

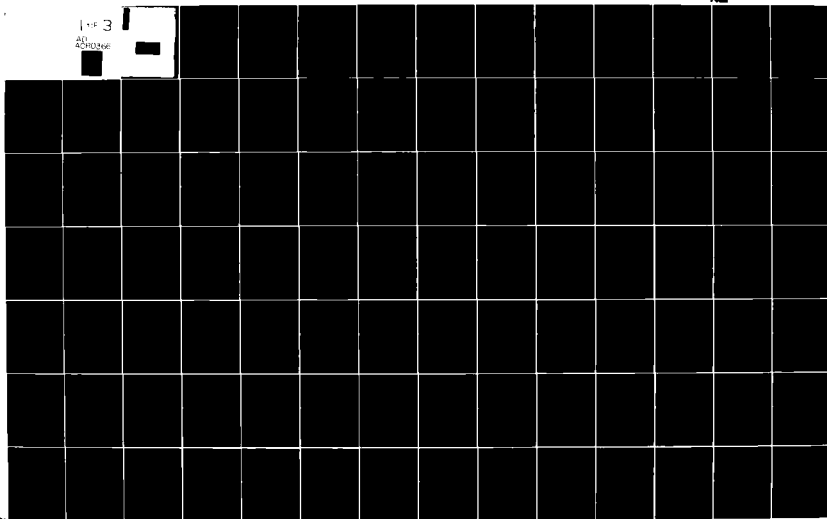
AD-A080 346

AIR FORCE INST OF TECH WRIGHT-PATTERSON AFB OH SCHOO--ETC F/O 20/12
PHOTOLUMINESCENCE OF UNDOPED, SEMI-INSULATING, AND NO-IMPLANTED--ETC(U)
DEC 79 G S POMRENKE
AFIT/DEP/PH/790-8

UNCLASSIFIED

NL

1-13
AD-A080 346



AFIT/GEP/PH/79D-8

1

6 PHOTOLUMINESCENCE OF UNDOPED,
SEMI-INSULATING, AND Mg-IMPLANTED
INDIUM PHOSPHIDE.

7 Masters THESIS

14 AFIT/GEP/PH/79D-8

10 Gernot Siefried Pomrenke
Capt USAF

DEC 6 1980

11 Dec 79

12 198

16 2306

17 R2

Approved for Public Release; Distribution Unlimited

012225

m+

Preface

All aspects of this study have been a most educational experience. Due to the lack of reported data on the photoluminescence of Mg-implanted InP, I believe this is one of the first investigations in this area. A voluminous amount of experimental data was obtained which could provide initiative for further analysis by others. As with many studies of this type, time becomes a factor in the final product.

I would like to express my thanks to Dr. Robert L. Hengehold for his suggestions and advice in particular problem areas; thanks also to George Gergal and Ron Gabriel for their technical assistance, and, of course, to Jim Miskimen whose invaluable help and advice kept the cryogenic and evacuation system operational. Appreciation also goes to Dr. Yoon Soo Park of the Air Force Avionics Laboratory for his suggestions and for providing the needed samples, and to Jim Ehret and Charles Geesner for their fine work in ion implantation and annealing. Interaction with doctoral students, Mike Sydenstricker and Orven Swenson brought light to various questions concerning the study. Finally, I would like to thank my wife, Erna, for her help and understanding.

Gernot S. Pomrenke

(This thesis was typed by Sharon Gabriel)

Contents

	Page
Preface.....	ii
List of Figures.....	vi
List of Tables.....	xii
Abstract.....	xiii
I. Introduction.....	1
Background.....	1
Problem.....	4
II. Theory.....	5
Semiconductor Characteristics.....	5
Radiative Transitions.....	8
Exciton Recombination.....	8
Conduction Band-to-Valence Band.....	10
Band-to-Impurity Level.....	11
Donor-to-Acceptor.....	12
Photoluminescence of Indium Phosphide.....	13
Semi-Insulating Indium Phosphide.....	15
Ion Implantation and Annealing.....	15
Mg-Implanted Indium Phosphide.....	16
III. Equipment, Procedure, and Sample Information.....	19
Equipment.....	19
Sample Environment.....	19
Illumination Source and Optics.....	23
Signal Processing.....	24
Procedure.....	27
Sample Mounting.....	27
Alignment.....	28
Laser and Optics.....	30
Signal Detection and Recording.....	31
Evacuation and Cryogenics.....	32
Data Collection.....	33
Data Analysis.....	34
Sample Data and Preparation.....	36
IV. Results and Discussion.....	40
Undoped Indium Phosphide.....	40
Representative Spectra.....	42
Peak Identification.....	47

	Page
Temperature Dependence.....	49
Emission Intensity.....	54
Semi-Insulating InP:Fe.....	57
Unannealed, Mg-Implanted InP:Fe.....	63
Mg-Implanted InP:Fe.....	65
750° C Annealed.....	65
700° C Annealed and 4.2° K Sample Temperature.....	72
700° C Annealed and 50° K Sample Temperature.....	74
700° C Annealed and at Various Sample Temperatures	78
VPE and LPE Grown InP.....	82
V. Conclusions and Recommendations.....	88
Bibliography.....	91
Appendix A: Polynomial Least Squares Fit Analysis of Indium Phosphide Peak Energy Versus Temperature Data.....	94
Appendix B: Photoluminescence Below 9700 Å of Undoped InP from 2.69° K to 225° K.....	103
Appendix C: Photoluminescence Between 9100 Å and 11700 Å of Undoped InP from 2.22° K to 100° K.....	118
Appendix D: Photoluminescence Below 3.0 µm of Undoped InP at 162° K.....	123
Appendix E: Photoluminescence Below 11700 Å of Semi-Insulating InP:Fe from 4.2° K to 100° K.....	125
Appendix F: Photoluminescence Below 3.0 µm of Semi-Insulating InP:Fe at 4.2° K.....	130
Appendix G: Photoluminescence Below 1.4 µm of Unannealed, Unimplanted and Mg-Implanted InP:Fe at 50° K.....	132
Appendix H: Photoluminescence of Mg-Implanted, 750° C Annealed InP:Fe at 50° K.....	136
Appendix I: Photoluminescence of Mg-Implanted, 700° C Annealed InP:Fe at 4.2° K.....	146
Appendix J: Photoluminescence of Mg-Implanted, 700° C Annealed InP:Fe at 50° K.....	155
Appendix K: Photoluminescence of Unimplanted (Wafer 6), 700° C Annealed InP:Fe from 4.2° K to 100° K.....	163
Appendix L: Photoluminescence of Mg-Implanted ($1 \times 10^{15} \text{ cm}^{-2}$), 700° C Annealed InP:Fe from 4.2° K to 100° K.....	167

	Page
Appendix M: Photoluminescence of VPE InP.....	171
Appendix N: Photoluminescence of Undoped LPE InP at 77.3° K and 100° K.....	177
Vita.....	180

List of Figures

<u>Figure</u>		<u>Page</u>
1	Conduction and Valence Bands of a Pure Semiconductor at Absolute Zero and Room Temperature.....	6
2	Radiative Transitions.....	9
3	Experimental Setup.....	20
4	Cryogenic and Evacuation System.....	21
5	Spectral Response of S-1 Photomultiplier.....	25
6	Photoconductor Location and Associated Electronics....	26
7	Spectral Response of PbS Photoconductor.....	27
8	Background Spectrum of Sample Environment at 50° K....	29
9	Photoluminescence Below 9700 Å of Undoped InP at 20°K.	43
10	Photoluminescence Between 9100 Å and 11700 Å of Undoped InP at 77.3° K.....	44
11	Photoluminescence Below 3.0 μm of Undoped InP at 162° K.....	45
12	Detail in Near-Bandedge Peak of Undoped InP at 4.2°K..	46
13	Detail in 1.37 eV Peak of Undoped InP at 2.69° K.....	48
14	Temperature Dependence of Near-Bandedge Peak in Undoped InP.....	50
15	Temperature Dependence of Donor-Acceptor (8900 Å) Peak Energy for Undoped InP.....	51
16	Temperature Dependence of Emission Spectra for Undoped InP.....	52
17	Temperature Dependence of Emission Intensity for Undoped InP.....	55
18	Temperature Dependence of Ratio of Relative Peak Intensity for Undoped InP.....	56
19	Photoluminescence of Undoped InP at 4.2° K at Various Excitation Intensities.....	58

List of Figures (Cont'd)

<u>Figure</u>		<u>Page</u>
20	Emission Intensity Dependence on Excitation Intensity for Undoped InP at 4.2° K.....	59
21	Photoluminescence Below 11700 Å of Semi-Insulating InP:Fe at 10° K.....	61
22	Photoluminescence Below 1.4 μm of Unannealed, Mg-Implanted ($1 \times 10^{13} \text{ cm}^{-2}$) InP:Fe at 50° K.....	64
23	Photoluminescence of Mg-Implanted ($1 \times 10^{14} \text{ cm}^{-2}$), 750° C Annealed InP:Fe at 50° K.....	66
24	Mg-Implanted, 750° C Annealed InP:Fe at 50° K.....	69
25	Ion Dose Dependence of Peak Energy for Mg-Implanted, 750° C Annealed InP:Fe at 50° K.....	70
26	Ion Dose Dependence of Emission Intensity for Mg-Implanted, 750° C Annealed InP:Fe at 50° K.....	71
27	Magnesium Peak in Photoluminescence Spectra of Mg-Implanted ($3 \times 10^{13} \text{ cm}^{-2}$) InP:Fe at 50° K.....	73
28	Ion Dose Dependence of Peak Energy for Mg-Implanted, 700° C Annealed InP:Fe at 50° K.....	77
29	Ion Dose Dependence of Emission Intensity for Mg-Implanted, 700° C Annealed InP:Fe at 50° K.....	80
30	Temperature Dependence of Photoluminescent Spectra in Annealed, Unimplanted, and Mg-Implanted InP.....	81
31	Photoluminescence of Undoped VPE InP at 4.2° K.....	84
32	Photoluminescence of Mg-Implanted ($1 \times 10^{12} \text{ cm}^{-2}$) VPE InP at 4.2° K.....	85
A-1	Temperature Dependence of Exciton-Related (8700 Å) Peak Energy in Undoped InP.....	99
A-2	Temperature Dependence of Donor-Acceptor (8900 Å) Peak Energy in Undoped InP.....	101
A-3	Empirical Band Gap.....	102
B-1	Photoluminescence Below 9700 Å of Undoped InP at 2.69°K	104
B-2	Photoluminescence Below 9700 Å of Undoped InP at 4.2°K	105

List of Figures (Cont'd)

<u>Figure</u>		<u>Page</u>
B-3	Photoluminescence Below 9700 Å of Undoped InP at 5° K....	106
B-4	Photoluminescence Below 9700 Å of Undoped InP at 10° K...	107
B-5	Photoluminescence Below 9700 Å of Undoped InP at 20° K...	108
B-6	Photoluminescence Below 9700 Å of Undoped InP at 30° K...	109
B-7	Photoluminescence Below 9700 Å of Undoped InP at 40° K...	110
B-8	Photoluminescence Below 9700 Å of Undoped InP at 50° K...	111
B-9	Photoluminescence Below 9700 Å of Undoped InP at 60° K...	112
B-10	Photoluminescence Below 9700 Å of Undoped InP at 77.3° K.	113
B-11	Photoluminescence Below 9700 Å of Undoped InP at 100° K..	114
B-12	Photoluminescence Below 9700 Å of Undoped InP at 125° K..	115
B-13	Photoluminescence Below 9700 Å of Undoped InP at 160° K..	116
B-14	Photoluminescence Below 9700 Å of Undoped InP at 225° K..	117
C-1	Photoluminescence Between 9100 Å and 11100 Å of Undoped InP at 2.22° K.....	119
C-2	Photoluminescence Between 9100 Å and 11900 Å of Undoped InP at 50° K.....	120
C-3	Photoluminescence Between 9100 Å and 11700 Å of Undoped InP at 77.3° K.....	121
C-4	Photoluminescence Between 9100 Å and 11700 Å of Undoped InP at 100° K.....	122
D-1	Photoluminescence Below 3.0 μm of Undoped InP at 162° K...	124
E-1	Photoluminescence Below 11700 Å of Semi-Insulating InP:Fe at 4.2° K.....	126
E-2	Photoluminescence Below 11700 Å of Semi-Insulating InP:Fe at 10° K.....	127
E-3	Photoluminescence Below 11700 Å of Semi-Insulating InP:Fe at 50° K.....	128

List of Figures (Cont'd)

<u>Figure</u>		<u>Page</u>
E-4	Photoluminescence Below 11700 Å of Semi-Insulating InP:Fe at 100° K.....	129
F-1	Photoluminescence Below 3.0 μm of Semi-Insulating InP:Fe at 4.2° K.....	131
G-1	Photoluminescence Below 1.4 μm of Unannealed, Unimplanted InP:Fe at 50° K.....	133
G-2	Photoluminescence Below 1.4 μm of Unannealed, Mg-Implanted ($3 \times 10^{14} \text{ cm}^{-2}$) InP:Fe at 50° K.....	134
G-3	Photoluminescence Below 1.4 μm of Unannealed, Mg-Implanted ($1 \times 10^{13} \text{ cm}^{-2}$) InP:Fe at 50° K.....	135
H-1	Photoluminescence of Unimplanted (Wafer 4), 750° C Annealed InP:Fe at 50° K.....	137
H-2	Photoluminescence of Unimplanted (Wafer 5), 750° C Annealed InP:Fe at 50° K.....	138
H-3	Photoluminescence of Unimplanted (Wafer 6), 750° C Annealed InP:Fe at 50° K.....	139
H-4	Photoluminescence of Mg-Implanted ($1 \times 10^{15} \text{ cm}^{-2}$), 750° C Annealed InP:Fe at 50° K.....	140
H-5	Photoluminescence of Mg-Implanted ($3 \times 10^{14} \text{ cm}^{-2}$), 750° C Annealed InP:Fe at 50° K.....	141
H-6	Photoluminescence of Mg-Implanted ($1 \times 10^{14} \text{ cm}^{-2}$), 750° C Annealed InP:Fe at 50° K.....	142
H-7	Photoluminescence of Mg-Implanted ($3 \times 10^{13} \text{ cm}^{-2}$), 750° C Annealed InP:Fe at 50° K.....	143
H-8	Photoluminescence of Mg-Implanted ($1 \times 10^{13} \text{ cm}^{-2}$), 750° C Annealed InP:Fe at 50° K.....	144
H-9	Photoluminescence of Mg-Implanted ($5 \times 10^{12} \text{ cm}^{-2}$), 750° C Annealed InP:Fe at 50° K.....	145
I-1	Photoluminescence of Unimplanted (Wafer 4), 700° C Annealed InP:Fe at 4.2° K.....	147
I-2	Photoluminescence of Unimplanted (Wafer 6), 700° C Annealed InP:Fe at 4.2° K.....	148

List of Figures (Cont'd)

<u>Figure</u>		<u>Page</u>
I-3	Photoluminescence of Mg-Implanted ($1 \times 10^{15} \text{ cm}^{-2}$), 700° C Annealed InP:Fe at 4.2° K.....	149
I-4	Photoluminescence of Mg-Implanted ($3 \times 10^{14} \text{ cm}^{-2}$), 700° C Annealed InP:Fe at 4.2° K.....	150
I-5	Photoluminescence of Mg-Implanted ($1 \times 10^{14} \text{ cm}^{-2}$), 700° C Annealed InP:Fe at 4.2° K.....	151
I-6	Photoluminescence of Mg-Implanted ($3 \times 10^{13} \text{ cm}^{-2}$), 700° C Annealed InP:Fe at 4.2° K.....	152
I-7	Photoluminescence of Mg-Implanted ($1 \times 10^{13} \text{ cm}^{-2}$), 700° C Annealed InP:Fe at 4.2° K.....	153
I-8	Photoluminescence of Mg-Implanted ($5 \times 10^{12} \text{ cm}^{-2}$), 700° C Annealed InP:Fe at 4.2° K.....	154
J-1	Photoluminescence of Unimplanted, 700° C Annealed InP:Fe at 50° K.....	156
J-2	Photoluminescence of Mg-Implanted ($1 \times 10^{15} \text{ cm}^{-2}$), 700° C Annealed InP:Fe at 50° K.....	157
J-3	Photoluminescence of Mg-Implanted ($3 \times 10^{14} \text{ cm}^{-2}$), 700° C Annealed InP:Fe at 50° K.....	158
J-4	Photoluminescence of Mg-Implanted ($1 \times 10^{14} \text{ cm}^{-2}$), 700° C Annealed InP:Fe at 50° K.....	159
J-5	Photoluminescence of Mg-Implanted ($3 \times 10^{13} \text{ cm}^{-2}$), 700° C Annealed InP:Fe at 50° K.....	160
J-6	Photoluminescence of Mg-Implanted ($1 \times 10^{13} \text{ cm}^{-2}$), 700° C Annealed InP:Fe at 50° K.....	161
J-7	Photoluminescence of Mg-Implanted ($5 \times 10^{12} \text{ cm}^{-2}$), 700° C Annealed InP:Fe at 50° K.....	162
K-1	Photoluminescence of Unimplanted (Wafer 6), 700° C Annealed InP:Fe at 4.2° K.....	164
K-2	Photoluminescence of Unimplanted (Wafer 6), 700° C Annealed InP:Fe at 50° K.....	165
K-3	Photoluminescence of Unimplanted (Wafer 6), 700° C Annealed InP:Fe at 100° K.....	166

List of Figures (Cont'd)

<u>Figure</u>		<u>Page</u>
L-1	Photoluminescence of Mg-Implanted ($1 \times 10^{15} \text{ cm}^{-2}$), 700° C Annealed InP:Fe at 4.2° K.....	168
L-2	Photoluminescence of Mg-Implanted ($1 \times 10^{15} \text{ cm}^{-2}$), 700° C Annealed InP:Fe at 50° K.....	169
L-3	Photoluminescence of Mg-Implanted ($1 \times 10^{15} \text{ cm}^{-2}$), 700° C Annealed InP:Fe at 100° K.....	170
M-1	Photoluminescence of Undoped VPE InP at 4.2° K.....	172
M-2	Photoluminescence of Undoped VPE InP at 50° K.....	173
M-3	Photoluminescence of Undoped VPE InP at 77.3° K.....	173
M-4	Photoluminescence of Mg-Implanted ($1 \times 10^{13} \text{ cm}^{-2}$) VPE InP at 50° K.....	174
M-5	Photoluminescence of Mg-Implanted ($1 \times 10^{12} \text{ cm}^{-2}$) VPE InP at 4.2° K.....	175
M-6	Photoluminescence of Mg-Implanted ($1 \times 10^{12} \text{ cm}^{-2}$) VPE InP at 50° K.....	176
N-1	Photoluminescence of Undoped LPE InP at 77.3° K.....	178
N-2	Photoluminescence of Undoped LPE InP at 100° K.....	179

List of Tables

<u>Table</u>		<u>Page</u>
1	Sheet Hole Concentration (N_S) and Mobility (μ_S) for Magnesium Implants in InP.....	18
2	Sample Conditions.....	35
3	Sample Data.....	37
4	Photoluminescence of Undoped InP at 2.22° K to 225° K..	41
5	Photoluminescence of Semi-Insulating InP:Fe at 4.2° K to 100° K.....	60
6	Photoluminescence of Unannealed, Mg-Implanted InP:Fe at 50° K.....	63
7	Photoluminescence of Mg-Implanted, 750° C Annealed InP:Fe at 50° K.....	67
8	Photoluminescence of Mg-Implanted, 700° C Annealed InP:Fe at 4.2° K.....	75
9	Photoluminescence of Mg-Implanted, 700° C Annealed InP:Fe at 50° K.....	76
10	Photoluminescence of Unimplanted (Wafer 6), 700° C Annealed InP:Fe from 4.2° K to 100° K.....	79
11	Photoluminescence of Mg-Implanted ($1 \times 10^{15} \text{ cm}^{-2}$), 700° C Annealed InP:Fe from 4.2° K to 100° K.....	79
12	Photoluminescence of VPE InP.....	83
13	Photoluminescence of Undoped LPE at 77.3° K and 100P K.	87

Photoluminescence power
to the left
power

Abstract

A photoluminescent investigation was made of undoped, semi-insulating, unannealed and annealed Mg-ion implanted, indium phosphide which originated from Czochralski, vapor, and liquid grown crystals. Ion implantation was performed at fluences of 5×10^{12} ions/cm² to 1×10^{15} ions/cm² with an energy of 120 keV at room temperature, followed by annealing at 700° C and 750° C for fifteen minutes using a Si₃N₄ encapsulant.

Luminescence of undoped InP was studied with respect to temperature, emission intensity, and excitation intensity; results included the possible identification of the following radiative recombinations: free exciton, bound exciton, donor-to-valence, and donor-to-acceptor. Broad, low intensity peaks were identified at 1.0541 eV, 0.9374 eV, and 1.15 eV. Spectral results of the less intense semi-insulating InP:Fe were identical to undoped InP aside from a 1.38 eV high energy shoulder and low intensity peak at 1.31 eV.

Photoluminescence of unannealed, implanted samples resulted in a 0.9643 eV peak with a long, low energy shoulder. Emission intensity and peak energy of annealed, implanted samples were studied as a function of dosage and anneal temperature. The post-implantation annealing at 750° C was sufficient to obtain efficient luminescence. Analysis of the 750° C annealed samples indicates that the peak due to recombinations involving implanted Mg acceptors is located between 1.384 eV and 1.388 eV at 50° K. Superior spectral results from VPE InP places the Mg peak position at 1.3801 eV. Full width at half maximum for

2

direct
↓
the 1.41 eV peak at 77.3° K was 10.32 meV for Czochralski grown
InP, 5.67 meV for LPE grown InP, and 4.99 meV for VPE grown InP. *X*

PHOTOLUMINESCENCE OF UNDOPEO,
SEMI-INSULATING, AND Mg-IMPLANTED INDIUM PHOSPHIDE

I. Introduction

Background

The Electronic Research Branch (DHR) of the Air Force Avionics Laboratory (AFAL) has been providing the Air Force with material research for solid state devices with very-high-speed, digital integrated circuits for applications requiring data rates of 10 gigabits per second and up where silicon integrated circuit technology has been unsuccessful. These microwave semiconductors, which are used for power generation and amplification, include field effect transistors (FETs) and transferred-electron (TE) devices. Requirements for this new device technology are derived from needs for high-speed signal processing in electromagnetic warfare, real-time digital radar, reconnaissance, communications, and satellites. Research emphasis for material to be used in these devices has basically been placed on gallium arsenide (GaAs), a III-V group semiconductor (Ref 1:33); however, as GaAs technology matured, a search took shape for finding new materials with improved transport properties. The investigation by government and industry identified the binary III-V compound, indium phosphide (InP), as a material with high potential for application in TE devices which depend for their operation on internal negative resistance due to carrier motion in the semiconductor at high electric

fields. The high mobility of InP is also thought to extend the frequency and power ranges in FETs (Ref 2:4); hence making indium phosphide very attractive for various high-speed device applications in both the microwave and opto-electronic areas (Ref 3).

A key element in studying semiconductors such as InP lies in the ability to change their electrical properties by introducing impurities into the pure or intrinsic material. Donor impurities for InP are many, with the following elements used to create n-type material: silicon (Si), germanium (Ge), tin (Sn), bismuth (Bi), sulfur (S), selenium (Se), and tellurium (Te). Typical acceptor dopants for creating p-type InP are as follow: zinc (Zn), cadmium (Cd), mercury (Hg), copper (Cu), manganese (Mn), and beryllium (Be) (Refs 3:418-420 and 4:1741-1749). By controlling the doping, the material's electrical parameters can be changed as desired. To do this may only require impurity levels of a few parts per million, and such levels are difficult to produce in a reliable fashion with the conventional melt-grown, vapor-grown, and solution-grown techniques. In recent years the advances in the field of semiconductor devices have depended on the ability to accurately control these dopants. Ion implantation has proven to be extremely helpful in achieving this objective (Ref 5:1669). Other advantages of implantation include control of design through masking, control of implant depth, low process temperature, uniform junctions, and an increase in production of reliable devices (Ref 6:329).

Ions are implanted into indium phosphide most commonly with energies of 50 to 400 keV (Ref 3:418) to yield the required doping;

however, these ions are not necessarily at the proper lattice positions and the lattice itself may be rather badly damaged as a result of the ion-bombardment. In order to position the ions into lattice sites and to remove the residual damage, one must anneal the surface of the material. This is done by thermally heating the implanted sample, causing the defects to migrate to the appropriate sites. Once the sample is implanted and annealed, characterization is performed in order to assess the properties of the chosen implant and the efficiency of the anneal conditions.

Currently the Air Force Office of Scientific Research (AFOSR) is supporting the study of n- and p-implants into indium phosphide and their behavior under various annealing conditions. The n-implants are required for high drift velocity layers for high frequency devices, while p-implants support junction field-effect transistor (JFET) fabrication (Ref 2:2-3). Electrical results are available for n-implants (Se, Si, S) and p-implants (Be, Mg, Cd) (Refs 3, 7) with n-implants being well-behaved throughout low and high dopant concentrations and with p-implants creating problems over consistent activation. The latter problem area is less evident in Be and Mg-implants (Ref 2:2). In response to the interest in implanted indium phosphide, AFAL/DHR recently started investigating Mg-implanted InP. Lack of published luminescence data for this p-implant prompted support from AFIT to perform a photoluminescence study.

Photoluminescence occurs as the result of radiative recombination of electron-hole pairs when a material is excited by photons. As an experimental technique, photoluminescence uses light of a particular

wavelength to excite electrons in the sample material to higher energy states. The light emitted from the sample during the subsequent relaxation of the electrons is collected by lenses, directed through a spectrometer, and detected by a photomultiplier or photoconductor; the spectrum is recorded on an x-y plotter.

Problem

The purpose of this study is to optically characterize undoped, semi-insulating, and Mg-implanted indium phosphide using photoluminescence. Initially, the goal is to understand the basic optical properties of the intrinsic material by identifying the various impurity and defect levels as reported in the literature. These observations shall be made over a wide range of temperatures starting at least at 4.2° K and extending beyond 77.3° K, where limited published data are available. The substrate material for the ion implantation is iron-doped, semi-insulating indium phosphide; hence, the luminescence resulting from excitation of this substrate material is also investigated over a range of temperatures. This information should facilitate the identification of spectra due to implants. Magnesium ions are implanted at 120 keV at room temperature with fluences of 5×10^{12} ions/cm² to 1×10^{15} ions/cm² and the resulting samples are annealed at temperatures of 700° C and 750° C for fifteen minutes. Each of these samples, including some unannealed specimens, is investigated for impurity and defect levels and efficacy of the implant and anneal condition. Finally, a comparison of the emission spectra is made of liquid phase epitaxial and vapor phase epitaxial crystals and the InP crystals grown by the Czochralski technique.

II. Theory

Semiconductor Characteristics

Instead of discrete levels, electronic energy states exist as bands in crystals. In semiconductors this energy level structure consists of a band in which all electronic states are filled at absolute zero and a band that is completely empty (Figure 1). The region separating the bands is the energy gap and is normally no wider than 2 eV (Ref 9:505). The filled band is called the valence band; the empty band, the conduction band. At higher temperatures a few electrons acquire enough thermal energy to cross the energy gap and to fill the empty band, therefore becoming conduction electrons in the previously empty conduction band. Whenever sufficient energy in the form of heat, photons, or voltage is applied to the material to excite electrons from the valence to the conduction band, a hole is created in the valence band. This "absent electron" state behaves much as a positive charge in the crystal; it responds to applied electrical field and has an effective mass (Ref 8:256-263; 10:1-2).

Pure or intrinsic semiconductors contain an equal number of holes and electrons; however, crystals in this form have an extremely low conduction. Usable semiconductors are therefore desired to be extrinsic rather than intrinsic. These are semiconductors to which dopants or impurities have been added in carefully controlled amounts. In terms of the energy bands, a donor or n-type impurity (donates electrons) produces a new narrow band of allowed energy below, but very close to, the bottom edge of the conduction band. Similarly,

the p-type or acceptor impurity (accepts electrons) produces a narrow allowed energy band above, but very close to, the top of the valence band (Ref 10:1-2).

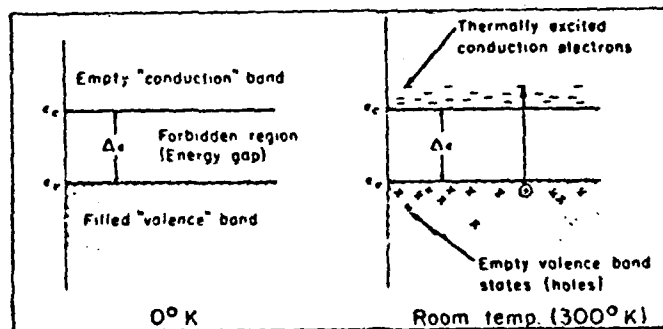


Figure 1. Conduction and Valence Bands of a Pure Semiconductor at Absolute Zero and Room Temperature (Ref 8:257).

Most commonly, dopants are introduced as substitutional impurities in which one of the crystal's constituent atoms is replaced. For example, by introducing sulfur (Group VI impurity) into indium phosphide, the sulfur replaces phosphorus in the lattice site. Sulfur, which acts as a donor in this case, has six electrons per atom in the valence band, while phosphorus has five electrons per atom in the valence band; hence, five sulfur electrons are bound and the sixth is nearly free. The sixth electron is bound to the sulfur atom only by weak electrostatic forces and, hence, is easily ionized into the conduction band at a much lower temperature than would be required for electrons in the valence band. The donor ionization energy (E) is given in CGS units by the following modified Bohr model expression (Ref 11:232):

$$E = \frac{e^4 m_e}{2\epsilon^2 \hbar^2} \quad (1)$$

where e is the electrical charge, m_e is the effective mass, ϵ is the dielectric constant of the host material, and \hbar is Planck's constant. This extra electron, therefore, occupies a narrow range of energy levels below the conduction band into which it may be easily excited.

If, instead, a Group II impurity such as magnesium is substituted for indium, a hole is introduced. Magnesium has only two electrons in the valence band, while indium has three electrons in the valence band. The hole can easily drift away from the magnesium impurity site since neighboring electrons migrate to the site to fill the third electron position in the band. This impurity, or acceptor, introduces thus a narrow band of energy levels above the top of the valence band into which valence electrons are easily excited, consequently leaving holes in the valence band (Ref 9:506-507).

If the dopant is introduced in such a manner as to occupy one of the spaces between the constituent atoms of the semiconductor material, it is called an interstitial impurity. The outer-shell electrons become available for conduction and the interstitial impurity is considered a donor. Conditions also occur where an atom is missing in the lattice, which results in a vacancy and deprives the crystal of one electron per broken bond; hence, the vacancy becomes an acceptor. Under the condition where the valence of the substitutional impurity is the same as that of the atom it replaces, an isoelectronic center is formed (Ref 12:8, 61).

Electron-hole recombinations are categorized according to two types of centers, simple and complex, which are responsible for the transition. A simple center is defined as an impurity which sits, for example, in a binary compound, on either one of the host's lattice sites and contributes an additional carrier to the binding. The radiative recombinations considered in this study will all be of this type. A complex center is defined as a radiative center which produces an emission peak too broad and too low in energy to be a hydrogenic center and the temperature dependence of the peaks is opposite to that of the band gap (Ref 13:8-9).

Radiative Transitions

Photoluminescence in semiconductors occurs as the result of optical excitation of the material and the subsequent recombination of electrons and holes with the simultaneous emission of photons. A variety of recombinations are possible (Ref 12); however, only a limited number of transitions are relevant to this study and these are depicted in Figure 2. The transitions are identified as free exciton (recombination A1 in Figure 2), bound exciton (A2), conduction band-to-valence band (B), conduction band-to-acceptor (C1), donor-to-valence band (C2), and donor-to-acceptor (D). Only transitions for direct gap material are discussed; material for which an electron in the conduction band and a hole in the valence band recombine without the assistance of an intermediate state (Ref 8:361).

Exciton Recombination. The first transition to be considered is the free exciton recombination. An exciton is an electron and hole bound together by their attractive electrostatic interaction, similar

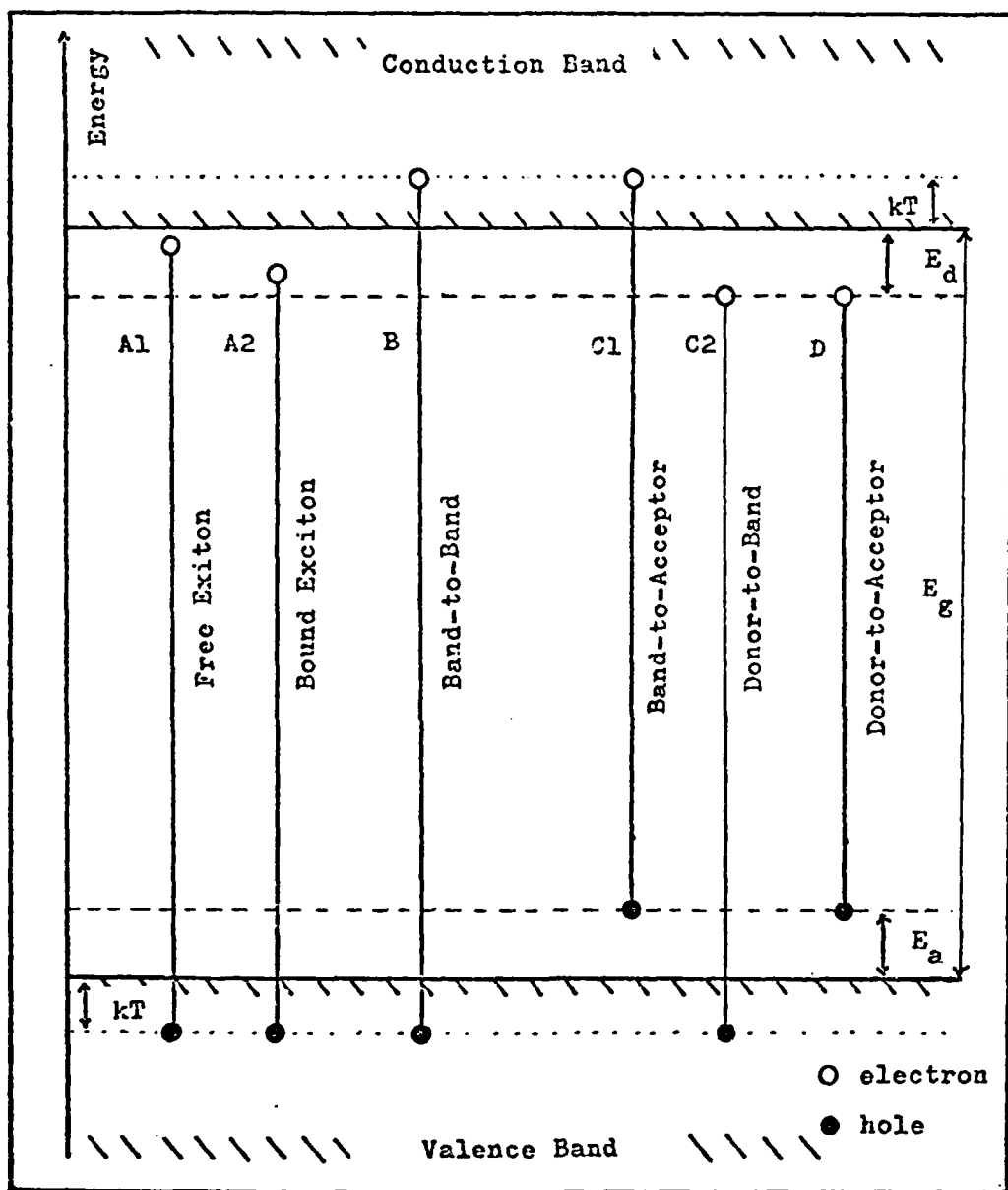


Figure 2. Radiative Transitions

to an electron bound to a proton in a hydrogen atom. As a free exciton, the electron-hole pair moves freely through the crystal; however, due to its unstable nature, the electron and hole eventually recombine, emitting a photon (Ref 11:332). In a direct-gap semiconductor, such as indium phosphide, where momentum is conserved in the transition, the energy (E) of the emitted photon is estimated as:

$$E = E_g - E_x \quad (2)$$

where E_g is the band gap energy and E_x is the binding energy of the exciton (equivalent to the ionization energy given by Equation (1)). Lower probability exciton transitions are also possible where one or more phonons are involved (Ref 12:114). Bound exciton recombinations may occur in the presence of impurities since the exciton may become bound to a donor or acceptor center. The energy emitted in this transition is less than that for a free exciton by the amount equal to the binding energy of the exciton to the impurity (Ref 14:107).

Conduction Band-to-Valence Band. Excitons are formed most easily in the purest material and at low temperatures. At higher temperatures and less pure crystals, the electron-hole pairs actually become free carriers occupying the conduction and valence bands; hence, the electrons and holes recombine in a band-to-band transition (Figure 2, transition B). The transition has a low energy threshold at bandgap energy. As the excitation rate and temperature increase, states deeper in the band recombine; hence, emitting photons of higher energy. Band-to-band transitions are therefore characterized by a

temperature dependent high-energy tail with low energy edge cutoff at band gap energy. Actual experimental emission peaks show a more Gaussian appearance at low energy; this suggests transitions from tails of states and impurity bands (Ref 12:124-126). The emission intensity of the band-to-band recombination will also decrease with increasing temperature. This is because band-to-band transitions provide the maximum lifetime that carriers can attain in a semiconductor, but capture into various impurity levels is usually far more rapid; thus, with increasing temperature, carriers migrate faster to impurity sites before recombination (Ref 15:16-17; 16:297). Since states deeper in the band recombine at higher temperature, luminescence at high temperatures will be characterized by low intensity broad peaks.

Band-to-Impurity Level. Although transitions between a band and nearest impurity level exist, experimental determination of such is difficult. Deeper transitions are usually observed, such as the conduction band-to-acceptor level (Figure 2, transition C1) in indium phosphide. These recombinations emit photons of the following energy (E) (Ref 17:744):

$$E = E_g - E_i + kT - nE_p \quad (3)$$

where E_g is the band gap energy; E_i is the impurity (acceptor or donor) binding energy; kT is the kinetic energy of the free electron, where k is the Boltzmann constant and T is the absolute temperature; and nE_p represents the change in energy due to the simultaneous

emission of $n = 0, 1, 2, \dots$ phonons of energy E_p . Due to the thermal energy (kT) of the free electron, the luminescence peak will be broader than in a bound exciton transition (Ref 18:40). Band-to-impurity transitions are basically limited to semiconductors with a relatively low concentration of impurities (Ref 12:133-134).

Donor-to-Acceptor. The final transition (Figure 2, transition D) to be discussed involves the recombination of an electron bound to a donor with a hole bound to an acceptor. Energy (E) of the emitted radiation is given by:

$$E = E_g - (E_a + E_d) - nE_p + \frac{e^2}{\epsilon r} \quad (4)$$

where E_a and E_d are the acceptor and donor binding energies, respectively; and the last term represents the Coulomb attraction between the hole and the electron where ϵ is the dielectric constant of the host material, e is the electronic charge, and r the donor-acceptor pair separation (Ref 17:743-744). (The remaining terms were identified in Equation (3)). As indicated by the nE_p term, phonon-emission replicas may extend the low energy edge of the emission spectrum over a large range. Transitions for distances greater than the effective Bohr radius are assisted by a tunneling process (Ref 12:143). Many discrete values of r may occur; hence, a series of sharp emission lines should be expected for donor-acceptor recombination. However, for the majority of transitions the separation r is greater than 40 Å, preventing donor-acceptor pair emission lines from being resolved. The result is a rather broad peak which is the envelope of the unresolvable sharp lines (Ref 18:40; 12:143).

Transitions between near donor-acceptor pairs are more probable than between distant pairs; therefore, emission intensity is skewed toward higher energy. However, since the number of possible donor-acceptor pairings decreases as r decreases, the emission intensity must go through a maximum as the separation decreases (Ref 12:143). Impurity concentration affects pair separation. As the concentration is decreased, the average donor-acceptor separation is increased, and the donor-acceptor peak position is shifted toward lower energy (Ref 19:1000).

Temperature dependence of the donor-acceptor transitions is discussed by Halperin and Zacks (Ref 20:2237-2242). At very low temperature, peak energy decreases as the temperature is increased until a minimum is reached beyond which the peak shifts to higher energy; however, the decrease in band gap energy with temperature counteracts the peak shift to higher energy. The net result is that the donor-acceptor peak energy decreases with increasing temperature, but by a smaller amount than the band gap energy. Intensity decreases with temperature since the impurity sites become more rapidly depopulated with increased temperature.

Photoluminescence of Indium Phosphide

Heim, et al. (Ref 21) identified at low temperature, a near edge emission at 1.416 eV and a further emission at 1.36 eV. At low temperature (1.8° K) and low intensity four lines are reported in the near edge emission: a narrow dominant line at 1.4165 eV is ascribed to free exciton recombination, a relatively narrow line at 1.4143 eV is due to bound exciton recombination, the 1.4123 eV line

is a donor-valence transition, and the 1.418 eV shoulder is of unknown origin. At higher intensities a new line emerges at 1.407 eV and is interpreted as a band-to-band transition. In a more detailed study of bound excitons in indium phosphide at 1.8° K, White, et al. (Ref 22) ascribe the 1.4144 eV emission to excitons bound to neutral acceptors. The 1.4165 eV emission is ascribed to excitons bound to neutral donors and the 1.4178 eV emission is identified as being due to free excitons. Higher temperatures result in near edge emission merging into a single peak which is ascribed to the exciton recombinations. At low temperature, the 1.38 eV peak is the strongest emission and is attributed to donor-acceptor recombination. Accompanying this peak are subsidiary peaks separated by 43 meV which can be associated with longitudinal optical (LO) phonon emission. A weak line at 1.358 eV may be due to a slightly deeper acceptor and the high energy side of the 1.38 eV emission may be partly due to conduction band-to-acceptor level transitions (Ref 21:542-551).

Williams, et al. (Ref 4) concentrated on doped indium phosphide; data are reported for the effect on electrical and luminescence properties of InP with the following impurities: Zn, Hg, Cu, Cd, B, Si, Ge, Sn, Bi, S, Se, Te, and Mn. A broad emission peak at 1.16 eV is also reported and is ascribed to phosphorus vacancies. Turner and Petit (Ref 23) identified two very broad peaks at lower photon energy, specifically at 1.04 eV and 0.72 eV at 6° K; the peaks are believed to arise from recombination at some unknown deep levels.

Band gap energy for InP is reported by Kittel as 1.42 eV at 0° K and 1.35 eV at 300° K (Ref 11:210). The extinction coefficient of

indium phosphide as a function of wavelength is tabulated by Willardson and Beer (Ref 24:527-531); from these data, the absorption coefficient at 5145 Å (wavelength of sample excitation source used in this study) is calculated to be $1.06466 \times 10^7 \text{ m}^{-1}$. By using Beer's law, the distance over which the irradiance falls by a factor of e is determined to be 939.3 Å.

Semi-Insulating Indium Phosphide

The InP substrate (VIPC 156) which served as host for ion implants was iron (Fe) doped to create semi-insulating or compensated material. Unless great care is taken in the preparation and growth of the semiconductor, there will be a significant density of donor and acceptor flaws in the intrinsic material at various energies within the energy gap. In order that the material behaves like an intrinsic semiconductor, the number of donor and acceptor flaws or unintentional dopants must be equal. In typical commercial InP, these flaws range around 10^{16} cm^{-3} ; hence, enough dopant is added to compensate for the unintentional added carriers. Photoluminescent studies show that Fe in InP provides four well-defined peaks; however, these studies of semi-insulating InP:Fe by the Naval Research Laboratory remain unpublished (Ref 2:12).

Ion Implantation and Annealing

As mentioned in the introduction, ion implantation is one of the main methods of accurately introducing dopants into the semiconductor substrate. The dopant is initially ionized and accelerated through a high potential field. The various species of the beam are

then separated by a magnetic field, and the desired ions are then directed to the target material. By controlling certain aspects of the implant process such as the potential field and implant time, various impurity concentrations may be entered into the substrate. Complete understanding of the implant process, however, requires an in-depth study of the mechanisms of energy loss which control the implant depth distribution and radiation damage; therefore, for most practical applications, range-energy tables from the theory of Lindhard, Scharff, and Schiott are utilized (Ref 25:1-5). The impurity depth distribution developed from this theory is described by a Gaussian function; for magnesium implanted at 120 keV, the mean projected range (R_p) was calculated to be 0.1432 μm with a projected standard deviation (σ_p) of 0.062 μm (Ref 26).

Aside from surface damage, collisions of the ions with the host nuclei remove atoms from their lattice sites creating crystal defects, interstitials and vacancies. To remove the defects and obtain useful electrical and optical properties, the implanted samples are annealed. During this process the samples are heated to high temperatures so that they may recrystallize and aid impurities in moving into substitutional sites (Ref 13:13).

Mg-Implanted Indium Phosphide

Limited profile data on magnesium implants in InP:Fe are reported by Eldridge and Wrick for an implant energy of 140 keV. The samples were annealed at 600° C for one hour under a SiO₂ encapsulant. It is believed that magnesium has its advantage as a p-type dopant as it is relatively nontoxic and both shallow and deep Mg profiles

should be achievable. Profiles by secondary ion mass spectrometry (SIMS) indicated a projected range and standard deviation ($R_p = 1700 \text{ \AA}$, $\sigma_p = 1000 \text{ \AA}$) which were significantly greater than the theoretical values ($R_p = 1470 \text{ \AA}$, $\sigma_p = 670 \text{ \AA}$). The profile was also characterized by an exponential tail between a depth of 0.5 \mu m and 1.2 \mu m ; this may be an actual tail or it may be a result of the redeposition of sputtered material. Finally, diffusion characteristics of implanted Mg in InP are not known (Ref 2:94-96).

Although luminescence data for Mg-implanted InP remain unreported, Donnelly and Hurwitz have published electrical results for 150 keV Mg implants in InP:Fe at various implant and anneal temperatures. The sheet hole concentration and mobility are listed in Table 1 for implantations at room temperature and 200° C ; samples implanted at 77° K gave results identical to those reported at 25° C . Annealing temperatures were 700° C , 725° C , and 750° C , and the encapsulant was pyrolytic phosphosilicate glass (PSG). The highest sheet concentration of $5.2 \times 10^{13} \text{ cm}^{-2}$ was reported for a sample implanted at a dosage of $1 \times 10^{14} \text{ Mg ions/cm}^2$ and annealed at 750° C . The data show that sheet hole concentration for a $1 \times 10^{14} \text{ cm}^{-2}$ implant is higher at room temperature than at 200° C . Investigations with implants of Kr^+ indicated that residual implantation damage is n-type, therefore making it more difficult to achieve high activation with implanted acceptors (Ref 3).

TABLE 1

Sheet Hole Concentration (N_s) and Mobility (μ_s)
for Magnesium Implants in InP (Ref 2:420)

Energy (keV)	Dose (cm^{-2})	Anneal temp. ($^{\circ}\text{C}$)	25 $^{\circ}\text{C}$ implants		200 $^{\circ}\text{C}$ implants	
			N_s (cm^{-2})	μ_s ($\text{cm}^2/\text{V sec}$)	N_s (cm^{-2})	μ_s ($\text{cm}^2/\text{V sec}$)
150	1×10^{14}	700	4.5×10^{13}	68	1.5×10^{13}	95
		725	4.4×10^{13}	92		
		750	5.2×10^{13}	83		

III. Equipment, Procedure, and Sample Information

Basic components for this photoluminescence study, as depicted in Figure 3, included a temperature-controlled sample environment, illuminating source, signal processing elements, and a signal recorder. Indium phosphide (InP) samples were located in the "detachable tail" section of a cryogenic dewar where they were excited by a light of a particular wavelength from an argon-ion laser. The emitted luminescence was collected by a system of lenses, chopped, and directed through a spectrometer. The signal was then detected by a photomultiplier, amplified, compared to the reference signal from the mechanical chopper by a lock-in amplifier, and finally recorded on an x-y recorder.

Equipment

Sample Environment. A Janis Detachable Tail 7 D.T. research dewar, operating from 2.22° K to room temperature, served as the sample environment throughout the experiment (Figure 4). The dewar consisted of a stainless steel, cylindrical body housing an outer three and one-half liter reservoir, filled with liquid nitrogen (LN_2); and an inner three liter reservoir, filled with liquid helium (LHe). Each of the reservoirs was surrounded by a vacuum wall. A tail assembly, with three quartz windows for viewing the sample, extended below the body and formed the lower section of the gas exchange column. This hollow shaft ran along the central axis of the system and housed the sample transfer rod. The valve-operator on top of the body controlled the flow rate of liquid helium into the gas exchange column. The

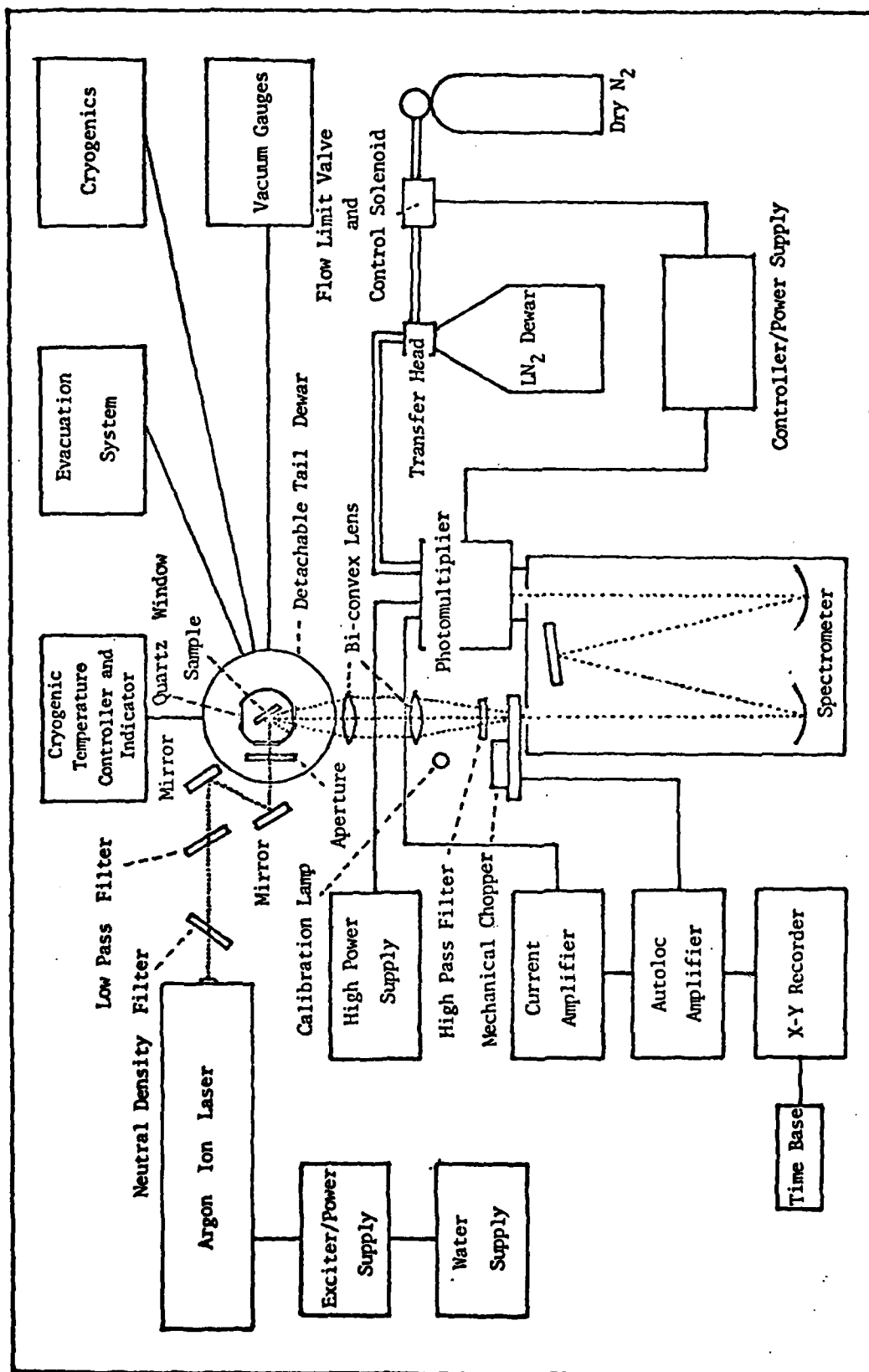


Figure 3. Experimental Setup

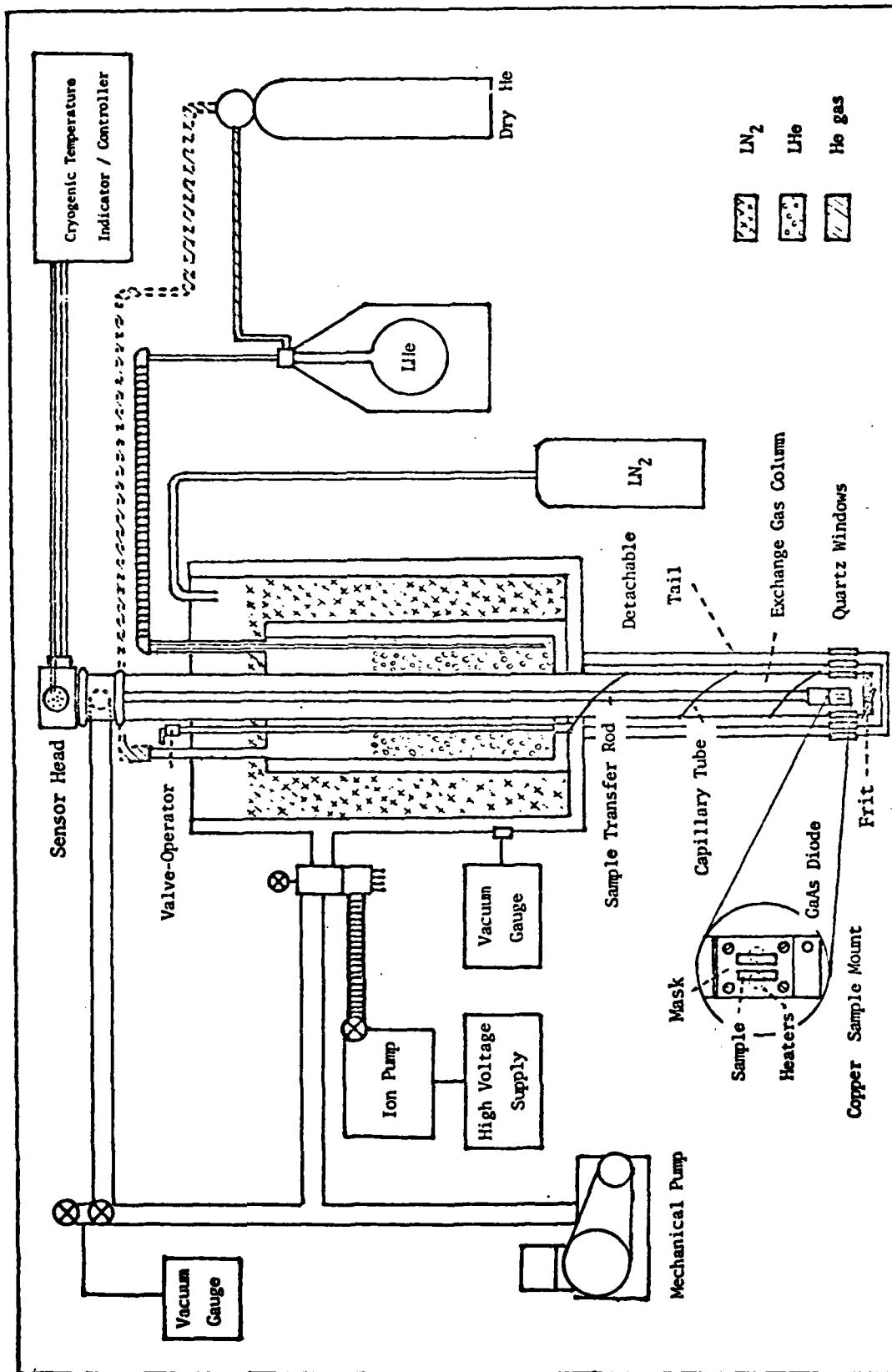


Figure 4. Cryogenic and Evacuation System

helium fed into this column and over the sample via a capillary tube by means of a gravity feed or pumping on the column.

Vacuum was maintained in the reservoirs' vacuum walls and gas exchange column by a Welch Scientific Company mechanical pump and an Ultek ion pump. In a non-cryogenic environment, the fore-pump achieved a 5 - 15 micron pressure, while with a liquid nitrogen environment the system achieved a 5×10^{-6} to 1×10^{-5} torr pressure which allowed operation of the ion pump. After the vacuum walls were isolated from the rest of the system and liquid helium supplied to the inner reservoir, pressures in the 10^{-7} torr region were possible. Power to the ion pump was supplied by a Varian 8 kV VacIon Pump Control Unit.

The sample transfer rod (Figure 4), to which the InP sample or samples were mounted, consisted of a sensor head, a 110 cm long stainless steel rod, and a copper sample mount. The mount was a 7.0 cm long, 2.1 cm wide, and 0.6 cm thick copper block which served as sample holder, heat sink, and point of connection for the temperature sensor and controller. A 2 cm by 2 cm thin copper sheet, which was fastened by four screws onto the mount, retained the InP sample. This copper mask contained apertures (sizes depended on sample size) for control of the irradiance on the sample. Two sample heaters and a temperature sensor were located, respectively, behind and below the specimen, and were electrically connected to the sensor head.

The sensor, a calibrated GaAs temperature-sensing diode, and resistive heaters were connected via the sensor head to a Lake Shore Cryotronics DTC-500 cryogenic temperature indicator and controller. The system determined the difference between the diode voltage and

the voltage dialed into the system (set point voltage). When the voltage difference was zero, the set point voltage corresponded to a particular temperature. In the temperature control mode, a particular voltage was selected and, by increasing or decreasing the current across the heaters, the system stabilized at the desired sample environment temperature. The degree of stability depended on the flow rate of helium over the sample.

Illumination Source and Optics. The InP sample was optically excited with a Spectra-Physics Model 164 Ion Laser. This water-cooled argon-ion laser was operational at eight wavelengths in the 4579 Å to 5145 Å region. (Sensitivity of the laser to water pressure changes prevented operation in a continuous and stable mode.) Peak power at the most intense line, 5145 Å, was measured with a power meter to be 1.43 watts (W). Optical elements (Figure 3) between the laser and dewar quartz window decreased the power to 0.757 W. By using neutral density filters, this latter output was further reduced to 0.310 W at 0.5 OD (optical density), to 0.075 W at 1.0 OD, and 0.010 W at 2.0 OD. Beam diameter at the $1/e^2$ point is 1.5 mm for the 5145 Å line and 1.2 mm for the 4579 Å line.

The laser's inherent violet/ultraviolet and infrared output at all wavelength selections was filtered with transmission type (90%) filters. Two 3 cm by 3 cm mirrors were used to direct the beam through a 1 mm aperture, the quartz windows, and onto the sample. The luminescence was focused by a 75.2 mm and a 200 mm bi-convex lens onto the entrance slit of the spectrometer.

Signal Processing. A SPEX 1702 3/4-meter Czerny-Turner Spectrometer was used to disperse the photoluminescent signal. Varying slit widths of 100 μm to 3 mm were used throughout the experiment in conjunction with a 10 mm slit height. A 102 mm by 102 mm grating blazed at 5000 \AA with 1200 grooves/mm served in making observations below the 12000 \AA region. An identically dimensioned grating blazed at 1.6 μm with 600 gr/mm was used for observations up to the 3.0 μm region. The spectral range was from 1750 \AA to 15000 \AA with a factory-calibrated scanning accuracy of -0.7 \AA at 2535 \AA and $+0.7 \text{ \AA}$ at 13075.6 \AA . Scanning speed ranged from 0.5 $\text{\AA}/\text{min}$ to 5000 $\text{\AA}/\text{min}$. At a scanning speed of 100 $\text{\AA}/\text{min}$ and a slit width of 100 μm , the resolution (width at half maximum) was better than 2.7 \AA . At a scanning speed of 250 $\text{\AA}/\text{min}$ and a slit setting of 400 μm , the resolution was 3.0 \AA . Calibration of the spectrometer in the 8500 \AA to 9800 \AA region with a low pressure Krypton lamp resulted in an error of less than ± 0.6 compared to peak positions reported in the literature.

For observations in the 8500 \AA to 12000 \AA region, the dispersed light was detected by an RCA C70007A, S-1 type, photomultiplier tube housed in a liquid-nitrogen-cooled Products for Research photomultiplier housing. With a controlled 15 psi pressure of dry nitrogen applied to a liquid nitrogen dewar, the nitrogen was transferred to the photomultiplier housing to cool the tube to a constant temperature of -50°C . A stable environment at this temperature is maintained by a Products for Research controller, flow limit valve and control solenoid, and a housing heater (Figure 1). Manufacturer's data for maximum tube sensitivity was used to operate the photomultiplier at a 1260 V bias

with a Keithley 244 High Voltage Supply. The relative sensitivity ranged from 95% at 8500 Å to 50% at 9500 Å with sensitivity rapidly dropping off after 12000 Å (Figure 5).

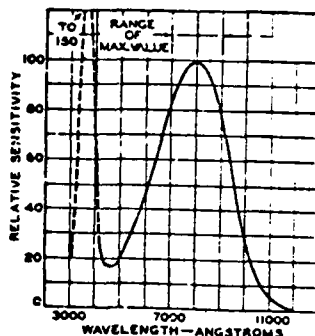


Figure 5. Spectral Response of S-1 Photomultiplier (Ref 27)

The photomultiplier output was connected to a Keithley 417 Current Amplifier which was operated at the minimum rise time setting of 0.01 msec and in the 10^4 to 10^{11} gain region. Output from the current amplifier was connected to the signal input of a Keithley Model 840 Autoloc Amplifier whose reference signal originated from a 225 Hz mechanical chopper positioned between the 200 mm bi-convex lens and spectrometer. This phase-lock technique minimized noise by passing only the luminescent signal in phase with the reference signal. The output from the Autoloc became the y-input of a Hewlett-Packard 7045-A x-y recorder. A Hewlett-Packard 17108AM Time Base served as the x-input to drive the recorder at 25 sec/cm. (Chopping the signal when using the photomultiplier proved basically to be an academic exercise, as the noise to be eliminated with the phase-lock technique lies beyond the 12000 Å region. Sample studies, other than the

undoped InP, and observations above 12000 Å, utilized the output of the Keithley 427 for input to the x-y recorder.)

An Infrared Industries Model 2767 Lead Sulfide (PbS) Detector was used to detect the luminescence in the 1.2 μm to 3.0 μm region. The photoconductor and electronics were positioned on top of a detector housing which was fastened to the spectrometer (Figure 6). A concave

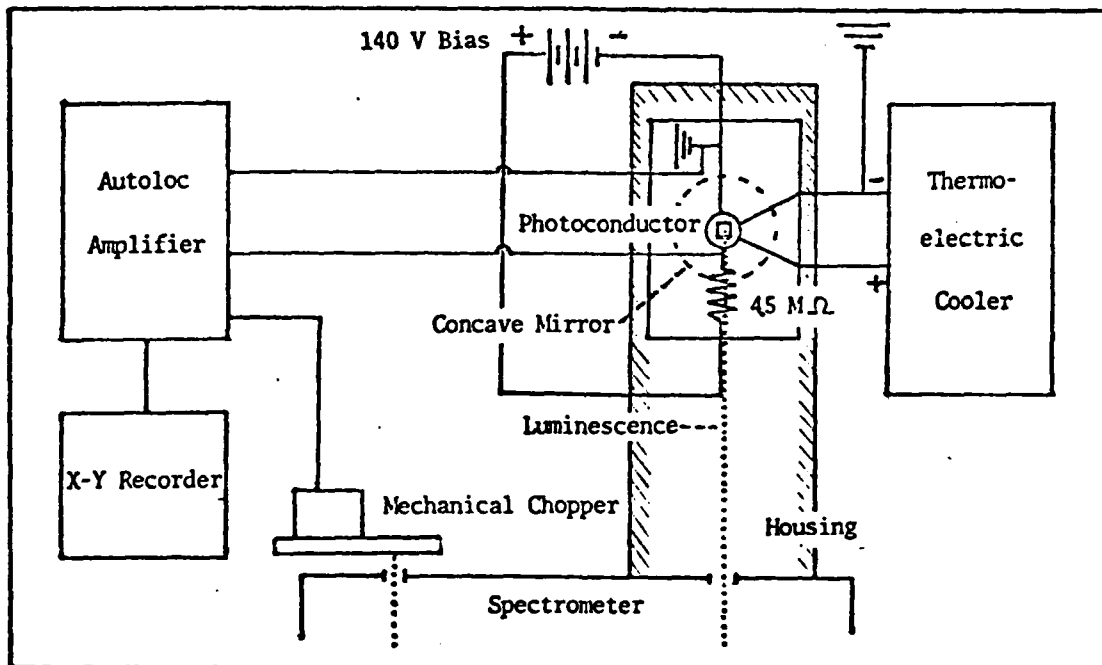


Figure 6. Photoconductor Location and Associated Electronics

mirror, located in the housing, of 1.3 cm focal length brought the luminescence on the sensor which was thermo-electrically cooled to -20° C by a Power/Mate Corporation power supply operated at 1.5 A and 1.0 V. For the 3 mm by 4 mm element size, a bias of 140 V was used.

As seen in Figure 7, the photoconductor's spectral response varied from 65% at 1.2 μm to 30% at 3.0 μm . The signal from the sensor is brought to the Keithley Autoloc amplifier which operated at the 225 Hz reference signal from the mechanical chopper.

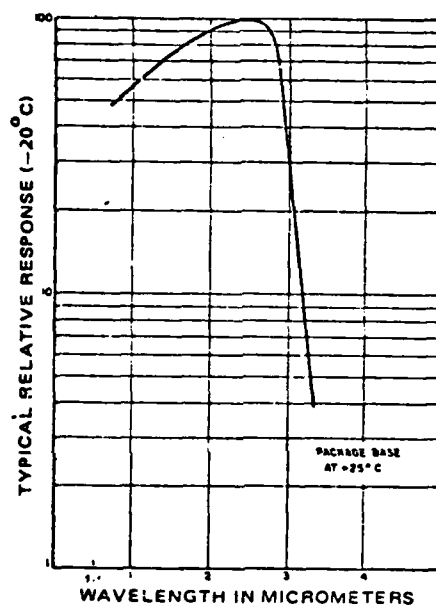


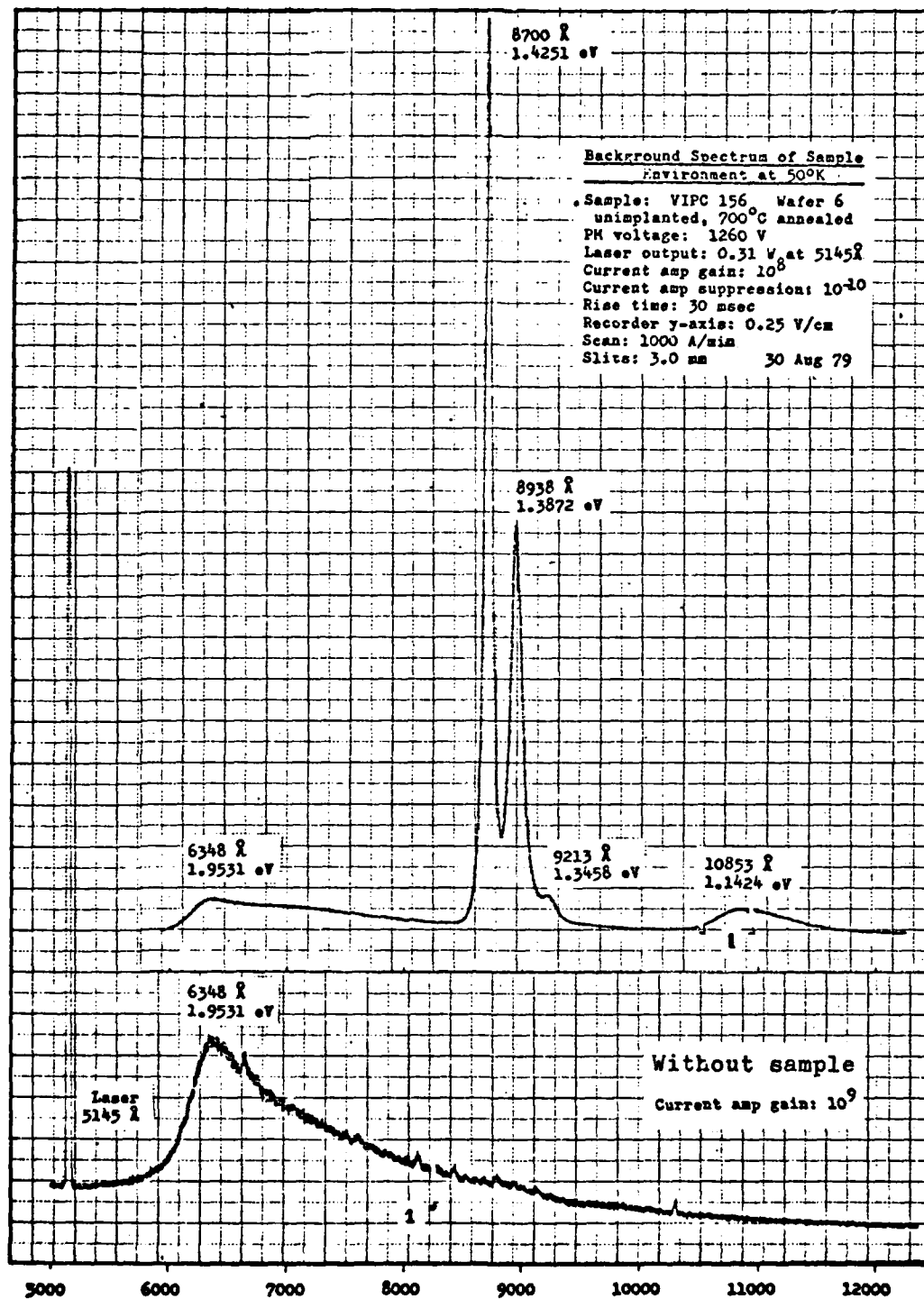
Figure 7. Spectral Response of PbS Photoconductor (Ref 28)

Procedure

Sample Mounting. The initial step in mounting the InP samples was to prepare an appropriate mask which held them onto the copper sample mount (Figure 4). To minimize sample handling and transferring from the sample chamber or exchange gas column, up to four specimens were positioned on the copper mount; hence, a mask with four 4.0 mm diameter apertures was utilized. Each aperture's dimension was larger

than the incident laser beam's diameter so that the beam irradiated only the sample, hence minimizing any luminescence from the copper. Photoluminescence from the copper mask and excessive reflections and scattering of the incident light within the sample chamber were further decreased by painting the mask with aquadag, a colloidal dispersion of graphite in alcohol. (The resulting background spectrum, after filtering, for a representative photoluminescent study is given by Figure 8 which shows the luminescence with an InP sample and the luminescence without a sample.) The samples were positioned on the copper mount of the transfer rod and held in place through the back pressure applied by the mask. The transfer rod was placed into the gas exchange column of the dewar which was subsequently evacuated to prevent excessive atmospheric exposure to the sample surfaces.

Alignment. Initial equipment setup was concerned with the placement of the spectrometer and laser, as the relatively fixed position of the detachable-tail dewar and evacuation system controlled the location of the remaining equipment. After positioning and leveling the spectrometer on a rigid, stable platform, the dewar, which was fastened to an adjustable table, was vertically adjusted such that the sample in the detachable-tail was at the same height as the spectrometer entrance slit. The laser was positioned on a wooden platform, which was fastened to jacks, and was leveled and brought to the height of the sample and entrance slit. Further fine adjustment was performed by bringing the laser beam (set at minimum power) onto the sample; the reflected light was then directed onto a mirror which reflected the beam back onto the laser exit port so that the levelness



¹ Laser turned off due to low water pressure or overheating.

Figure 8. Background Spectrum of Sample Environment at 50° K

of the beam could be determined. After removal of the mirror, the spectrometer was horizontally adjusted to bring the laser beam onto the center of the spectrometer's optics.

Laser and Optics. The 5145 \AA line of the argon-ion laser was used for sample excitation as it lies above the bandgap energy of InP; this setting also allowed the greatest range of power operation (0.01 W to 0.75 W). Although one particular wavelength was used, background spectra from the laser in the violet and near ultraviolet (3400 \AA to 4800 \AA) range and in the infrared range were also present. By using two low pass filters (600 nm and 700 nm), between the laser and the InP sample, the infrared was removed; while a high pass filter (650 nm), between the sample and spectrometer, removed the violet/ultraviolet and the 5145 \AA radiation (Figure 3). This arrangement gave a relatively "clean" photoluminescence spectra for indium phosphide (Figure 8).

The laser was always operated at maximum power, 1.43 W, but the incident power on the samples, varying from 757 mW to 10 mW, was controlled by the optics in the laser beam path and a set of neutral density filters, located between the laser and low pass filters. To prevent physical movement of the laser in the horizontal direction, two 3 cm by 3 cm mirrors were used to bring the laser beam through the quartz windows of the dewar and onto the sample. A 2.5 mm aperture stop was utilized between the quartz windows and the mirrors to block excessive reflections into and out of the sample chamber. Since the spectrometer was located at approximately a right angle to the laser, the mirrors and sample had to be oriented in such a direction as to prevent the reflected beam from entering the spectrometer.

A system of bi-convex lenses (76.2 mm and 200 mm focal length), located on a 1/3 meter optical bench, were used to gather the luminescence from the InP sample and focus it onto the spectrometer entrance slit.

Signal Detection and Recording. The photomultiplier was fastened to the spectrometer at the exit slit and then connected to the thirty liter liquid nitrogen dewar with an insulated transfer hose (Figure 3). A flow limit valve and control solenoid was installed on the low pressure outlet of the dry nitrogen tank to control the gas flow to the dewar. This action subsequently also controlled the flow of cold nitrogen gas from the dewar to the photomultiplier housing. The gas flow and housing heater maintained the photomultiplier environment at -50° C. A 1260 V bias was supplied to the photomultiplier. The signal from the detector was then brought to the current amplifier, the output of which was sent to the Autoloc amplifier. The mechanical chopper which produces the reference signal for the Autoloc was placed between the high pass filter and entrance slit. Finally, the Autoloc was connected to the x-y recorder.

Use of the lead sulfide detector was necessary in the $1.2\text{ }\mu\text{m}$ to $3.0\text{ }\mu\text{m}$ region. The dispersed light from the exit slit was collected by a concave mirror and focused onto the photoconductor (Figure 5). Since the detector output was voltage, it was directly connected into the Autoloc amplifier. The output signal was maximized by rotating the photoconductor into its optimum position. Grounding of the thermoelectric cooler was required for acceptable signal to noise ratio.

Evacuation and Cryogenics. To maintain a relatively long and stable cryogenic environment, the dewar needed to be evacuated. The mechanical pump evacuated the gas exchange tube and the two vacuum walls to a pressure of approximately 5 microns (determined by one of the two vacuum gauges). The liquid helium reservoir, capillary tube, and frit were purged with dry helium to eliminate water vapor and atmospheric gases. The outer reservoir was then filled with liquid nitrogen which allowed the system to be further evacuated to 1×10^{-5} torr. By isolating the vacuum walls from the mechanical pump and operating the ion pump, the pressure in the vacuum walls was brought into the 10^{-7} torr region.

After the detachable-tail system was sufficiently cooled, liquid helium was transferred from a dewar or tank via an evacuated transfer hose into the inner reservoir (Figure 4). While the mechanical pump was operating, the valve-operator was opened to allow the flow of liquid helium or helium gas over the sample. After a particular volume of helium had settled into the gas exchange column, a liquid helium environment, 4.2° K, was maintained by isolating the column from the pump and letting the gas vent through a pressure relief valve or by unclamping the sensor head. By pumping on the liquid helium, temperatures below 4.2° K were obtained. Temperatures above 4.2° K were achieved by opening the valve-operator by one fourth to one full turn and pumping on the gas exchange column at different rates, depending on the temperature desired. Particular temperature stability was further maintained through the cryogenic temperature indicator/controller which operated the two heaters in the copper sample mount.

Data Collection. Once all system components were operational and the spectrometer calibrated, data collection was initiated. The desired sample was placed on the copper sample mount and into the gas exchange column, the dewar was evacuated and cooled, a stable observation temperature was acquired, the photomultiplier was cooled to -50°C or the lead sulfide detector components were connected, and the laser and all signal processing elements were turned on. The image of the illuminated sample was focused on the entrance slit and the photoluminescent spectrum in InP was manually scanned for the maximum peak so that proper gain, sensitivity, and x-y recorder settings could be chosen. When utilizing the phase-lock technique, the mechanical chopper and Autoloc amplifier were entered into the system and the dominant peak signal was phase-locked to the 225 Hz reference signal and amplified. Peak intensity was finally maximized by fine adjustment of the mirrors, optical bench, and lenses.

Luminescence of the undoped InP sample, which resulted in a relatively strong signal, was analyzed with a $100\text{ }\mu\text{m}$ slit width and a 75 mW laser power setting. A temperature profile was performed for the $8500\text{ }\text{\AA}$ to $9700\text{ }\text{\AA}$ region with the following temperature settings in degrees Kelvin: 2.69, 4.2, 5, 10, 20, 30, 40, 50, 60, 77.3, 100, 125, 160, and 225. The sequence of events for a particular spectrum resulted in room lights off; start of the spectrometer $100\text{ }\text{\AA}/\text{min}$ scan and x-y recorder sweep; the recorder pen in down position; insertion and withdrawal of the calibration lamp at the desired wavelength locations ($8505.8\text{ }\text{\AA}$ and $9751.7\text{ }\text{\AA}$); and, finally, the recorder pen in up position, recorder sweep and spectrometer scan stopped. (Displacing

the krypton calibration lamp instead of turning it off prevented noise in the spectrum.)

Luminescence of undoped InP in the 9100 Å to 11700 Å region was performed at 757 mW; 250 Å/min scan; a 3.0 mm entrance and exit slit; and at temperatures of 4.2° K, 50° K, 77.3° K, and 100° K. Similar conditions existed for the spectra of semi-insulating InP. Observations of Mg-implanted samples were made at 4.2° K and 50° K, using a 310 mW laser power setting, 100 Å/min and 250 Å/min scans, and 400 µm slit widths. Each emission spectrum was taken under unique conditions; hence, equipment settings had to be adopted accordingly. Due to the many samples and various conditions (Table 2), each observed spectrum, as found in the appendices, is completely documented and therefore should allow reproducibility. (Representative spectra in the appendices are photocopied reductions of the originals at varying scales.)

Data Analysis

Although data analysis in this study essentially consisted of interpreting graphs which were generated directly from the luminescence data, a DuPont 310 Curve Resolver was used to resolve overlapping spectral peaks and computer software was used to create polynomial curves to fit spectral data. The Curve Resolver is a modified analog computer which takes a series of overlapping peaks and reduces them to individual components. The instrument utilizes a series of function generators which are capable of creating a single distribution function on a cathode ray tube. Any given number of these functions can be positioned, shaped, and summed until a trace is obtained that will match the experimental curve envelope. The CDC 6600 computer and its

TABLE 2

Sample Conditions

Sample	Spectral Range	Temperature ($^{\circ}\text{K}$)														
		2.22	2.69	4.2	5	10	20	37	43	50	63	77.3	100	125	160	225
6-41	.85 μ - .97 μ											○	○			
Undoped InP VIPC 201	.85 μ - .97 μ		○	○	○	○	○	○	○	○	○	○	○	○	○	○
	.9 μ - 1.17 μ	○								○		○	○			
	.85 μ - 3.00 μ														○	
Semi-insulated InP:Fe VIPC 124	.85 μ - 1.17 μ			○		○				○			○			
	.85 μ - 3.00 μ			○												
Unannealed Mg-implanted InP:Fe																
	Substrate									○						
	$3 \times 10^{14} \text{ cm}^{-2}$									○						
	$1 \times 10^{13} \text{ cm}^{-2}$									○						
700 $^{\circ}\text{C}$ Annealed Mg-implanted InP:Fe																
	V4 substrate			○												
	V6 substrate			○						○			○			
	V6 $1 \times 10^{15} \text{ cm}^{-2}$			○						○			○			
	V5-6 $3 \times 10^{14} \text{ cm}^{-2}$			○						○						
	V5 $1 \times 10^{14} \text{ cm}^{-2}$			○						○						
	V4-5 $3 \times 10^{13} \text{ cm}^{-2}$			○						○						
	V4 $1 \times 10^{13} \text{ cm}^{-2}$			○						○						
	V4 $5 \times 10^{12} \text{ cm}^{-2}$			○						○						
750 $^{\circ}\text{C}$ Annealed Mg-implanted InP:Fe																
	V4 substrate									○						
	V5 substrate									○						
	V6 substrate									○						
	V6 $1 \times 10^{15} \text{ cm}^{-2}$									○						
	V5-6 $3 \times 10^{14} \text{ cm}^{-2}$									○						
	V5 $1 \times 10^{14} \text{ cm}^{-2}$									○						
	V4-5 $3 \times 10^{13} \text{ cm}^{-2}$									○						
	V4 $1 \times 10^{13} \text{ cm}^{-2}$									○						
	V4 $5 \times 10^{12} \text{ cm}^{-2}$									○						
VPE SSU 29-1																
	Substrate			○												
Mg-implanted ($1 \times 10^{13} \text{ cm}^{-2}$)	.85 μ - .97 μ									○		○				
	.85 μ - .97 μ									○						
VPE SSU 20-1																
	Mg-implanted ($1 \times 10^{12} \text{ cm}^{-2}$)			○						○						

associated software and graphic peripherals were used to run the program listed in Appendix A. This program takes the energy of spectral peaks and their associated temperature and performs polynomial least squares fit analysis on the data points to arrive at polynomials of degree one to six. The data points and their polynomial curves are then plotted on an energy versus temperature graph and compared to the temperature dependence of the bandgap.

Sample Data and Preparation

Samples originated from Varian Associates and Mining Chemical Products, Ltd., and were made available to AFIT by the AFAL/DHR (Table 3). Sample 6-1A, which had been used in a previous study at AFIT (Ref 15), was produced through liquid phase epitaxy, the process by which a thin single-crystal film is grown from a dilute molten solution on a crystallographically oriented, single-crystal substrate (Ref 29). The main samples under investigation, VIPC 201 and VIPC 156, were produced by the Czochralski technique, the process of growing single crystals from a molten phase. A single, oriented crystal seed is dipped into appropriately doped and molten InP; then, while the heat input to the melt is reduced, the seed is slowly raised and rotated out of the molten material to produce the desired crystal (Ref 8:377). Three crystals (wafers) cut from the same boule were utilized in this study. In vapor phase epitaxy, the process which produced SSW 20-1 and SSW 29-1, the reactant ($n^+ \text{Sn} - \text{InP}$) is in a gaseous phase which precipitates out on a high-purity single crystal of InP (Ref 8:375). Aside for VIPC 201, electrical information for the samples was not available.

TABLE 3

Sample Data

Type	Sample Information	Origin	Identification Code
LPE InP	Liquid phase epitaxy: InP grown on an InP substrate	Varian Assoc.	6-1A
Undoped InP	Czochralski technique $n = 7.1 \times 10^{15}$ carriers/cm ² $\mu = 3900$ cm ² /V sec $\rho = 0.236$ Ω .cm	Mining Chemical Products Ltd.	VIPC 201
Semi-insulated InP:Fe	Czochralski technique	Mining Chemical Products Ltd.	VIPC 156
Semi-insulated InP:Fe (serving as substrate for Magnesium implant)	Czochralski technique	Mining Chemical Products Ltd.	VIPC 156 Wafer 4 (W4) Wafer 5 (W5) Wafer 6 (W6)
VPE InP (n/n ⁺ Sn)	Vapor phase epitaxy: (n ⁺ Sn)-InP grown on n-type substrate -3 1. $N_D - N_A = 9 \times 10^{14}$ cm ⁻³ 5.6 μ layer 2. $N_D - N_A = 2 \times 10^{14}$ cm ⁻³	Varian Assoc.	SSW 20-1 SSW 29-1

The undoped and semi-insulating substrate specimens were cut from wafers of 55 mm diameter and 0.5 mm thickness, and required no special preparation aside from cutting odd shaped samples to sizes that could be accommodated on the sample holder. Implanted samples required cutting, washing, implantation, encapsulation, and annealing. A diamond stylus of a dicer/cutter assembly was used to cut the wafer of the semi-insulating substrate into 5 mm by 5 mm squares which were subsequently washed with 10% aquasol solution, deionized water, trichloroethylene, acetone, and methanol.

The ion implantation which followed was performed by using an Accelerators, Inc. modified Implanter-I which consisted of a high voltage terminal where the ions are produced, an accelerating column, a magnetic mass analyzer, beam line optics for beam control, and an eight-position sample chamber. Implantations were made at room temperature at a pressure of less than 5×10^{-6} torr. Ions were produced by a hot cathode source (tungsten filament heating solid magnesium); extracted from the high voltage terminal; accelerated across a 120 kV potential; and brought into the mass analyzer where the ions of various species were separated into beams of mass and charge. The beam line optics were utilized to attenuate the ion current, clean the beam of neutral components, focus the ions with an electrostatic quadrupole, and scan the beam to eliminate implant non-uniformity and produce a large implantation area (Ref 30). Finally, the ion beam was brought onto the samples at seven degrees off from the $\langle 100 \rangle$ crystalline direction in order to inhibit channeling. To prevent current measurement problems, the system also included a method of reducing secondary

electron emission by utilizing a -500 V suppression. Implant dosage, which is a function of time and beam current, varied from 5×10^{12} ions/cm² to 1×10^{15} ions/cm².

After implantation with magnesium, the InP samples were again washed with the various solvents and placed into a plasma reactor for encapsulation. Silicon nitride (Si_3N_4), which was used as the encapsulant for InP, was produced by the reaction of silane (SiH_4) and nitrogen (N_2) at radio-frequency energy. The plasma reactor was evacuated and purged of impurities with a gas mixture of 2% silane and 98% argon. The second reactant, nitrogen, was added to the gas mixture and the RF source (13.5 MHz) was turned on to initiate the reaction. The capping process lasted for seven minutes at a temperature of 210° C to 230° C and a pressure of 0.5 torr, and resulted in a 1000 Å cap on the InP sample. The integrity of the cap was then checked with an ellipsometer for an index of refraction of 1.99 to 2.1. Finally, the samples were placed into the annealing furnace, face down on a strip of semi-insulating InP:Fe and annealed for fifteen minutes in flowing hydrogen gas at 700° C for one set and at 750° C for another set. Although not required for photoluminescence, the caps may be etched off with hydrofluoric acid.

IV. Results and Discussion

This section presents the spectral results for the various samples and various sample conditions as summarized in Table 2. The emission spectra of undoped indium phosphide is discussed with respect to temperature, emission intensity, and variation in excitation intensity. The spectra of semi-insulating indium phosphide is analyzed and compared to the spectra of undoped InP. The photoluminescence spectra of Mg-implanted semi-insulating (InP:Fe) is examined prior to and after annealing at temperatures of 700° C and 750° C, and the annealed samples are studied as a function of implant dosage and annealing temperature. Finally, vapor phase epitaxial InP is examined, both as undoped and Mg-implanted material; and the peak widths of the emission spectra of Czochralski, LPE, and VPE grown indium phosphide are compared.

Undoped InP

The photoluminescent data acquired in this study for undoped indium phosphide are in agreement with published data. The results extended the temperature data for the luminescence of InP beyond what is normally published; laboratory observations ranged beyond 2.22° K to 225° K. Table 4 catalogs all observed peak and shoulder positions from 2.22° K to 225° K, and Appendices B, C, and D contain the actual spectra from which these results were obtained. It is appropriate to indicate on Table 4 the days during which each spectrum was taken since experimental conditions are not completely stable; for example,

TABLE 4

Photoluminescence of Undoped InP at 2.22° K to 225° K

Date	Temp (°K)	Peak and Shoulder(s) Position in Wavelength(Å) and Energy (ev)									
10 Aug	2.22									9300.0	9613.7 1.2897
9 Aug	2.69	8744.9 = 1.4178	8751.9 = 1.4167	8760.4 = 1.4153	8773.1 = 1.4132	8784.3 = 1.3768	9031.7 = 1.3758	9297.9 = 1.3335	9622.7 = 1.2885	9982.2 = 1.2421	
	4.2	8744.5 = 1.4179	8753.3 = 1.4164	8762.2 = 1.4150	8773.8 = 1.4131		9009.5 = 1.3762	9298.3 = 1.3334	9618.1 = 1.2891		
1 Aug	5.0		8753.1 = 1.4165	8762.9 = 1.4149			9010.4 = 1.3760	9296.7 = 1.3337	9612.8 = 1.2898		
	10.0		8765.3 = 1.4145	8773.8 = 1.4131			9009.2 = 1.3762	9295.8 = 1.3338	9607.1 = 1.2906		
	20.0		8765.7 = 1.4144				8998.6 = 1.3778	9283.1 = 1.3356	9602.5 = 1.2912		
	30.0		8769.6 = 1.4138				8997.9 = 1.3779	9283.3 = 1.3355			
	40.0		8772.8 = 1.4133				8998.6 = 1.3778	9258.9 = 1.3352	9611.7 = 1.2899		
	50.0		8780.2 = 1.4121				9003.9 = 1.3770	9287.7 = 1.3349	9594.4 = 1.2923	9942.5 = 1.2470	10785.2 = 265° 1.1496 = 0.283
	60.0		8789.0 = 1.4107				9009.9 = 1.3761	9294.7 = 1.3359			
	77.3		8807.4 = 1.4077				9025.1 = 1.3738	9304.3 = 1.3326	9613.6 = 1.2897	9975.9 = 1.2429	10712.0 = 1.1574
	100.0		8835.3 = 1.4033				9042.8 = 1.3711	9324.4 = 1.3297	9634.9 = 1.2868		10776.0 = 1.1506
8 Aug	125.0		8866.1 = 1.3984				9098.7 = 1.3627				
	160.0		8924.9 = 1.3892				9161.6 = 1.3533				
22 Aug	162.0		8936.1 = 1.3875				9165.9 = 1.3527	9424.9 = 1.3155			11762.0 = 1.0541
14 Aug	225.0		9050.4 = 1.3699								13226.0 = 0.9374

** Data from a slower scan of the 9009 Å peak. Data from 10 Aug

equipment may become slightly displaced during cryogenic transfers and evacuating procedures.

Representative Spectra. A typical photoluminescence spectrum of undoped InP is depicted in Figure 9 (also see Appendix B). This spectrum, taken at 20° K, is dominated by two peaks centered at 1.4144 eV (8765.7 Å) and 1.3778 eV (8998.6 Å) with the latter the more dominant. There are also two low energy peaks; one is at 1.3356 eV, separated from the dominant peak by 42.2 meV, and the other peak is at 1.2912 eV, separated from the dominant peak by 86.6 meV and is at very low intensity. Full width at half maximum is 5.4 meV for the 1.4144 eV peak and 8.4 meV for the 1.3778 eV peak.

By increasing the photomultiplier's sensitivity and extending observations to higher wavelengths (low energy region), as seen in the spectrum of Figure 10 (also see Appendices C and D), peaks are observed which are separated by multiples (up to four) of 43 meV from the dominant peak of 1.3778 eV. Also seen in Figure 10 is a very broad low intensity peak around 1.15 eV. Peaks at even lower energy were observed with the photoconductor experimental setup at 162° K; these broad low intensity peaks were seen at 1.0541 eV and 0.9374 eV (Figure 11, Appendix D). The 0.69 eV peak in Figure 11 is the higher order emission of the 1.38 eV peak.

Observations below 20° K showed detail in the 1.41 eV peak. At 10° K and 5° K, a low energy shoulder emerged (Figures B-3 and B-4), while at 4.2° K and below further structure developed. Spectra at increased sensitivity and decreased excitation intensity (Figure 12) revealed the following at 4.2° K: a high energy shoulder at 1.4174 eV;

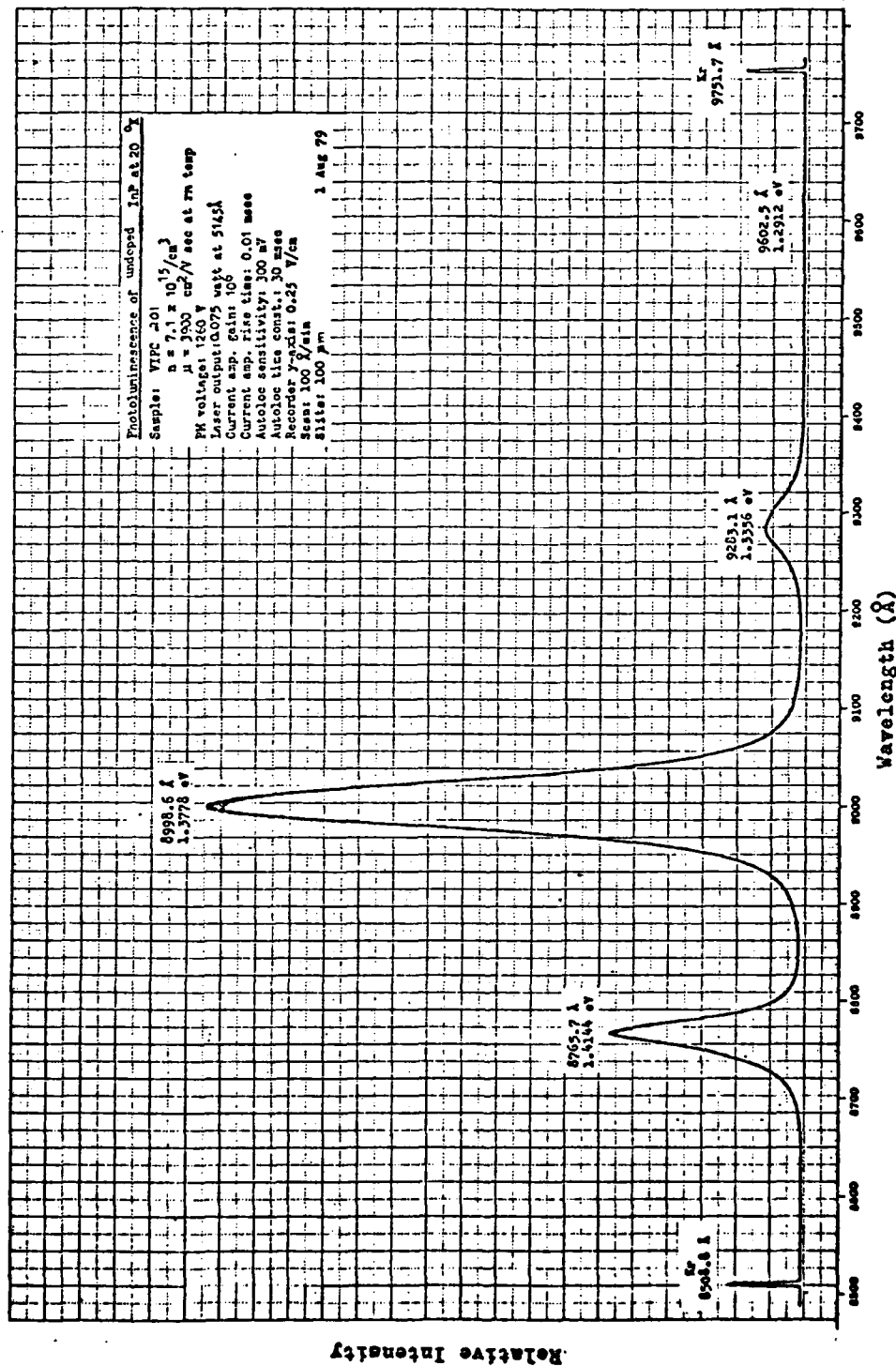


Figure 9. Photoluminescence Below 9700 Å of Undoped InP at 20° K

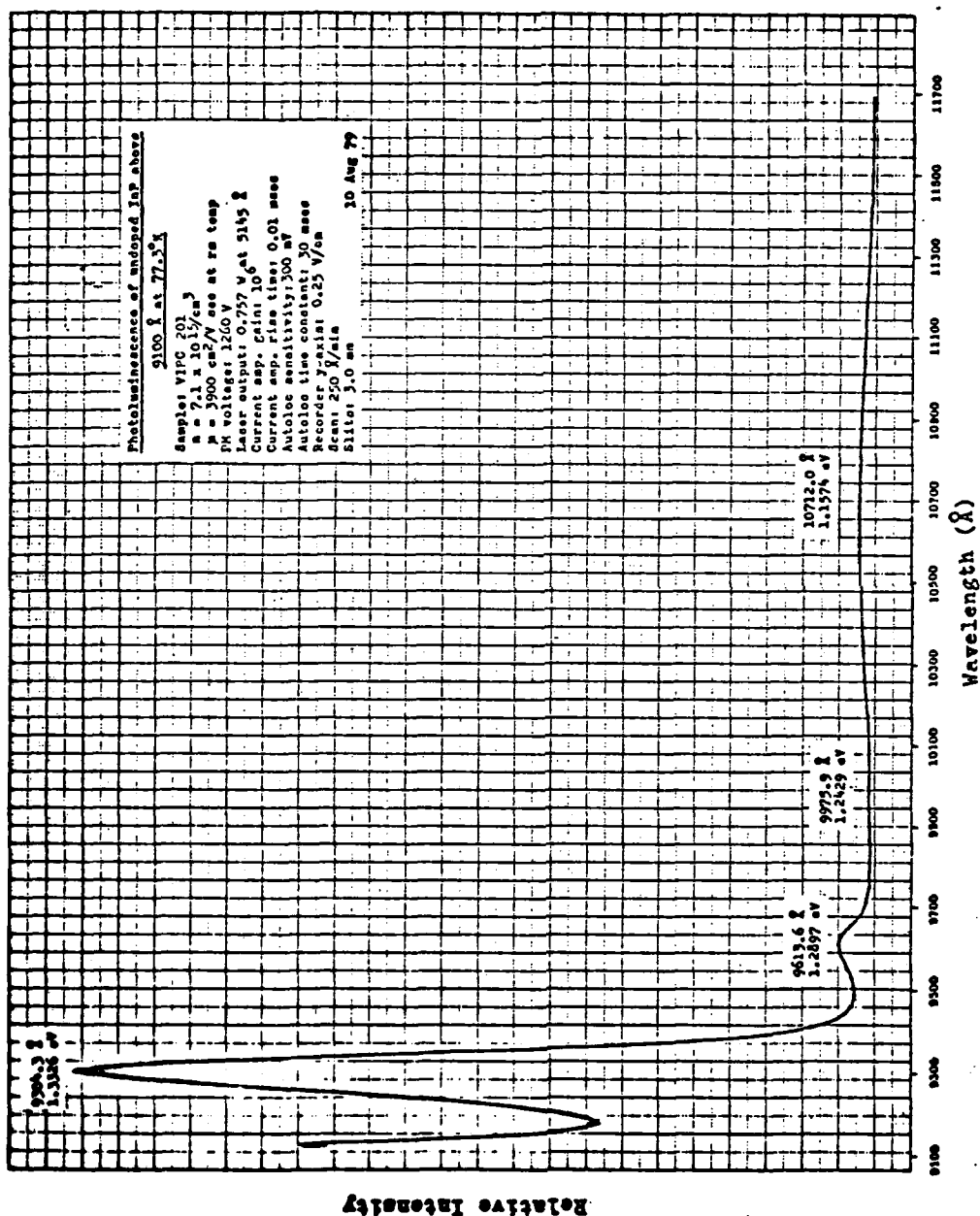


Figure 10. Photoluminescence Between 9100 Å and 11700 Å of Undoped InP at 77.3° K

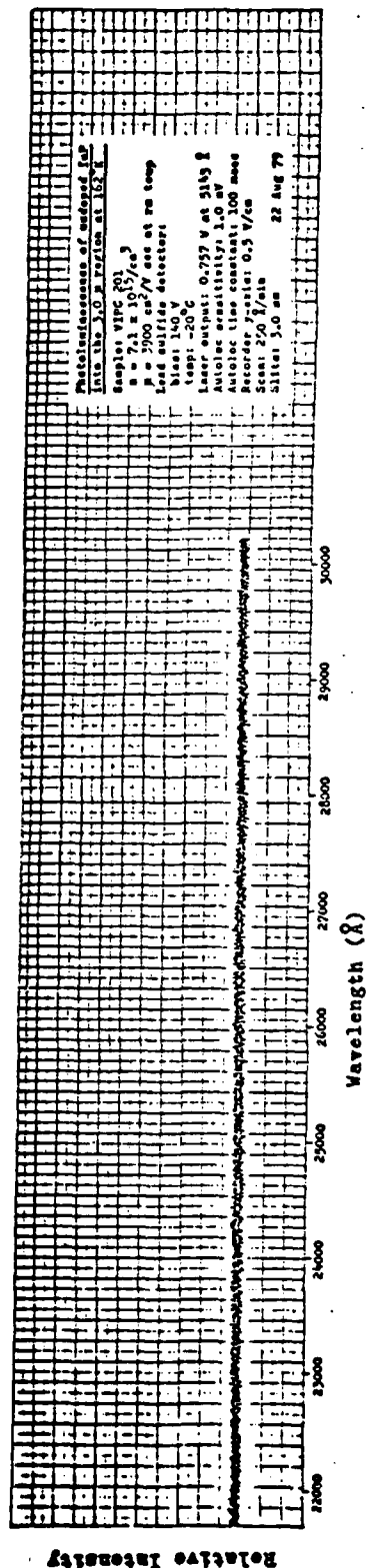
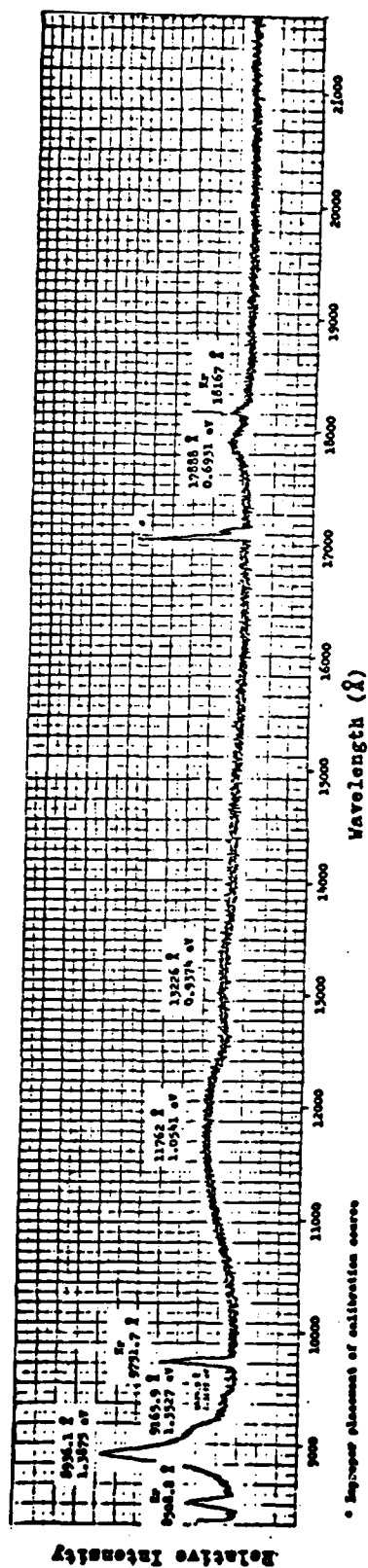


Figure 11. Photoluminescence Below 3.0 μ m of Undoped InP at 162° K

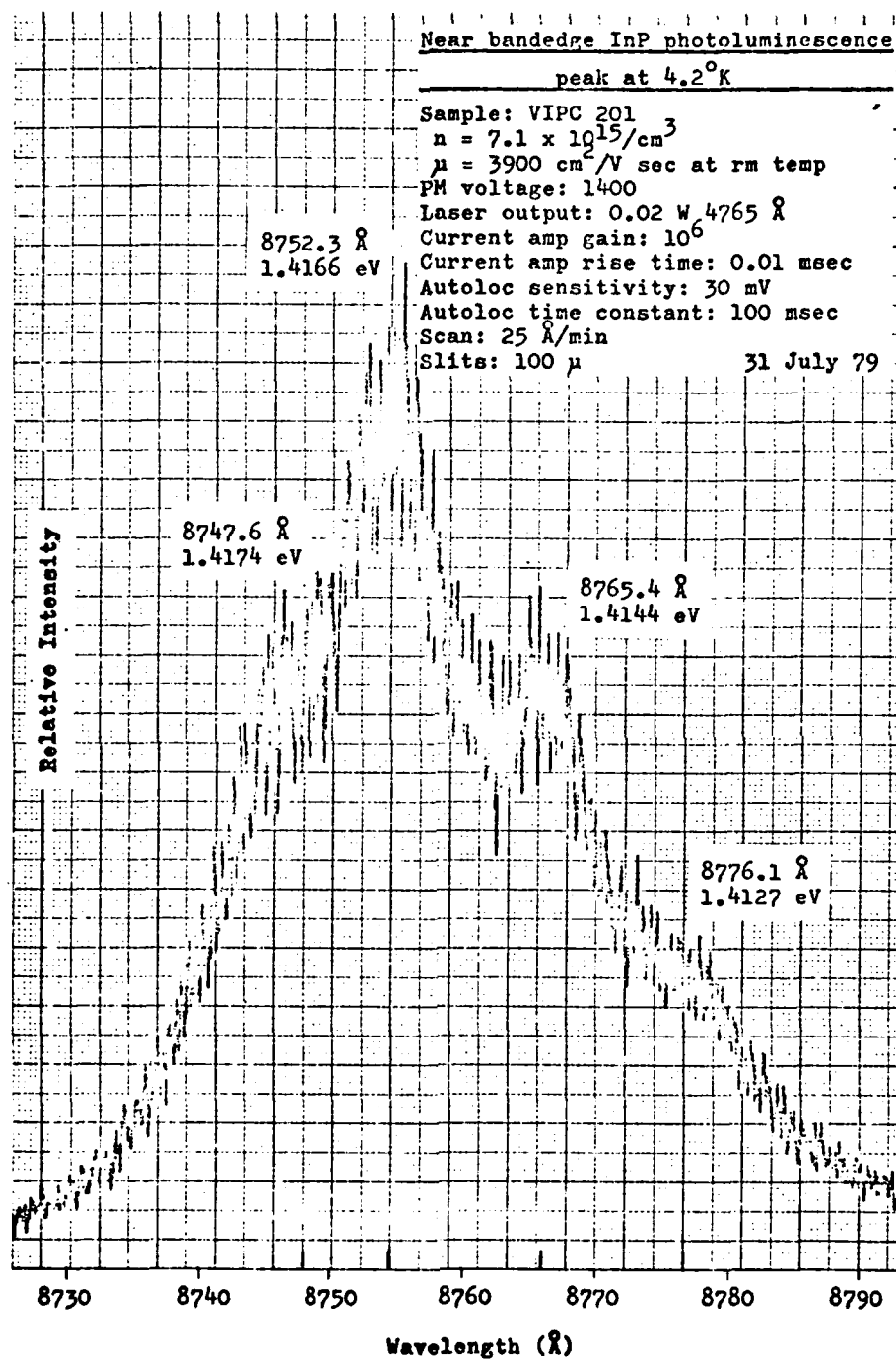


Figure 12. Detail in Near-Bandedge Peak
of Undoped InP at 4.2°K

a relatively high intensity narrow peak at 1.4166 eV; a peak at 1.4144 eV; and a low energy shoulder at 1.4127 eV. The only structure observed in the 1.37 eV peak was a high energy shoulder of 1.3768 eV at a sample temperature of 2.69° K (Figure 13).

Peak Identification. By referencing various publications, the processes behind the different emission structures may be identified. Using the results of Heim, et al. (Ref 21), the fine structure of the 1.41 eV peak in Figure 12 may be classified as follows: the relatively intense 1.4166 eV peak may be due to the free exciton, the 1.4144 eV peak is ascribed to a bound exciton, the 1.4127 eV shoulder is ascribed to the donor-to-valence band transition, and the 1.4174 eV high energy shoulder is of unknown origin. (A similar identification may be made for the 1.41 eV structure at 2.69° K in Figure B-1.) However, a more recent publication by White, et al. (Ref 22) assigns to the structure the following recombination mechanisms: the 1.4174 eV shoulder identifies with the free exciton, the 1.4166 eV peak is an exciton bound to a neutral donor, the 1.4144 eV peak is an exciton bound to a neutral acceptor, and the 1.4127 eV shoulder is believed to be due to the resonant coupling of the 1.4144 eV exciton complex to acoustic phonons. Above 4.2° K, the exciton related recombinations merge to create the 1.41 eV peak as seen in Figure 9. Peak intensity decreases with increasing temperature and peak width increases with temperature, as observed in Appendix B. (Heim, et al. [Ref 21] assigned band-to-band transitions to the 1.41 eV peak at high temperatures.)

The 1.37 eV peak is primarily due to donor-to-acceptor transitions and the low energy peaks, at multiples of 43 meV from the 1.37 eV peak,

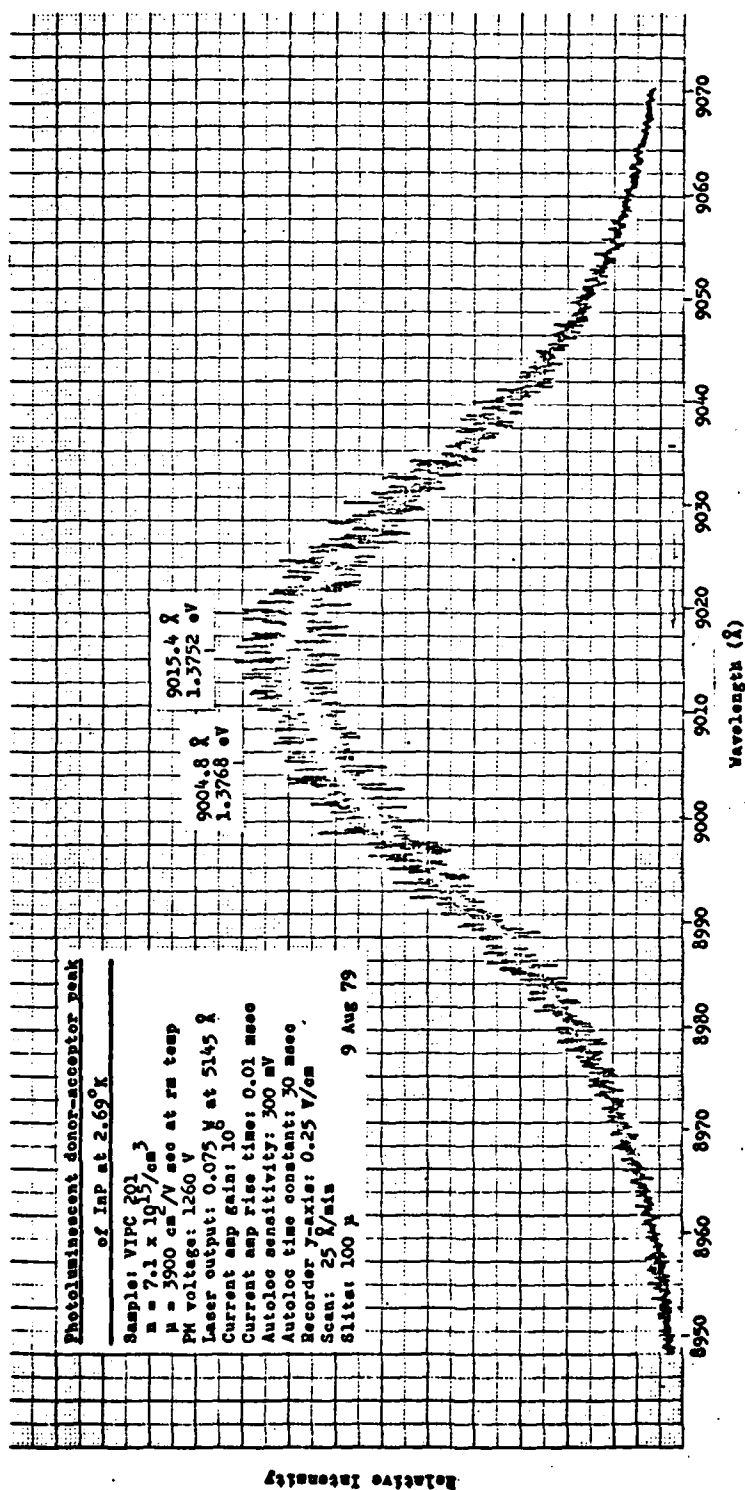


Figure 13. Detail in 1.37 eV Peak of Undoped InP at 2.69° K

are attributed to LO phonon emissions ($\hbar\omega_{ph} = 43 \text{ meV}$) (Ref 21). More specifically, in Figure 13, the 1.3752 eV peak is attributed to donor-acceptor transitions while the 1.3768 eV shoulder remains unidentified. Finally, the broad low intensity peak at 1.15 eV may be due to phosphorus vacancies, as identified by Williams (Ref 4). The low intensity broad peaks at 1.0541 eV and 0.9374 eV in Figure 11 correspond to similar peaks reported by Turner and Petit (Ref 24) and are ascribed to recombinations at unknown deep levels.

Temperature Dependence. The availability of data from 2.22° K to 225° K allowed the observation of the behavior of the emission spectra of undoped indium phosphide over a wide range of temperatures. The structure (Figures 12 and 13) seen in the 1.41 eV peak and 1.37 eV peak disappears above 10° K. When peak energy is plotted as a function of temperature as in Figure 14, then with increasing temperature the 1.41 eV peak shifts toward lower energy; a trend also exhibited, in general, by the 1.37 eV peak. This behavior is related to the temperature dependence of the bandgap which is given by the following empirical relationship (Ref 12:27):

$$E_f(T) = E_g(0) - \frac{\alpha T^2}{T + \beta} \quad (5)$$

where $E_g(0)$ is the value of the energy gap at 0° K, T is the absolute temperature, α and β are constants which, for InP, are equal to the numerical values of 4.906×10^{-4} and 327.0, respectively. The expression is graphically displayed in Figure 16. Using a polynomial least squares fit technique as shown in Appendix A, the following

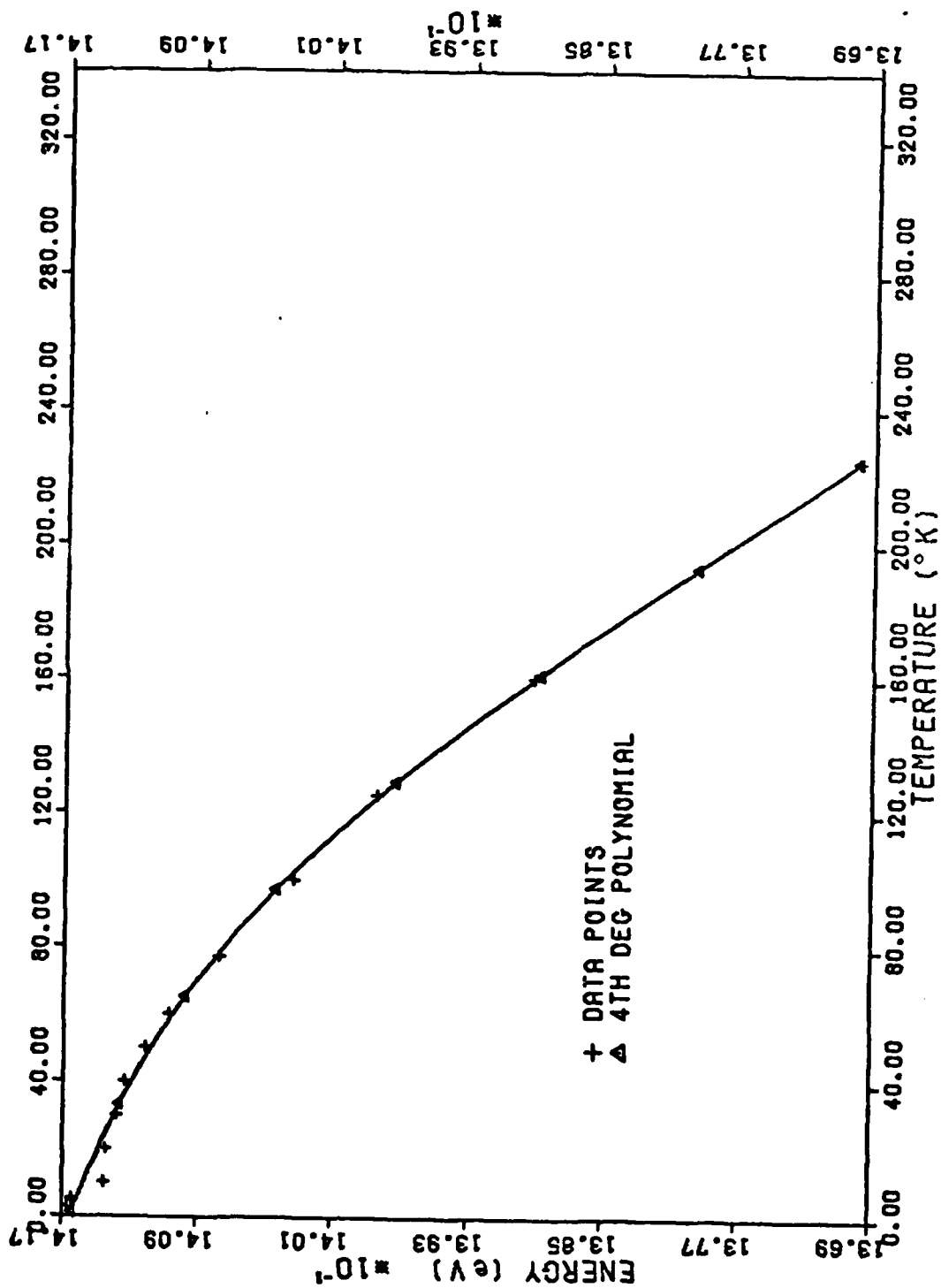


Figure 14. Temperature Dependence of Near-Bandedge Peak in Undoped InP

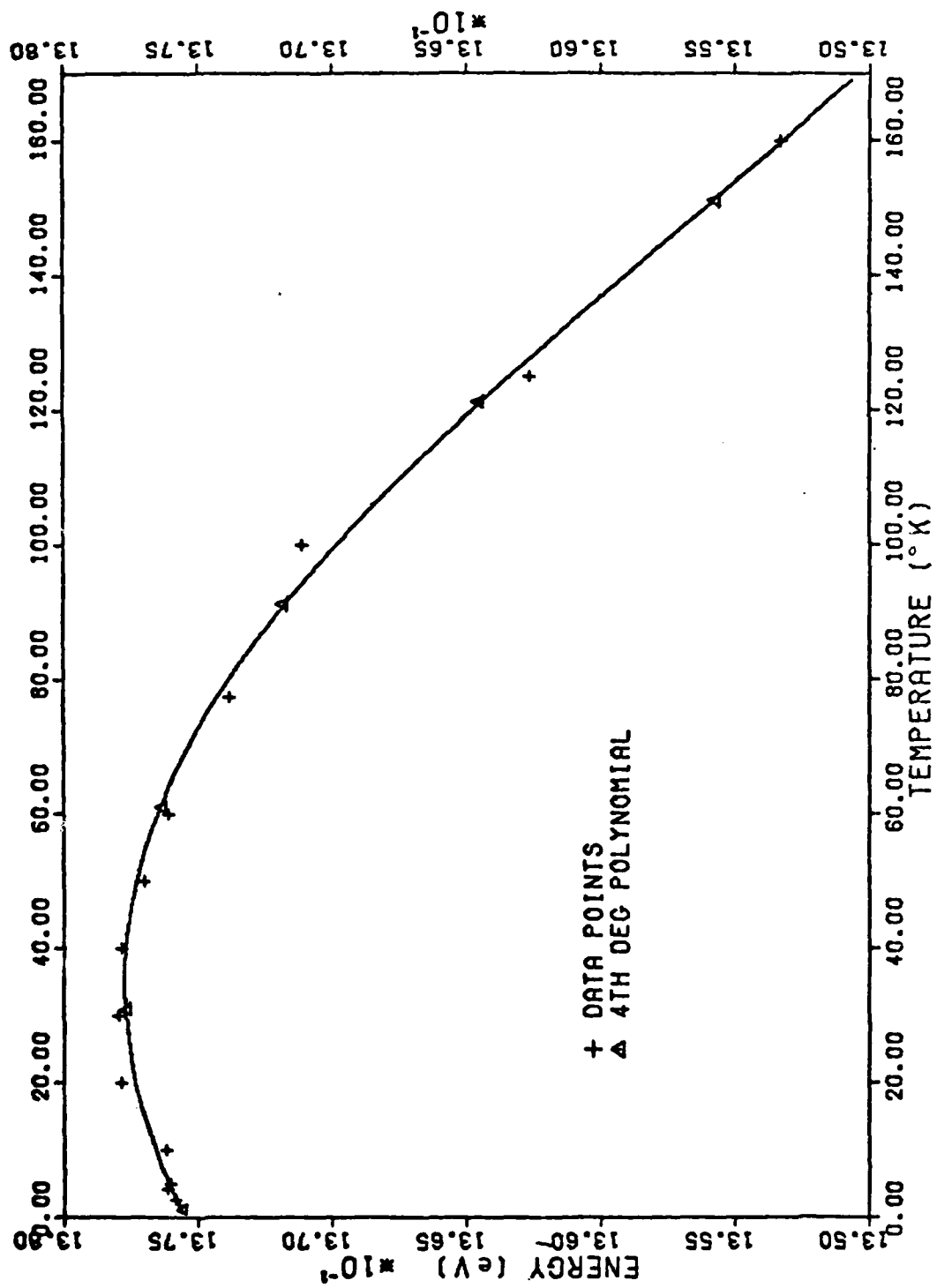


Figure 15. Temperature Dependence of Donor-Acceptor Peak in Undoped InP

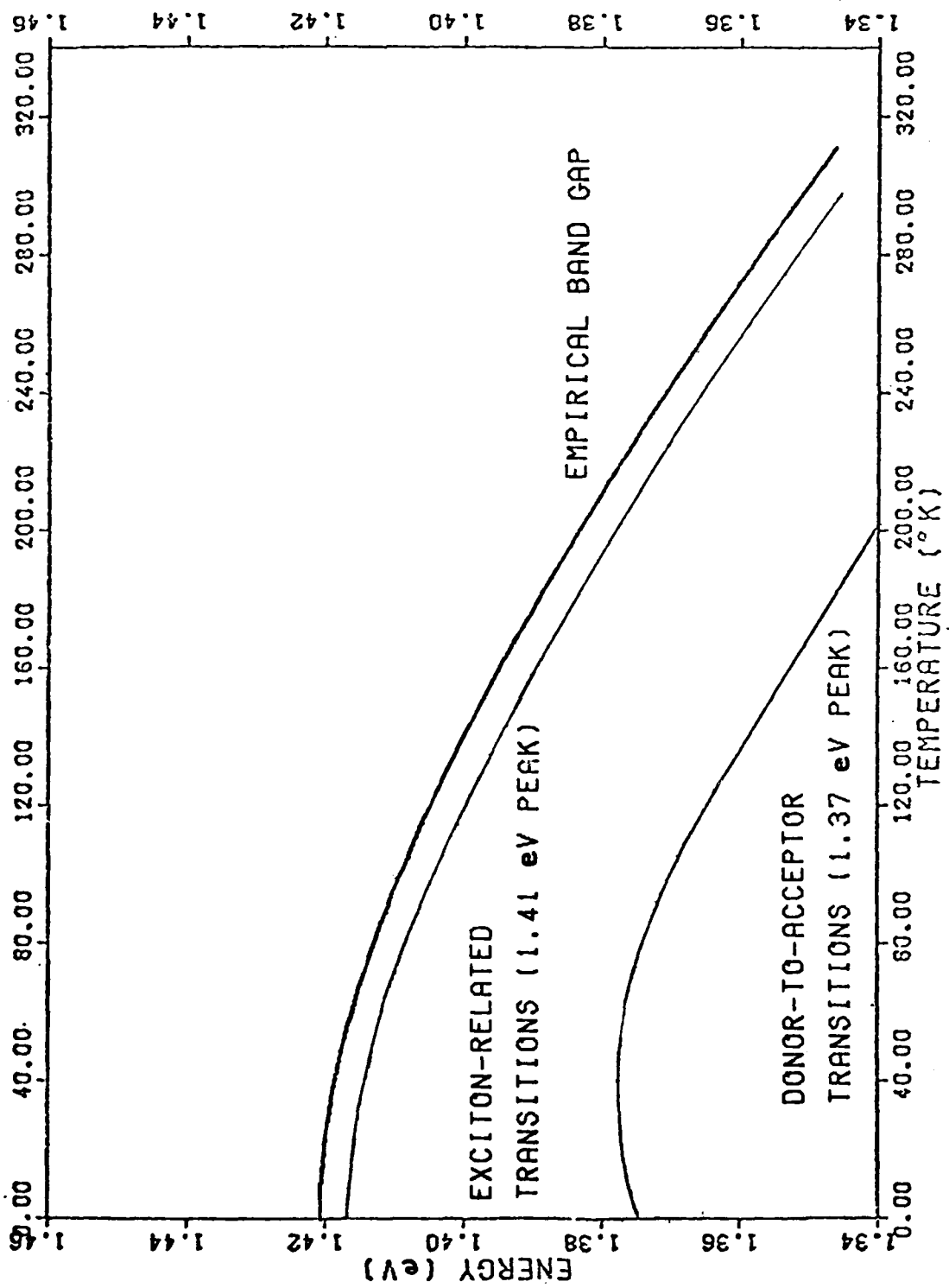


Figure 16. Temperature Dependence of Emission Spectra for Undoped InP

fourth degree polynomial was calculated to determine an expression for the temperature dependence of the 1.41 eV peak:

$$E(T) = 1.416477826 - 0.000076304T - 0.000000172T^2 - 0.0000000046T^3 + 0.0000000000124T^4 \quad (6)$$

where T is the absolute temperature; the expression is plotted in Figures 14 and 16. As seen in Figure 16, the plot of the 1.41 eV peak follows a parabolic lineshape and parallels the bandgap lineshape at a slightly lower energy. This relatively small energy difference between the 1.41 eV peak and the bandgap energy supports the argument that the peak's origin is due to exciton recombinations.

As depicted in Figure 15, the 1.37 eV peak increases with temperature between 2.69° K and 30° K, and then decreases with temperature, paralleling the bandgap at a relatively constant value below bandgap (Figure 6). The same polynomial least squares fit technique was used to calculate an expression for the temperature dependence of the 1.37 eV peak energy; the resulting fourth degree polynomial which appeared to give the best fit is as follows:

$$E(T) = 1.375546206 + 0.000122771T - 0.000001559T^2 - 0.0000000056T^3 + 0.0000000000318T^4 \quad (7)$$

where T is the absolute temperature.

Emission Intensity. Intensity studies for this experimental setup were somewhat difficult to make due to the problem of maintaining a constant data gathering environment. However, measurements from 5° K to 100° K appear to be stable, and the results are relatively consistent except, perhaps, at 30° K. These results, emission intensity versus temperature, are plotted in Figure 17 for the 1.41 eV (8760 Å), the 1.37 eV (9009 Å), and the 1.33 eV (9298 Å) peaks. The 1.33 eV peak is a phonon replica of the 1.37 eV peak; hence, the emission intensities parallel each other with the phonon replica at a lower intensity. All peaks slowly decrease in intensity up to about 50° K, after which the 1.37 eV and 1.33 eV peaks decrease more rapidly. The 1.37 eV peak is the dominant peak until around 77.3° K, after which the 1.41 eV peak is the more intense. From Figure 17 it appears that the 1.41 eV peak intensity changes less rapidly after 80° K.

In comparing the ratio of peak intensities between the 1.41 eV peak and the 1.37 eV peak (Figure 18), it can be seen that the 1.41 eV (8760 Å) peak becomes the dominant peak around 77.3° K. Aside from the ratio decrease between 10° K and 30° K (which may be an experimental anomaly or due to the fact that the 1.37 eV peak increases in energy when temperature is increased from 2.69° K to 30° K), the ratio between the two main peaks increases until at 160° K where the 1.41 eV peak is four times more intense than the 1.37 eV peak. (Data above 100° K are somewhat unreliable and above 160° K it is very difficult to resolve the 1.37 eV peak and its phonon replicas.) The ratio between 1.37 eV and 1.33 eV remain relatively constant over temperature.

By varying the intensity of the excitation source, another factor

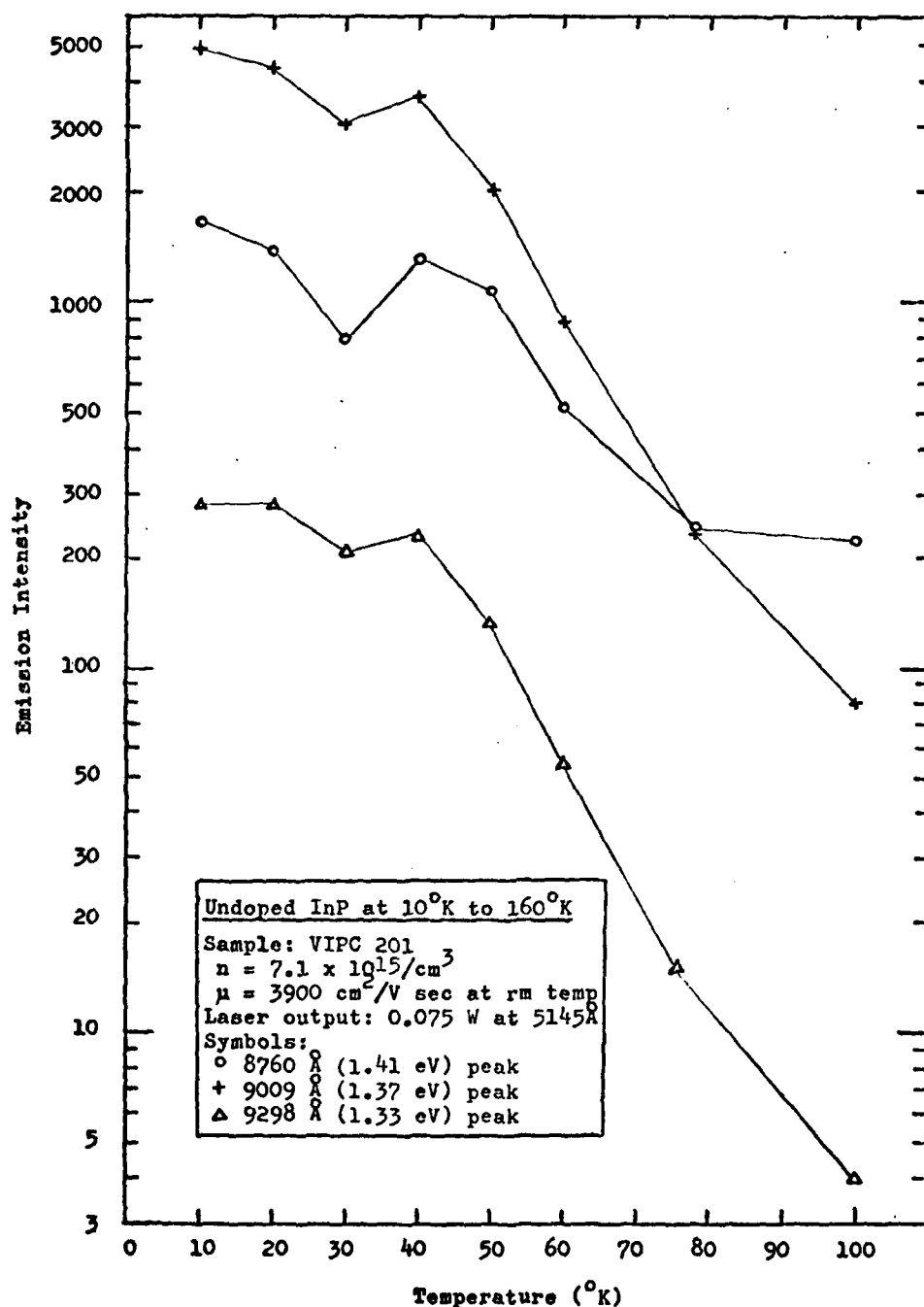


Figure 17. Temperature Dependence of Emission Intensity for Undoped InP

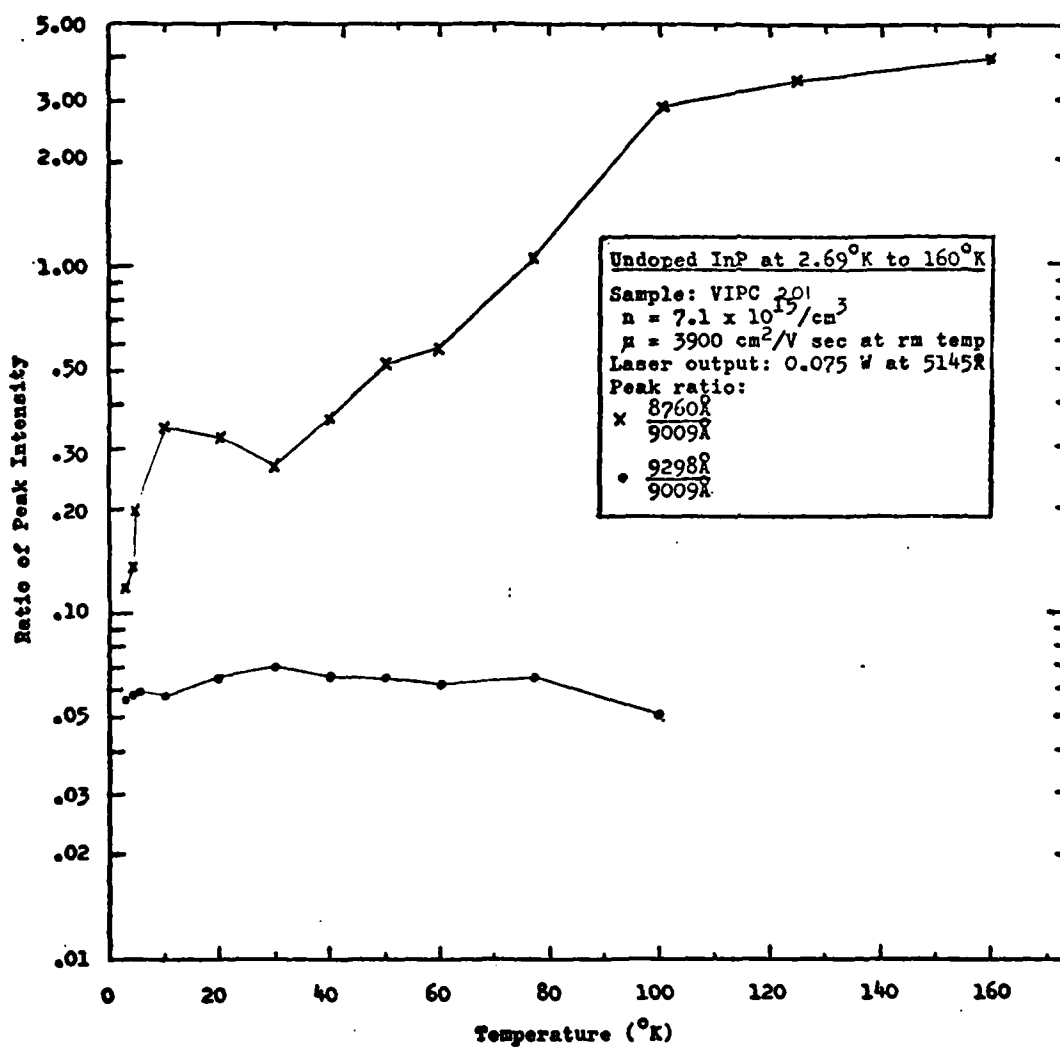
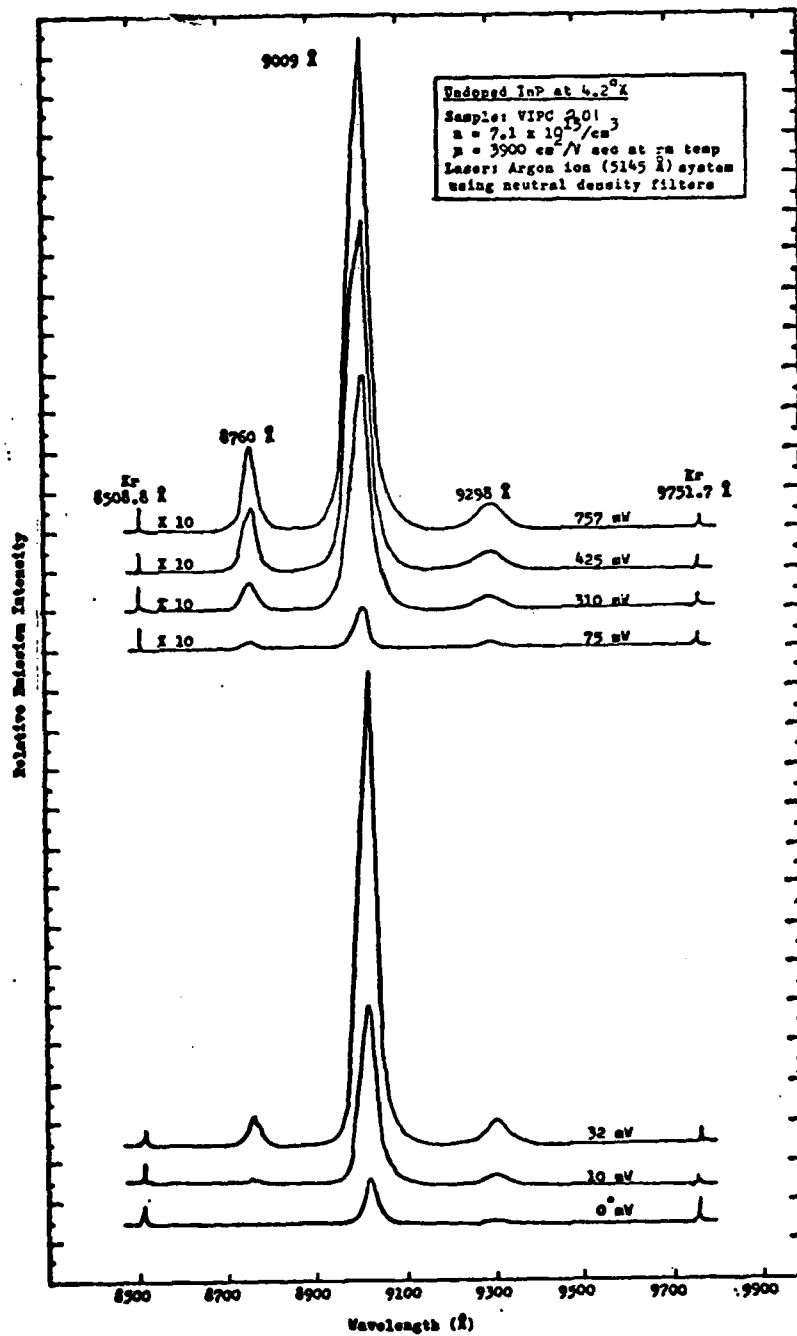


Figure 18. Temperature Dependence of Ratio of Relative Peak Intensity for Undoped InP

affecting luminescence may be studied. A constant sample environment of 4.2° K was maintained and the sample illumination was changed in varying increments from 757 mW to less than 10 mW (Figure 19). The dependence of emission intensity on excitation intensity is depicted in Figure 18 as a logarithmic relationship. Change in excitation power also had an effect on peak structure. At higher power, above 75 mW, a high energy shoulder appeared to be forming in the 1.37 eV peak; the origin of this shoulder is not known. In retrospect, the fine structure in the 1.41 eV peak (Figure 12) was dependent on the excitation intensity, since it did not emerge until the laser power had been lowered to 20 mW.

Semi-Insulating InP:Fe

Observed photoluminescence spectra for semi-insulating InP:Fe is similar to that of undoped InP aside from several distinct structures. Detection sensitivity, required to observe the InP:Fe spectra, had to be increased on the average by two orders of magnitude over the settings used for undoped InP. Table 5 lists the peak and shoulder positions from 4.2° K to 100° K; the plots of the corresponding spectra are shown in Appendix E and a representative spectrum is given in Figure 21. The radiative recombination processes are assigned as in undoped InP with the 1.41 eV peak being ascribed to exciton recombinations. It should be noted that the 1.41 eV peak and structure are at somewhat higher energy in this semi-insulating material than in undoped material. The 1.4294 eV high energy shoulder at 4.2° K (Figure E-1) appears to be more dominant than in undoped InP. The 1.37 eV peak is due to donor-acceptor transitions and the 1.33 eV peak is a phonon replica



* Data unattainable with available equipment for power measurement when using a neutral density filter of OD of 3.0

Figure 19. Photoluminescence of Undoped InP at 4.2° K at Various Excitation Intensities

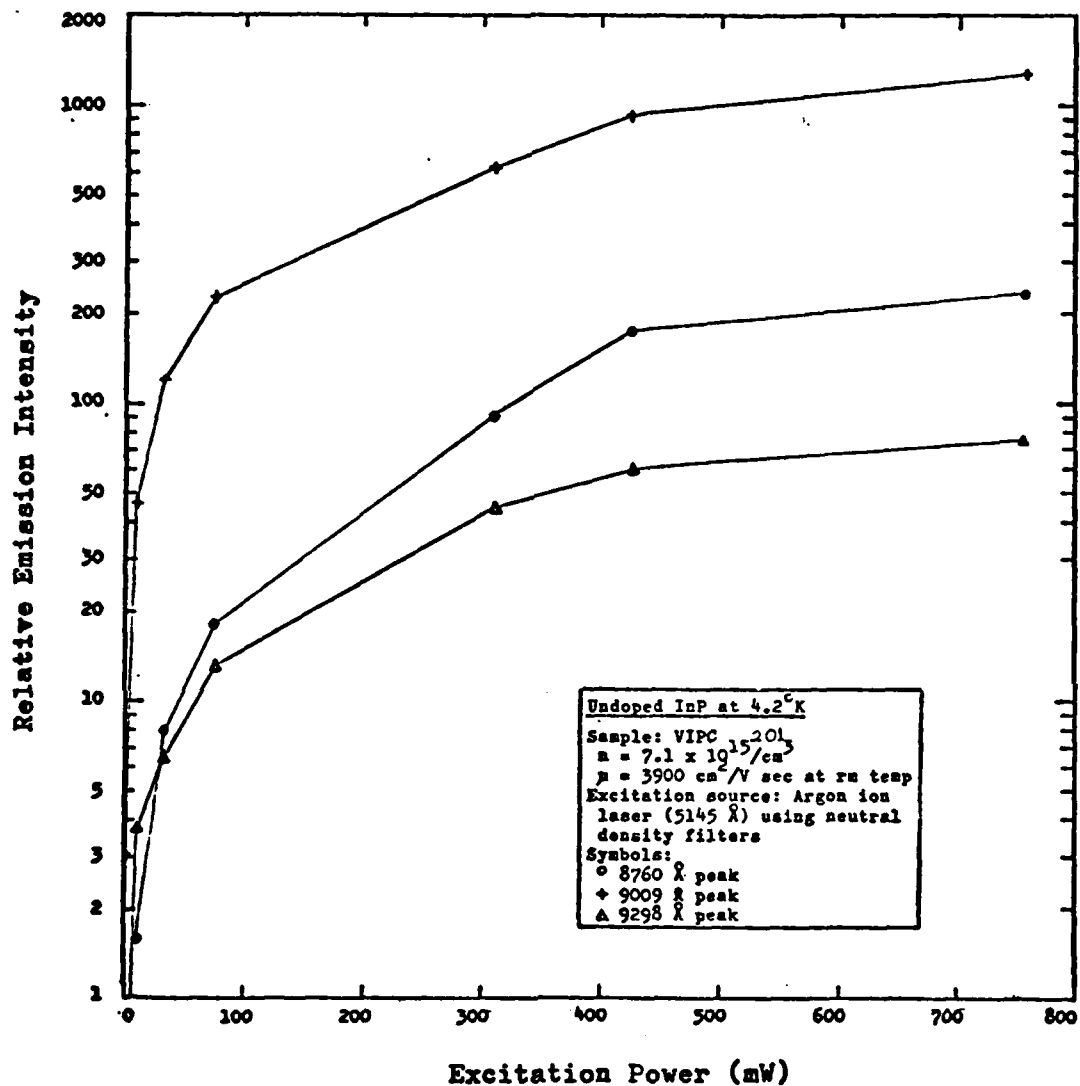


Figure 20. Emission Intensity Dependence on Excitation Intensity for Undoped InP at 4.2° K

TABLE 5

Photoluminescence of Semi-Insulating InP:Fe at 4.2° K to 100° K

Temp. (°K)	Peak and Shoulder(s) Position in Wavelength(Å) and Energy (eV)					
4.2	8673.9 s 1.4294	8732.1 1.4199	8943.0 s 1.3864	9013.6 1.3755	9311.0 1.3316	10873. 1.1403
10		8734.6 1.4195	8961.3 1.3836 s	9011.5 1.3759	9301.7 1.3329	10888.3 1.1387
50		8747.8 1.4173		8989.5 1.3792	9285.9 1.3352	10894.9 1.1380
100		8791.2 1.4103		8923.6 s 1.3894		10900.9 1.1374

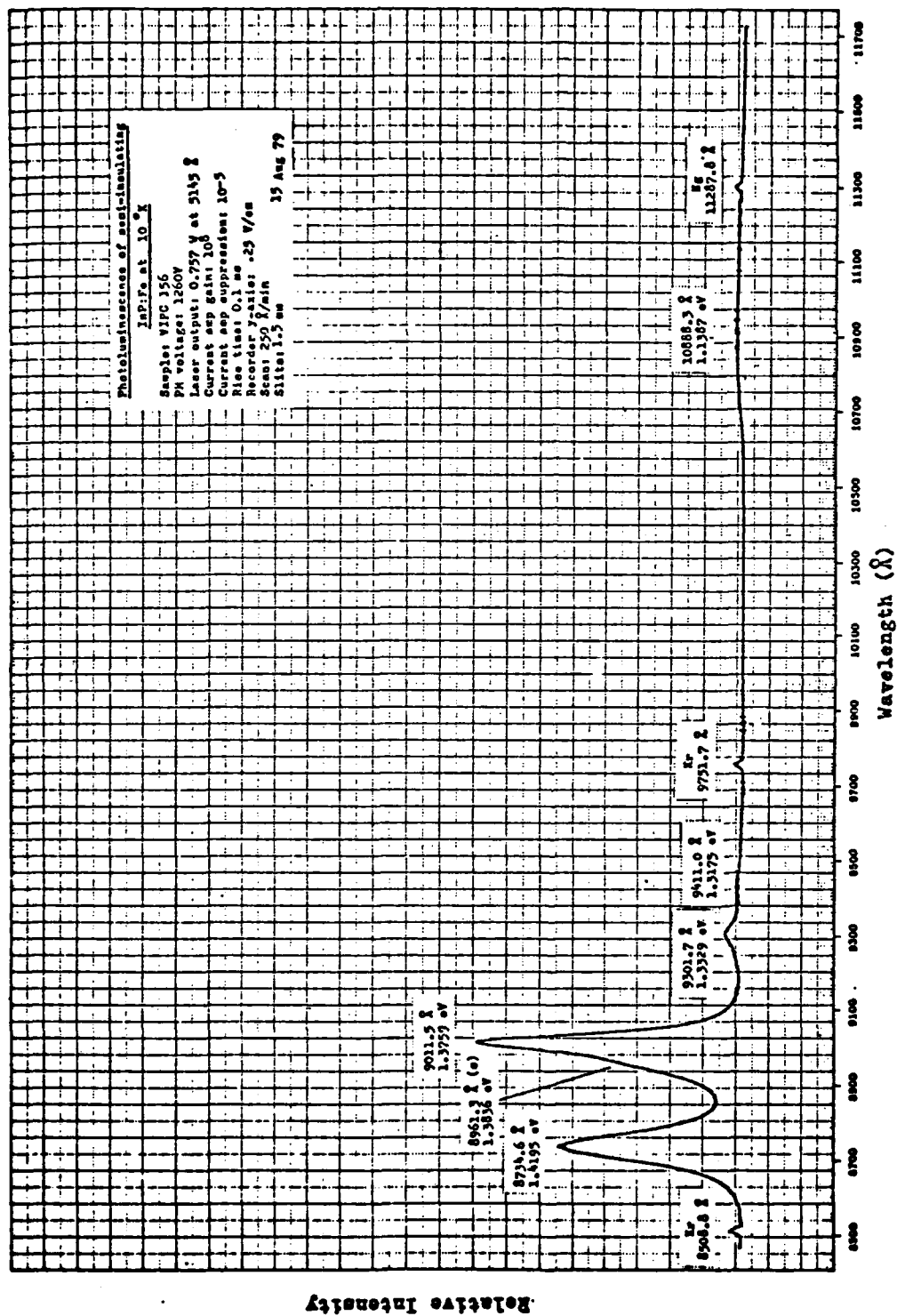


Figure 21. Photoluminescence Below 11700 Å
of Semi-Insulating InP:Fe at 10°K

of 1.37 eV emission; however, both of these peaks have an anomalous temperature behavior, peak energy increasing with increasing temperature. This effect could possibly be related to the rather dominating behavior of the 1.41 eV peak which rapidly increases in intensity such that at 50° K it is seven times more intense than the 1.37 eV peak.

The 1.3864 eV (Figure E-1) and 1.3836 eV (Figure 21) high energy shoulders of the 1.37 eV peak are present at low temperature; they are unobserved at 50° K and 100° K. Both the high energy shoulders and the 1.31 eV peak seen in Figure 21 are of unknown origin. The 1.31 eV peak is evident at all three higher temperature settings (10° K, 50° K, 100° K) and is separated from the first phonon peak by less than 25 meV. The broad low intensity peak in the 1.14 eV region, ascribed to phosphorus vacancies, is also present in semi-insulating indium phosphide. Its temperature behavior contradicts that of undoped InP; the 1.14 eV peak energy decreases with increasing temperature. However, as seen in undoped InP, as the temperature increases, the relative intensity of the 1.14 eV peak appears to decrease at a slower rate than the intensity of the remaining peaks.

The 1.05 eV peak, identified in undoped InP, also appears in InP:Fe when using a PbS detector, but the 1.14 eV peak is unobserved (Figure F-1). This low intensity and broad peak could possibly be ascribed to deep impurity levels due to one of the following major contaminants usually present in InP:Fe: O, Na, K, Fe, Si, and Al (Ref 2:23). Iron (Fe) being the source of this peak may be ruled out as its luminescence lies in the 3.5 μ m region (Ref 31). Donnelly and Hurwitz suggest that implantation damage is n-type (Ref 3); therefore, it may be possible to trace the impurity to either oxygen or silicon.

TABLE 6

Photoluminescence of Unannealed, Mg-Implanted InP:Fe at 50° K

Sample	Peak Position in Wavelength (Å) and Energy (eV)			
unimplanted substrate	8759.5 1.4154	8996.1 1.3782	9287.4 1.3350	10922.2 1.1352
Mg-implanted ($3 \times 10^{14} \text{ cm}^{-2}$)				12870 0.9643
Mg-implanted ($1 \times 10^{15} \text{ cm}^{-2}$)	8884. [*] 1.3956		9876. [*] 10596. [*] 1.2554 1.1701	12853. [*] 0.9643

^{*} Very low intensity and broad peaks

Unannealed, Mg-Implanted InP:Fe

Unannealed, implanted samples were investigated to determine spectral characteristics before crystal defects were removed (see Appendix G). As mentioned previously, the substrate material for the Mg implant was semi-insulating InP:Fe and its spectra was consistent with previous luminescence data of InP:Fe; however, the 1.1352 eV peak, ascribed to phosphorus vacancies, was relatively intense and contained a high energy shoulder. Peak positions for Mg-implanted, unannealed InP:Fe are listed in Table 6; but only one dominant peak at 0.9643 eV was observed for either implant dosage. This peak is characterized by a very wide low energy shoulder as seen in Figure 22. The exact origin for the peak or any of the low intensity peaks and structure is unidentified, but is probably due to interstitials or vacancies created by the implant.

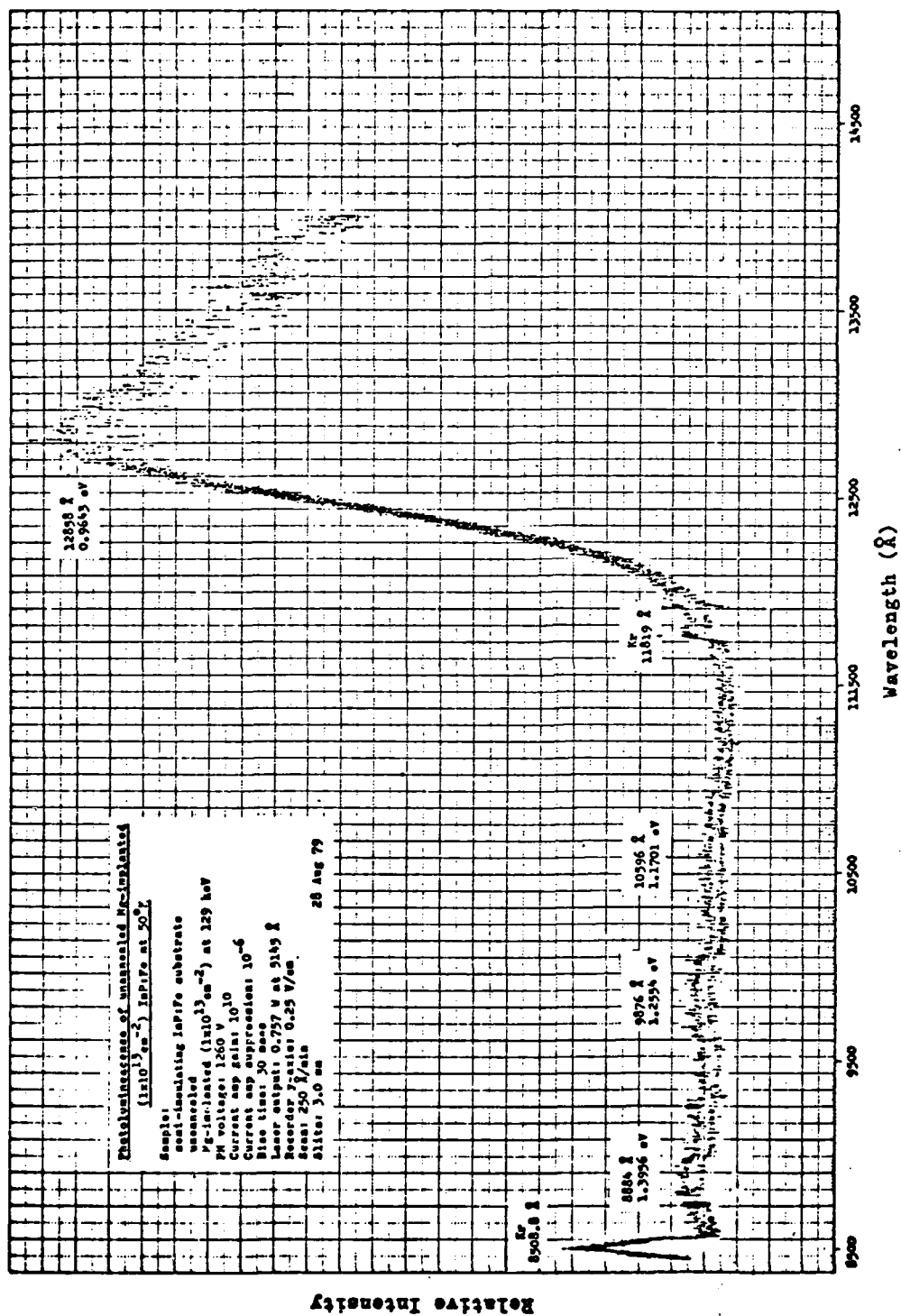


Figure 22. Photoluminescence Below 1.4 μm of Unannealed, Mg-Implanted ($1 \times 10^{13} \text{ cm}^{-2}$) InP:Fe at 50° K

Mg-Implanted InP:Fe

Just as ion-implantation of Mg in GaAs (Ref 32), Mg-implanted in InP provided a convenient method of doping. In this part of the experiment, the objective was to implant samples with various fluences of Mg, anneal a set of samples at 700° C and 750° C, and observe the luminescence as a function of fluence and anneal temperature. Observation temperatures were primarily at 50° K as both exciton-related recombinations and acceptor-to-donor recombinations are dominant at this temperature. Three different semi-insulating substrates were used in the implant process; however, these were wafers (identified as W4, W5, W6) originating from the same crystal (VIPC 156) and therefore should have relatively consistent characteristics. When the 700° C annealed samples were initially received, there was some question as to the integrity of the anneal due to problems with the encapsulant. After recording the spectra of both the 700° C and 750° C annealed samples and comparing them (see Appendices H, I, J), these doubts were confirmed. Compared to the 750° C anneal spectra, the 700° C anneal spectra was very noisy and had considerable structure. In light of this fact, the 750° C anneal data received more emphasis and shall be discussed first. However, one cannot rule out that the 700° C annealing temperature may not produce sufficient activation to obtain efficient luminescence.

750° C Annealed. Figure 23 depicts a representative spectra of Mg-implanted InP:Fe, annealed at 750° C for fifteen minutes. The spectra for all of the fluences are compiled in Appendix H and the individual peak positions are listed in Table 7. Spectra for the

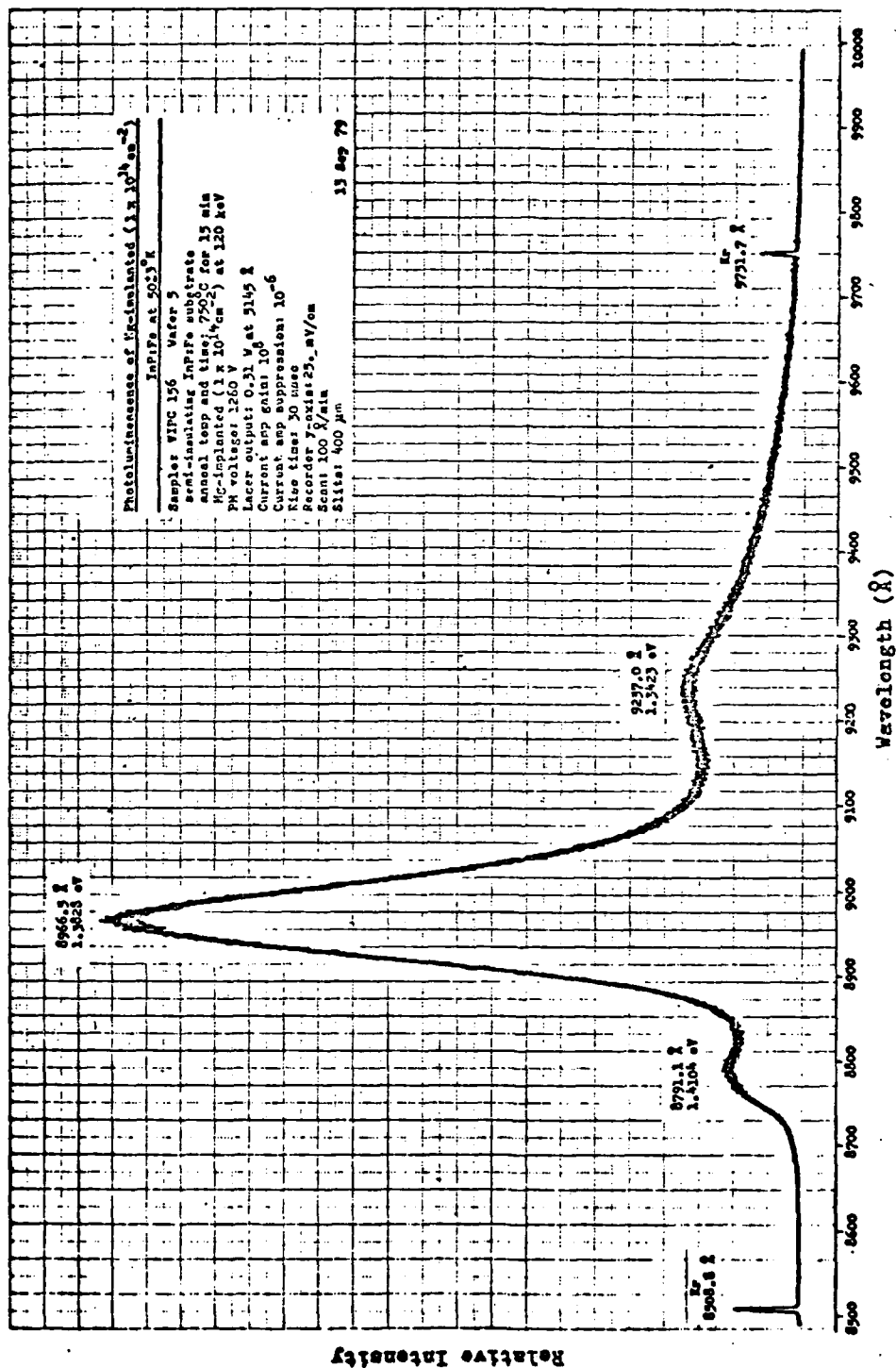


Figure 23. Photoluminescence of Mg-Implanted
 $(1 \times 10^{14} \text{ cm}^{-2})$, 750° C Annealed
InP:Fe at 50° K

TABLE 7

Photoluminescence of Mg-Implanted,
750° C Annealed InP:Fe at 50°K

Dose	Peak Position in Wavelength (Å) and Energy (eV)		
substrate Wafer 4	8758.8 1.4156	8992.2 1.3788	9275.7 1.3367
substrate Wafer 5	8758.0 1.4157	8991.0 1.3790	9276.5 1.3366
substrate Wafer 6	8760.0 1.4154	8990.4 1.3791	9270.2 1.3375
$1 \times 10^{15} \text{ cm}^{-2}$	8801.5 1.4087	8968.1 1.3825	9227.6 1.3436
$3 \times 10^{14} \text{ cm}^{-2}$	8788.6 1.4108	8969.8 1.3823	9247.2 1.3408
$1 \times 10^{14} \text{ cm}^{-2}$	8791.1 1.4104	8966.5 1.3828	9237.0 1.3423
$3 \times 10^{13} \text{ cm}^{-2}$	8774.3 1.4131	8966.1 1.3828	9234.5 1.3426
$1 \times 10^{13} \text{ cm}^{-2}$	8770.3 1.4137	8966.1 1.3828	9226.7 1.3438
$5 \times 10^{12} \text{ cm}^{-2}$	8766.6 1.4143	8964.5 1.3831	9235.7 1.3425

substrate material (Figures H-1, H-2, H-3) has already been extensively discussed; however, the differences in the relative intensity of the exciton related transitions and donor-acceptor recombinations of the three substrates should be noted.

As seen in Figure 23, the implant spectra exhibits essentially three peaks, with the dominant peak located around 1.38 eV. This is also observed when comparing the spectra of the various fluences and the substrate itself, as shown in Figure 24. Emission behavior is also characterized in Figure 25 where peak energy is plotted as a function of dosage. Hence, in analyzing the implant spectra, four conclusions may be reached: First, the 1.38 eV (8900 Å) peak is the most dominant peak at all doses; second, the 1.41 eV (8700 Å) peak increases slightly in energy with decreasing dosage; third, the 1.38 eV peak energy remains relatively constant at all fluences; and fourth, the 1.34 eV (9200 Å) peak remains relatively constant at all doses with an average energy separation from the 1.38 eV peak of 40.1 meV.

As before, intensity studies are somewhat unreliable due to an unstable sample environment; however, Figure 26 should give a general indication of how emission intensity is affected by dosage. The resulting variations in peak height with dosage is not necessarily anomalous; these variations are possibly a function of the crystal defects and the material's changing solubility caused by ion implantation (Ref 33).

When comparing the substrate spectra, specifically the 1.4156 eV and 1.3788 eV peaks, to the implant spectra, the key observation is the increase in the emission intensity of the implanted samples in the 1.38 eV region (Figure 24). This indicates that a dominant peak

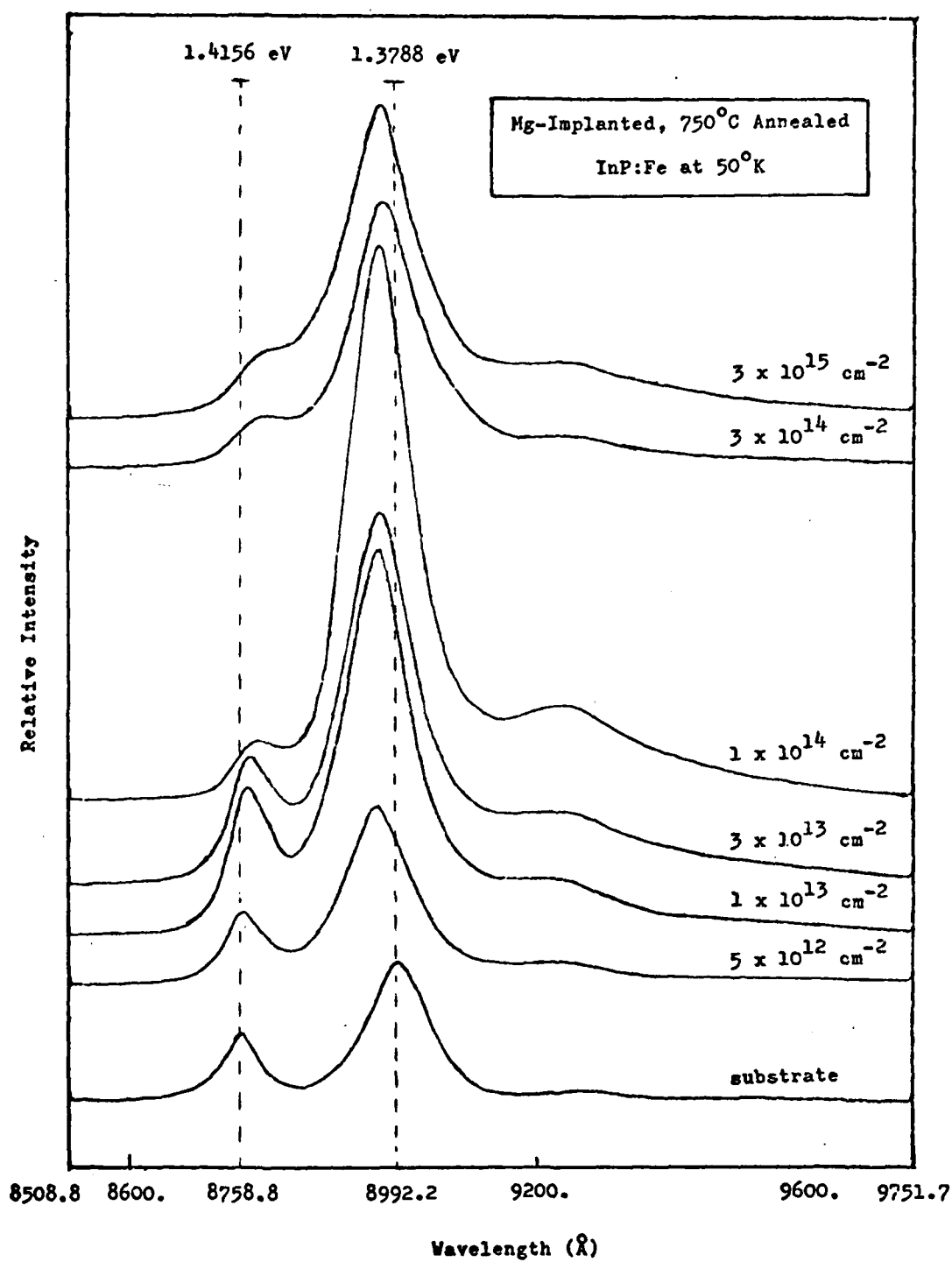


Figure 24. Mg-Implanted, 750° C Annealed InP:Fe at 50° K

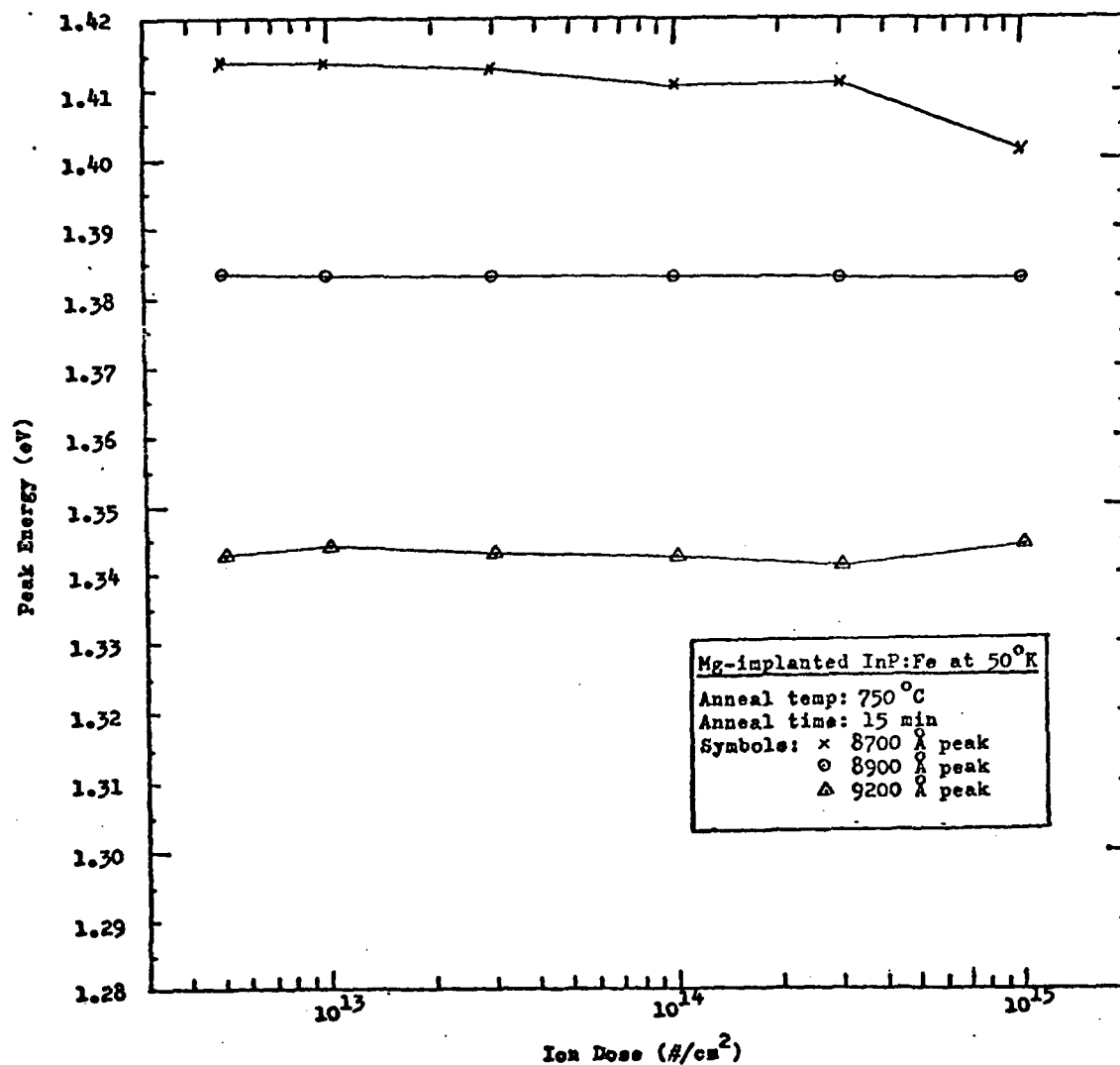


Figure 25. Ion Dose Dependence of Peak Energy for Mg-Implanted, 750° C Annealed InP:Fe at 50° K

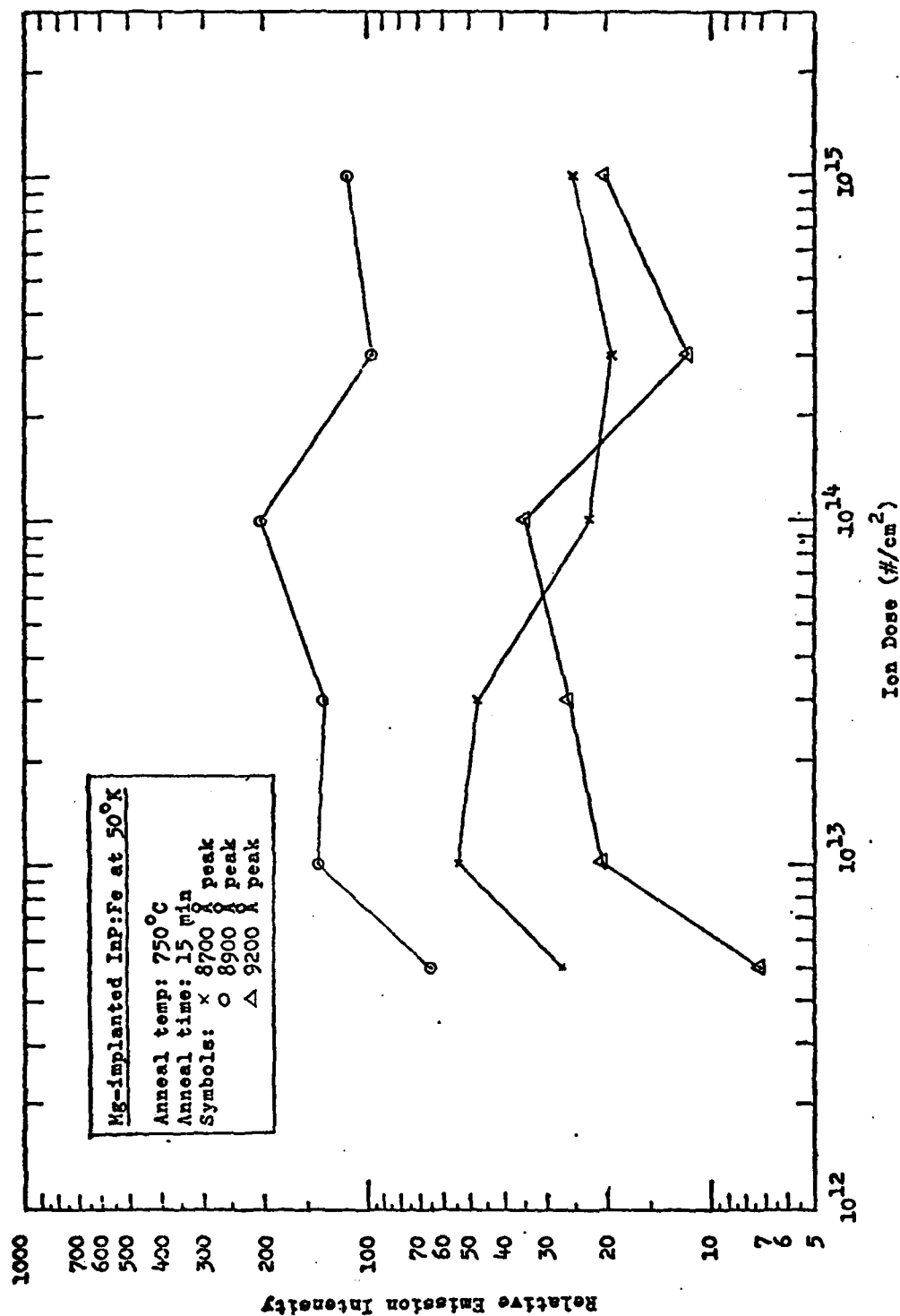


Figure 26. Ion Dose Dependence of Emission Intensity for Mg-Implanted, 750° C Annealed InP:Fe at 50° K

may lie in the implant spectra which is due to recombinations involving the magnesium acceptor. To determine the location of a magnesium peak, a DuPont 310 Curve Resolver was utilized to generate a function that, when summed to the substrate spectra, would result in the spectrum of the sample implanted with a $3 \times 10^{13} \text{ cm}^{-2}$ dose. The function that was generated is depicted in Figure 27 and roughly defines an emission peak at 1.3841 eV (8957.9 Å) with a full width at half-maximum of 29.9 meV. A similar result for this peak location may be derived when using the 28 meV binding energy for Mg in GaAs as estimated by Yu and Park (Ref 32:2434). Pankove's empirical relation (Equation 5) was used to determine a 1.4167 eV band gap for InP at 50° K. Then, by subtracting the 28 meV binding energy from this value, a difference of 1.3887 eV (8928.1 Å) was calculated. This is the energy of the photon given off by the recombination process; a value very close to that determined by the curve analyzer.

It is concluded that the peak due to recombinations involving implanted Mg acceptors is at a higher energy and greater intensity than the donor-acceptor recombination in substrate material, and is most probably located between 1.384 eV and 1.388 eV at 50° K. The radiative transition probably involves the recombination of free electrons with holes bound to Mg acceptors; a conclusion paralleling the results obtained for recombinations involving implanted Mg in GaAs (Ref 32).

700° C Annealed and 4.2° K Sample Temperature. Although photoluminescence observations for 700° C annealed samples were first performed at 50° K, the results of observations at 4.2° K shall be

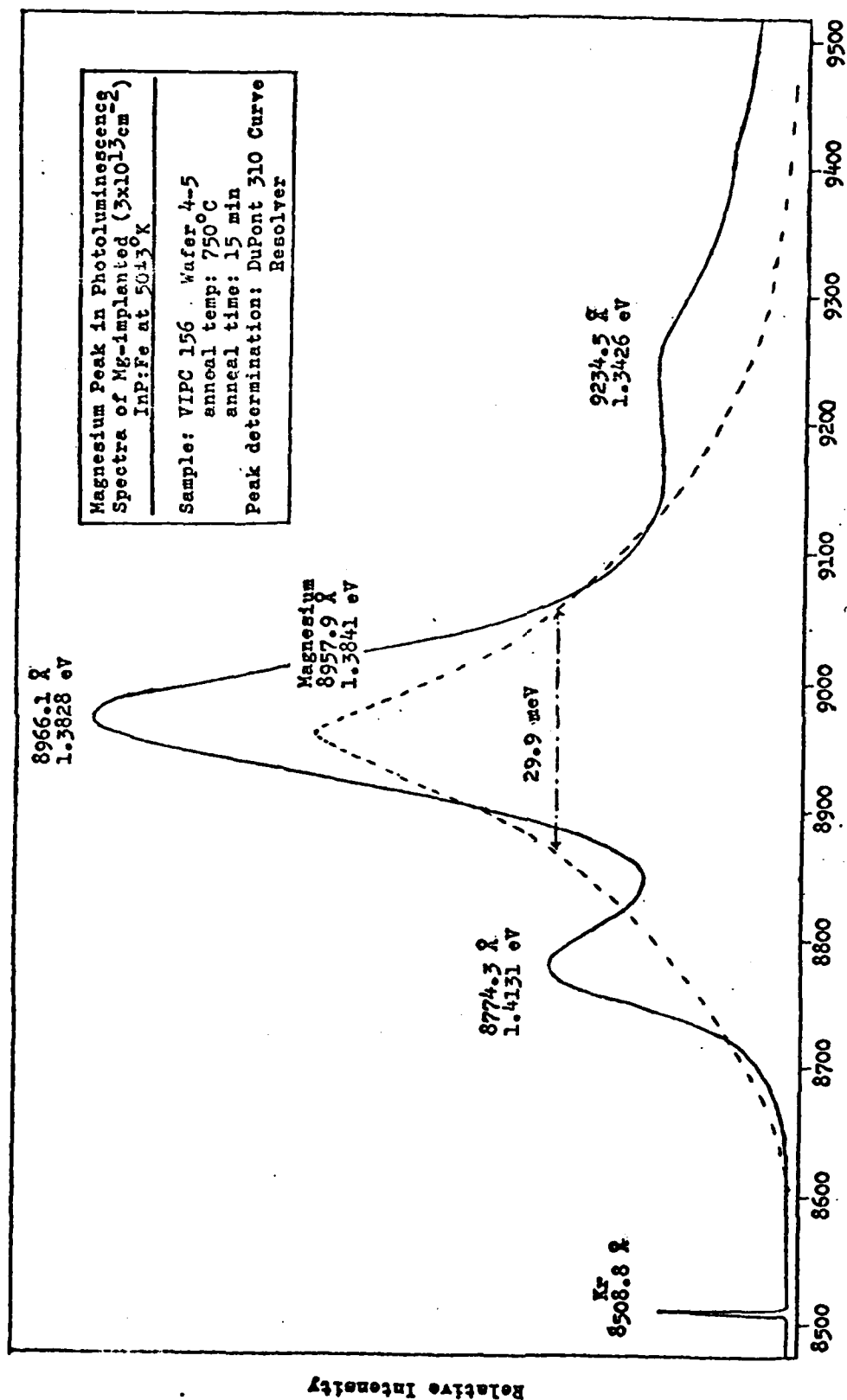


Figure 27. Magnesium Peak in Photoluminescence Spectra of Mg-Implanted ($3 \times 10^{13} \text{ cm}^{-2}$) InP:Fe at 50° K

discussed first. Figures I-1 through I-8 show the emission spectra at 4.2° K of unimplanted and Mg-implanted InP:Fe annealed at 700° C for fifteen minutes; Table 8 lists the observed emissions in order of decreasing Mg fluences. Four key observations may be made about the implant spectra: First, the 1.37 eV peak shifts toward lower energy for the $1 \times 10^{15} \text{ cm}^{-2}$ to $1 \times 10^{14} \text{ cm}^{-2}$ doses; second, the emission spectra develops considerable structure below the $1 \times 10^{14} \text{ cm}^{-2}$ dose; third, the emission spectra develops considerable noise beyond 1.37 eV at doses below $1 \times 10^{14} \text{ cm}^{-2}$; and fourth, the 1.37 eV peak and its low energy structure remain the dominant emission at all observations.

Assuming recombinations involving Mg are present in the 700° C anneal, 4.2° K spectra, then the spectral behavior at the three higher fluences is opposite to what is observed in the 750° C anneal spectra. The 1.37 eV peak is shifted toward lower energy. However, at fluences below $1 \times 10^{14} \text{ cm}^{-2}$ the 1.37 eV peak shifts again toward higher energy. Fluences below $1 \times 10^{14} \text{ cm}^{-2}$ also exhibit at least one phonon replica. Other peaks (1.3190 eV and 1.28 eV) are separated from the adjacent higher energy peaks at either less or greater than the 43 meV LO phonon energy.

700° C Annealed and 50° K Sample Temperature. Figures J-1 through J-7 contain the spectra for the sample temperature of 50° K for 700° C annealed Mg-implanted InP:Fe with peak positions listed in Table 9. General observations concerning the spectra show that there is considerable noise in the spectra of samples implanted at fluences below $1 \times 10^{15} \text{ cm}^{-2}$; compared to the 1.41 eV peak, the 1.38 eV peak and structure remain the dominant emission at all sample conditions;

TABLE 8

Photoluminescence of Mg-Implanted, 700° C Annealed InP:Fe at 4.2° K

Date	Dose	Peak and Shoulder (a) Position in Wavelength: (Å) and Energy (eV)			
7 Sep	Substrate Wafer 4	8749.8 1.4170	9004.8 1.3769	9283.0 1.3356	
12 Sep	Substrate Wafer 6	8747.1 1.4174	8993.4 1.3786	9276.8 1.3365	10883±40 1.1396±.0042
11 Sep	1x10 ¹⁵ cm ⁻²		9043.9 1.3709	9324.6 1.3297	
7 Sep	3x10 ¹⁴ cm ⁻²	8763.1 1.4149	9051.8 1.3697	9299 a 1.3333	10815±50 1.1464±.0053
11 Sep	1x10 ¹⁴ cm ⁻²	8760.4 1.4153	9097.8 1.3628	9165 a 1.3528	9983±40 1.2419±.0049
7 Sep	3x10 ¹³ cm ⁻²	8759.5 1.4154	8991.6 1.3789	9259.9 1.3389	9400±50 1.3190±.007
11 Sep	1x10 ¹³ cm ⁻²	8751.5 1.4167	8988.9 1.3793	9281.2 1.3359	9613.4 1.2897
7 Sep	5x10 ¹² cm ⁻²	8764.8 1.4146	8996.0 1.3782	9307.8 1.3321	9589.5 1.2929

TABLE 9

Photoluminescence of Mg-Implanted
700° C Annealed InP:Fe at 50° K

Dose	Peak Position in Wavelength (Å) and Energy (eV)				
substrate Wafer 6	8763.4 1.4148	8990.8 1.3790	9277.1 1.3365		
$1 \times 10^{15} \text{ cm}^{-2}$	8794.1 1.4099	8967.1 1.3827	9246.0 1.3410		
$3 \times 10^{14} \text{ cm}^{-2}$	8771.5 1.4135	8974.2 1.3816	9206.8 1.3467	9542.9 1.2992	
$1 \times 10^{14} \text{ cm}^{-2}$	8770.8 1.4136	8979.1 1.3808	9264.4 1.3383	9557.4 1.2973	
$3 \times 10^{13} \text{ cm}^{-2}$	8771.2 1.4136	8983.7 1.3801	9305.7 1.3327	9591.7 1.2926	
$1 \times 10^{13} \text{ cm}^{-2}$	8770.8 1.4136	8972.0 1.3819	9237.2 1.3422	9526.7 1.3015	9918 ⁺¹⁵ ₋₁ 1.2501 ⁺¹⁵ _{-0.004}
$5 \times 10^{12} \text{ cm}^{-2}$	8769.0 1.4139	8977.3 1.3811	9243.9 1.3413		9791 ⁺¹⁵ ₋₁ 1.2663 ⁺¹⁵ _{-0.004}

structure develops below the $1 \times 10^{15} \text{ cm}^{-2}$ dosage and extends over a considerable range into the low energy region; and all low energy peaks below the 1.38 eV peak are separated from each other at multiples of approximately 43 meV (aside from the broad 1.26 eV peak at $5 \times 10^{12} \text{ cm}^{-2}$ fluence). Figure 28 shows that the 1.41 eV and 1.38 eV peak energies, when plotted against dosage, remain relatively constant which is in good agreement with what was found for the 750° C annealed samples (Figure 25). Peaks due to phonon replicas show a variation

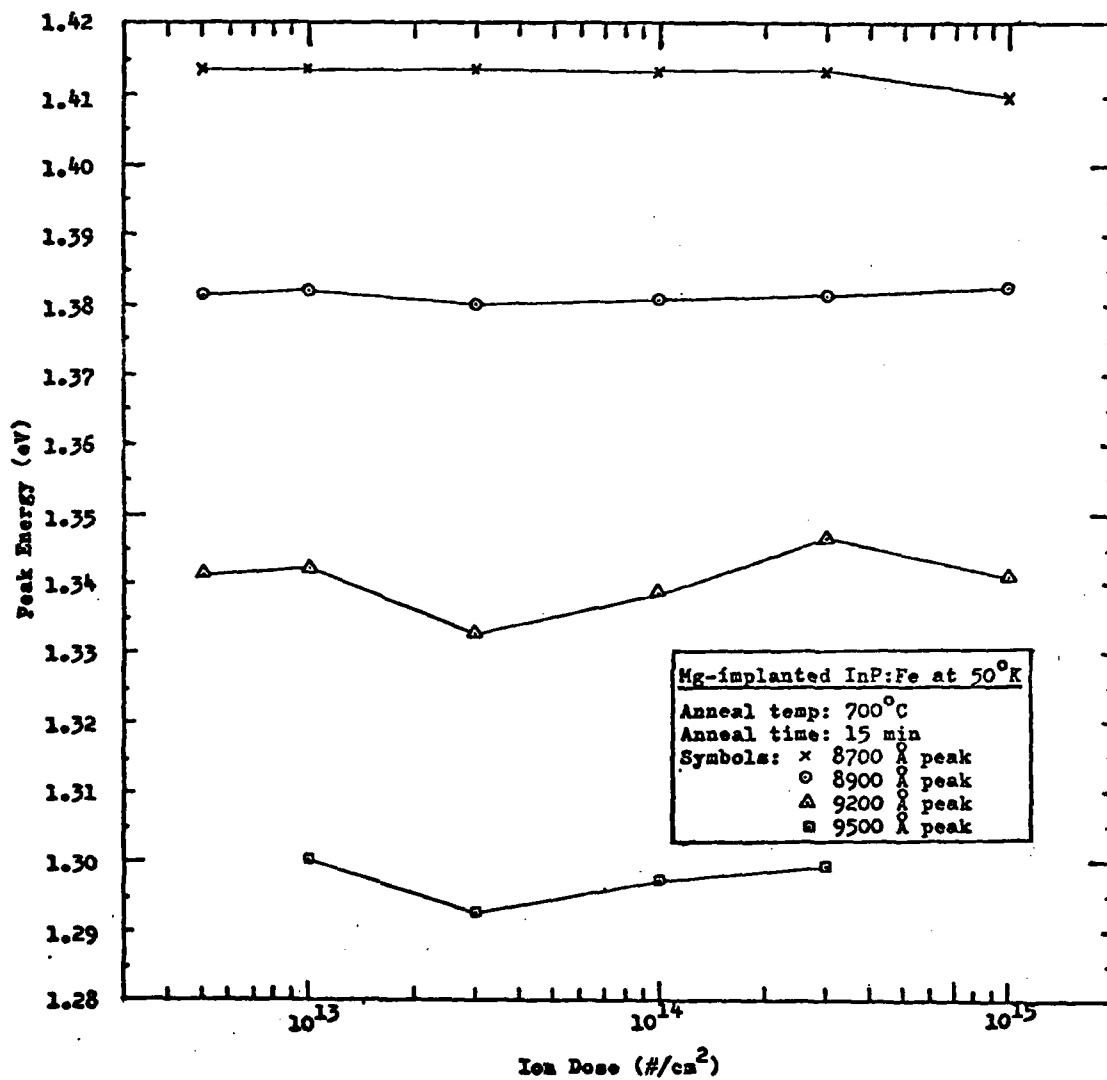


Figure 28. Ion Dose Dependence of Peak Energy for Mg-Implanted, 700° C Annealed InP:Fe at 50° K

from a constant value which is possibly due to the statistical nature of experimental data gathering. Emission intensity versus dosage (Figure 29) shows more of a parabolic behavior than the 750° C anneal data (Figure 26).

In comparing the substrate spectra to the implant spectra, the same high energy peak behavior as for the 750° C anneal is observed; the 1.41 eV substrate peak is slightly shifted toward lower energy in the implant spectra, and the 1.37 eV substrate peak is shifted toward higher energy in the implant spectra. These results and the corresponding intensity increase in the 1.37 - 1.38 eV peak, parallel previous conclusions that the Mg peak lies between the 1.41 eV and 1.37 eV substrate peaks.

700° C Annealed and at Various Sample Temperatures. The temperature dependence of the energy of the Mg-related peaks may be analyzed by using the results catalogued in Appendix K and Appendix L. For sample temperatures of 4.2° K, 50° K, and 100° K, Table 10 gives the results for the substrate and Table 11 gives the results for the sample implanted with Mg at a dosage of $1 \times 10^{15} \text{ cm}^{-2}$. Figure 30 shows that the data for the substrate agrees with previous results for the temperature dependence of undoped InP; in other words, the peak energy decreases with increasing temperature. However, the Mg-implanted sample shows the opposite effect for the 1.37 eV (8900 Å) peak. Although more data are required, especially at the 750° C annealing temperature, a preliminary conclusion is that the 1.36 - 1.38 eV peak, involving Mg acceptor recombinations, shifts to higher energy at increased temperature.

TABLE 10

Photoluminescence of Unimplanted (Wafer 6),
700° C Annealed InP:Fe from 4.2° K to 100° K

Temp (°K)	Peak Position in Wavelength (Å) and Energy (eV)		
4.2	8748.3 1.4173	8989.3 1.3793	9263.1 1.3385
50.0	8764.2 1.4147	8994.6 1.3784	9277.2 1.3365
100.0	8811.2 1.4071	9016.1 1.3751	

TABLE 11

Photoluminescence of Mg-Implanted ($1 \times 10^{15} \text{ cm}^{-2}$),
700° C Annealed InP:Fe from 4.2° K to 100° K

Temp (°K)	Peak Position in Wavelength (Å) and Energy (eV)		
4.2		9036.2 1.3721	9325.2 1.3296
50.0	8795.9 1.4096	8966.3 1.3828	9239.0 1.3420
100.0	8817.9 1.4061	8972.6 1.3818	9240.4 1.3419

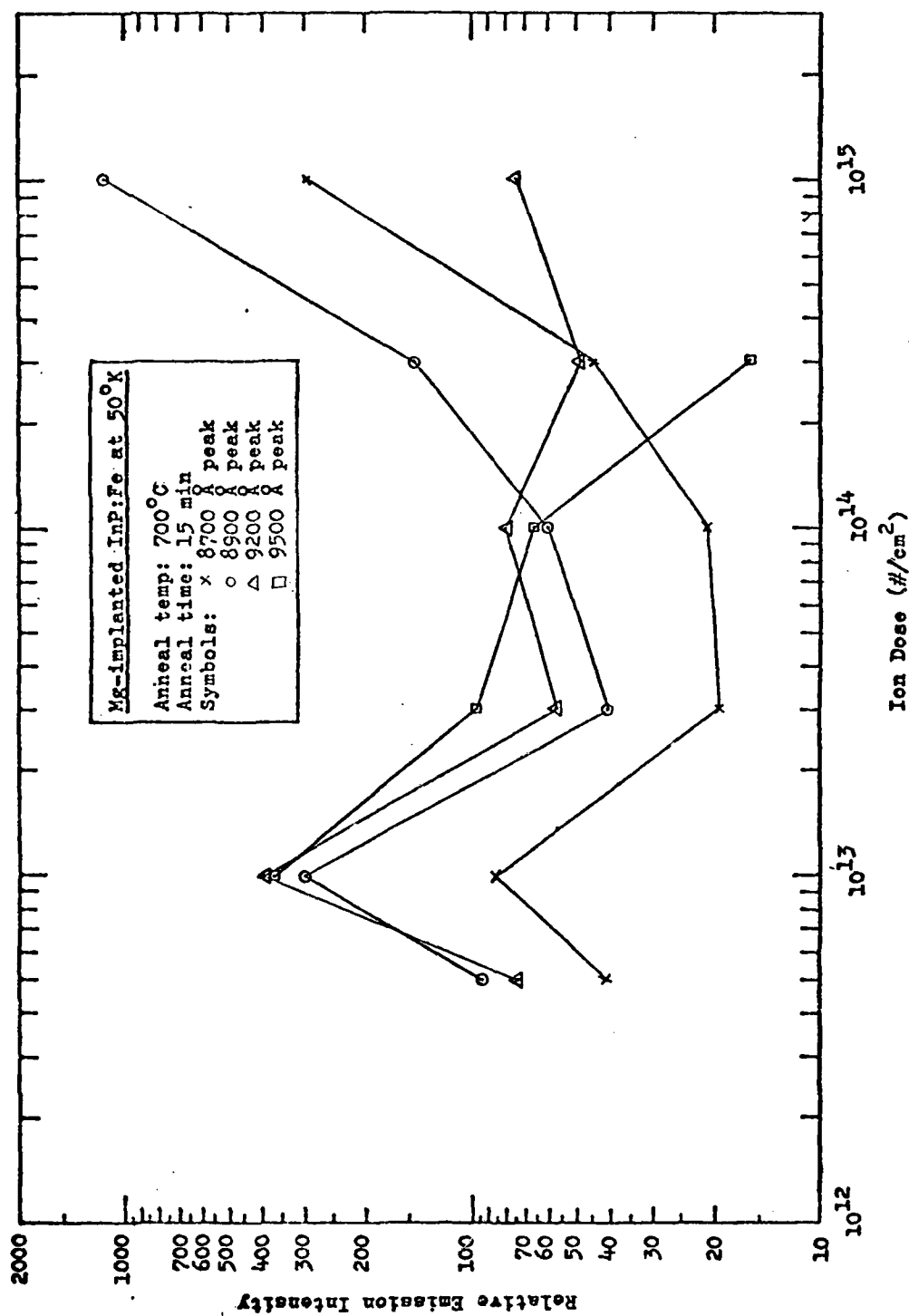


Figure 29. Ion Dose Dependence of Emission Intensity for Mg-Implanted, 700° C Annealed InP:Fe at 50° K

AD-A080 344

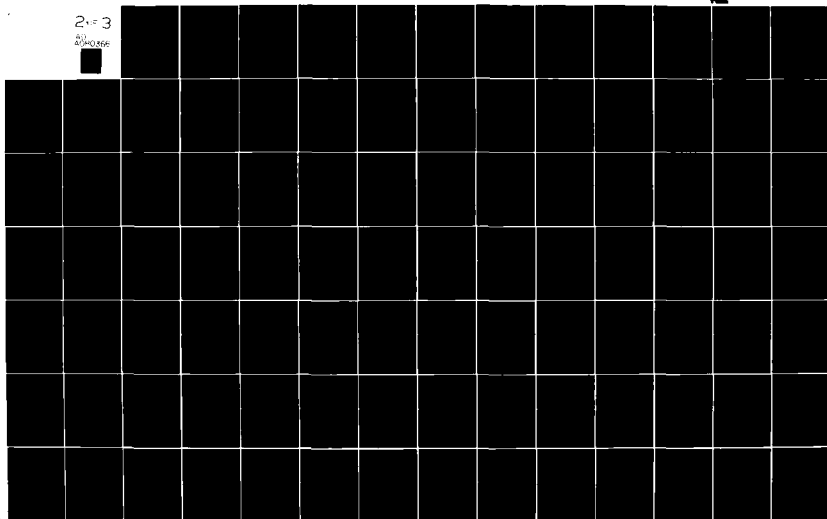
AIR FORCE INST OF TECH WRIGHT-PATTERSON AFB OH SCHOO--ETC F/S 28/12
PHOTOLUMINESCENCE OF UNDOPED, SEMI-INSULATING, AND MG-IMPLANTED--ETC(U)
DEC 79 G S POWRENKE
AFIT/SEP/PH/TWO-S

UNCLASSIFIED

NL

2 of 3

AD-A080 344



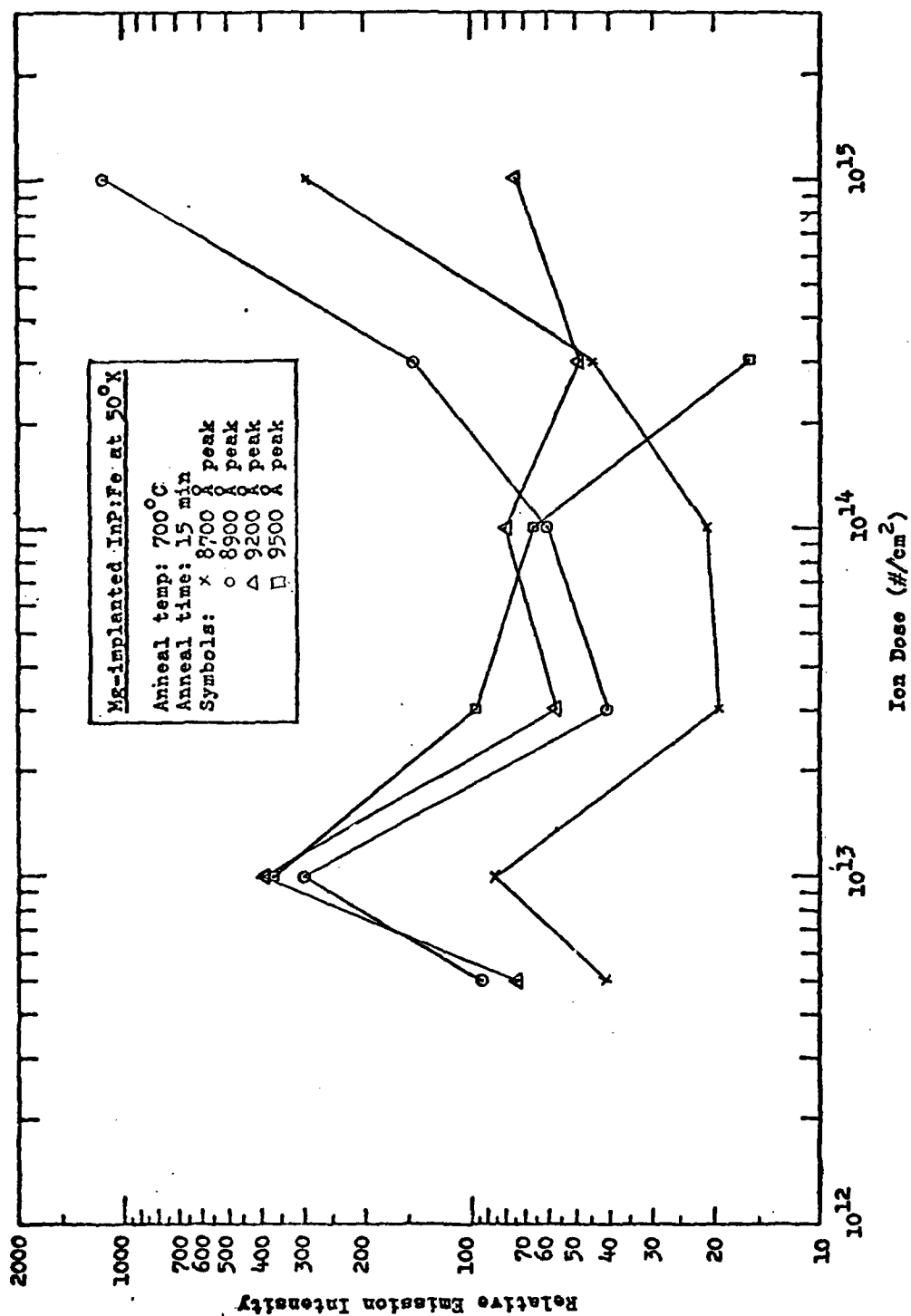


Figure 29. Ion Dose Dependence of Emission Intensity for Mg-Implanted, 700° C Annealed InP:Fe at 50° K

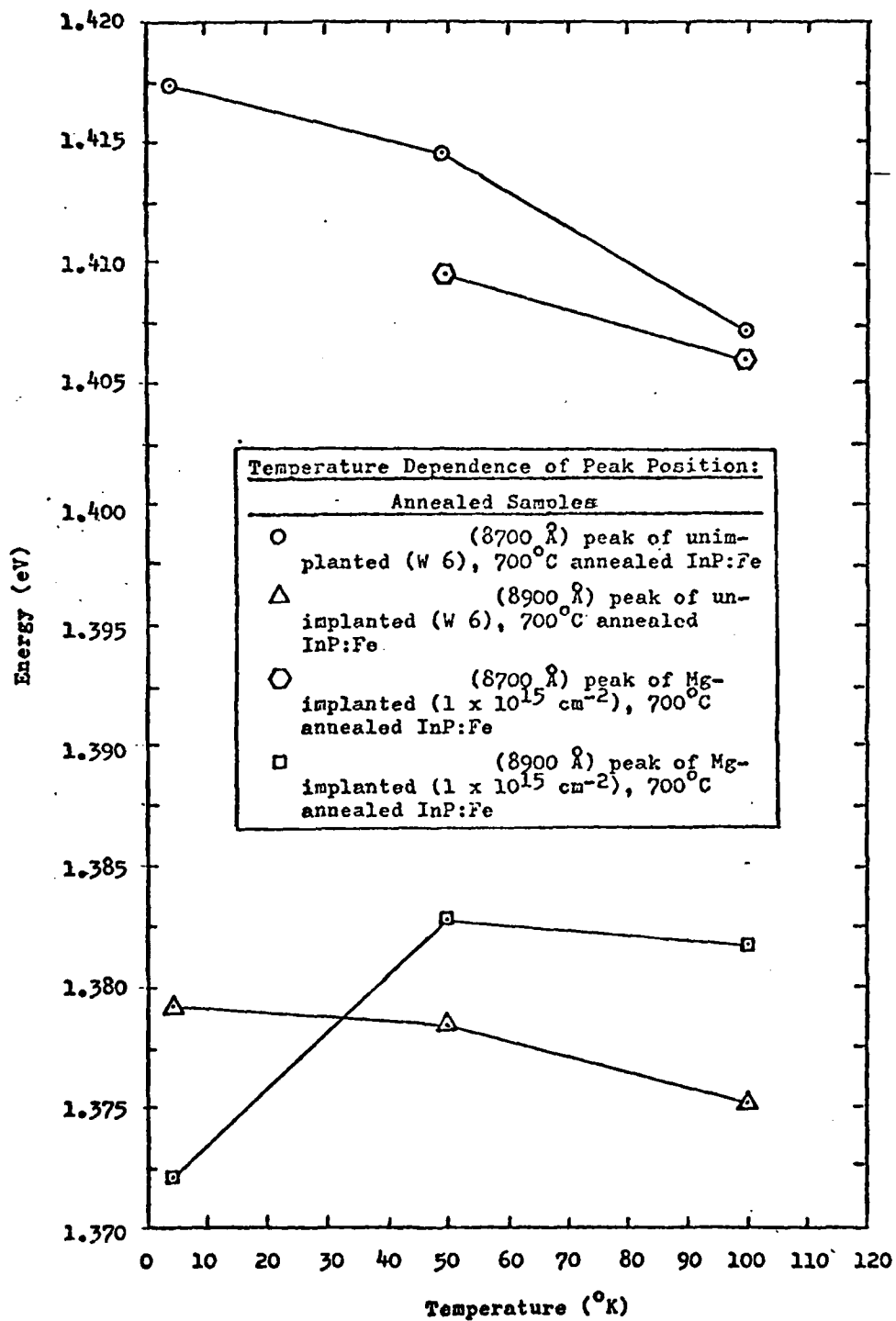


Figure 30. Temperature Dependence of Photoluminescent Spectra in Annealed, Unimplanted, and Mg-Implanted InP

VPE and LPE Grown InP

The availability of vapor phase epitaxial (VPE) and liquid phase epitaxial (LPE) indium phosphide allowed the comparison of the luminescence spectra of the three major crystal growth techniques presently used in semiconductor technology. VPE grown InP was examined both as an undoped and an implanted material at sample temperatures of 4.2° K, 50° K, and 77.3° K; the resulting emissions are listed in Table 12 and depicted in Appendix M. Of the three VPE samples, one was undoped and its spectra at 4.2° K is shown in Figure 31; and two were Mg-implanted at fluences of $1 \times 10^{13} \text{ cm}^{-2}$ and $1 \times 10^{12} \text{ cm}^{-2}$ with the emission spectra of the latter implant condition at 4.2° K depicted in Figure 32. Spectral detail in the 1.41 eV peak of unimplanted VPE InP at 4.2° K is significantly better than for Czochralski grown InP for the same emission region. The recombination processes for the individual peaks and shoulders in the structure are assigned as previously. The noticeable difference between the 1.41 eV structure in Figures 31 and 32 is probably due to the fact that the samples are from different substrates. More specific, the difference may be due to the variation in strain in the two crystals as shown in the study by White, et al. (Ref 22:1730-1731). The broad low intensity peak at 1.4041 eV is of unknown origin. The 1.37 eV peak identifies with donor-to-acceptor transitions, where the peak or maximum of this broad emission occurs at 1.37537 eV. The structure in the high energy shoulder of the peak suggests that with more sensitive detection the emission spectra might exhibit fine structure. The 1.3343 eV peak is a phonon emission.

TABLE 12

Photoluminescence of VPE InP

Sample	Peak and Shoulder (λ) Position in Wavelength and Energy							
Substrate 4.2°K	8739.8 λ 1.41563 eV	8745.1 λ 1.41777 eV	8760.4 λ 1.41529 eV	8769.9 λ s 1.41376 eV	8830.4 λ 1.4041 eV	9014.7 λ 1.37557 eV	9292.4 λ 1.3343 eV	
Substrate 50°K	8758.9 λ 1.41553 eV				8997.9 λ 1.3779 eV			
Substrate 77.3°K	8780.5 λ 1.41205 eV				8991.8 λ 1.3788 eV			
Mg-implanted 1x10 ¹² cm ⁻² 4.2°K	8733.4 λ 1.41967 eV	8749.4 λ 1.41707 eV	8761.2 λ 1.41516 eV	8769.4 λ s 1.41384 eV	8964.9 λ s 1.38301 eV	8993.4 A 1.37862 eV	9005.7 λ s 1.37674 eV	9286.5 λ 1.33511 eV 9310.9 λ 1.33161 eV
Mg-implanted 1x10 ¹² cm ⁻² 50°K	8752.7 λ s 1.41165 eV				8766.2 λ 1.41435 eV	8983.8 λ 1.3801 eV 9279.8 λ 1.3361 eV		
Mg-implanted 1x10 ¹³ cm ⁻² 50°K	9078.2 λ 1.3658 eV							

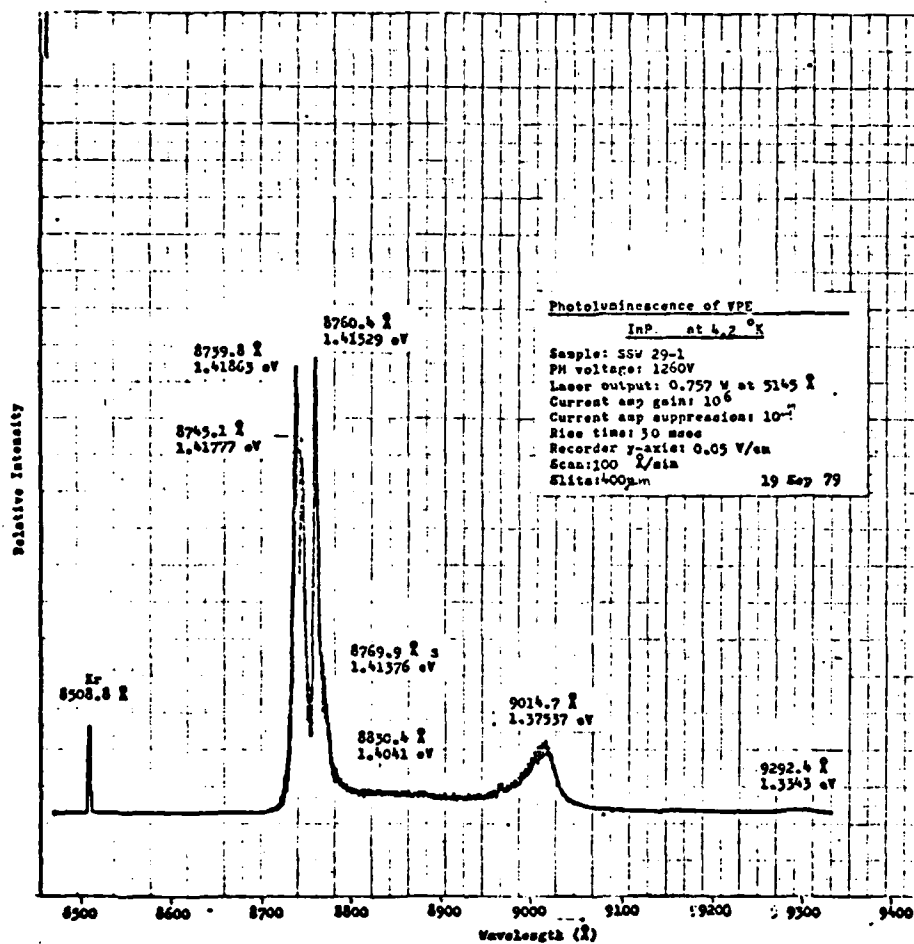


Figure 31. Photoluminescence of Undoped VPE InP at 4.2° K

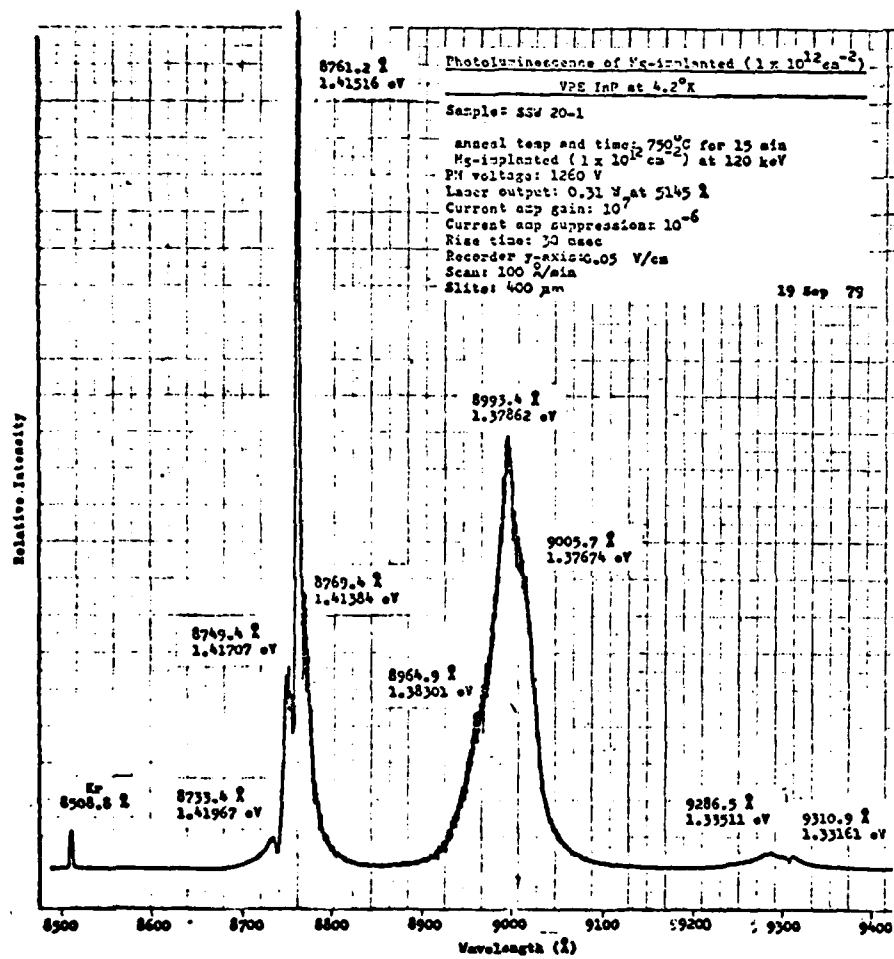


Figure 32. Photoluminescence of Mg-Implanted ($1 \times 10^{12} \text{ cm}^{-2}$) VPE InP at 4.2°K

When comparing the spectra of the unimplanted sample at 4.2° K with the $1 \times 10^{12} \text{ cm}^{-2}$ implant spectra at 4.2° K, the influence of the magnesium ions may be observed in the 1.37 eV peak. What was a relatively low intensity peak in the undoped material becomes the dominant peak in the implant material. The magnesium peak in the implanted VPE InP has also increased the structure in the 1.37 eV peak. A high energy shoulder is observed at 1.38301 eV and a low energy shoulder is observed at 1.3767 eV; both are of unknown origin. (The spectral results for the $1 \times 10^{13} \text{ cm}^{-2}$ implant were unsatisfactory.)

At 50° K the spectra of the unimplanted sample consists of basically a dominant peak at 1.41553 eV (Figure M-2), while the spectrum of implanted VPE InP (Figure M-6) consists of two dominant peaks at 1.4143 eV and 1.3801 eV. This confirms that the peak due to recombination involving implanted Mg acceptors is located at 1.38 eV, specifically at 1.3801 eV at a temperature of 50° K.

Table 13 lists the luminescence results for LPE InP with spectra depicted in Appendix N. In this study, spectral observations were made for the Czochralski, VPE, and LPE grown InP at 77.3° K; the spectrum of each is shown in Figures B-10, M-3, and N-1, respectively. The 1.41 eV peak was the most dominant peak in the LPE and VPE spectra, while for the spectra of Czochralski grown crystals, the 1.41 eV and 1.37 eV peaks were of about equal intensity. The availability of these data allows the comparison of the emission peak widths of the three growth techniques. Full width at half maximum for the 1.41 eV peak was 10.32 meV for the Czochralski technique, 5.67 meV for LPE, and 4.99 meV for VPE. These results support the superior characteristics of liquid and vapor grown material.

TABLE 13

Photoluminescence of Undoped LPE at 77.3° K and 100° K

Temp (°K)	Peak Position in Wavelength (Å) and Energy (eV)		
77.3	8781.4	9011.9	9300.3
	1.4119	1.3758	1.3331
100.	8864.2		
	1.3987		

V. Conclusions and Recommendations

Photoluminescence provided a method of optically characterizing indium phosphide. The emissions of this semiconductor material were studied with respect to temperature, emission intensity, and excitation intensity. Peak positions for undoped InP were in agreement with what has been published in the literature. At and below the sample temperature of 4.2° K, the following transitions were seen as identified by Heim, et al. (Ref 21): free exciton at 1.4166 eV, bound exciton at 1.4144 eV, and donor-to-valence at 1.4127 eV. White, et al. (Ref 22) respectively assigns these peaks to excitons bound to neutral donors, excitons bound to neutral acceptors, and acoustical phonon replicas of the 1.4144 eV peak; an emission at 1.4174 eV is ascribed to free excitons. Above 4.2° K, the 1.41 eV peak was identified with the recombination of exciton complexes, while the 1.38 eV peak was identified with donor-to-acceptor transitions which included up to four LO phonon replicas. Broad low intensity peaks were also identified at 1.054 eV, 0.937 eV, and 1.15 eV, with the latter ascribed to phosphorus vacancies.

Spectral results for semi-insulating InP:Fe are not available in the literature. When compared to undoped InP, the spectra is less intense and the high energy shoulder of the exciton related transitions is more dominant. The high energy shoulder at 1.3864 eV is of unknown origin, as is the 1.31 eV low intensity peak. Emission peak energies of the donor-to-acceptor transition also show an anomalous temperature dependence; this may be due to the dominant band-to-band transition.

The results from the Mg-implanted, 700° C annealed samples proved inconclusive due to the questionable integrity of the encapsulant, noisy spectra, and the inconsistencies with the 750° C anneal. However, preliminary observations from these data indicates a shift toward higher energy with decreasing temperature for the peak associated with the Mg acceptor recombination. Results from Mg-implanted InP:Fe, annealed at 750° C, indicate that at the same temperature the peak due to recombinations involving Mg acceptors is at a higher energy and greater intensity than the donor-to-acceptor recombination peak in substrate material. Analysis of the luminescence spectra results in identifying this peak position as being located between 1.384 eV and 1.388 eV at 50° K. The 0.9643 eV emission peak from unannealed, Mg-implanted InP:Fe is ascribed to lattice defects.

Superior spectral results of Mg-implanted VPE InP resulted in identifying the Mg peak at 1.3801 eV at 50° K. Using results from Mg-implanted GaAs, the Mg peak is ascribed to the recombination of free electrons with holes bound to the Mg acceptors. There was also considerable improvement in the resolution of structure in the 1.41 eV emission of VPE. Finally, at 77.3° K full peak width at half maximum for VPE and LPE InP was approximately one-half of the width of Czochralski grown InP.

The following are recommendations for further investigation of InP and recommendations for the experimental setup:

1. Photoluminescence studies of Mg-implanted InP annealed at the following temperatures: 800° C, 600° C, and 500° C.
2. Electrical measurements on Mg-implanted samples.

3. Investigate peak widths of undoped, semi-insulating, and Mg-implanted spectra.

4. Use of VPE InP for Mg-implant studies and examination of spectral detail of the 1.41 eV peak; specifically, re-investigate the questionable $1 \times 10^{13} \text{ cm}^{-2}$ Mg-implanted, 750° C annealed VPE InP.

5. Repeat investigation of Mg-implanted, 700° C annealed InP:Fe for dosages used in this study.

6. Investigate the emission intensity as a function of excitation intensity for specific Mg-implant dosages.

7. Correct spectra for photomultiplier and photoconductor response.

8. Prior to another photoluminescence study, the detachable tail dewar should be properly leak-checked and uncalibrated diodes used for cryogenic temperature measurements should be calibrated.

9. Acquire an improved cooling system for the argon-ion laser.

Bibliography

1. Air Force Avionics Laboratory, Technical Programs and Contacts, March 1979, 10th Ed.
2. Eldridge, G.W. and V.L. Wrick. Ion Implantation of Indium Phosphide: Interim Report. Pittsburgh PA: Westinghouse R&D Center, 30 November 1978.
3. Donnelly, J.P. and C.E. Hurwitz. "Ion-implanted n- and p-type Layers in InP," Applied Physics Letters, 31 (7): 418-420 (1 October 1977).
4. Williams, E.W., et al. "Indium Phosphide: I. A Photoluminescence Materials Study," Journal of Electrochemical Society: Solid-State Science and Technology, 120 (12): 1741-1749 (December 1973).
5. Rupprecht, H.S. "New Advances in Semiconductor Implantation," Journal of Vacuum Science Technology, 15 (5): 1669 (September/October 1978).
6. Mayer, J.W. and O.J. Marsh. "Ion-Implantation in Semiconductors," Applied Solid State Science, Edited by R. Wolfe and C.J. Kriessman. Volume 1. New York: Academic Press, 1969.
7. Davis, D.E. and J.P. Lorenzo. "Isolation and N-Type Conduction from Implantation in InP," IEEE Transistor Electron Devices, ED-24, (9): 1205 (September 1977).
8. McKelvey, John P. Solid State and Semiconductor Physics. New York: Harper and Row, 1966.
9. Eisberg, Robert and Robert Resnick. Quantum Physics of Atoms, Molecules, Solids, Nuclei, and Particles. New York: John Wiley and Sons, 1974.
10. Casasent, David. Electronic Circuits. New York: Quantum Publishers, Inc., 1973.
11. Kittel, C. Introduction to Solid State Physics. New York: John Wiley and Sons, Inc., 1976.
12. Pankove, Jacques I. Optical Processes in Semiconductors. Englewood Cliffs NJ: Prentice-Hall, Inc., 1971.
13. Lusk, Ronald L. Cathodoluminescence on the Effects of Te Implantation and Laser Annealing in Gallium Arsenide. Unpublished Thesis, Wright-Patterson AFB OH: Air Force Institute of Technology, December 1978.

14. Dexter, D.L. and R.S. Knox. Excitons. New York: John Wiley and Sons, Inc., 1965.
15. Varni, Jamie G.G. Photoluminescence of GaInAsP. Unpublished Thesis, Wright-Patterson AFB OH: Air Force Institute of Technology, September 1978.
16. Willardson, R.K. and Albert C. Beer. Semiconductors and Semimetals, Vol. 4 -- Physics of III-V Compounds. New York: Academic Press, 1968.
17. Colbow, K. "Free-to-Bound and Bound-to-Bound Transitions in CdS," Physical Review, 141: 742-749 (January 1966).
18. Pierce, B.J. Luminescence and Hall Effect of Ion Implanted Layers in ZnO. Unpublished Dissertation, Wright-Patterson AFB OH: Air Force Institute of Technology (September 1974).
19. Bogardus, E.H. and H.B. Bebb. "Bound-Exciton, Free-to-Bound, Band-Acceptor, Donor-Acceptor, and Auger Recombination in GaAs," Physical Review, 176: 993-1002 (15 December 1968).
20. Halperin, A. and E. Zacks. "Temperature Dependence of the 2.2-eV Pair-Recombination Band in GaP(S,C) Crystals," Physical Review B, 11: 2237-2242 (12 March 1975).
21. Heim, U. et al. "Photoluminescence of InP," Journal of Luminescence, 1-2: 542-551 (1970).
22. White, A.M., et al. "The Photoluminescence Spectrum of Bound Excitons in Indium Phosphide and Gallium Arsenide," Journal of Physics C: Solid State Physics, 5, 1972.
23. Turner, W.J. and G.D. Pettit. "Photoinduced Recombination Radiation in InP Diodes," Applied Physics Letters, 3 (6): 102-104, (15 September 1963).
24. Willardson, R.K. and Albert C. Beer. Semiconductors and Semimetals, Vol 3 -- Optical Properties of III-V Compounds. New York: Academic Press, 1967.
25. Townsend, Peter David, et al. Ion Implantation, Sputtering, and Their Application. London: Academic Press, 1976.
26. Yeo, Yung Kee. Personal Communication, 7 September 1979.
27. RCA Photomultiplier and Image Tubes. Harrison NJ: Radio Corporation of America, 1965.

28. IR Industries Technical Information Sheet on PbS Detector T0-2667.
29. Matthews, J.W. Epitaxial Growth, Pt. A. New York: Academic Press, 1975.
30. Woody, William R. Luminescence in Ion Implanted Zn Te. Unpublished Thesis, Dayton OH: University of Dayton, April 1975.
31. Koshel, W., V. Kaufmann, and S.G. Bishop. "Optical and ESR Analysis of the Fe Acceptor in InP," Solid State Communications, 21: 1069-1072, 1977.
32. Yu, Phil Won and Y.S. Park. "Temperature Dependence of Photo-luminescence from Mg-implanted GaAs," Journal of Applied Physics, 48 (6): 2434-2441, June 1977.
33. Park, Y.S. Personal Communication, 14 September 1979.

Appendix A

Polynomial Least Squares Fit Analysis of Indium Phosphide Peak Energy
Versus Temperature Data


```

1      PROGRAM POLY(INPUT=780,OUTPUT,TAPF5=INPUT,TAPF6=OUTPUT)
      C THIS PROGRAM TAKES PEAK ENERGY VERSUS TEMPERATURE DATA FROM A
      C PHOTOLUMINESCENCE EXPERIMENT: PERFORMS POLYNOMIAL LEAST SQUARE FIT
      C ANALYSIS ON THE DATA POINTS TO ARRIVE AT POLYNOMIALS OF DEGREE 1 TO 6:
5      C THE DATA POINTS AND POLYNOMIAL CURVES ARE PLOTTED ON A ENERGY
      C VERSUS TEMPERATURE GRAPH: ALSO PLOTTED IS THE THEORETICAL BANDGAP FOR INDIUM
      C PHOSPHIDE. --- GERNOT POMRENKE
      C
      C      DIMENSION X(30),Y(30),W(30),C1(2),C2(3),C3(4),C4(5),C5(6),C6(7)
10     DIMENSION W1(7),W2(12),W3(18),W4(23),W5(28),W6(32)
      DIMENSION S(60),T(50),O(60),R(60),P(30),D(10),E(50)
      DIMENSION F(60),G(60),A(70),B(70)
      C
      C READ DATA CARDS , INPUT IS IN TEMPERATURE, WAVELENGTH
15     READ(5,222)NP
222    FORMAT(I2)
      DO 20 J=1,NP
      READ(5,*)X(J),P(J)
20     CONTINUE
      C PRINT INITIAL INPUT
      WRITE(6,7)
7      FORMAT(" INITIAL INPUT DATA: (TEMPERATURE,WAVELENGTH)",/)
      DO 27 J=1,NP
      WRITE(6,*)X(J),P(J)
25     CONTINUE
      C CONVERT WAVELENGTHS TO ENERGY IN EV
      DO 25 J=1,NP
      Y(J)=(1.239856E3L)*(1./P(J))
25     CONTINUE
30     C ASSIGN WEIGHT TO EACH DATA POINT
      DO 30 J=1,NP
      W(J)=1
30     CONTINUE
      C PRINT OUT DATA POINTS AND WEIGHT
35     WRITE(6,3)
3      FORMAT(" ",/, " DATA POINTS (TEMPERATURE,ENERGY,WEIGHT):",/)
      DO 40 J=1,NP
      WRITE(6,*)X(J),Y(J),W(J)
40     CONTINUE
      C
      C POLYNOMIAL LEAST SQUARE FIT ROUTINES FOR GIVEN DATA POINTS FROM
      C DEGREE OF 1 TO 6
      C PROGRAM CALLS PLSCF FROM CCC 6600 LIBRARY
      C
45     WRITE(6,13)
13     FORMAT(" ",/, " POLYNOMIALS FROM DEGREE 1 TO 6 FOR DATA POINTS ",
5      " AS A RESULT OF LEAST SQUARES FIT CALCULATIONS.",/)
      IN=0
      C *****
50     NDEG1=1
      CALL PLSCF(X,Y,W,NP,NDEG1,NMAX,C1,IN,XD,XO,W1,IER)
      WRITE(6,403)C1(1),C1(2)
403    FORMAT(" P(X) = ",F12.9," + ",F12.9," X ",/)
      C *****
55     NDEG2=2
      CALL PLSCF(X,Y,W,NP,NDEG2,NMAX,C2,IN,XD,XO,W2,IER)
      WRITE(6,303)C2(1),C2(2),C2(3)
303    FORMAT(" P(X) = ",F12.9," + ",F12.9," X + ",F12.9," X**2 ",/)
      C *****
60     NDEG3=3
      CALL PLSCF(X,Y,W,NP,NDEG3,NMAX,C3,IN,XD,XO,W3,IER)
      WRITE(6,307)C3(1),C3(2),C3(3),C3(4)
307    FORMAT(" P(X) = ",F12.9," + ",F12.9," X + ",F12.9," X**2 ",
6      " + ",F12.9," X**3 ",/)
      C *****
65     NDEG4=4
      CALL PLSCF(X,Y,W,NP,NDEG4,NMAX,C4,IN,XD,XO,W4,IER)
      WRITE(6,309)C4(1),C4(2),C4(3),C4(4),C4(5)
309    FORMAT(" P(X) = ",F12.9," + ",F12.9," X + ",F12.9," X**2 ",
7      " + ",F12.9," X**3 ", + ",F15.13," X**4 ",/)
      C *****
70     NDEG5=5
      CALL PLSCF(X,Y,W,NP,NDEG5,NMAX,C5,IN,XD,XO,W5,IER)
      WRITE(6,311)C5(1),C5(2),C5(3),C5(4),C5(5),C5(6)
75     311    FORMAT(" P(X) = ",F12.9," + ",F12.9," X + ",F12.9," X**2 ",
8      " F12.10," X**3 ", + ",F15.13," X**4 ", + ",/, " ",
8      " F15.13," X**5 ",/)
      C *****

```

```

      NDEG(=6
      CALL PLSCF(X,Y,W,NP,NDEG6,NMAX,C3,I4,XD,XG,WE,IER)
      WRITE(6,313)C5(1),C5(2),C6(3),C6(4),C6(5),C6(6),C6(7)
313  FORMAT(" P(X) = ",F12.6," + ",F12.9," X + ",F12.9," X**2 ",F12.9," X**3 ",F12.16," X**4 ",F12.16," X**5 ",F12.16," X**6 ",/)
      C .....
85  C
      C
      C SET ORIGIN OF PLOT AND SCALE FACTOR
      CALL PLOT(1.0,3.0,-3)
      CALL FACTOR(1.0)
90  C PLOTTING DATA POINTS ON GRAPH
      CALL SCALE(X,3.3,NP,1)
      CALL SCALE(Y,5.3,NP,1)
      CALL LINE(X,Y,NP,1,-1,3)
95  C
      XMIN=X(NP+1)
      DX=X(NP+2)
      YMIN=Y(NP+1)
      DY=Y(NP+2)
100 C
      C UTILIZING POLYNOMIALS TO DRAW 'BEST FIT' CURVE THROUGH DATA POINTS
      C ON GRAPH
      C
      C FOURTH DEGREE POLYNOMIAL
      K=0
105  DO 701 I=1,225,4
      K=K+1
      S(K)=I
      T(K)=
      C4(1) + C4(2)*S(K) + C4(3)*S(K)**2 + C4(4)*S(K)**3
      C4(5)*S(K)**4
701  CONTINUE
      CALL SCALE(S,3.5,K,1)
      CALL SCALE(T,5.3,K,1)
115  S(K+1)=XMIN
      S(K+2)=DX
      T(K+1)=YMIN
      T(K+2)=DY
      CALL LINE(S,T,K,1,8,2)
120 C THIRD DEGREE POLYNOMIAL
      KK=0
      DO 711 I=1,225,4
      KK=KK+1
      Q(KK)=I
      R(KK)= C3(1)+C3(2)*Q(KK)+C3(3)*Q(KK)**2+C3(4)*Q(KK)**3
711  CONTINUE
      CALL SCALE(Q,3.5,KK,1)
      CALL SCALE(R,5.0,KK,1)
125  Q(KK+1)=XMIN
      Q(KK+2)=DX
      R(KK+1)=YMIN
      R(KK+2)=DY
130 C SECOND DEGREE POLYNOMIAL
      KM=0
      DO 733 I=1,225,4
      KM=KM+1
      F(KM)=I
      G(KM)=C2(1)+C2(2)*F(KM)+C2(3)*F(KM)**2
733  CONTINUE
      CALL SCALE(F,3.5,KM,1)
      CALL SCALE(G,5.0,KM,1)
140  F(KM+1)=XMIN
      F(KM+2)=DX
      G(KM+1)=YMIN
      G(KM+2)=DY
145 C FIRST DEGREE POLYNOMIAL
      KN=0
      DO 744 I=1,260,4
      KN=KN+1
      A(KN)=I
      B(KN)=C1(1)+C1(2)*A(KN)
744  CONTINUE
      A(KN+1)=XMIN
      A(KN+2)=DX
      B(KN+1)=YMIN
      B(KN+2)=DY
150 C .....
      C

```

THIS FILE IS BEST QUALITY PRINTABLE
FROM DATA FURNISHED TO IDG

```

160      C
      C PLOTTING AXES AND LABELING
      CALL AXIS(0.0,0.0,15,TEMPERATURE ( K),-16.5,0.0,XMIN,DX)
      CALL AXIS(0.0,0.0,11,ENERGY ( V),11.6,0.30,YMIN,DY)
      CALL AXIS(0.0,0.0,14,1,8.5,0.0,XMIN,DX)
      CALL AXIS(0.0,0.0,14,-1,6.0,90.0,YMIN,DY)
165      C SYMBOL IDENTIFICATION ON GRAPH
      CALL SYMBOL(1.25,2.36,.12,3,0.0,-1)
      CALL SYMBOL(1.5,2.0,0.12,11,DATA POINTS,0.0,11)
      CALL SYMBOL(1.25,1.36,.12,2,0.0,-1)
      CALL SYMBOL(1.5,1.3,0.12,18,WITH DEG POLYNOMIAL,0.0,18)
170      C
      C PRINT OUT XMIN,DX,YMIN,DY FOR ERROR CHECK
      WRITE(6,23)
23      FORMAT(" ERROR CHECK:")
      WRITE(6,*)XMIN,DX
175      WRITE(6,*)YMIN,DY
      C
      C ***** PLOT OF THEORETICAL BAND GAP VS TEMPERATURE *****
      C BAND GAP AT 0 DEG K = 1.42 eV
      C ALPHA AND BETA ARE CONSTANTS
180      C
      CALL FLOT(11.0,0.0,-3)
      CALL FACTOR(1.0)
      KL=0
      DO 722 I=1,318,6
      KL=KL+1
185      ALPHA=4.906E-04
      BETA=327.
      D(KL)=1
      E(KL)=1.4206-((ALPHA*D(KL)**2)/(3*(KL)+BETA))
190      722 CONTINUE
      CALL SCALE(0.5,5,KL,1)
      CALL SCALE(0.5,3,KL,1)
      XMINFG=D(KL+1)
      DXBG=D(KL+2)
195      YMINFG=E(KL+1)
      DYBG=E(KL+2)
      CALL LINE(3,E,KL,1,4,5)
      CALL AXIS(0.0,0.0,15,TEMPERATURE ( K),-16.5,0.0,XMINBG,DXBG)
      CALL AXIS(0.0,0.0,11,ENERGY ( V),11.6,0.30,YMINBG,DYBG)
200      CALL AXIS(0.0,0.0,14,1,8.5,0.0,XMINBG,DXBG)
      CALL AXIS(0.0,0.0,14,-1,6.0,90.0,YMINBG,DYBG)
      CALL SYMBOL(1.25,2.36,.12,5,0.0,-1)
      CALL SYMBOL(1.5,2.0,0.12,20,THEORETICAL BAND GAP,0.0,20)
205      C
      C
      CALL FLOTE(M)
      STOP
      END

```

THIS IS BEST QUALITY PRACTICE
 TO DO

INITIAL INPUT DATA:TEMPERATURE, WAVELENGTH

2.69 8751.9
4.2 8753.3
5. 8753.1
10. 8765.3
20. 8765.7
30. 8769.6
40. 8772.8
50. 8780.2
60. 8789.
77.3 8807.4
100. 8835.3
125. 8868.1
160. 8924.9
225. 9050.4

DATA POINTS (TEMPERATURE, ENERGY, WEIGHT)

2.69 1.41567816798 1.
4.2 1.41644083945 1.
5. 1.41647848364 1.
10. 1.41650422321 1.
20. 1.41444337555 1.
30. 1.413611348294 1.
40. 1.413295641072 1.
50. 1.41219458787 1.
60. 1.41099936322 1.
77.3 1.407731843 1.
100. 1.403298133623 1.
125. 1.398423207498 1.
160. 1.3923936117 1.
225. 1.363945079731 1.

POLYNOMIALS FROM DEGREE 1 TO 6 FOR DATA POINTS AS A RESULT OF LEAST SQUARES FIT CALCULATIONS.

P(X) = 1.419530504 + -.000193983 X
P(X) = 1.415497069 + -.000066178 X + -.000000630 X**2
P(X) = 1.416292289 + -.000046674 X + -.000000050 X**2 + .000000001 X**3
P(X) = 1.416677826 + -.000076304 X + -.000000172 X**2 -.000000006 X**3 + .00000000000124 X**4
P(X) = 1.416833676 + -.000251882 X + .000007774 X**2 -.0000000454 X**3 + .0000000002408 X**4 +
-.0000000000004 X**5
P(X) = 1.417670704 + -.000379093 X + .00001717 X**2
-.000010322 X**3 + .0000000030632 X**4 + -.000000000000022 X**5 + .000000000000000022 X**6

ERROR CHECK
0.40.
1.369 .008

THIS PAGE IS BEST QUALITY PRACTICE
COPY PROHIBITED

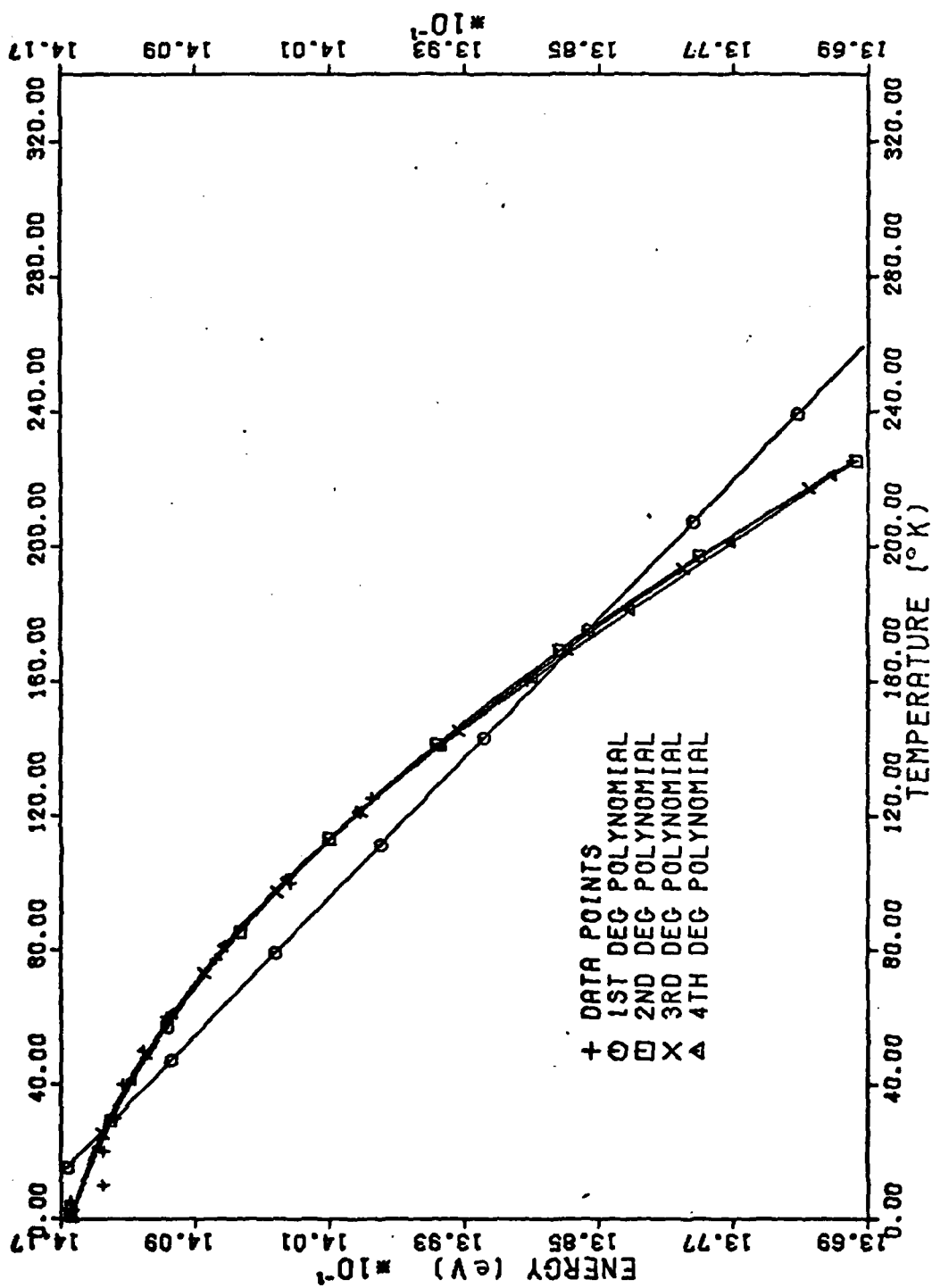


Figure A-1 Temperature Dependence of Exciton-Related (8700 Å) Peak Energy in Undoped InP

2.69 9011.7
4.2 9009.5
5. 9018.4
10. 9009.2
20. 9008.6
30. 8997.9
40. 8998.6
50. 9003.9
60. 9009.9
77.3 9025.1
100. 9042.8
125. 9098.7
160. 9161.6

2.69 1.375823199818 1.
 4.2 1.376165159999 1.
 5.2 1.376307131323 1.
 6.2 1.37644914327 1.
 7.2 1.376591155217 1.
 8.2 1.376733167161 1.
 9.2 1.376875179105 1.
 10.2 1.377017191049 1.
 11.2 1.377159202993 1.
 12.2 1.377301214937 1.
 13.2 1.377443226881 1.
 14.2 1.377585238825 1.
 15.2 1.377727250769 1.
 16.2 1.377869262713 1.
 17.2 1.378011274657 1.
 18.2 1.378153286601 1.
 19.2 1.378295298545 1.
 20.2 1.378437310489 1.
 21.2 1.378579322433 1.
 22.2 1.378721334377 1.
 23.2 1.378863346321 1.
 24.2 1.379005358265 1.
 25.2 1.379147370209 1.
 26.2 1.379289382153 1.
 27.2 1.379431394097 1.
 28.2 1.379573406041 1.
 29.2 1.379715417985 1.
 30.2 1.379857429929 1.
 31.2 1.379999441873 1.
 32.2 1.380141453817 1.
 33.2 1.380283465761 1.
 34.2 1.380425477705 1.
 35.2 1.380567489649 1.
 36.2 1.380709501593 1.
 37.2 1.380851513537 1.
 38.2 1.380993525481 1.
 39.2 1.381135537425 1.
 40.2 1.381277549369 1.
 41.2 1.381419561313 1.
 42.2 1.381561573257 1.
 43.2 1.381703585201 1.
 44.2 1.381845597145 1.
 45.2 1.381987609089 1.
 46.2 1.382129621033 1.
 47.2 1.382271632977 1.
 48.2 1.382413644921 1.
 49.2 1.382555656865 1.
 50.2 1.382697668809 1.
 51.2 1.382839680753 1.
 52.2 1.382981692697 1.
 53.2 1.383123704641 1.
 54.2 1.383265716585 1.
 55.2 1.383407728529 1.
 56.2 1.383549740473 1.
 57.2 1.383691752417 1.
 58.2 1.383833764361 1.
 59.2 1.383975776305 1.
 60.2 1.384117788249 1.
 61.2 1.384259800193 1.
 62.2 1.384401812137 1.
 63.2 1.384543824081 1.
 64.2 1.384685836025 1.
 65.2 1.384827847969 1.
 66.2 1.384969859913 1.
 67.2 1.385111871857 1.
 68.2 1.385253883801 1.
 69.2 1.385395895745 1.
 70.2 1.385537907689 1.
 71.2 1.385679919633 1.
 72.2 1.385821931577 1.
 73.2 1.385963943521 1.
 74.2 1.386105955465 1.
 75.2 1.386247967409 1.
 76.2 1.386389979353 1.
 77.2 1.386531991297 1.
 78.2 1.386674003241 1.
 79.2 1.386816015185 1.
 80.2 1.386958027129 1.
 81.2 1.387099999073 1.
 82.2 1.387242011017 1.
 83.2 1.387384022961 1.
 84.2 1.387526034905 1.
 85.2 1.387668046849 1.
 86.2 1.387810058793 1.
 87.2 1.387952070737 1.
 88.2 1.388094082681 1.
 89.2 1.388236094625 1.
 90.2 1.388378106569 1.
 91.2 1.388520118513 1.
 92.2 1.388662130457 1.
 93.2 1.388804142401 1.
 94.2 1.388946154345 1.
 95.2 1.389088166289 1.
 96.2 1.389230178233 1.
 97.2 1.389372190177 1.
 98.2 1.389514202121 1.
 99.2 1.389656214065 1.
 100.2 1.389798226009 1.

```

P(X) = 1.373953326 + -.000126070 X
P(X) = 1.373986553 + .000095410 X + -.000001507 X**2
P(X) = 1.373982056 + .000153352 X + -.000002530 X**2 + .000000000 X**3
P(X) = 1.373546206 + .000122771 X + -.0000004559 X**2 -.0000000056 X**3 + .000000000000310 X**4
P(X) = 1.374427026 + .000302608 X + -.000010451 X**2 .0000001550 X**3 + -.00000000011197 X**4 +
.00000000000031 X**5
P(X) = 1.375986917 + -.000056424 X + .000011941 X**2
-.000000552 X**3 + .000000078679 X**4 + -.0000000000000303 X**5 + .000000000000000000118 X**6

```

ERROR CHECK
0.20.
1.35 .005

100

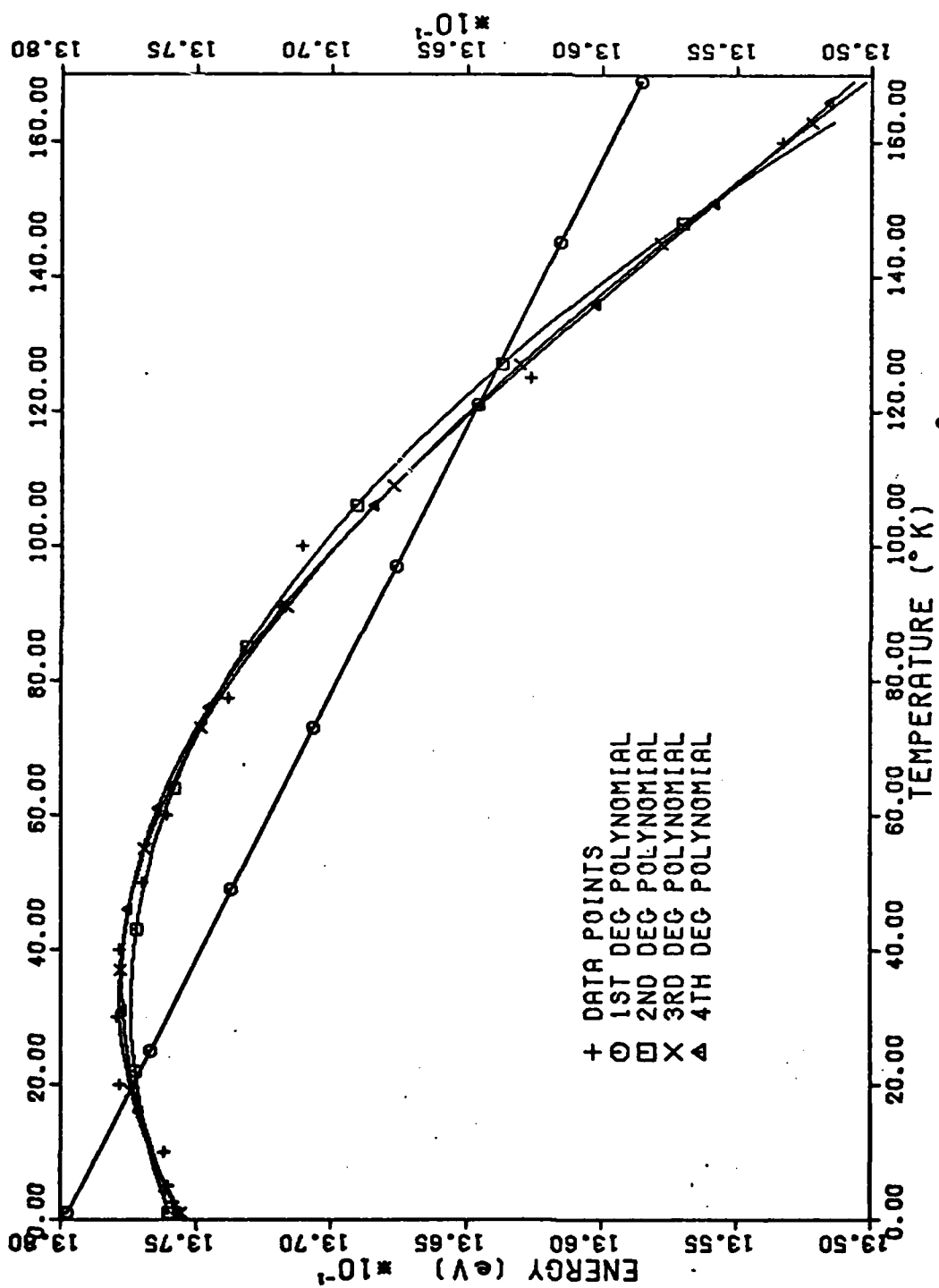


Figure A-2 Temperature Dependence of Donor-Acceptor (8900 Å) Peak Energy in Undoped InP

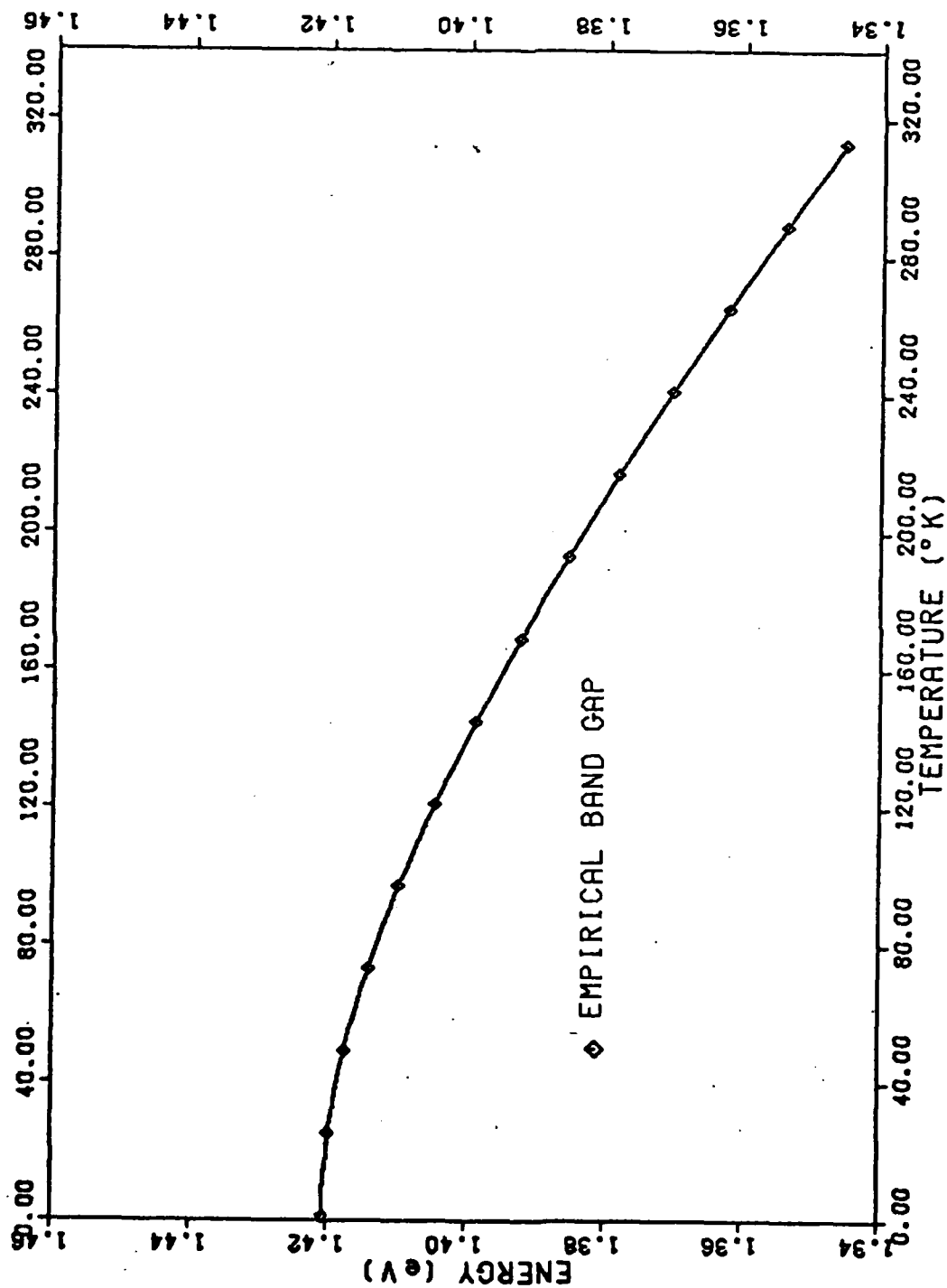


Figure A-3 Empirical Band Gap

Appendix B

Photoluminescence Below 9700 Å of Undoped InP from 2.69°K to 225°K

Identification of anomalies in spectra:

- 1 Accidental movement of equipment
- 2 Laser turned off due to low water pressure or overheating
- 3 System temperature restabilized
- 4 Calibration lamp turned off
- 5 Unknown noise
- 6 Secondary peaks from krypton calibration lamp

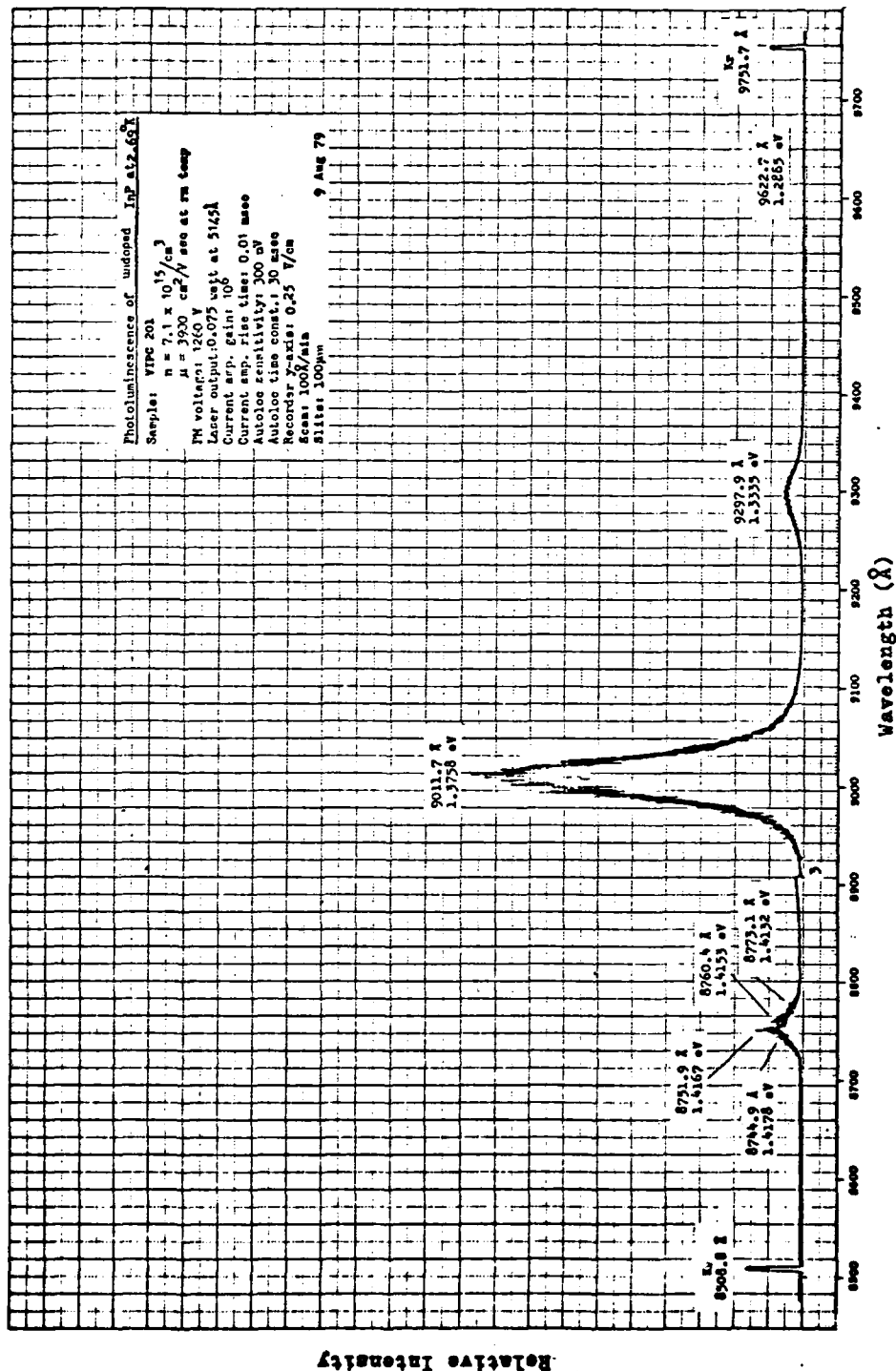


Figure B-1 Photoluminescence Below 9700 Å of Undoped InP at 2.69°K

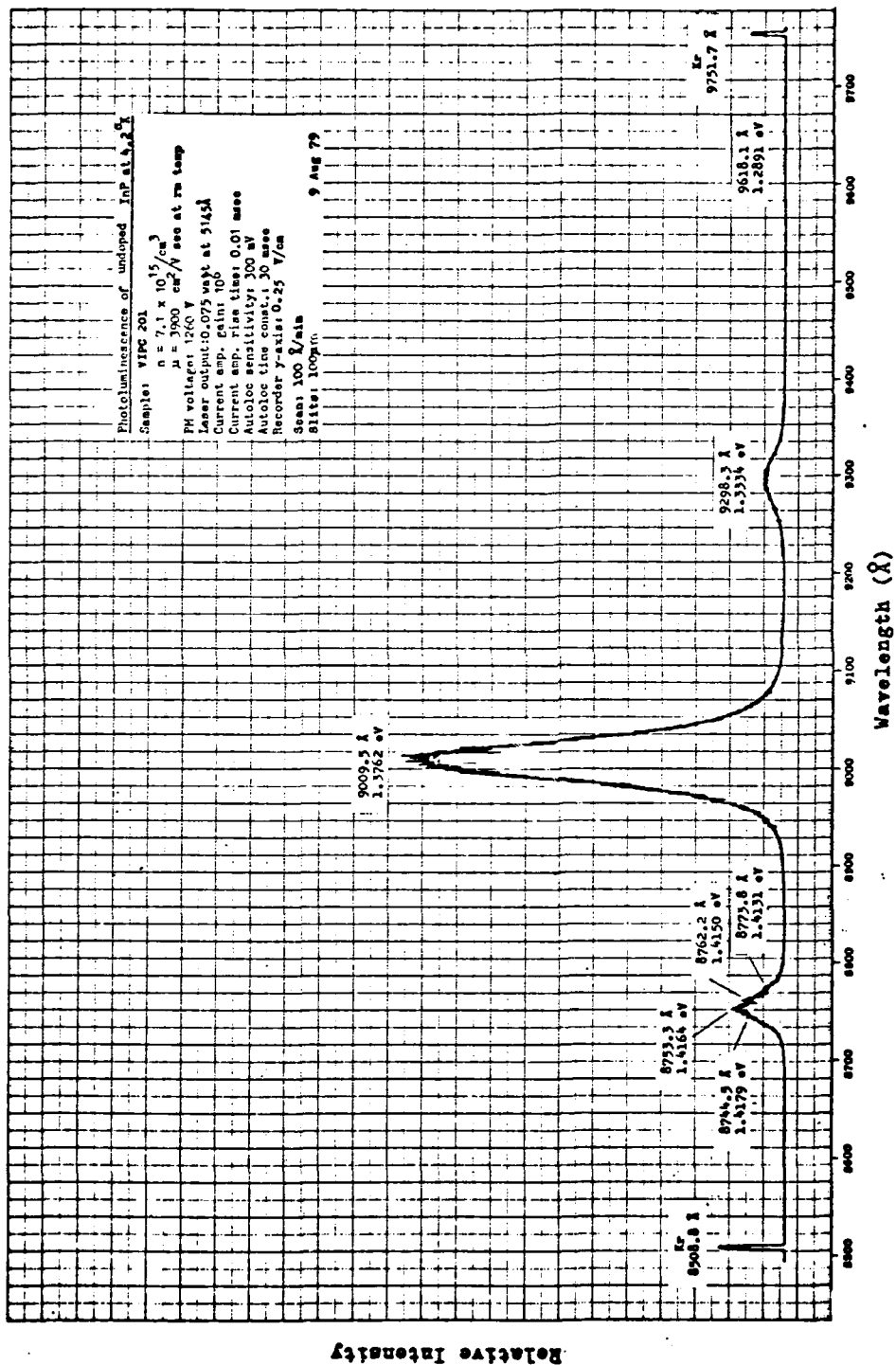


Figure B-2 Photoluminescence Below 9700 Å of Undoped InP at 4.2°K

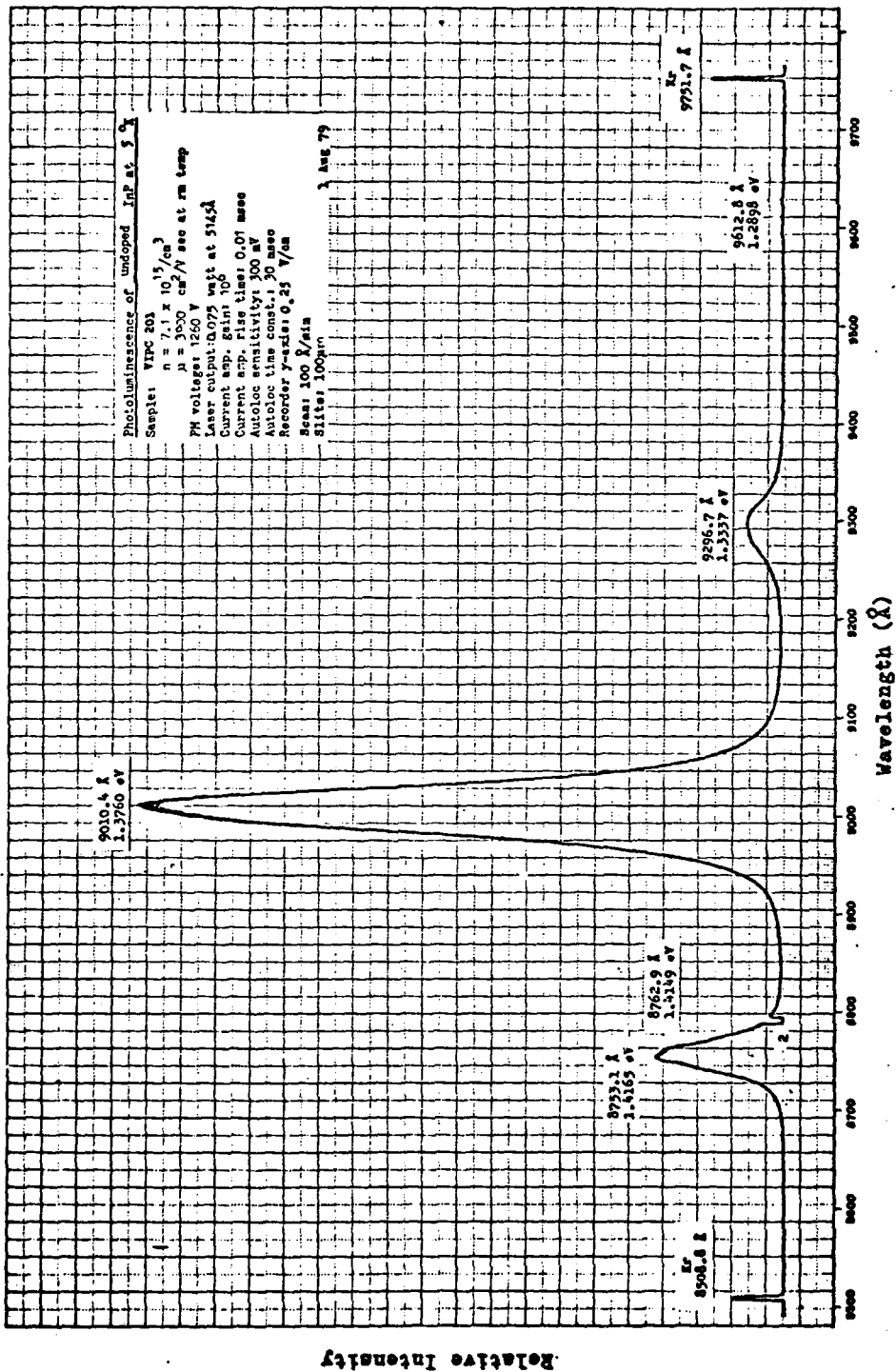


Figure B-3 Photoluminescence Below 9700 Å of Undoped InP at 5°K

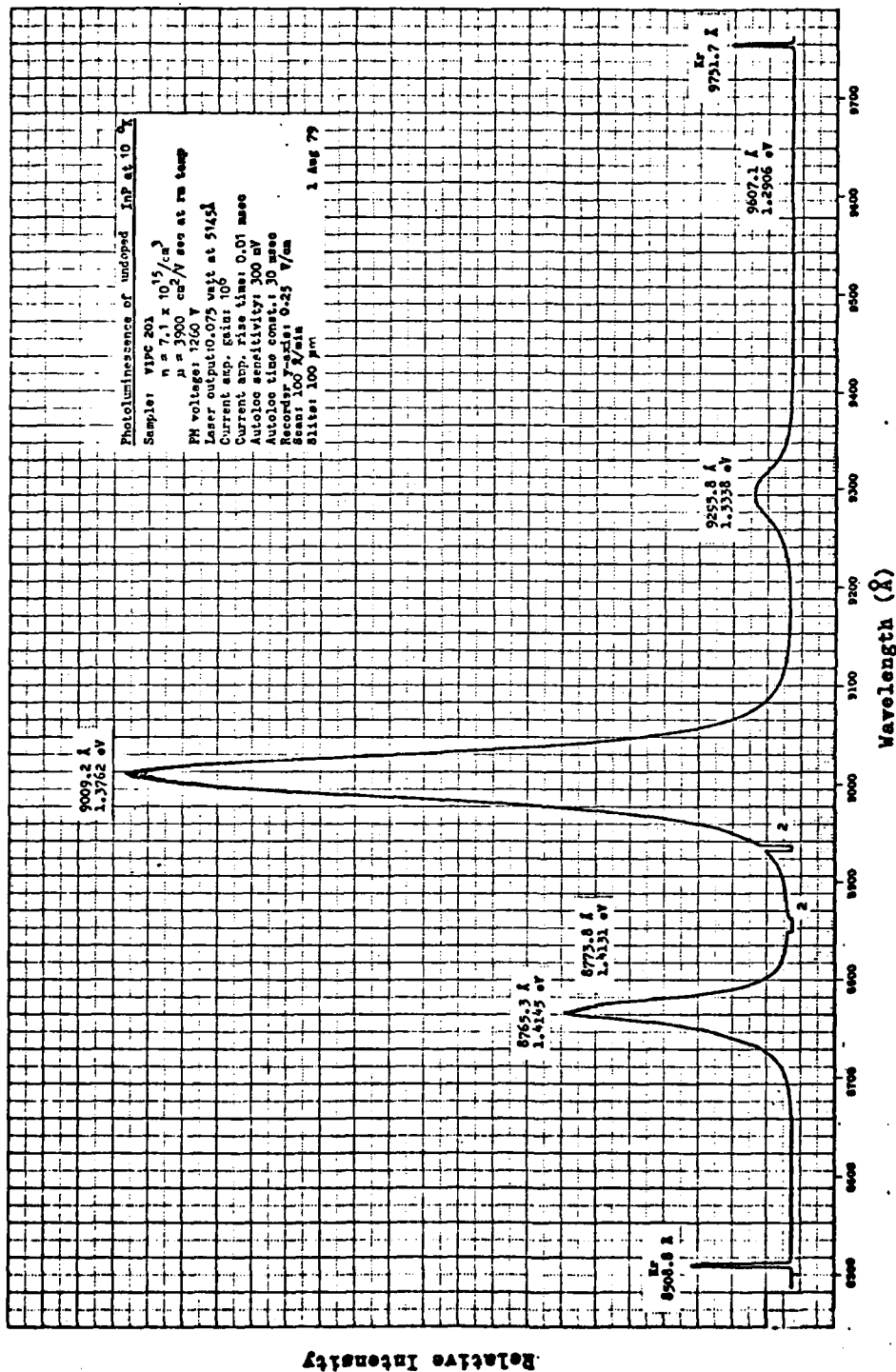


Figure B-4 Photoluminescence Below 9700 Å of Undoped InP at 10°K

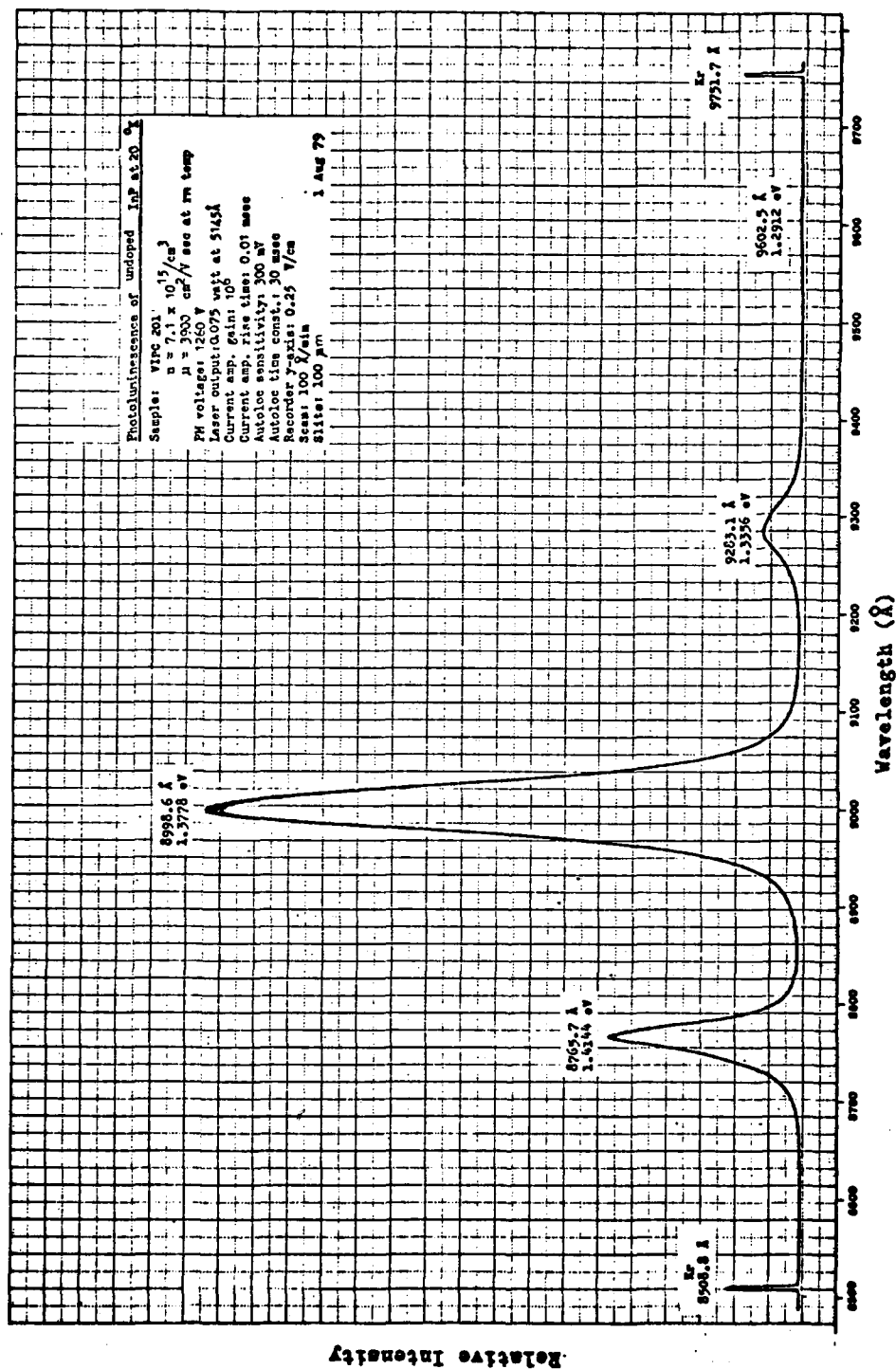


Figure B-5 Photoluminescence Below 9700 Å of Undoped InP at 20 °K

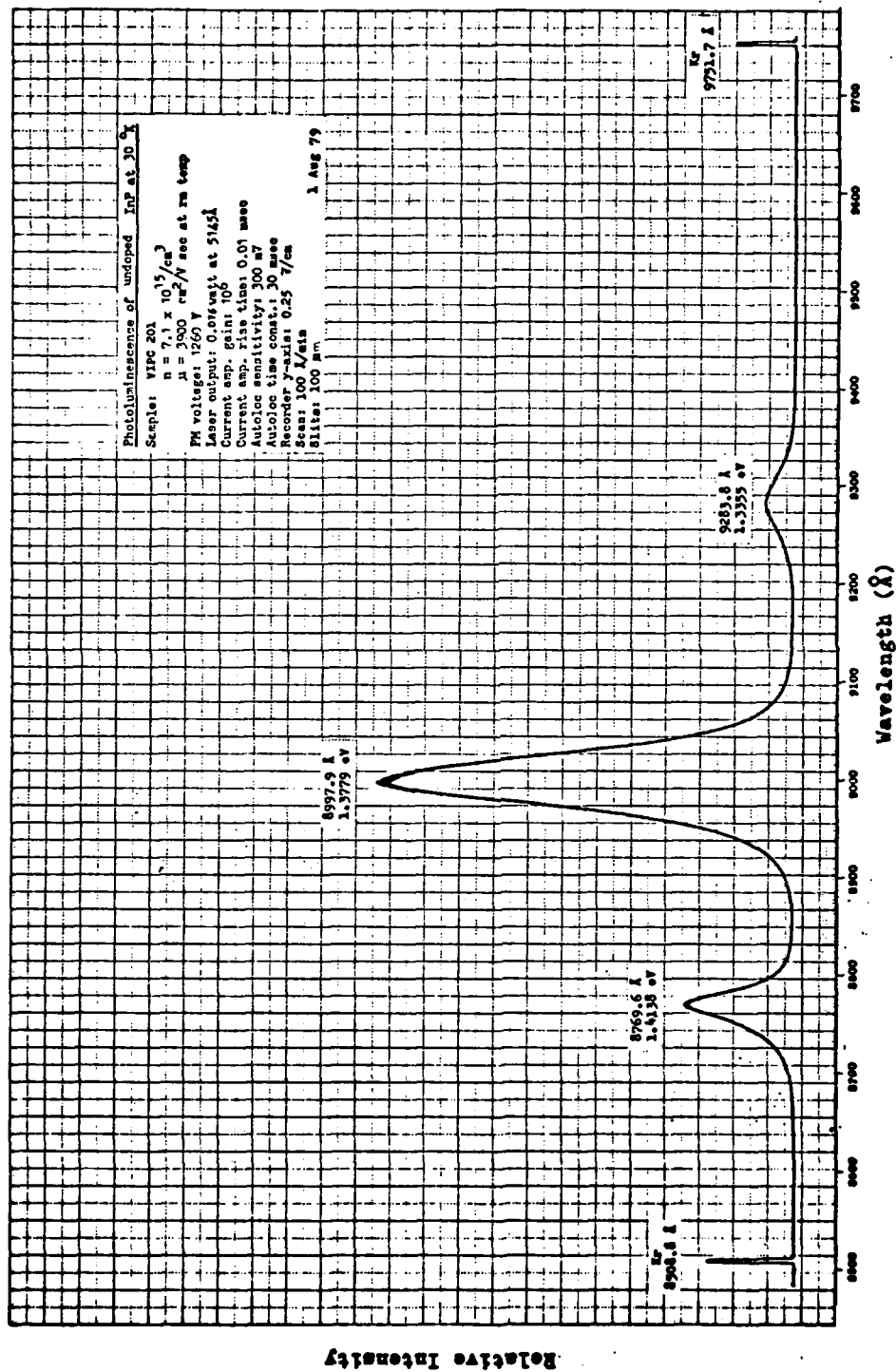


Figure B-6 Photoluminescence Below 9700 Å of Undoped InP at 30 °K

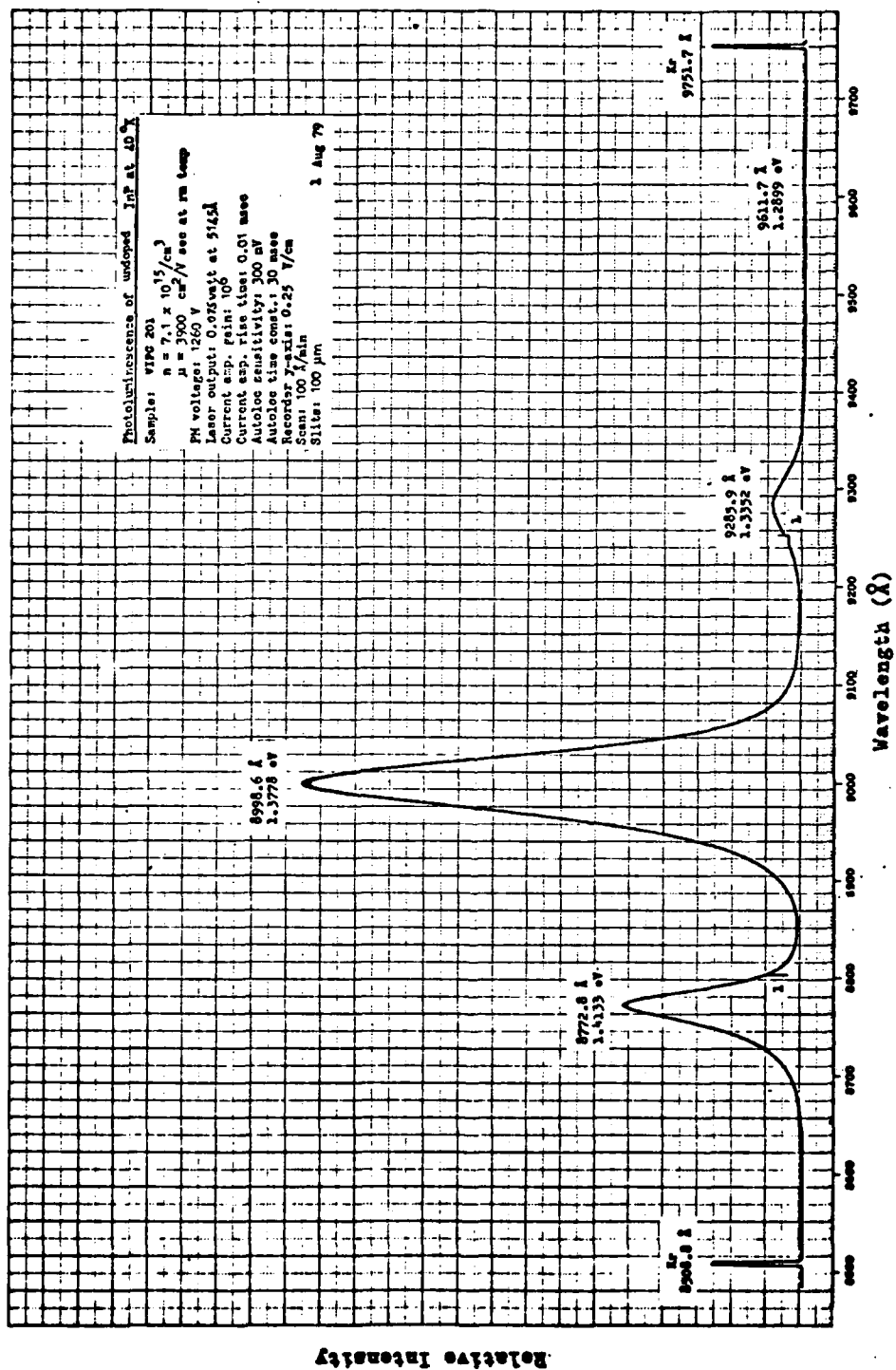


Figure B-7 Photoluminescence Below 9700 Å of Undoped InP at 40°K

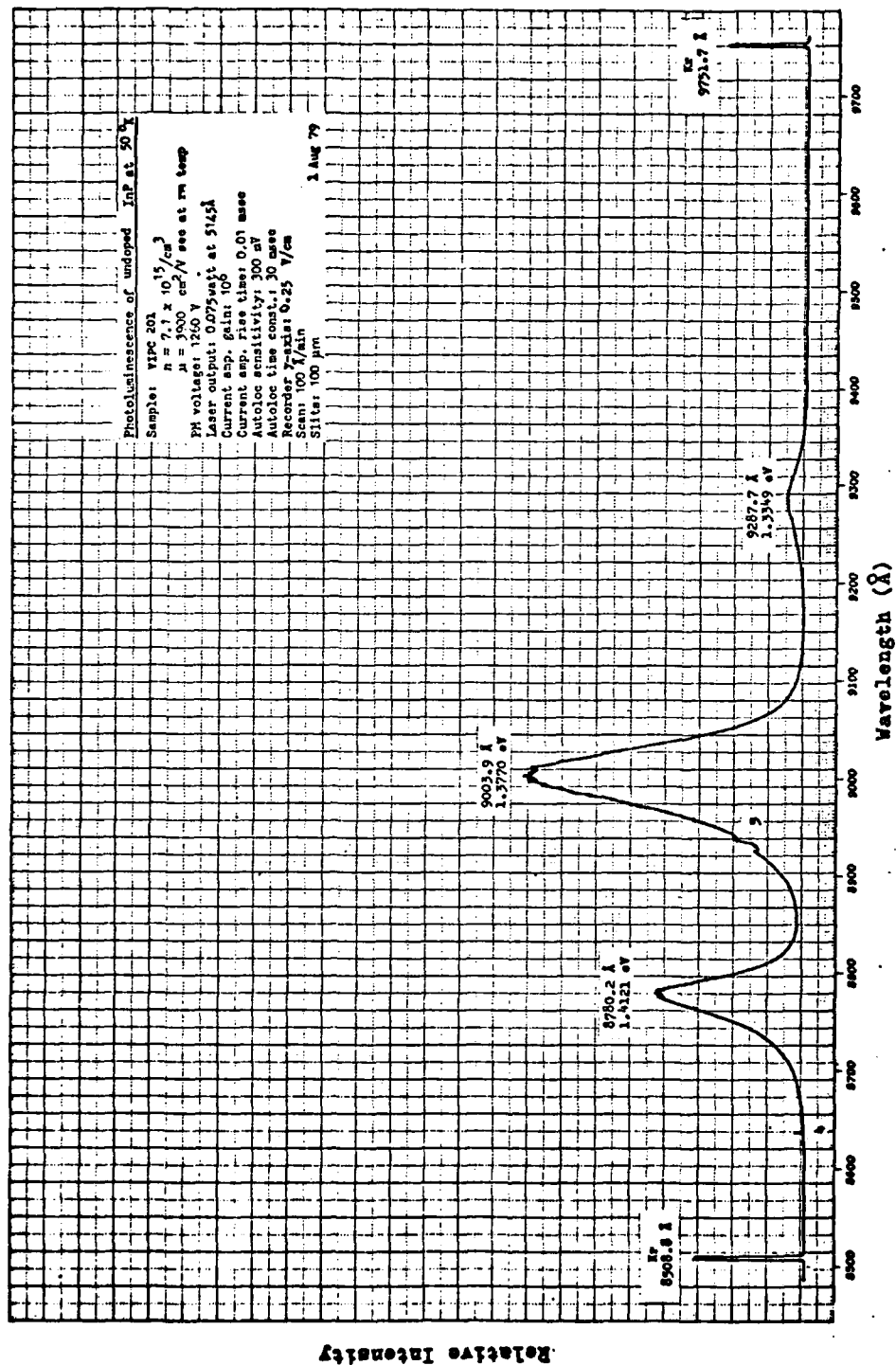


Figure B-8 Photoluminescence Below 9700 Å of Undoped InP at 50°K

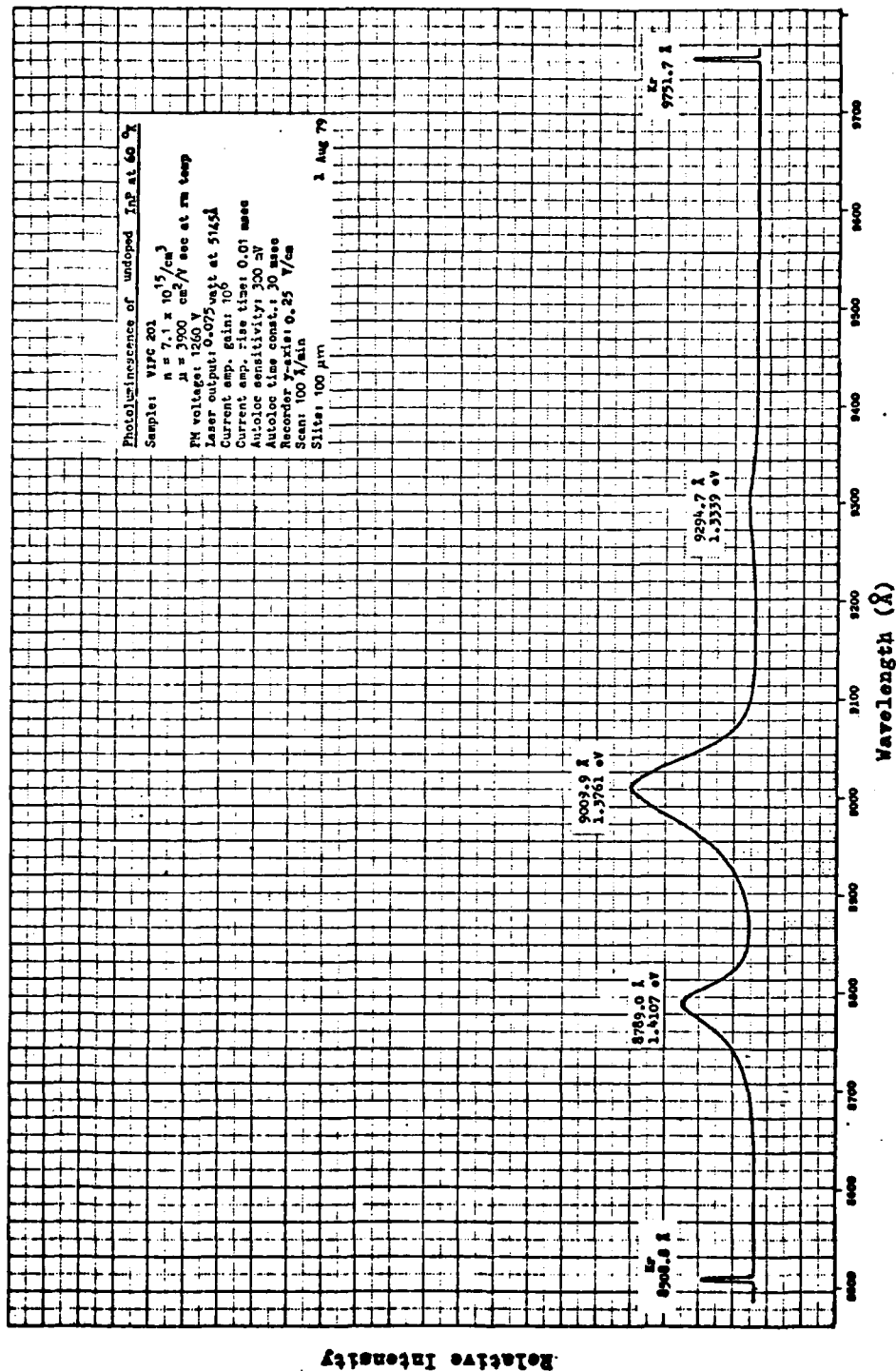


Figure B-9 Photoluminescence Below 9700 Å of Undoped InP at 60°K

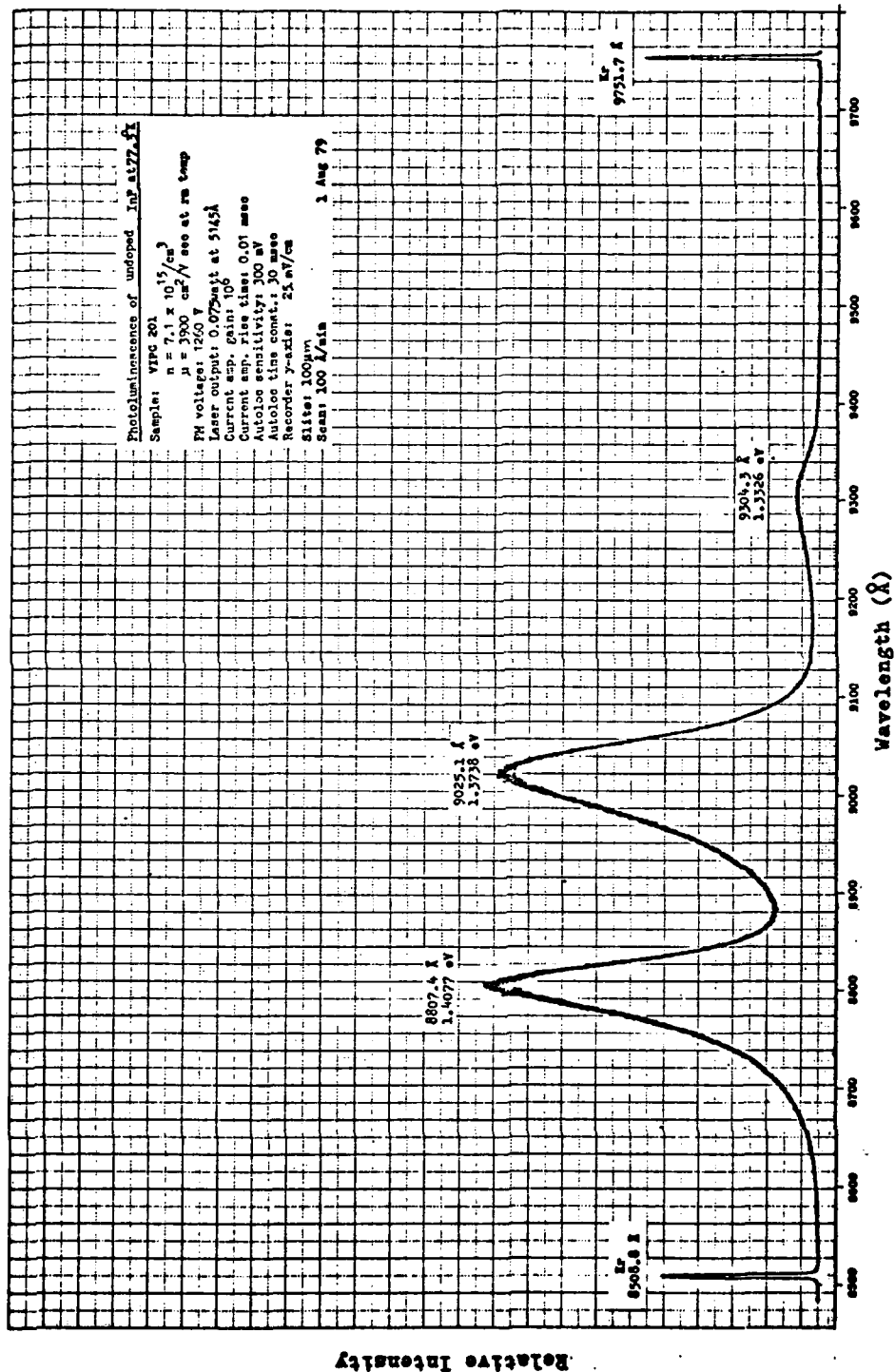


Figure B-10 Photoluminescence Below 9700 Å of Undoped InP at 77.3°K

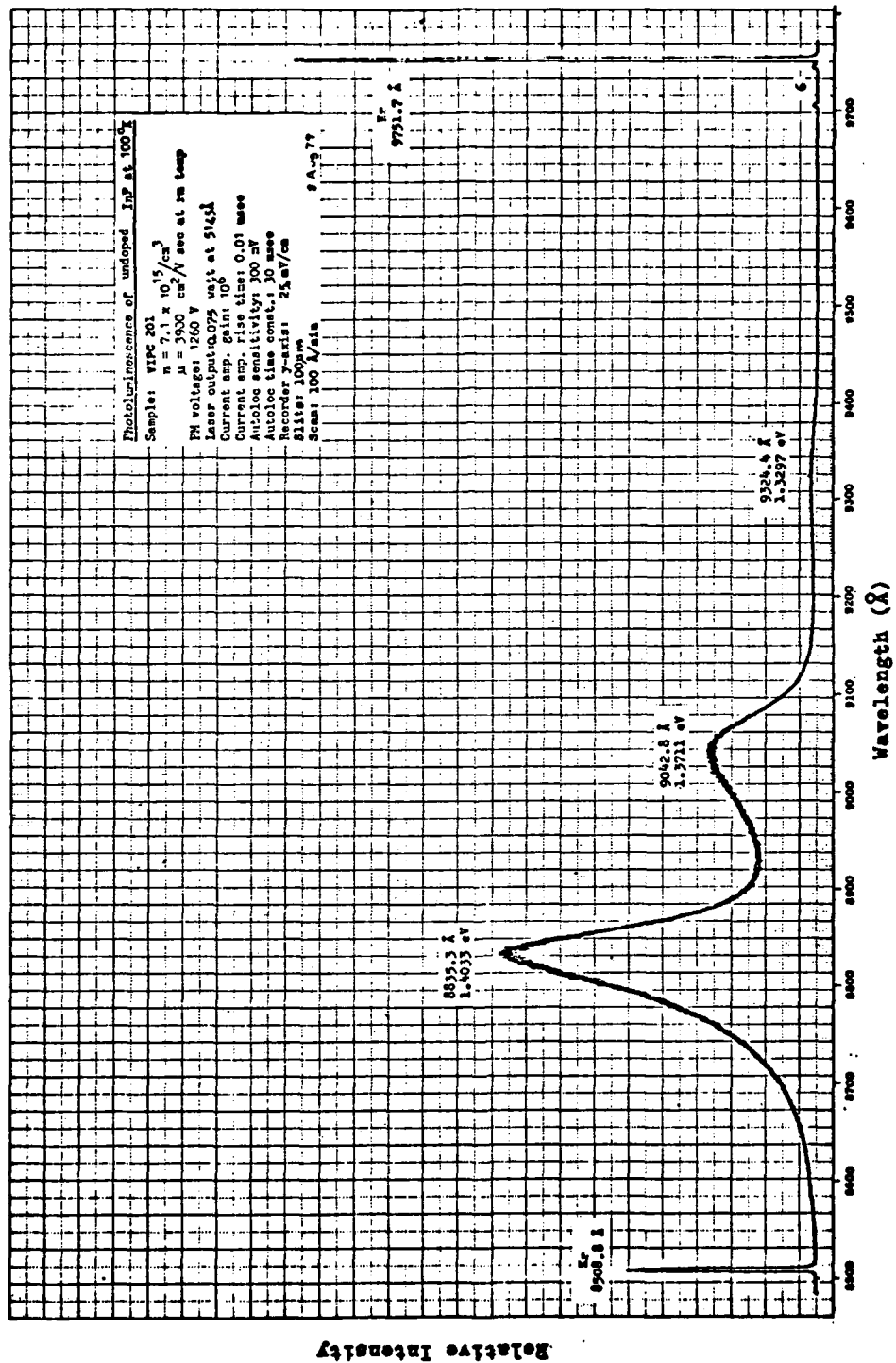


Figure B-11 Photoluminescence Below 9700 Å of Undoped InP at 100°K

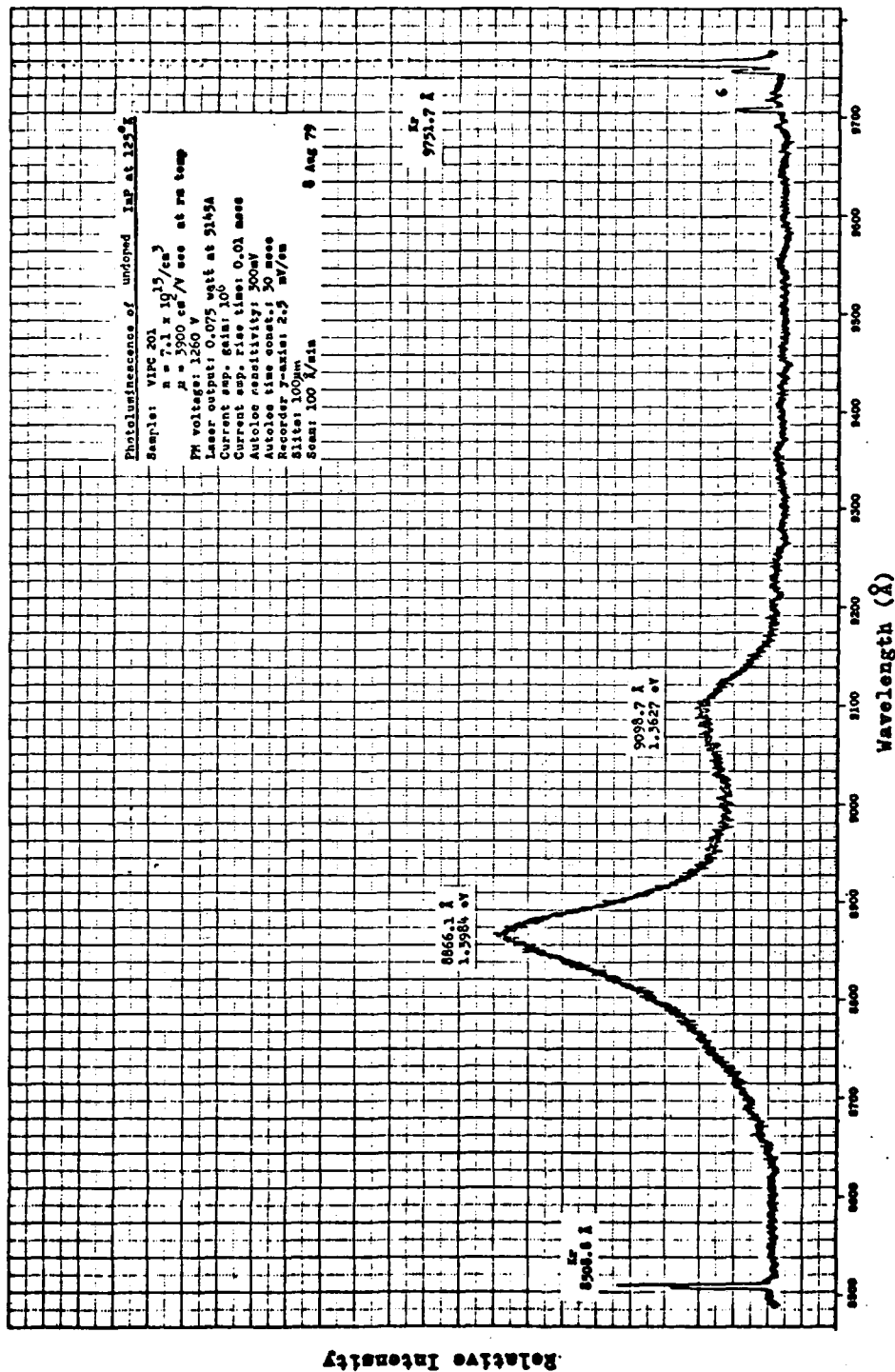


Figure B-12 Photoluminescence Below 9700 Å of Undoped InP at 125°K

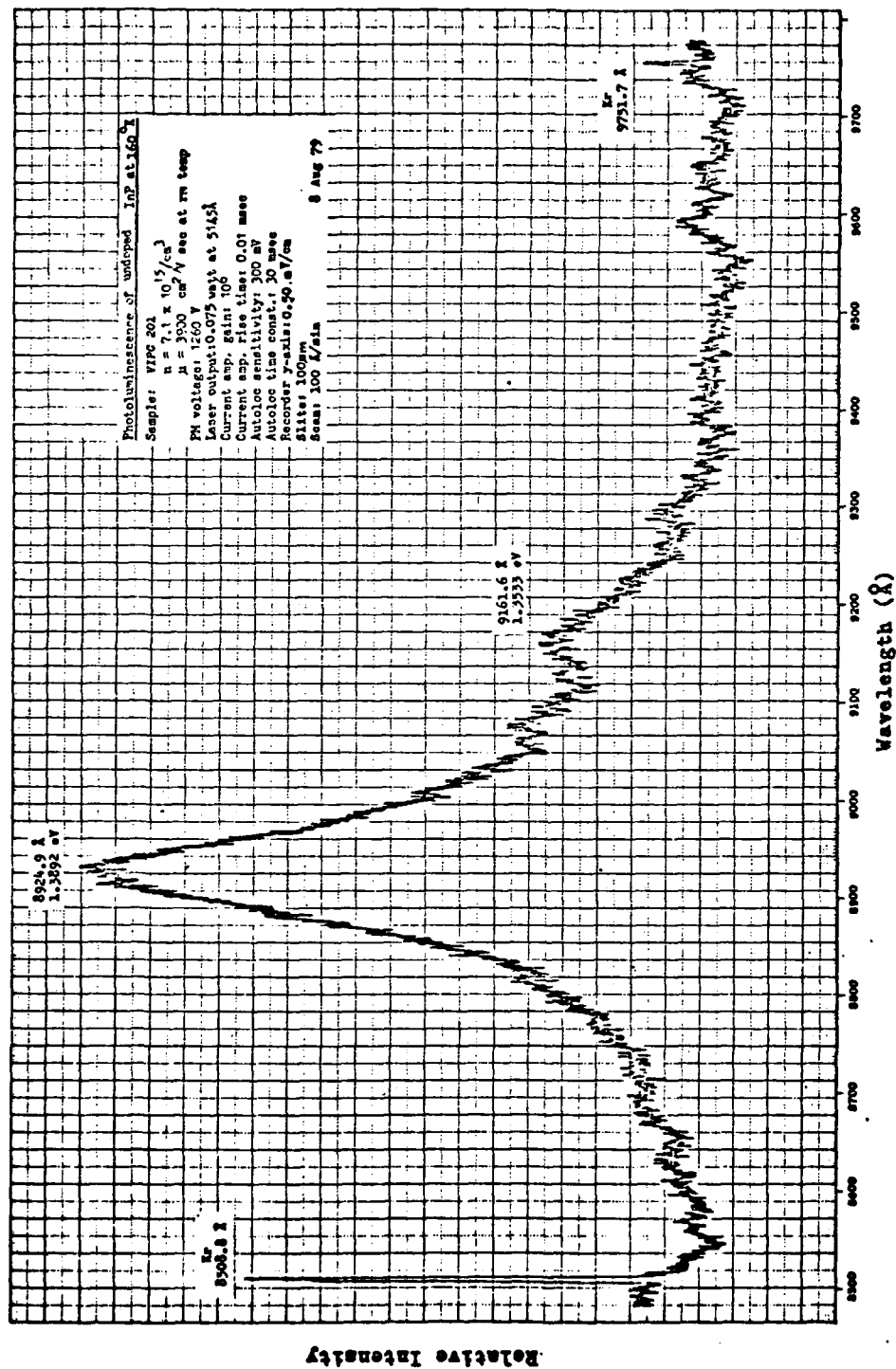


Figure B-13 Photoluminescence Below 9700 Å of Undoped InP at 160°K

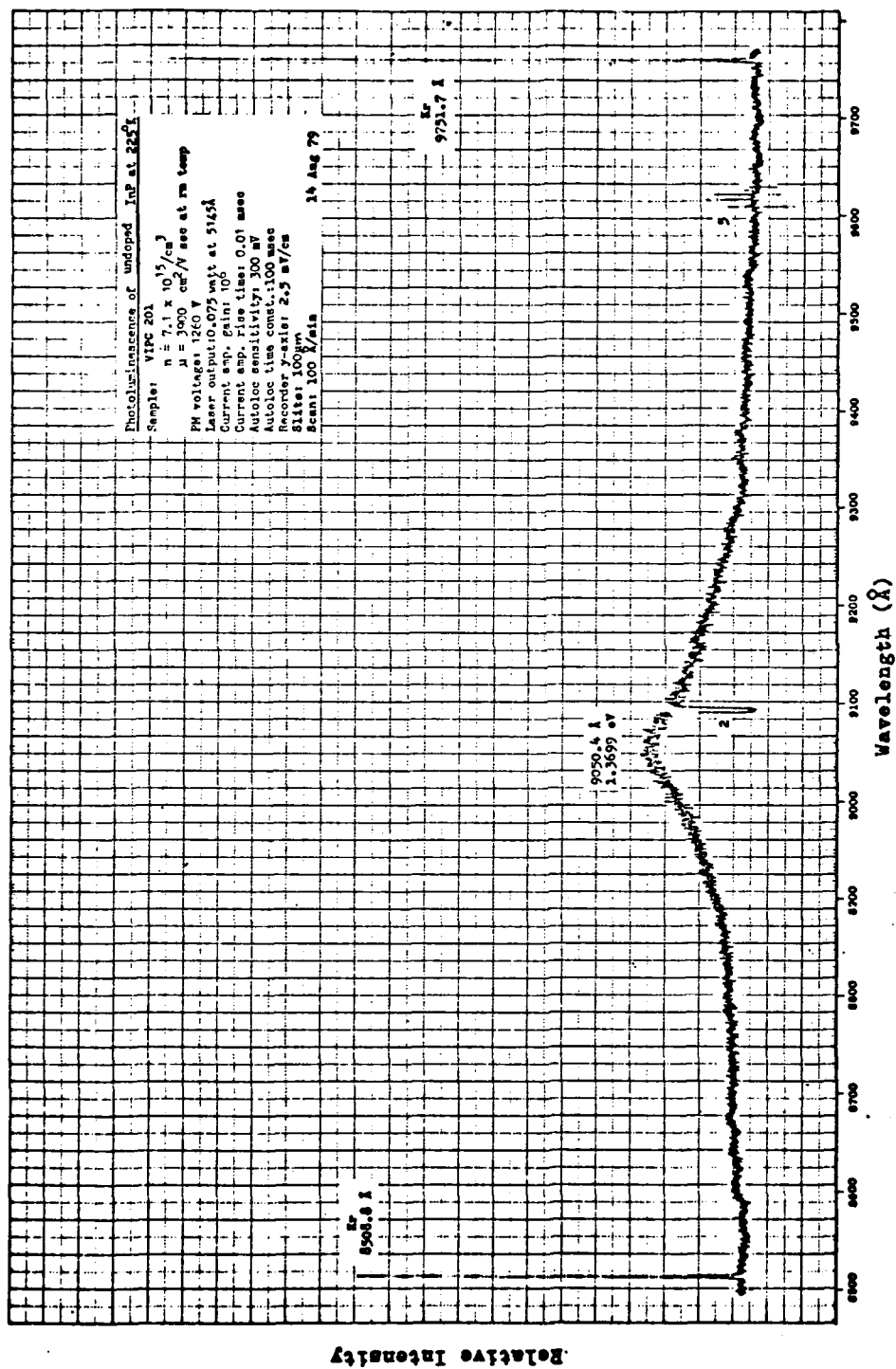


Figure B -14 Photoluminescence Below 9700 Å of Undoped InP at 225°K

Appendix C

Photoluminescence Between 9100 Å and 11700 Å of Undoped InP
from 2.22°K to 100°K

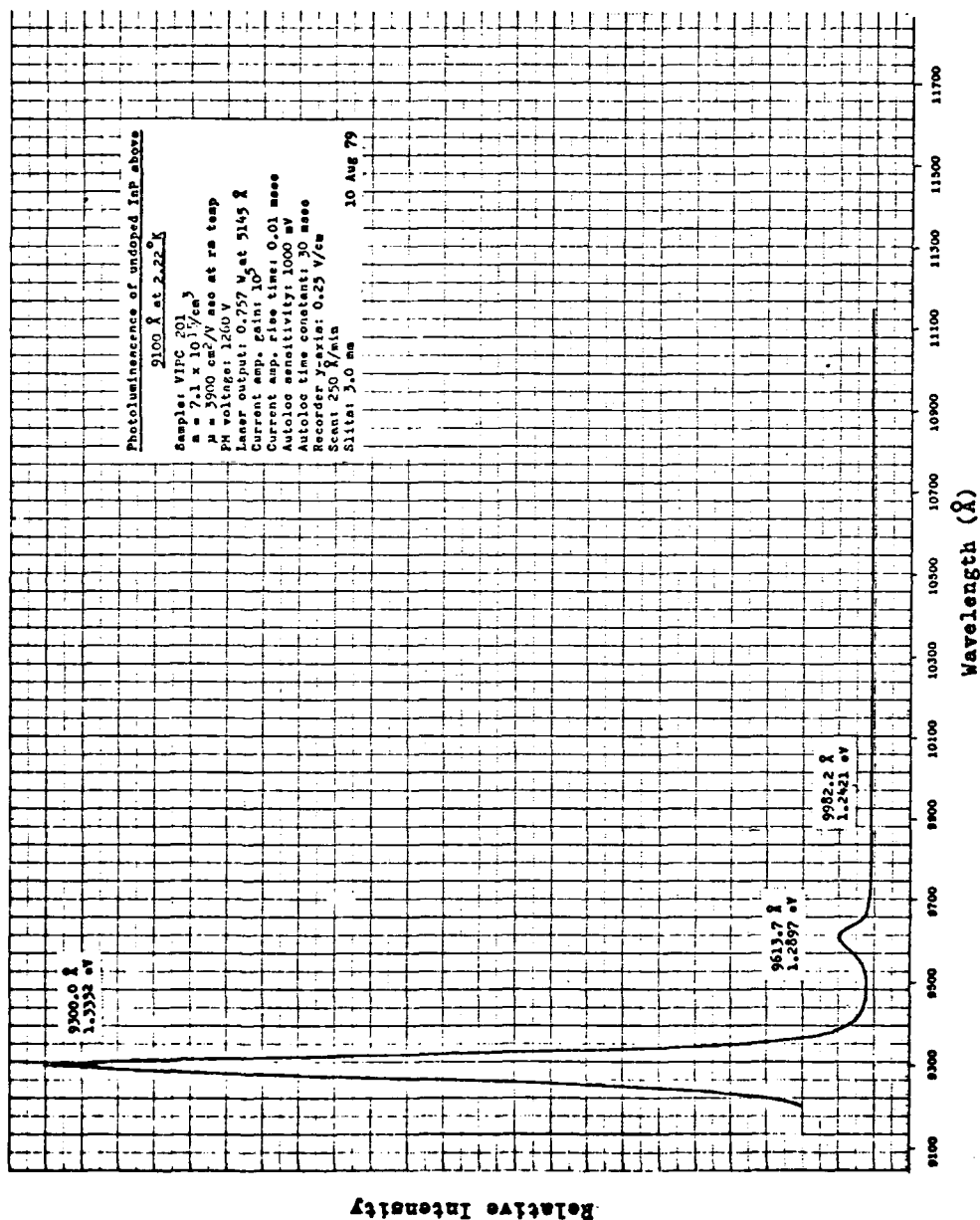


Figure C-1 Photoluminescence Between 9100 Å and 11100 Å of Undoped InP at 2.22°K

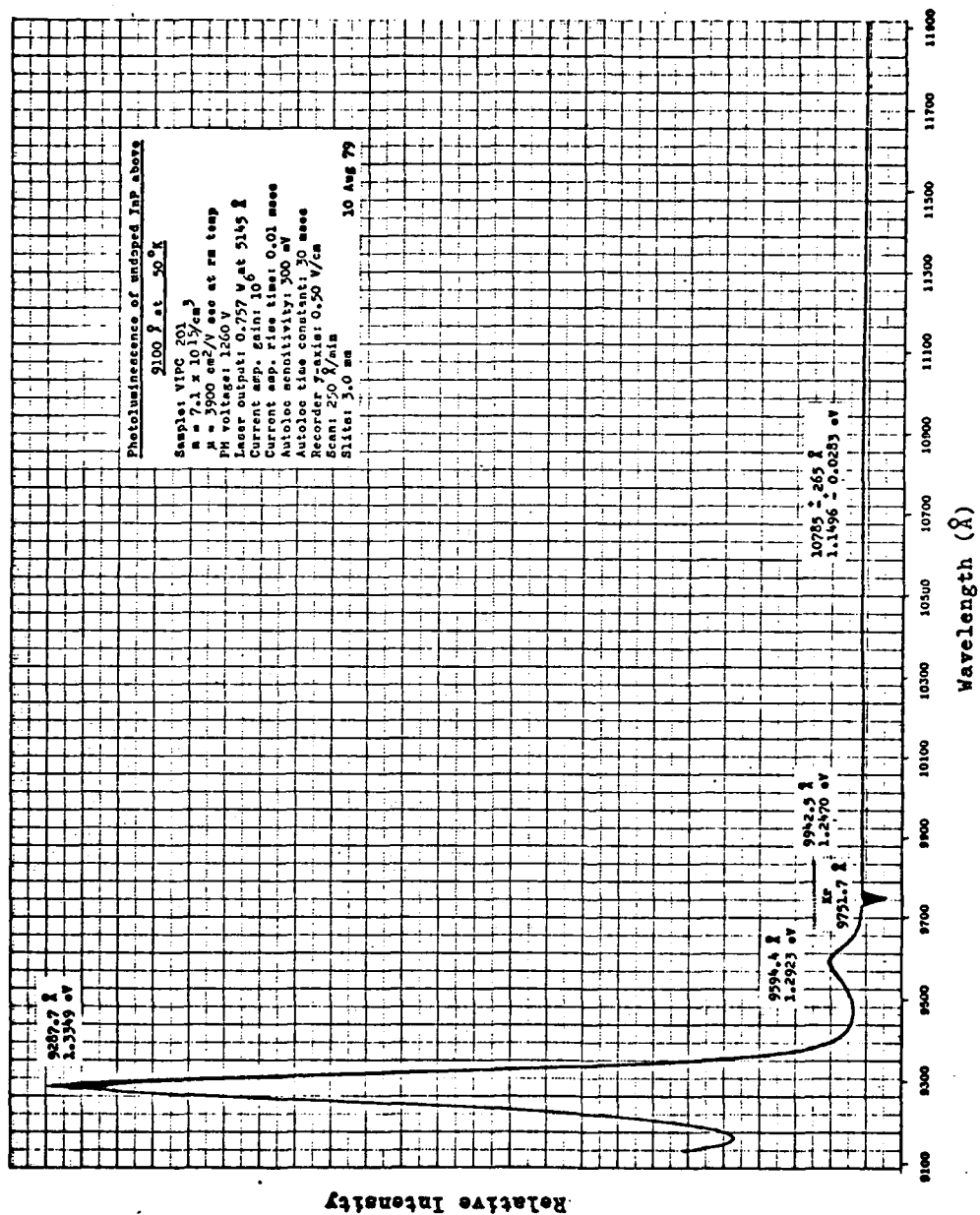


Figure C-2 Photoluminescence Between 9100 Å and 11900 Å of Undoped InP at 50°K

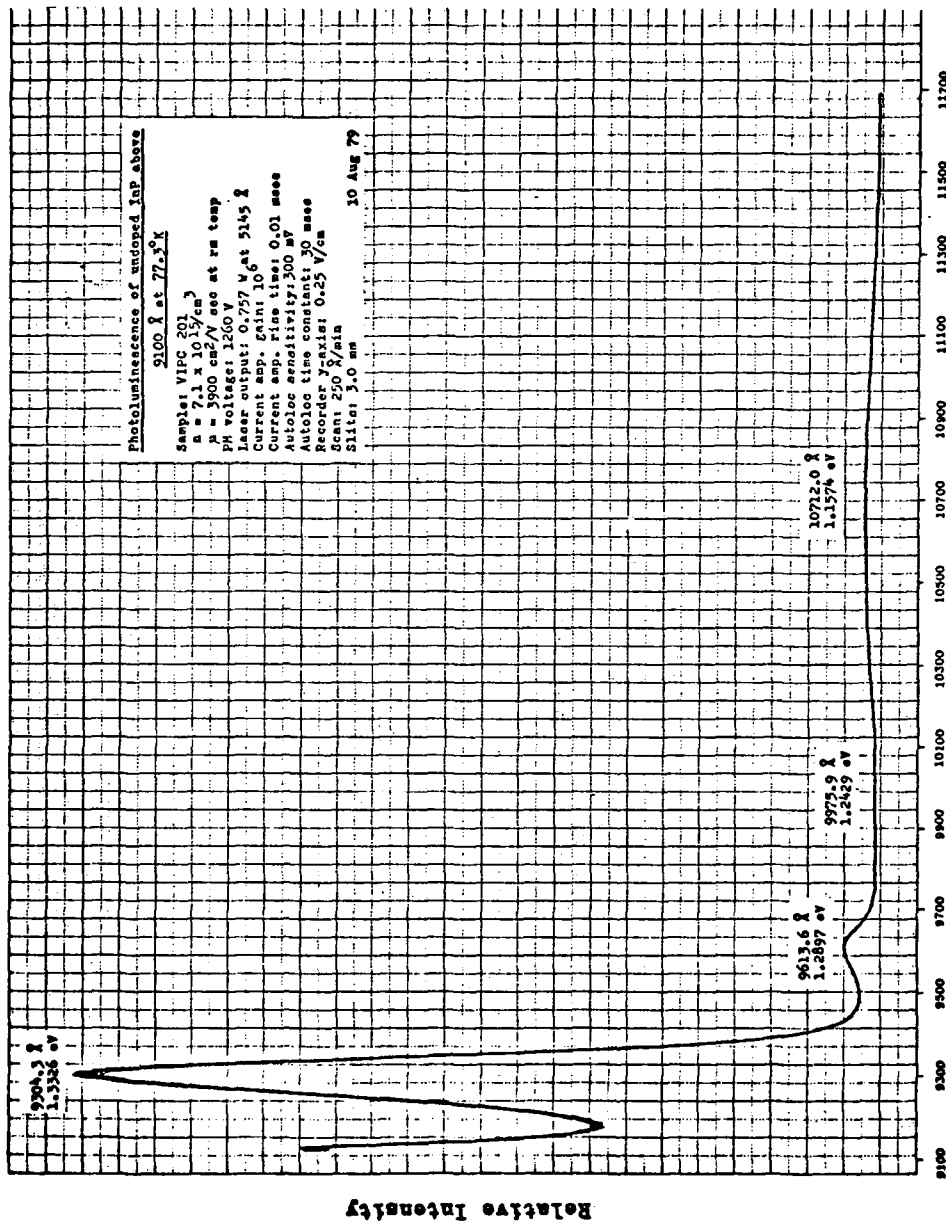


Figure C-3 Photoluminescence Between 9100 Å and 11700 Å of Undoped InP at 77.3°K

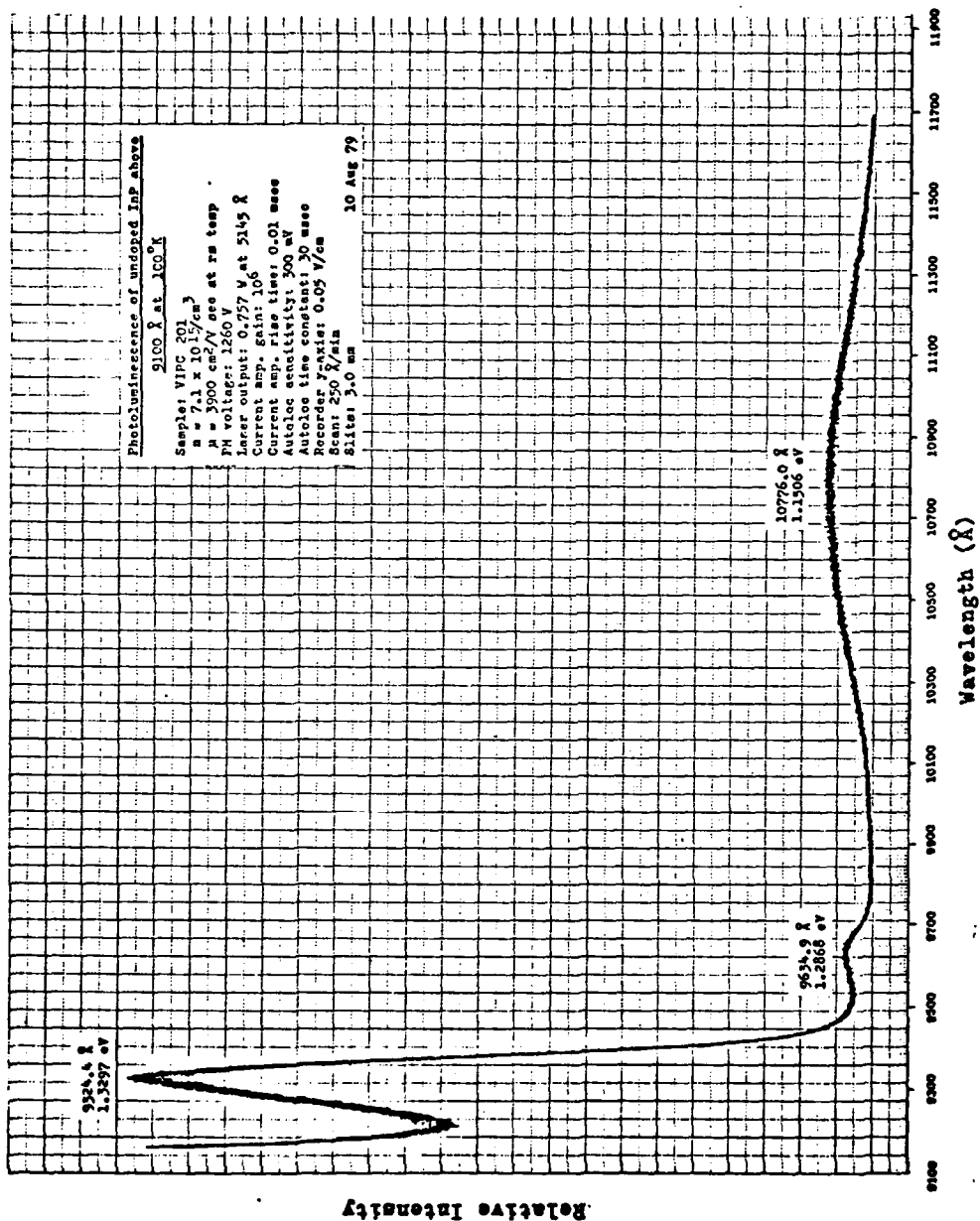


Figure C-4 Photoluminescence Between 9100 Å and 11700 Å of Undoped InP at 100°K

Appendix D

Photoluminescence Below 3.0 μm of Undoped InP at 162°K

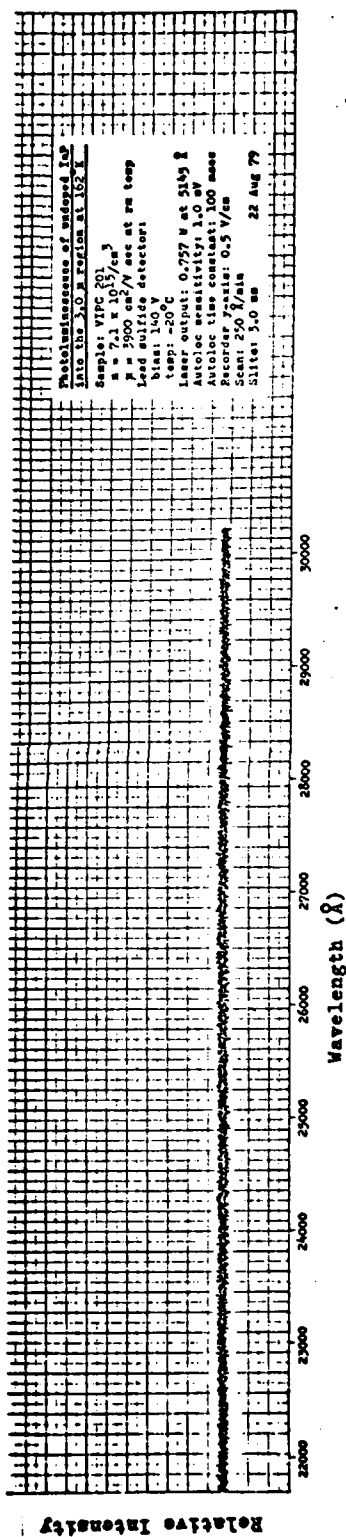
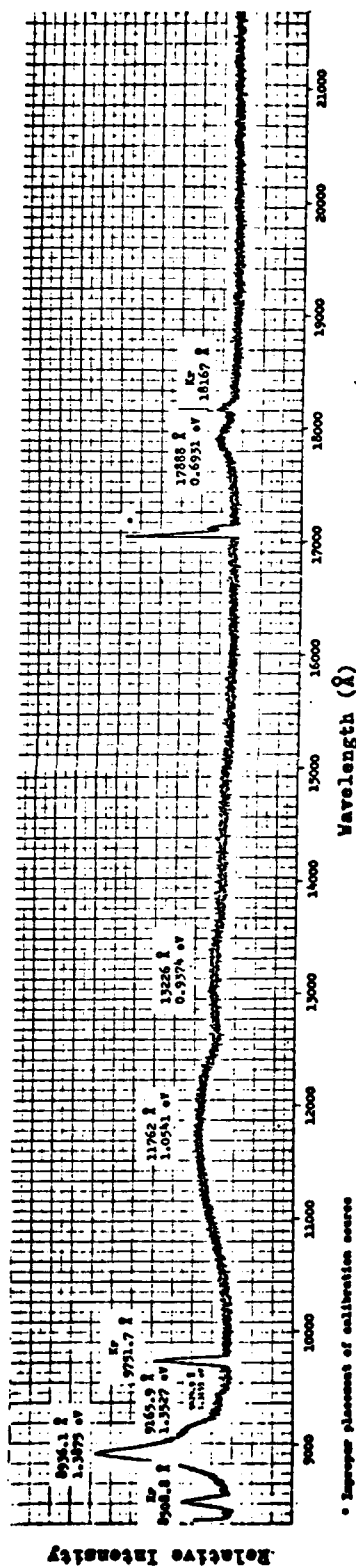


Figure D-1 Photoluminescence Below 3.0 μ of Undoped InP at 162°K

Appendix E

Photoluminescence Below 11700 Å of Semi-insulating InP:Fe from 4.2°K
to 100°K

Identification of anomalies in the spectra:

- 1 Laser turned off due to low water pressure or overheating
- 2 Unknown peak
- 3 Noise from x-y recorder
- (s) Shoulder

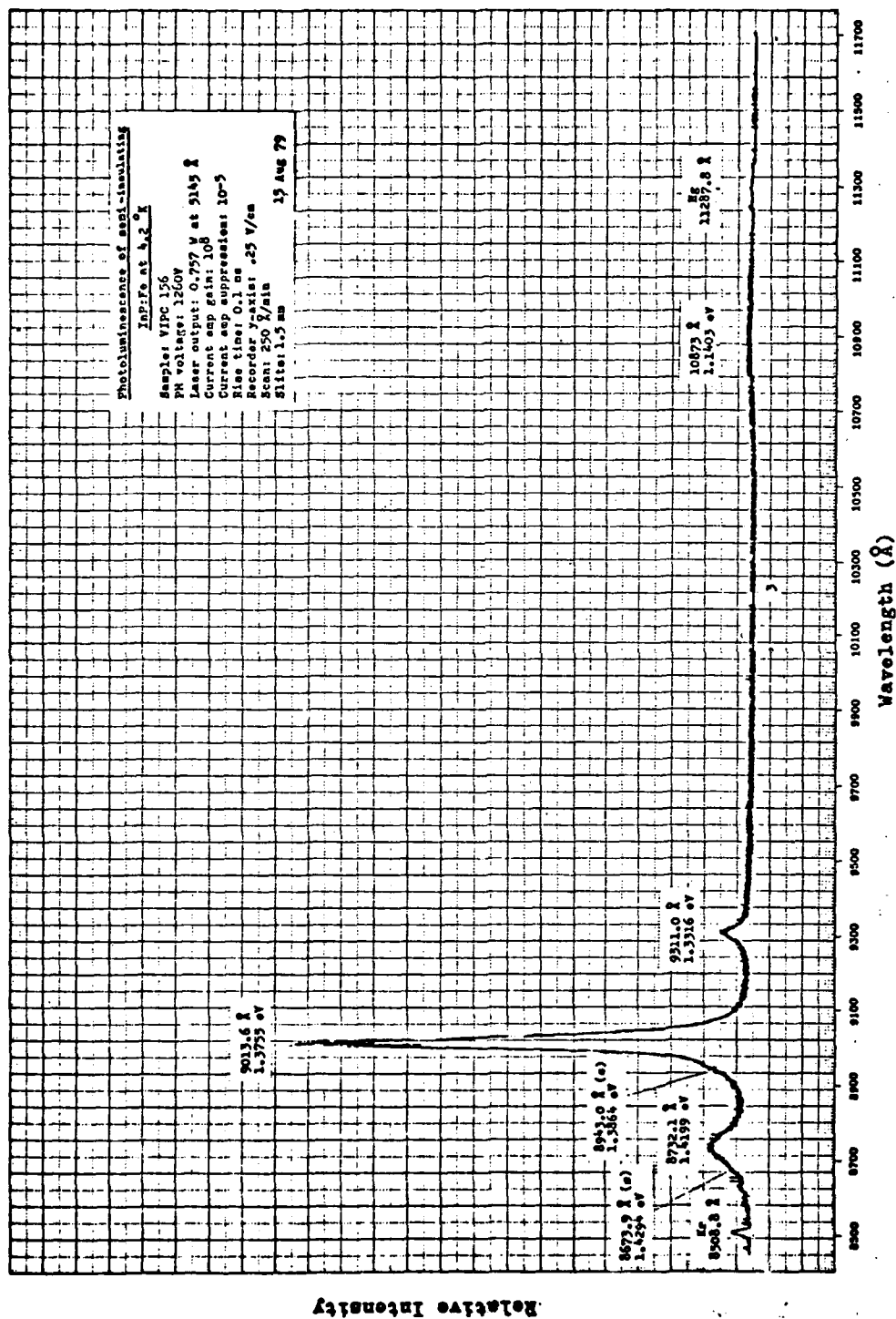


Figure E-1 Photoluminescence Below 11700 Å of Semi-insulating InP:Fe at 4.2°K

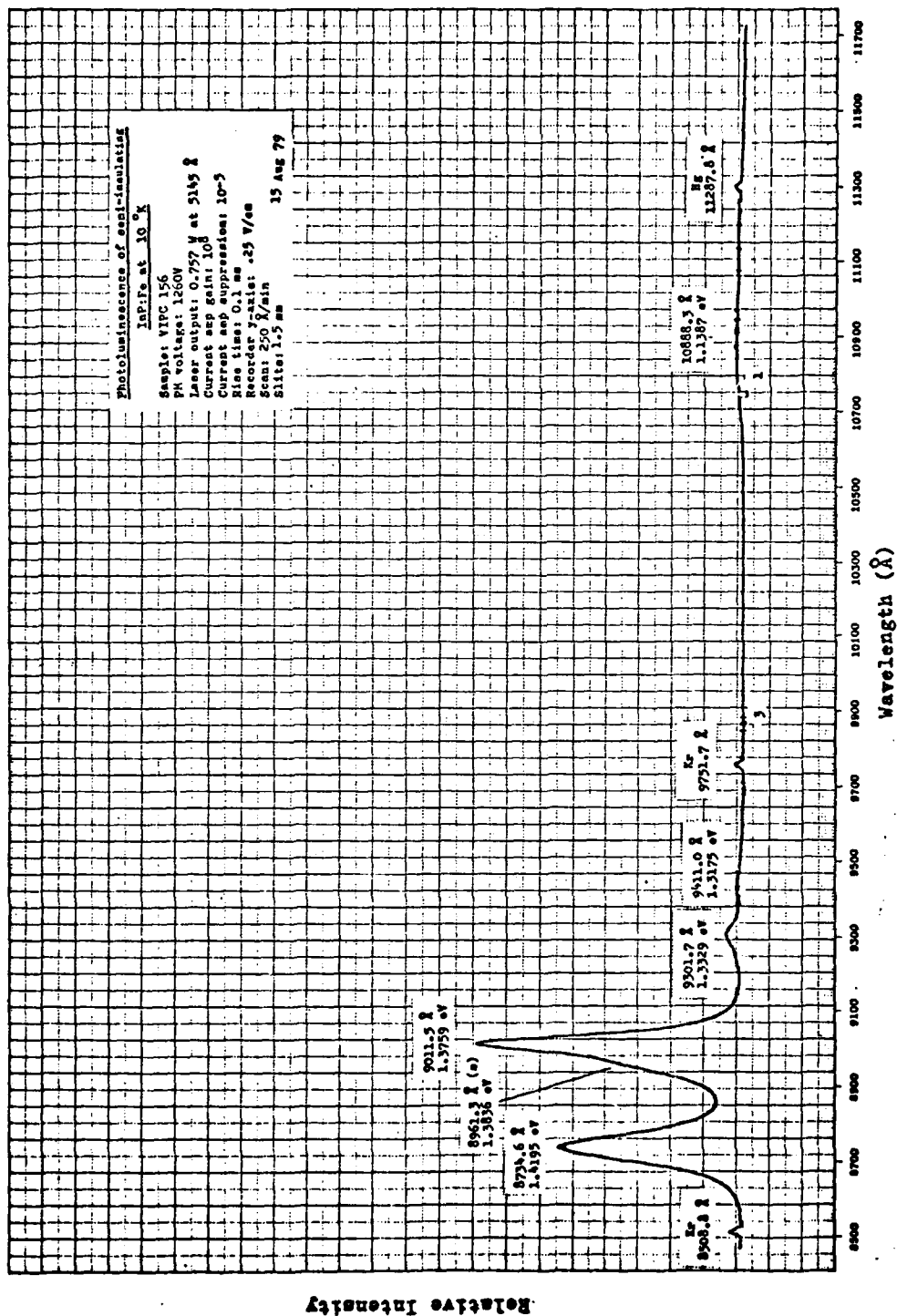


Figure E-2 Photoluminescence Below 11700 Å of Semi-insulating
InP:Fe at 10°K

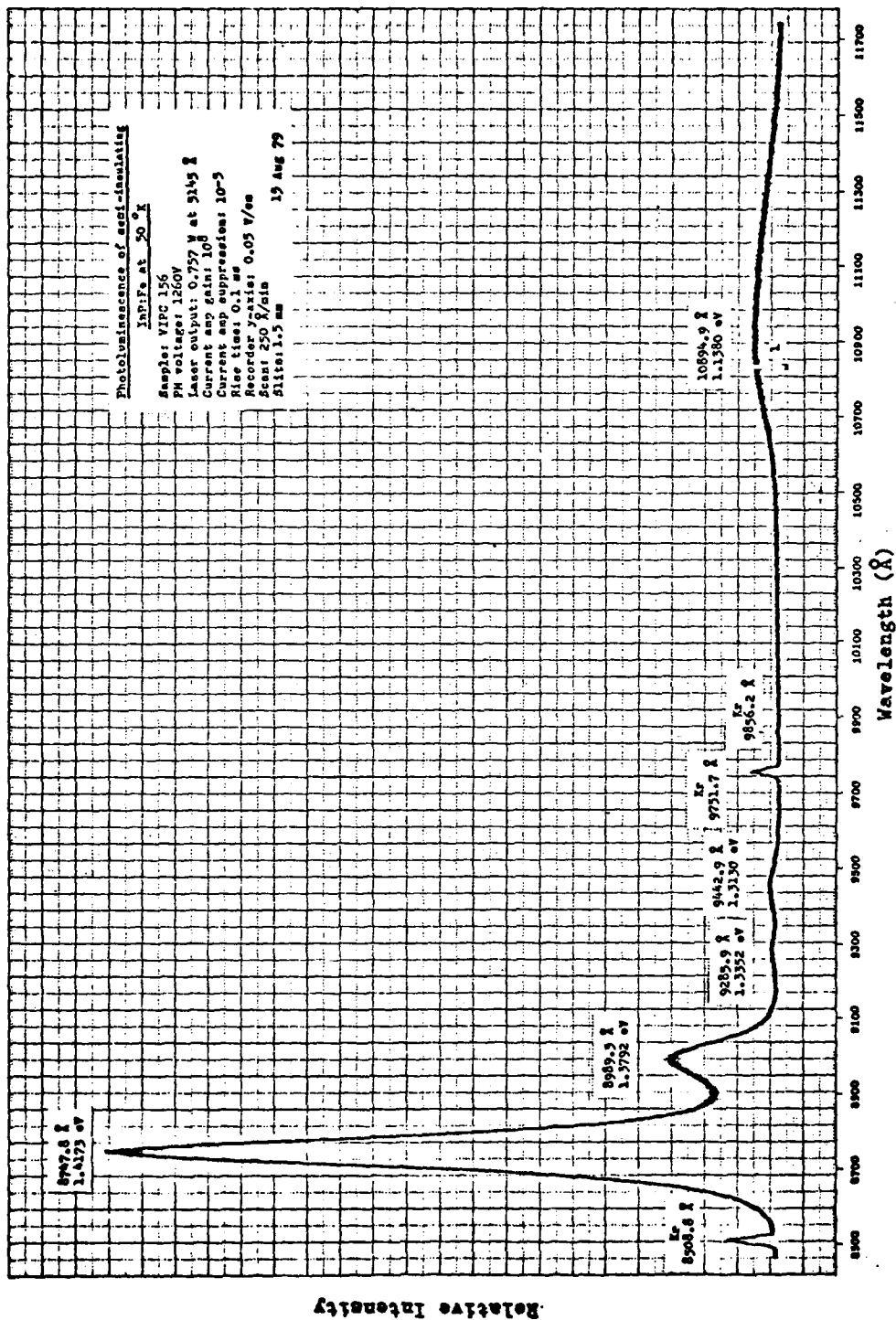


Figure E-3 Photoluminescence Below 11700 Å of Semi-insulating
InP:Fe at 50°K

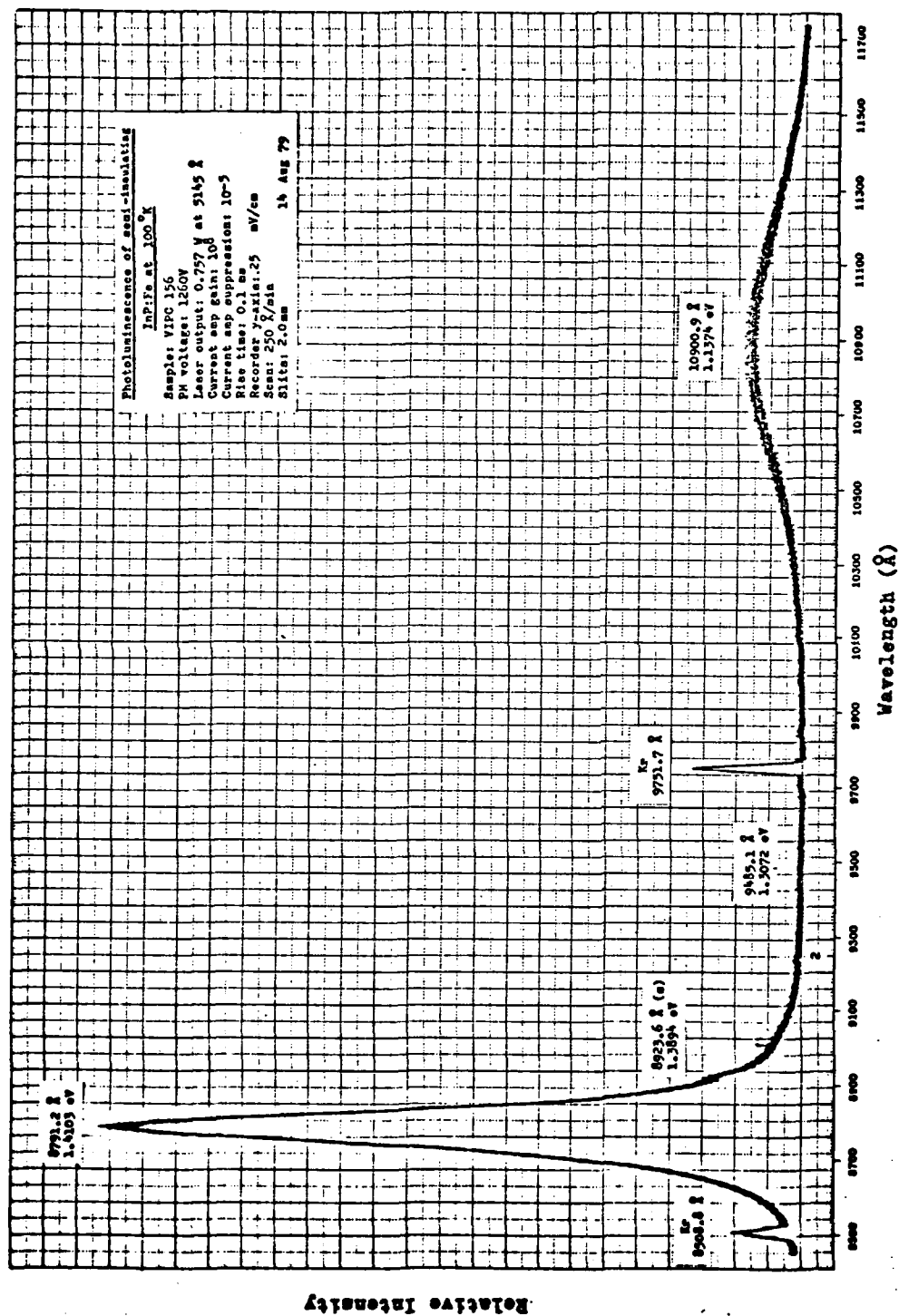


Figure E-4 Photoluminescence Below 11700 Å of Semi-insulating
InP:Fe at 100°K

Appendix F

Photoluminescence Below 3.0 μm of Semi-insulating InP:Fe at 4.2°K

Identification of anomalies in spectra:

- 1 Laser turned off due to low water pressure or overheating
- 2 Noise

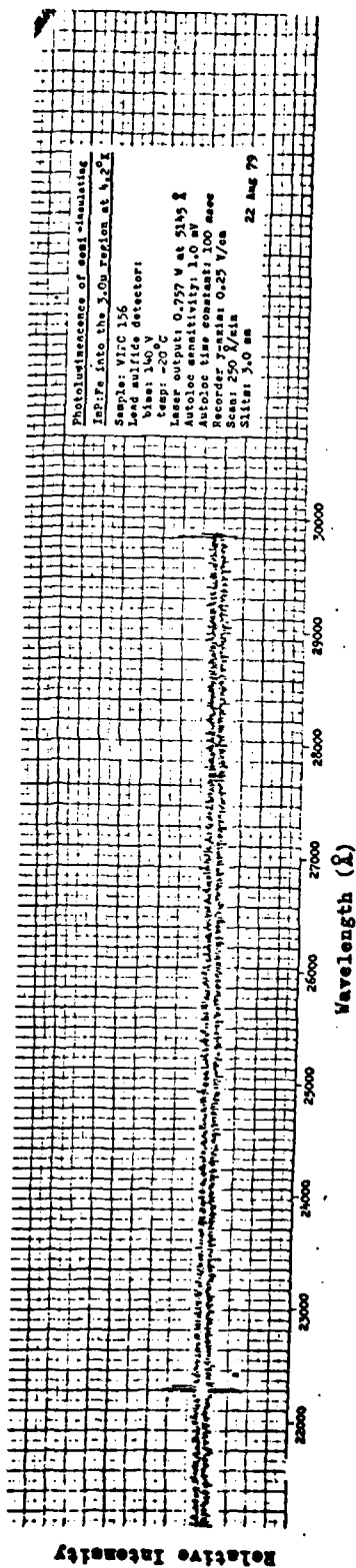
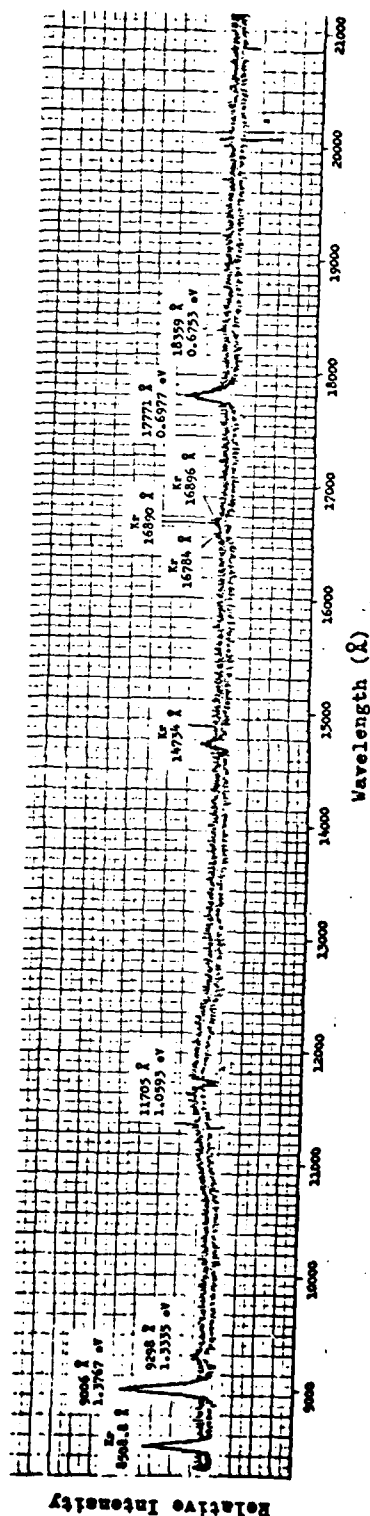


Figure F-1 Photoluminescence Below 3.0 μm of Semi-insulating InP:Fe at 4.2°K

Appendix G

Photoluminescence Below 1.4 μm of Unannealed, Unimplanted and

Mg-implanted InP:Fe at 50°K

Identification of anomalies in spectra:

- 1 Improper placement of calibration lamp
- 2 Laser turned off due to low water pressure or overheating

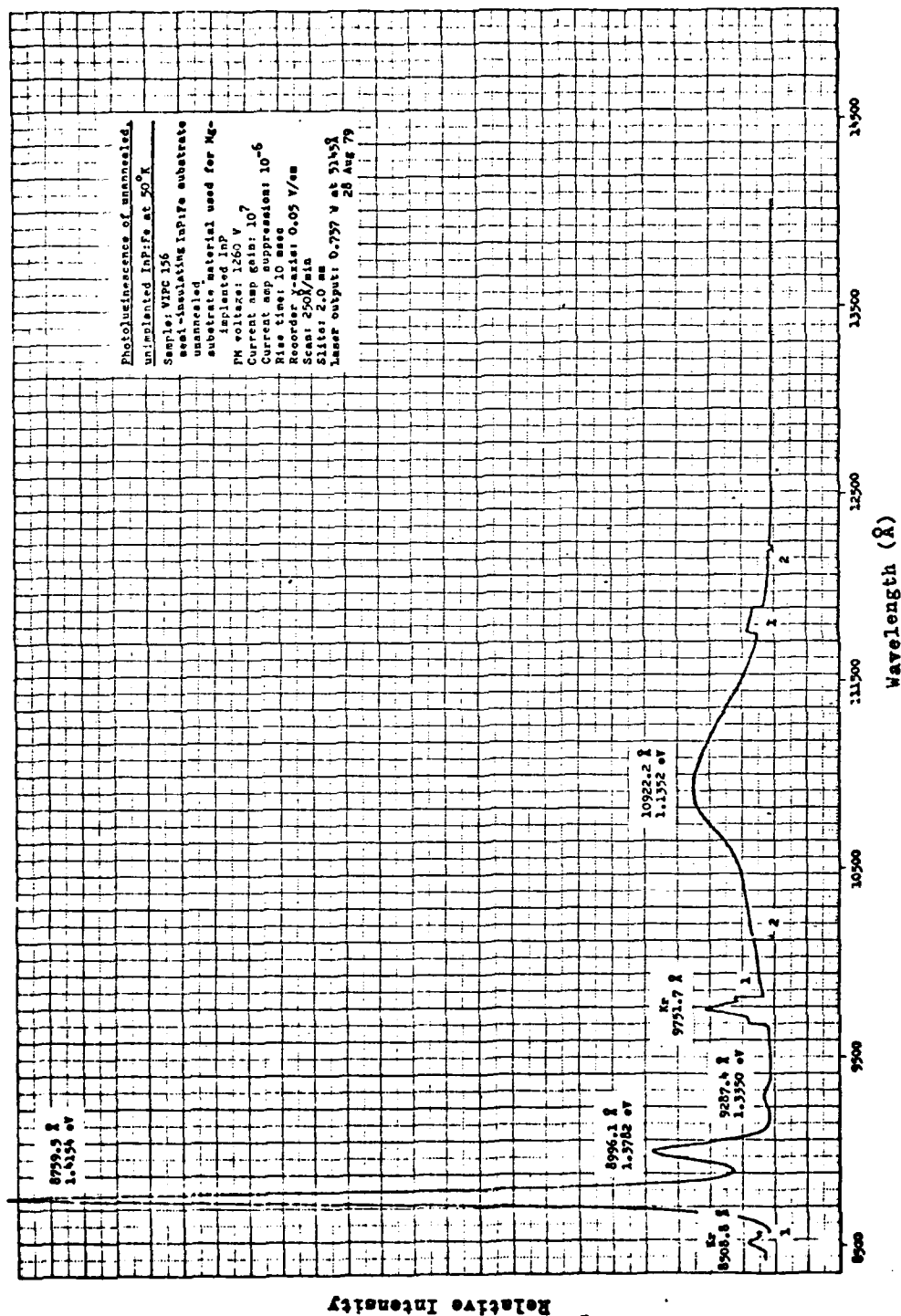


Figure G-1 Photoluminescence Below 1.4 μ m of Unannealed, Unimplanted InP:Fe at 50°K

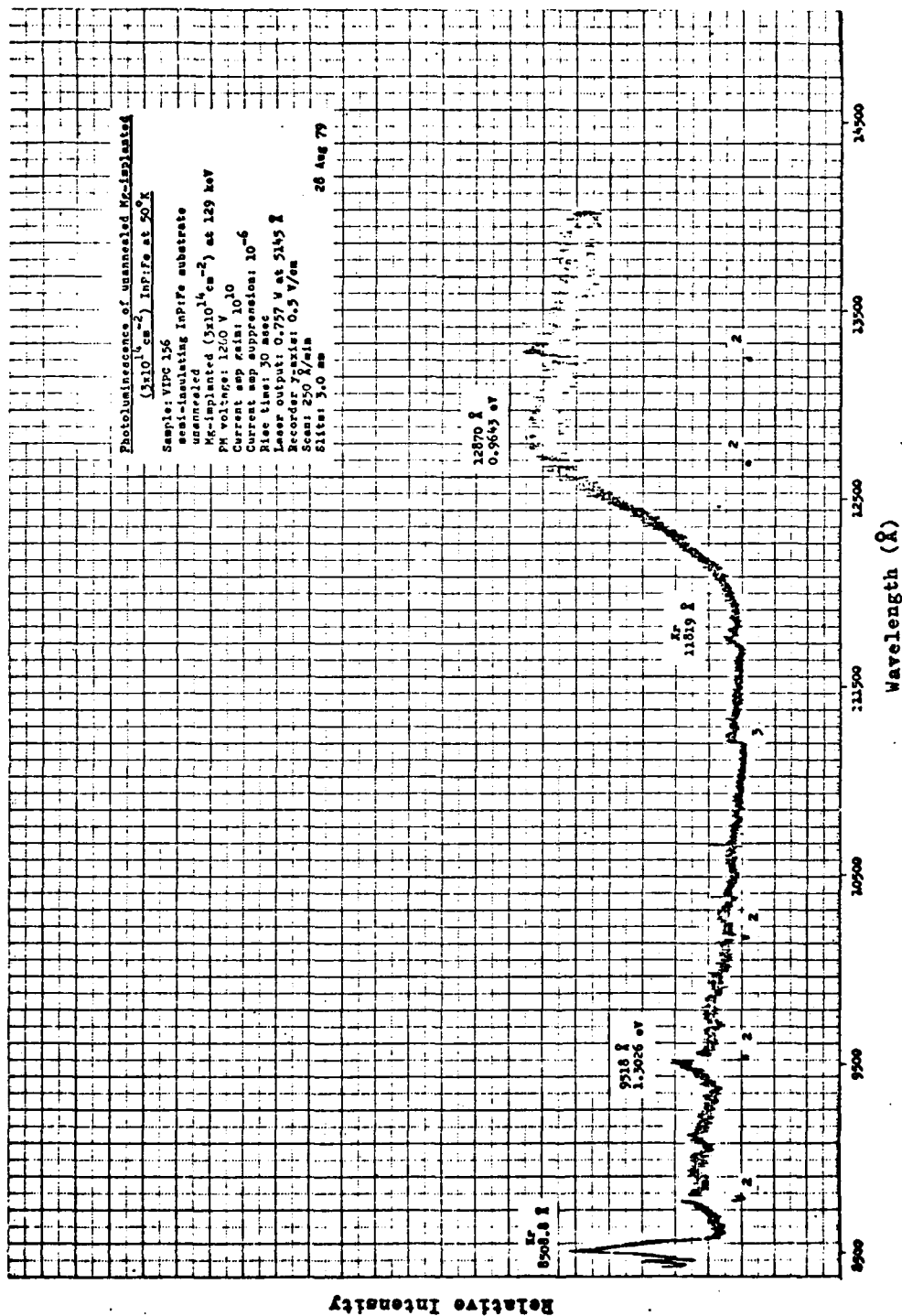


Figure G-2 Photoluminescence Below 1.4 μm of Unannealed, Mg-implanted ($3 \times 10^{14} \text{ cm}^{-2}$) InP:Fe at 50°K

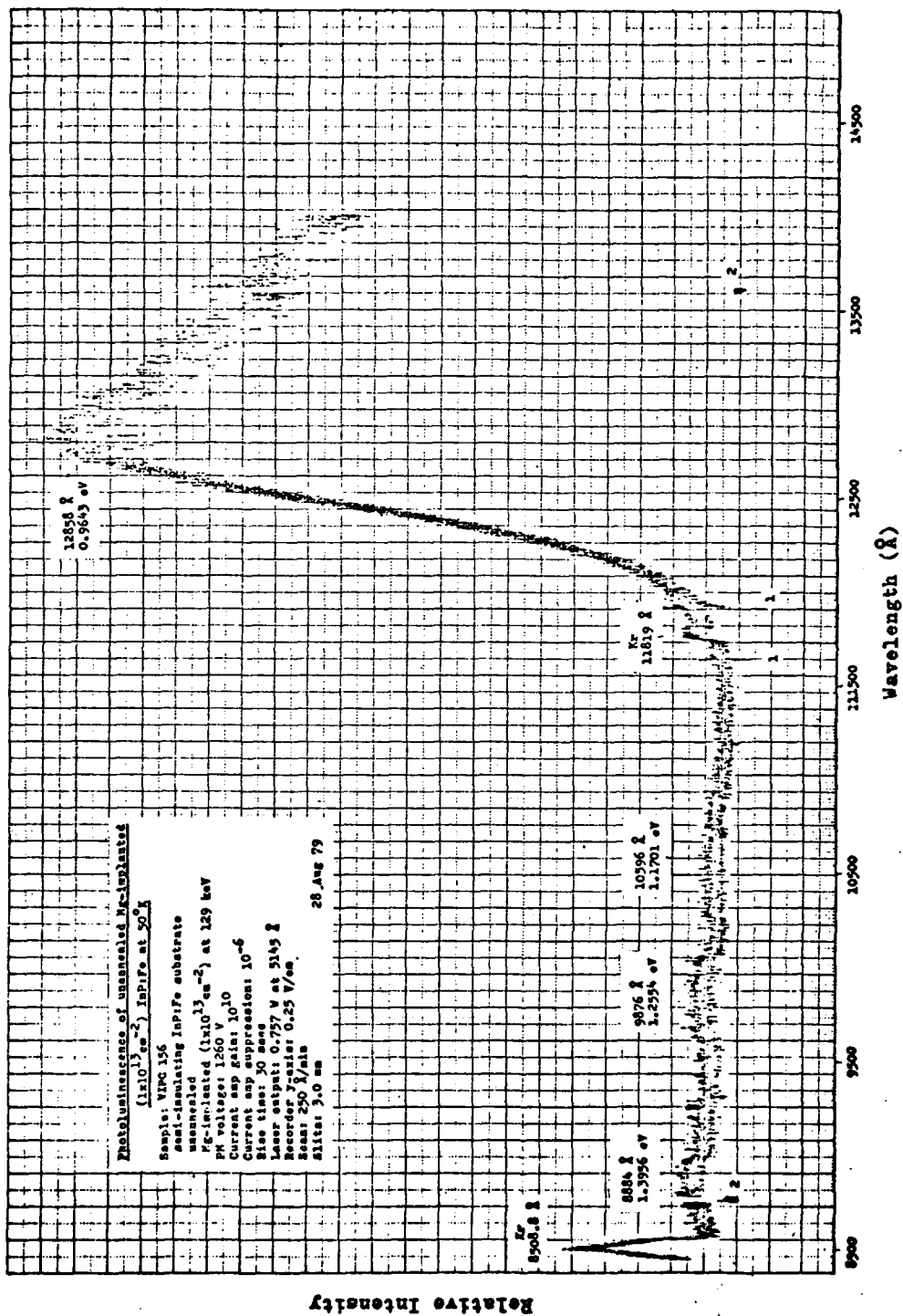


Figure G-3 Photoluminescence Below $1.4 \mu\text{m}$ of Unannealed, Mg-implanted ($1 \times 10^{13} \text{ cm}^{-2}$) InP:Fe at 50°K

Appendix H

Photoluminescence of Mg-implaned, 750°C Annealed InP:Fe at 50°K

Identification of anomalies in spectra:

- 1 Improper placement of krypton calibration lamp
- 2 Laser turned off due to low water pressure or overheating
- 3 Secondary line of calibration source

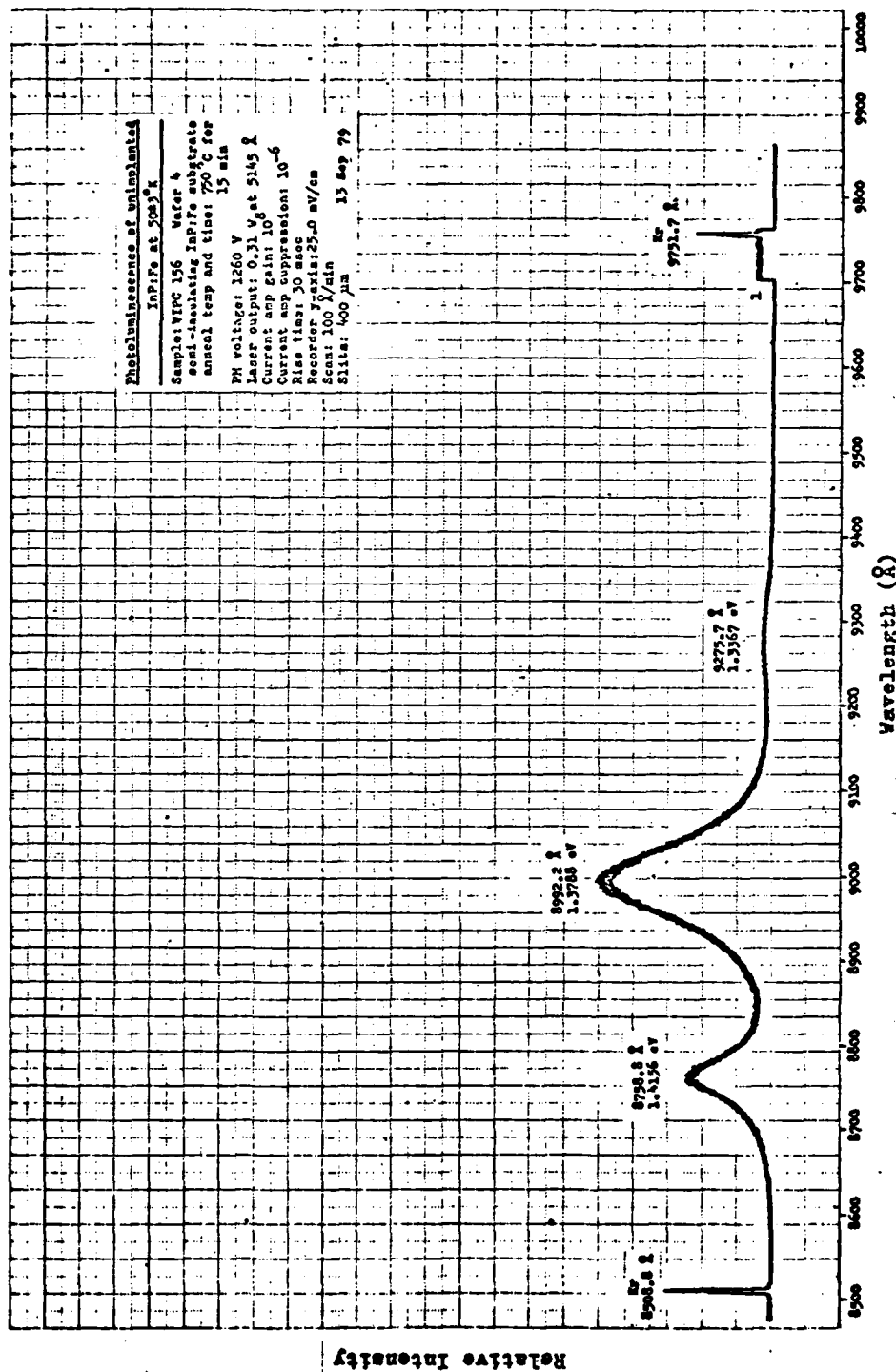


Figure H-1 Photoluminescence of Unimplanted (Wafer 4), 750°C
Annealed InP:Fe at 50°K

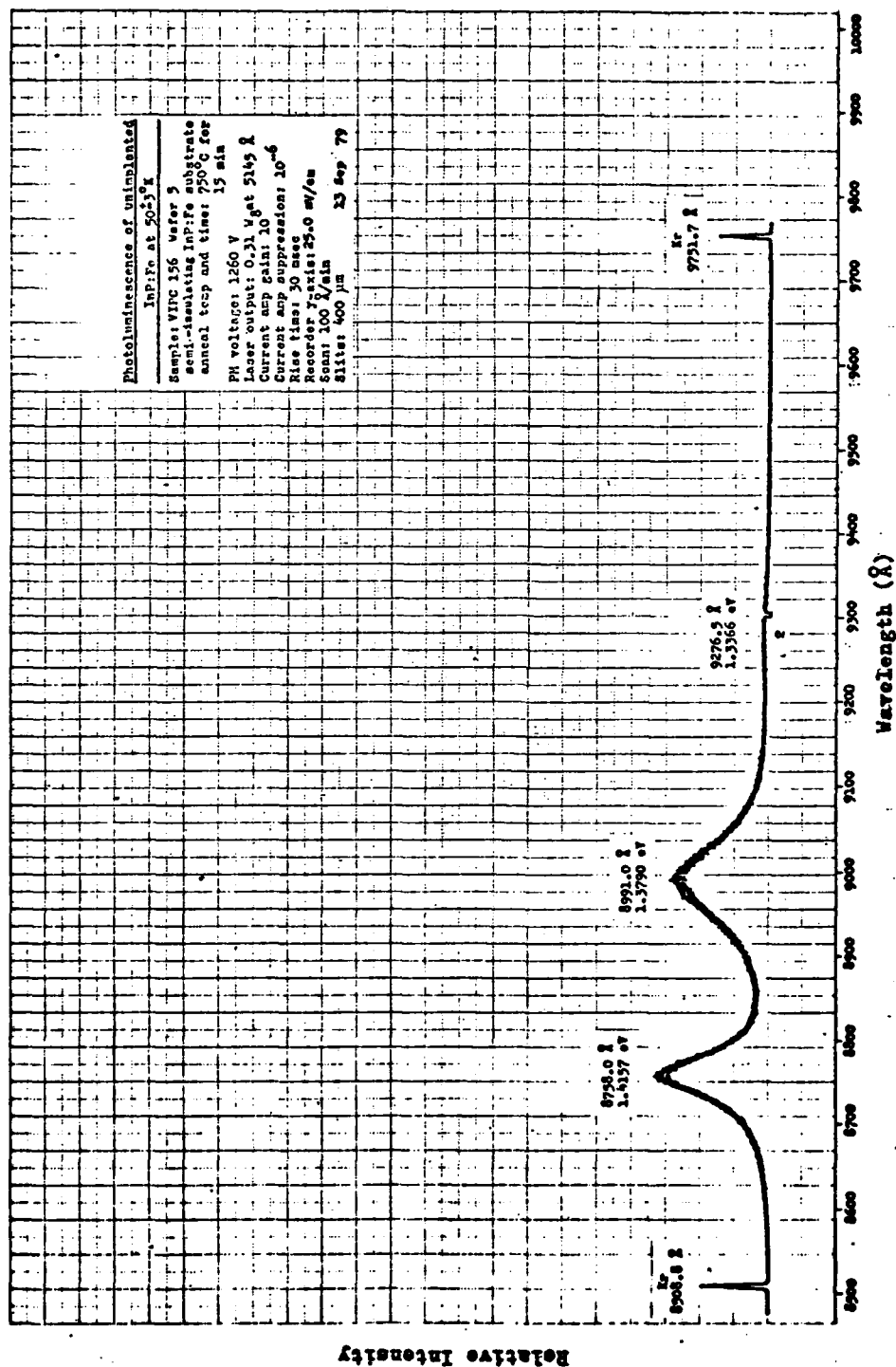


Figure H-2 Photoluminescence of Unimplanted (Wafer 5), 750°C
Annealed InP:Fe at 50°K

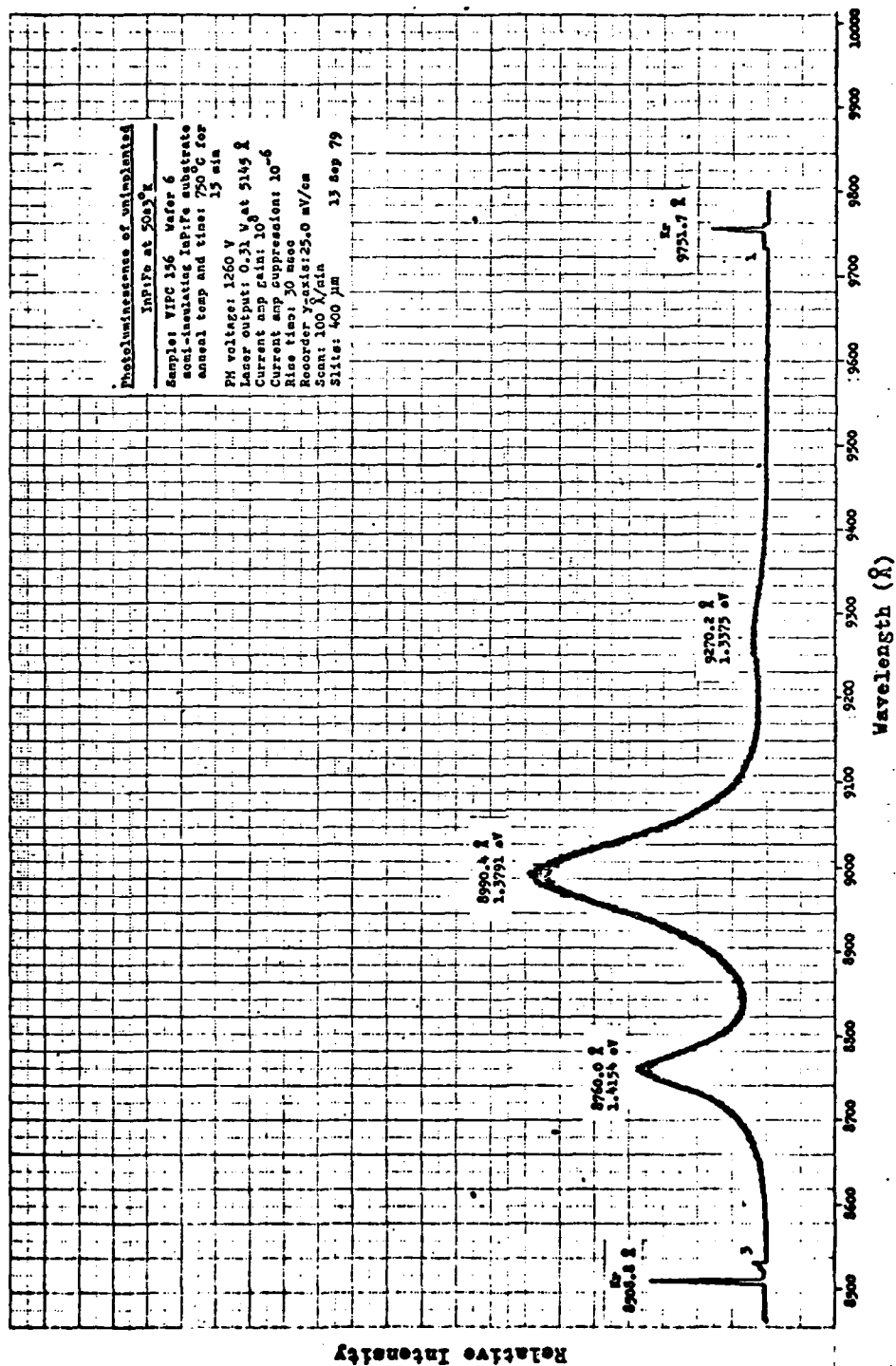


Figure H-3 Photoluminescence of Unimplanted (Wafer 6), 750°C
 Annealed InP:Fe at 50°K

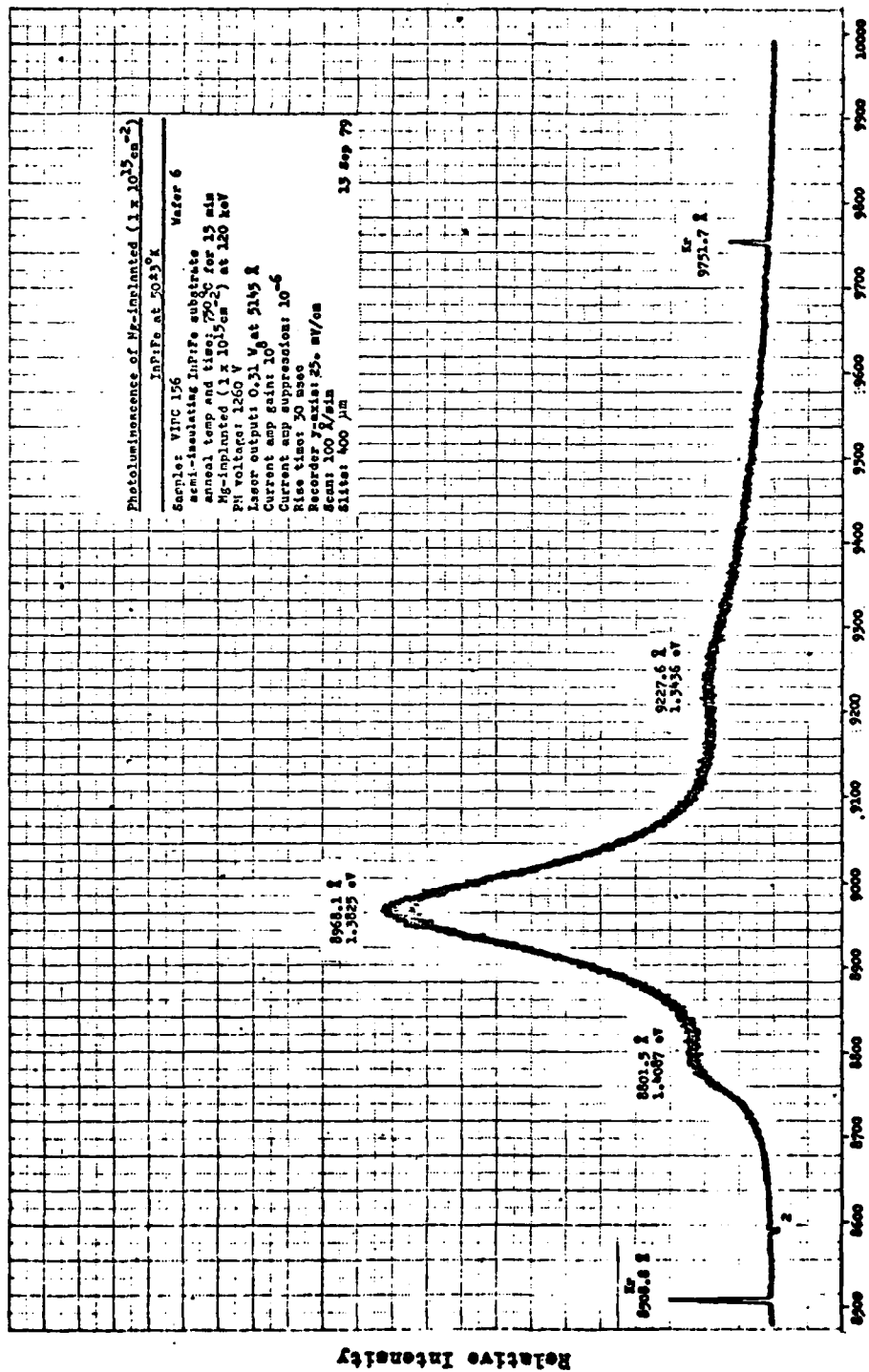


Figure H-4 Photoluminescence of Mg-implanted ($1 \times 10^{15} \text{ cm}^{-2}$), 750°C Annealed InP:Fe at 50°K

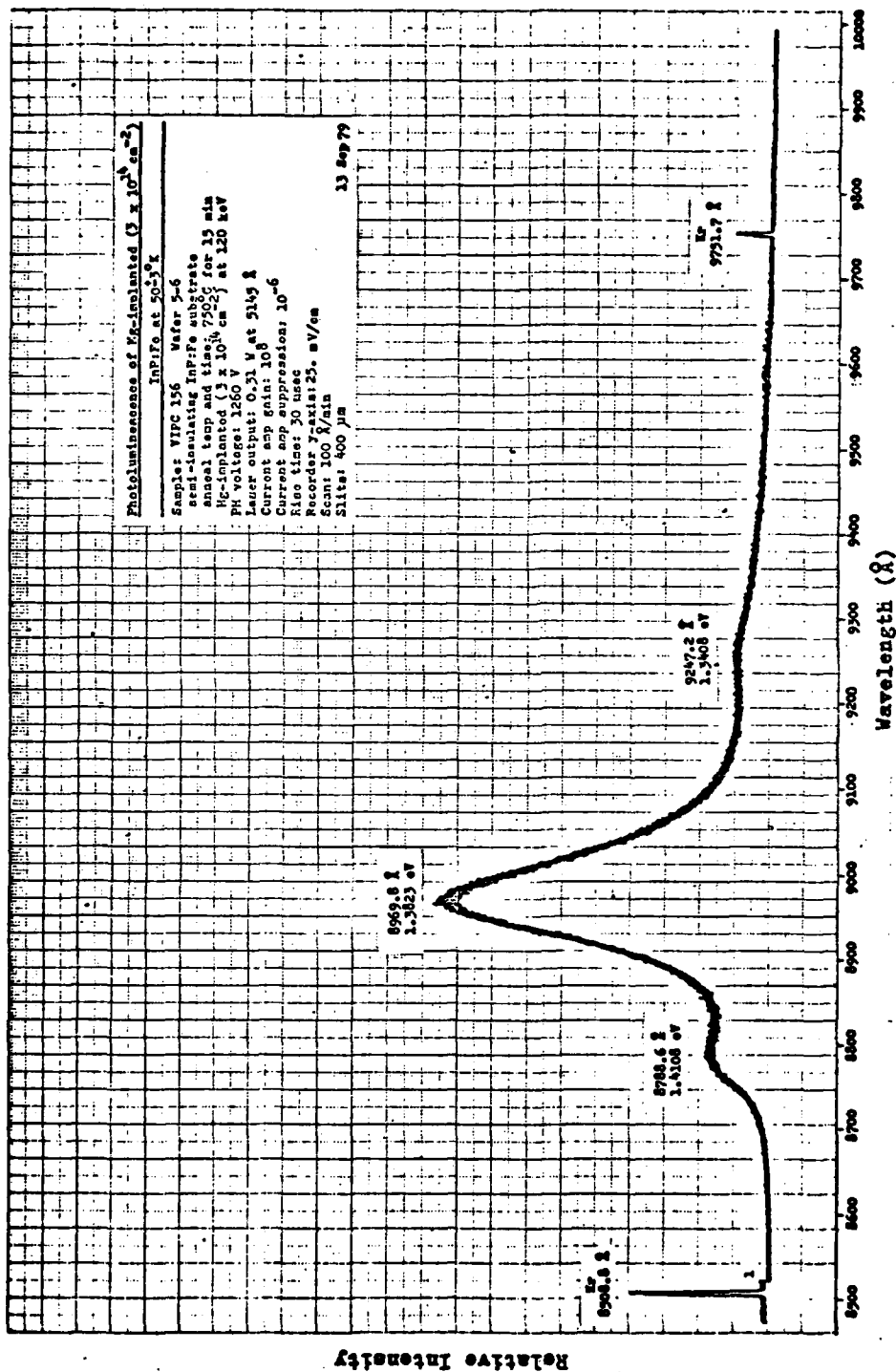


Figure H-5 Photoluminescence of Mg-implanted ($3 \times 10^{14} \text{ cm}^{-2}$), 750°C Annealed InP:Fe at 50°K

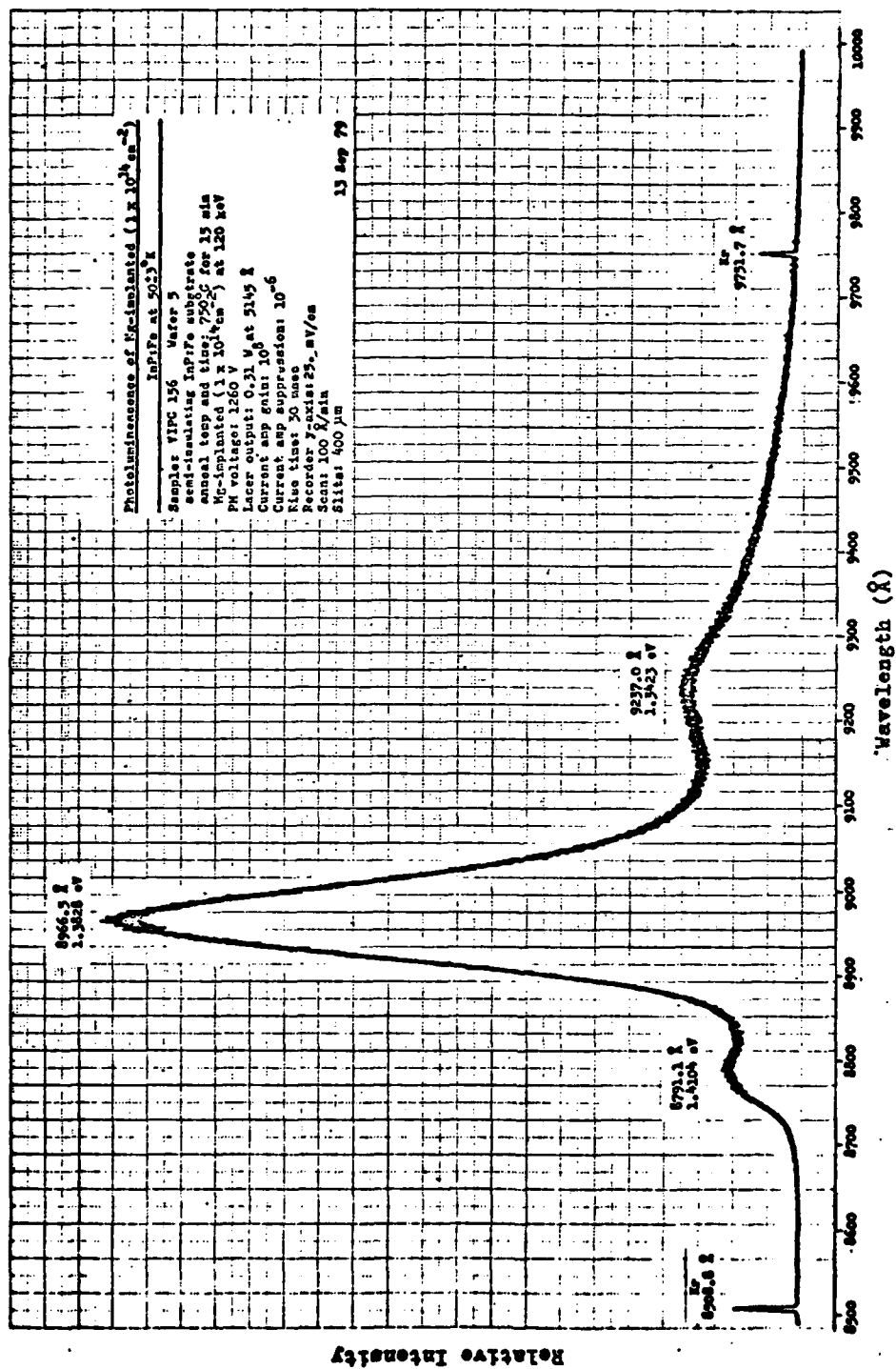


Figure H-6 Photoluminescence of Mg-implanted ($1 \times 10^{14} \text{ cm}^{-2}$),
 750°C Annealed InP:Fe at 50°K

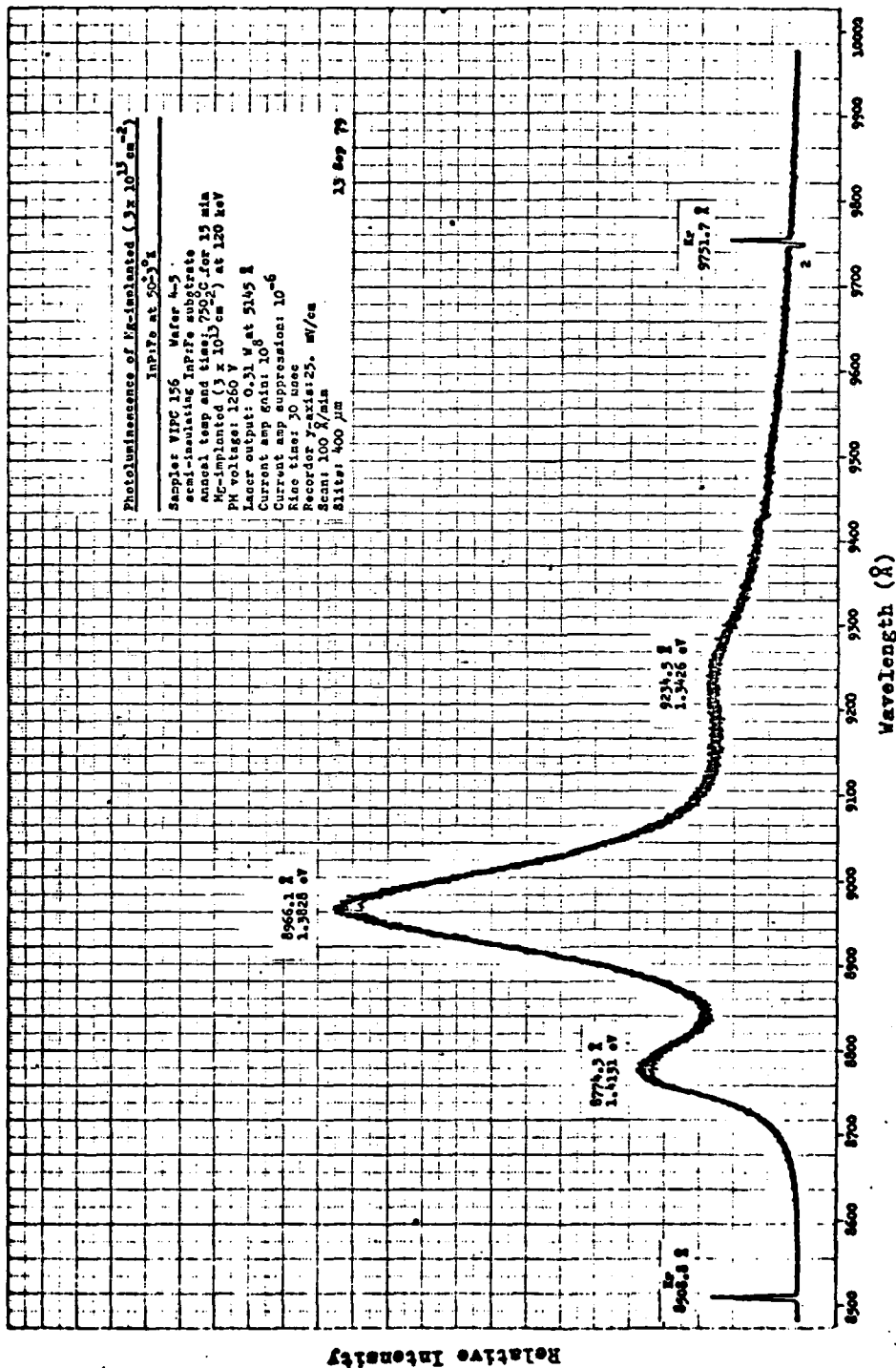


Figure H-7 Photoluminescence of Mg-implanted ($3 \times 10^{13} \text{ cm}^{-2}$), 750°C Annealed InP:Fe at 50°K

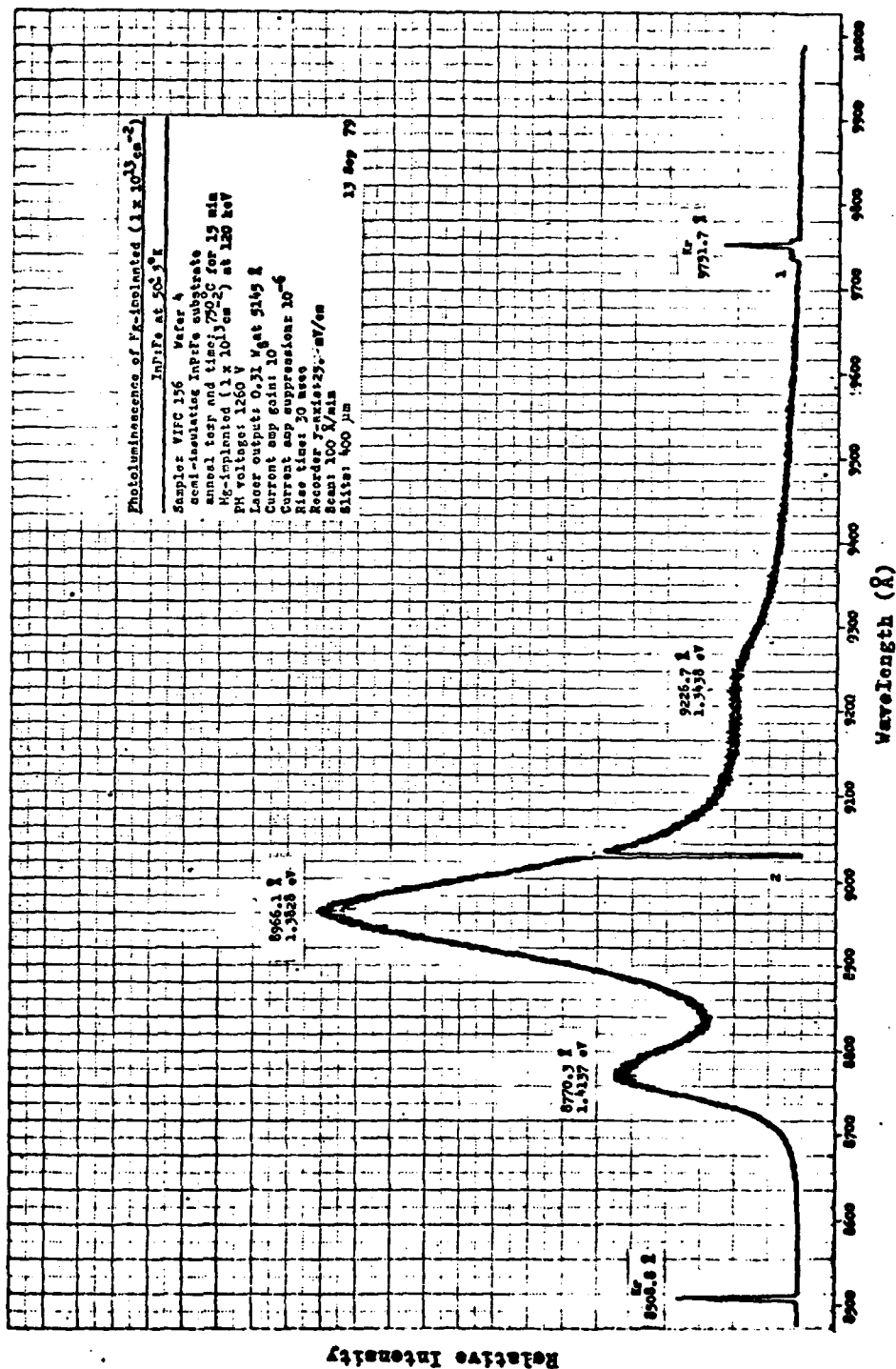


Figure H-8 Photoluminescence of Mg-implanted ($1 \times 10^{13} \text{ cm}^{-2}$),
 750°C Annealed InP:Fe at 50°K

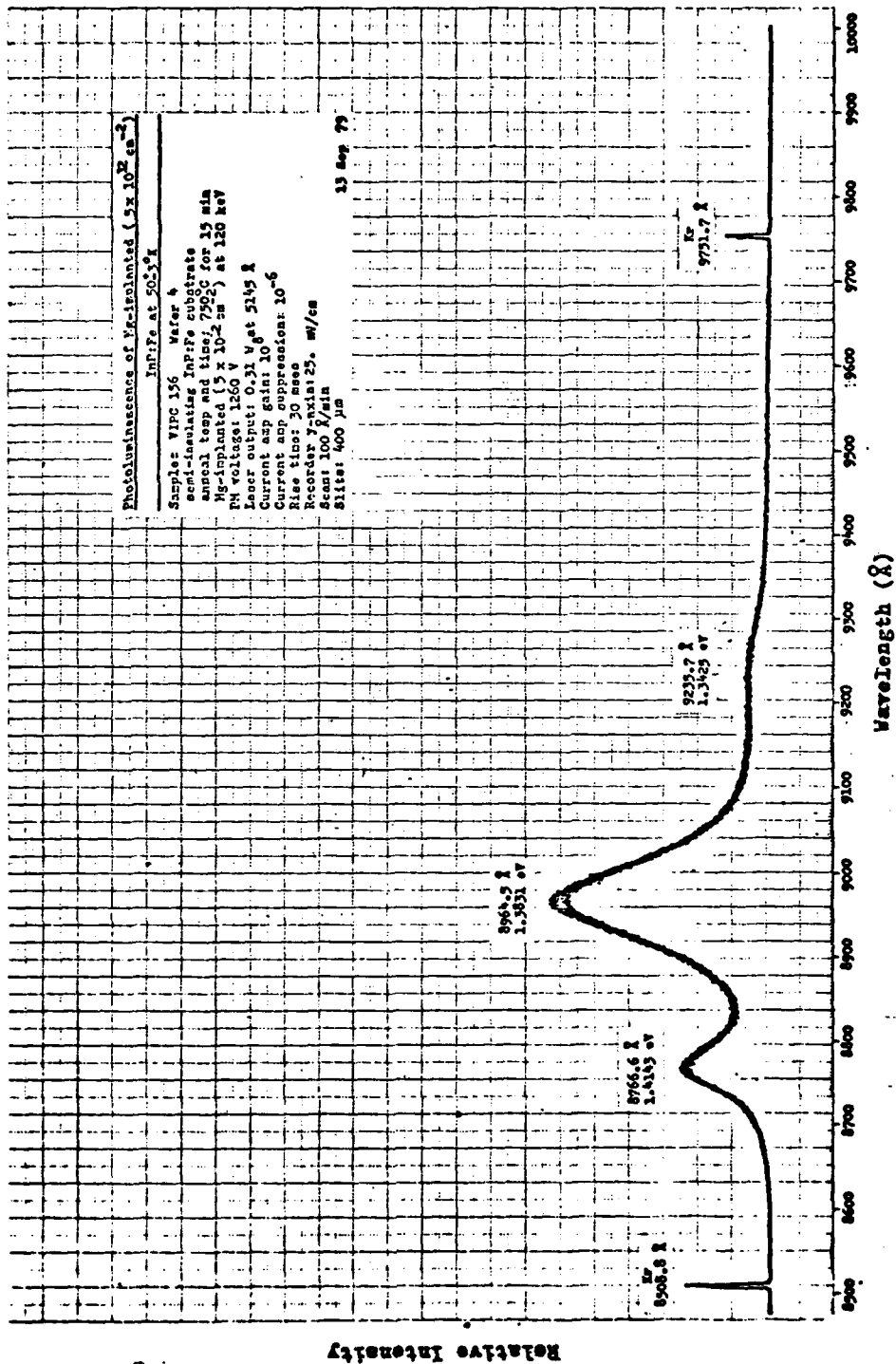


Figure H-9 Photoluminescence of Mg-implanted ($5 \times 10^{12} \text{ cm}^{-2}$),
 750°C Annealed InP:Fe at 50°C

Appendix I

Photoluminescence of Mg-implanted, 700°C Annealed InP:Fe at 4.2°K

Identification of anomalies in spectra:

- 1 Improper placement of krypton calibration lamp
 - 2 Laser turned off due to low water pressure of overheating
 - 3 Secondary line of calibration source
- (s) Shoulder

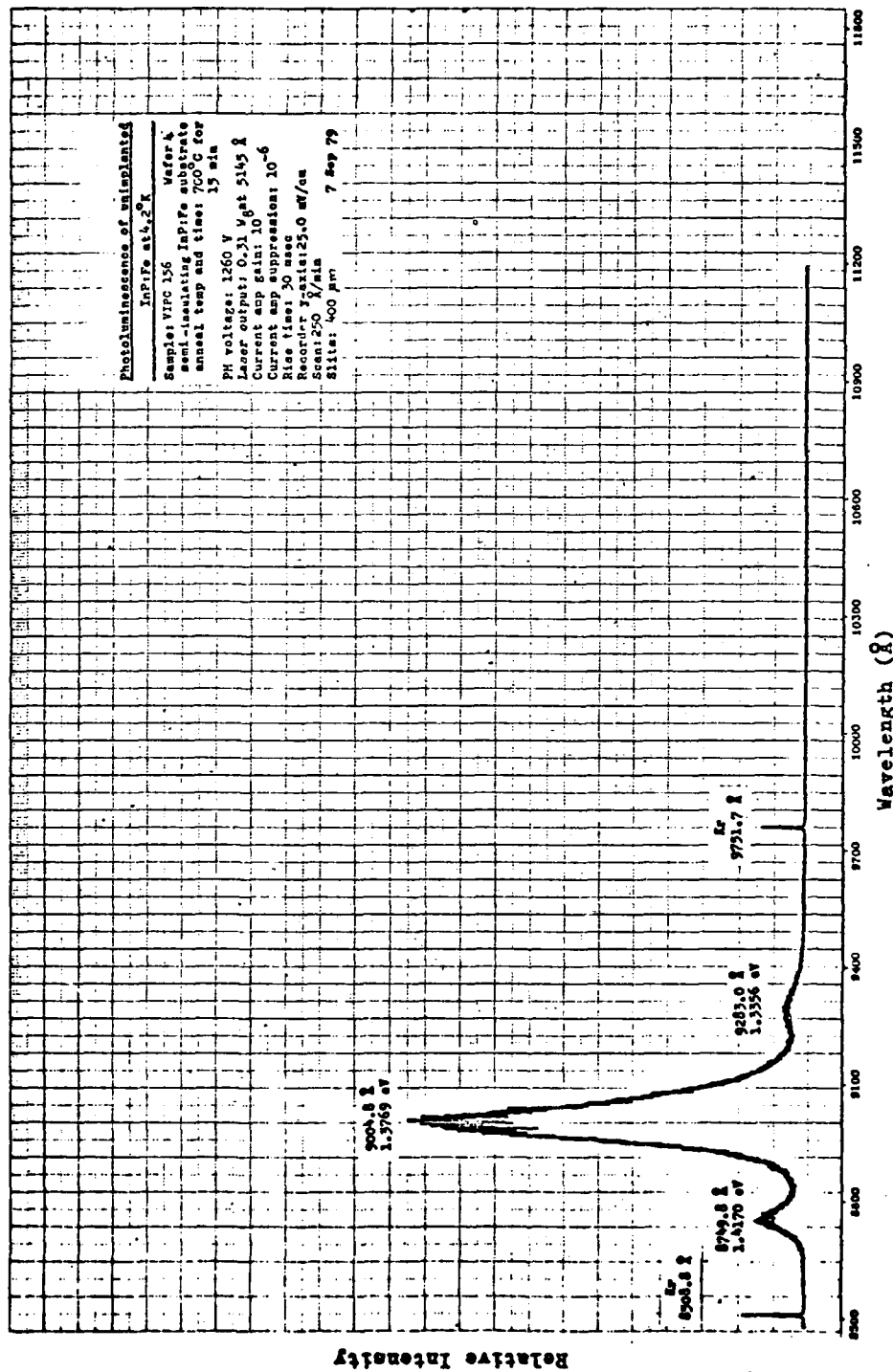


Figure I-1 Photoluminescence of Unimplanted (Wafer 4), 700°C
Annealed InP:Fe at 4.2°K

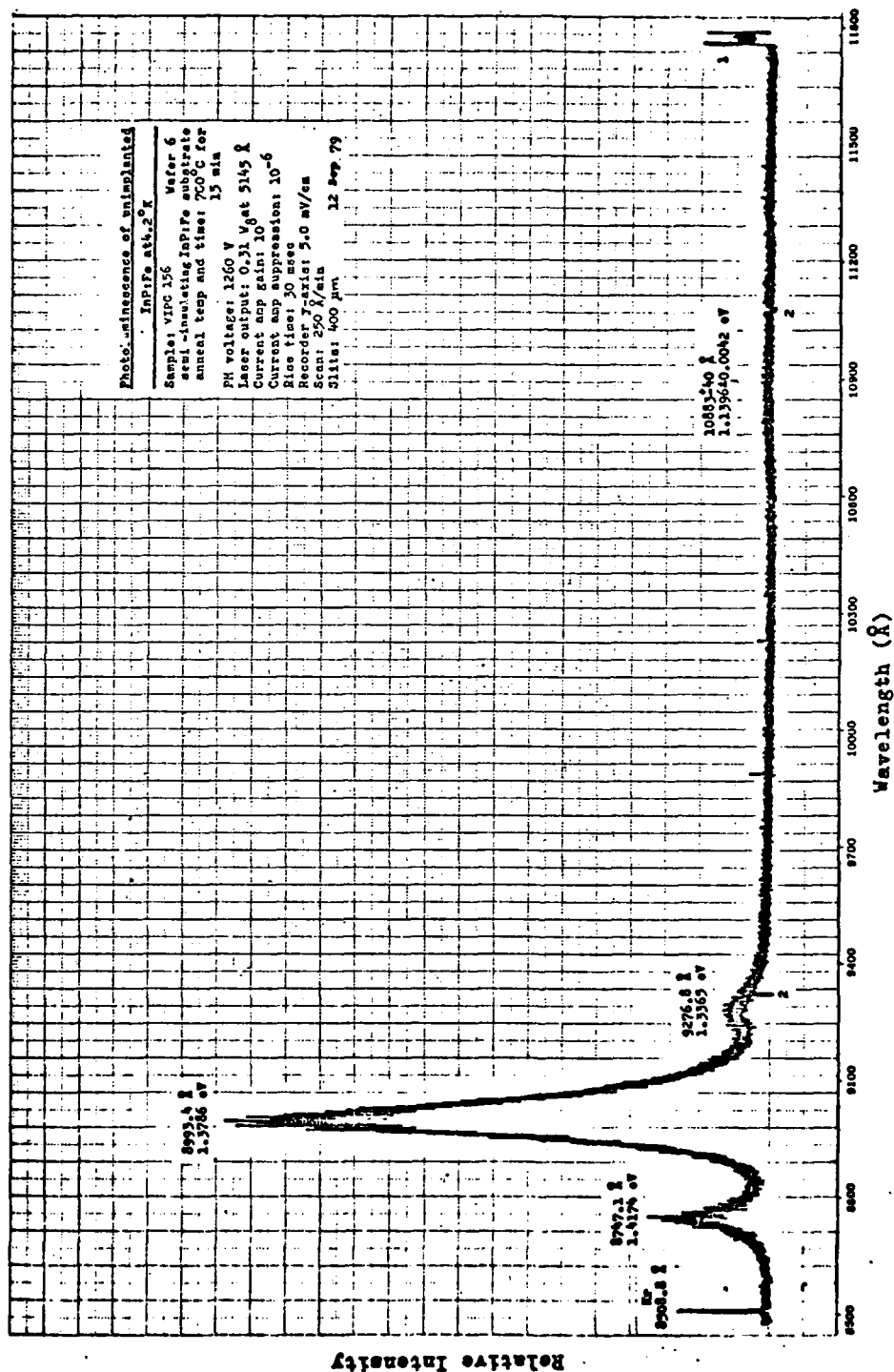


Figure I-2 Photoluminescence of Unimplanted (Wafer 6), 700°C
Annealed InP:Fe at 4.2°K

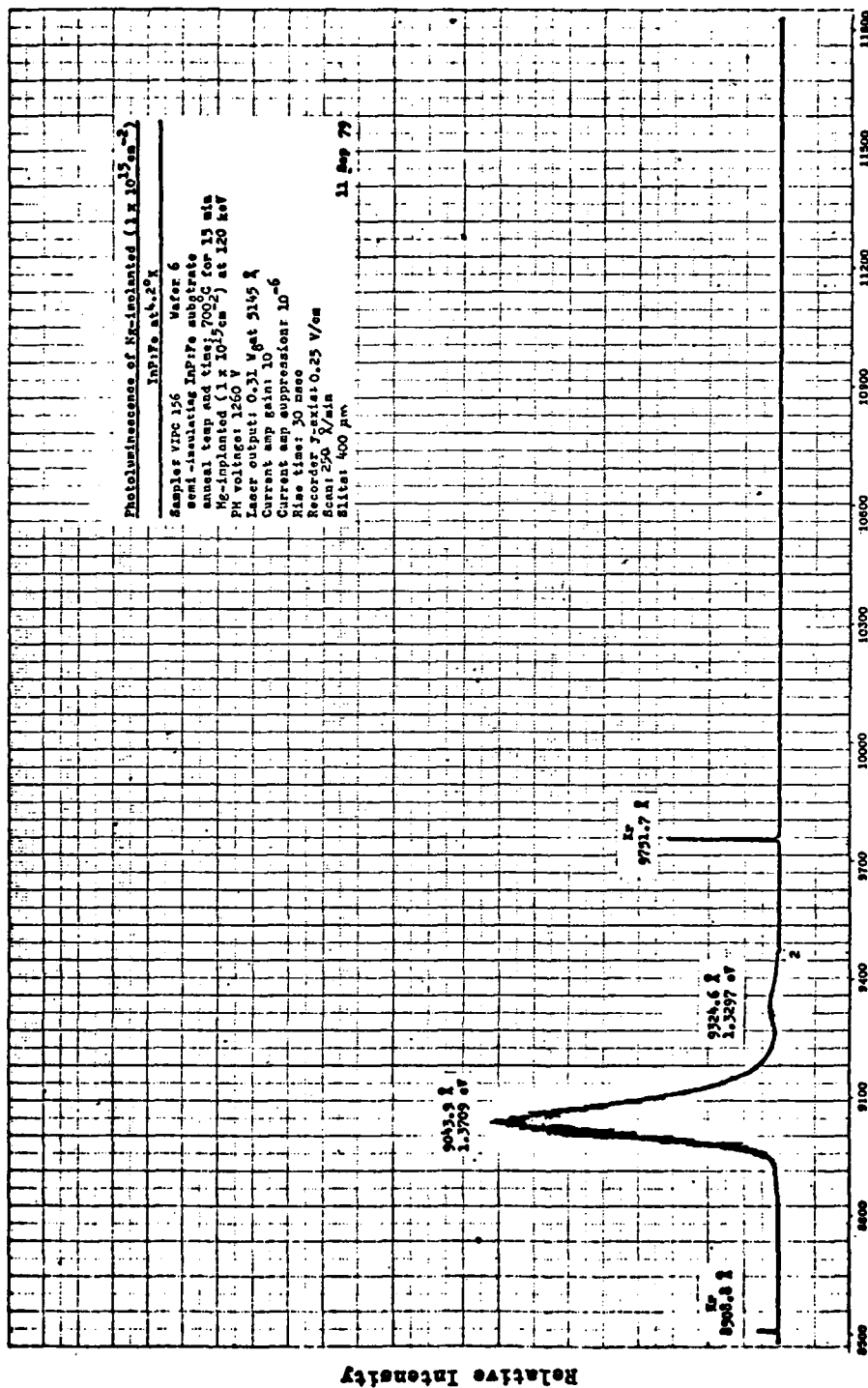


Figure I-3 Photoluminescence of Mg-implanted ($1 \times 10^{15} \text{ cm}^{-2}$),
 700°C Annealed InP:Fe at 4.2°K

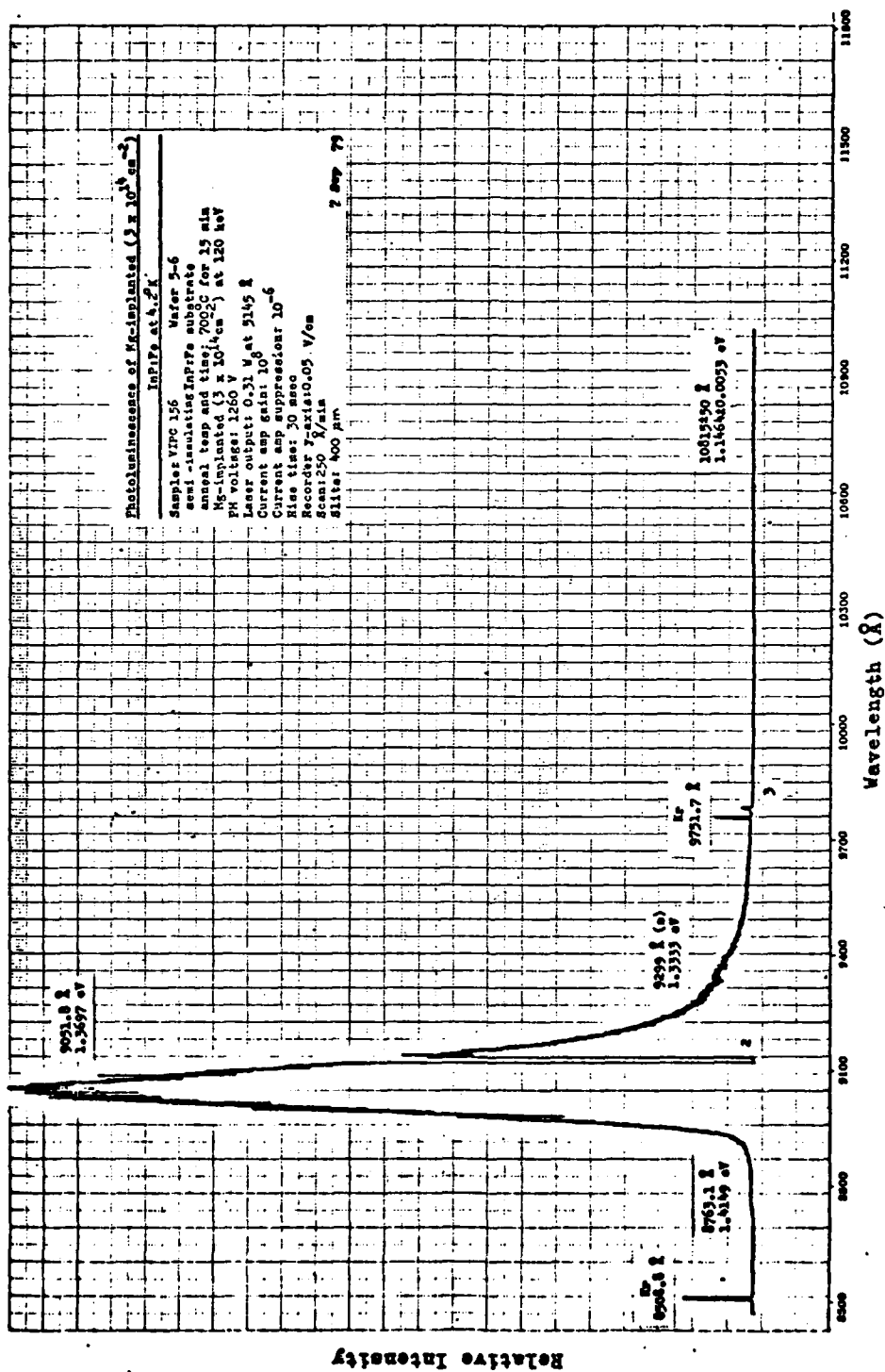


Figure I-4 Photoluminescence of Mg-implanted ($3 \times 10^{14} \text{ cm}^{-2}$),
 700°C Annealed InP:Fe at 4.2°K

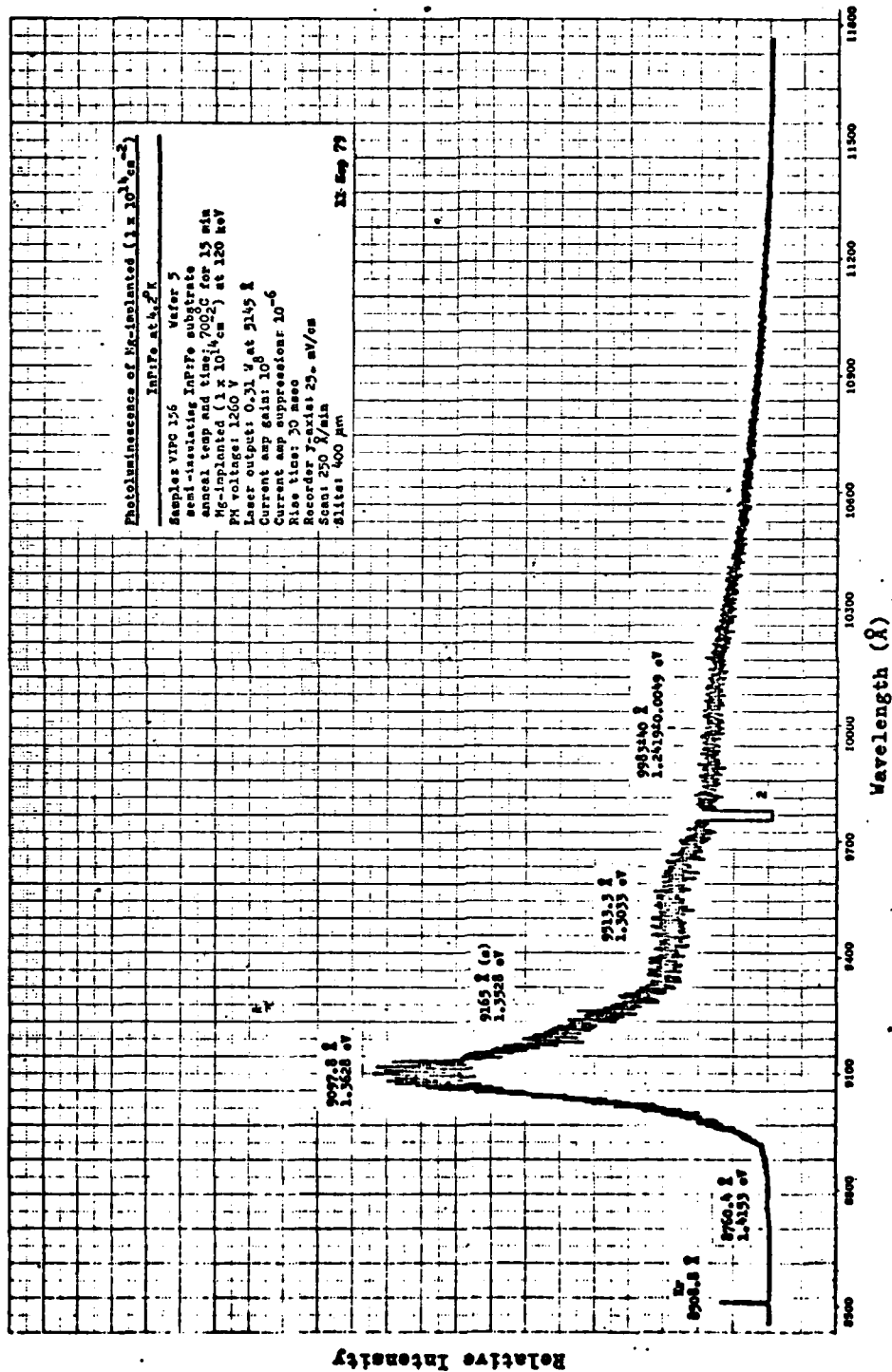


Figure I-5 Photoluminescence of Mg-implanted ($1 \times 10^{14} \text{ cm}^{-2}$), 700°C Annealed InP:Fe at 4.2°K

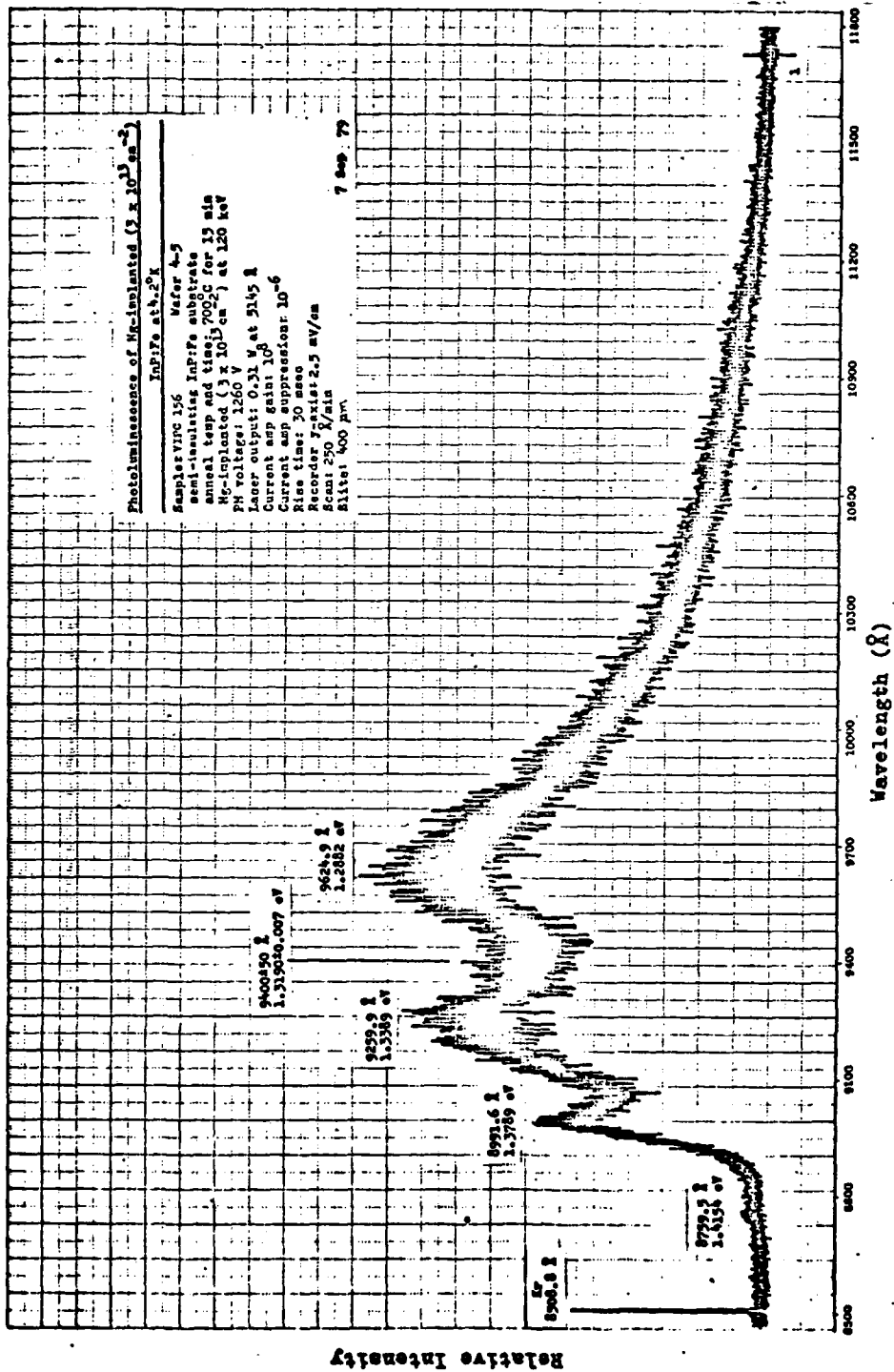


Figure I-6 Photoluminescence of Mg-implanted ($3 \times 10^{13} \text{ cm}^{-2}$),
 700°C Annealed InP:Fe at 4.2°K

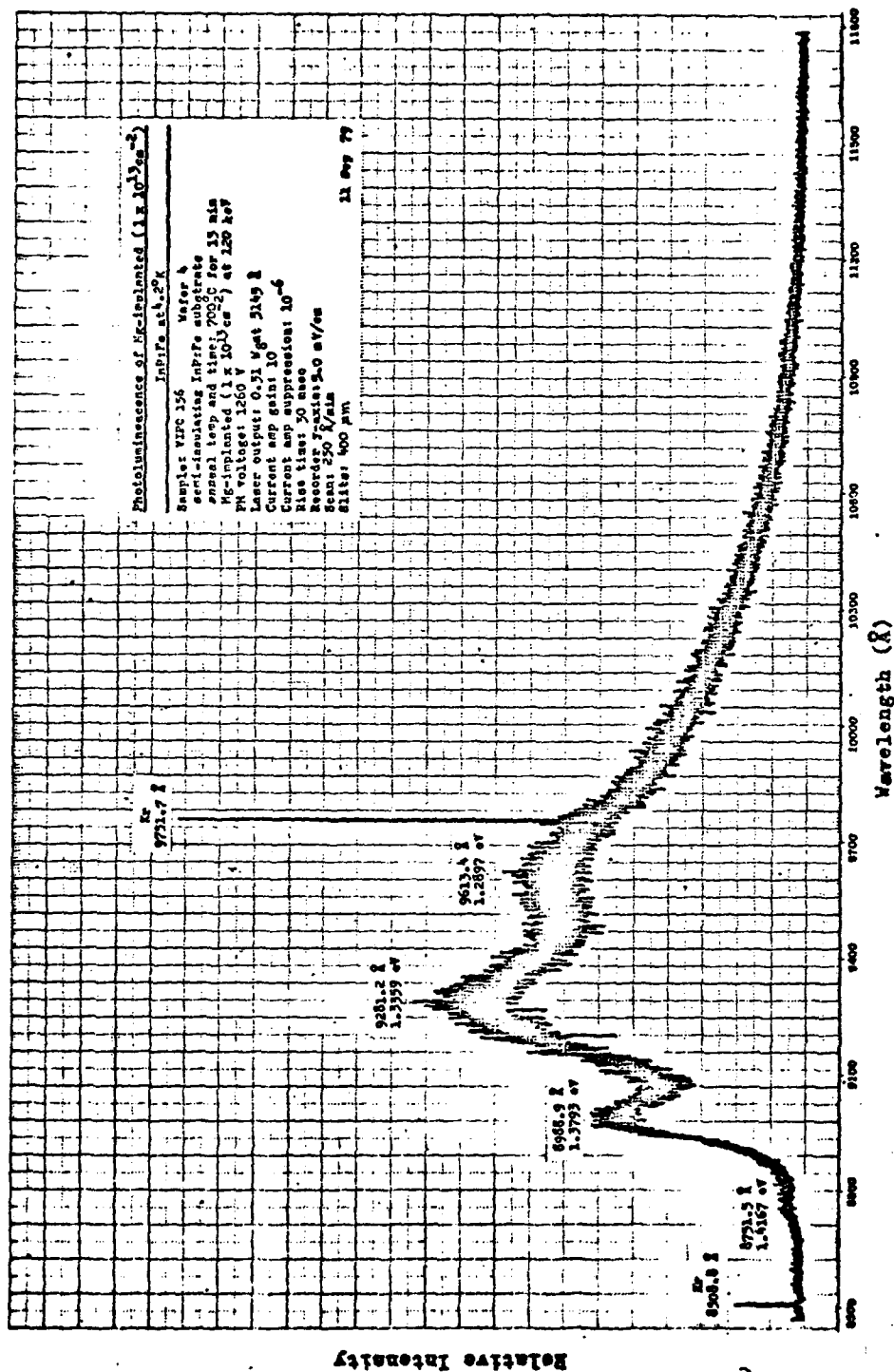


Figure I-7 Photoluminescence of Mg-implanted ($1 \times 10^{13} \text{ cm}^{-2}$),
 700°C Annealed InP:Fe at 4.2°K

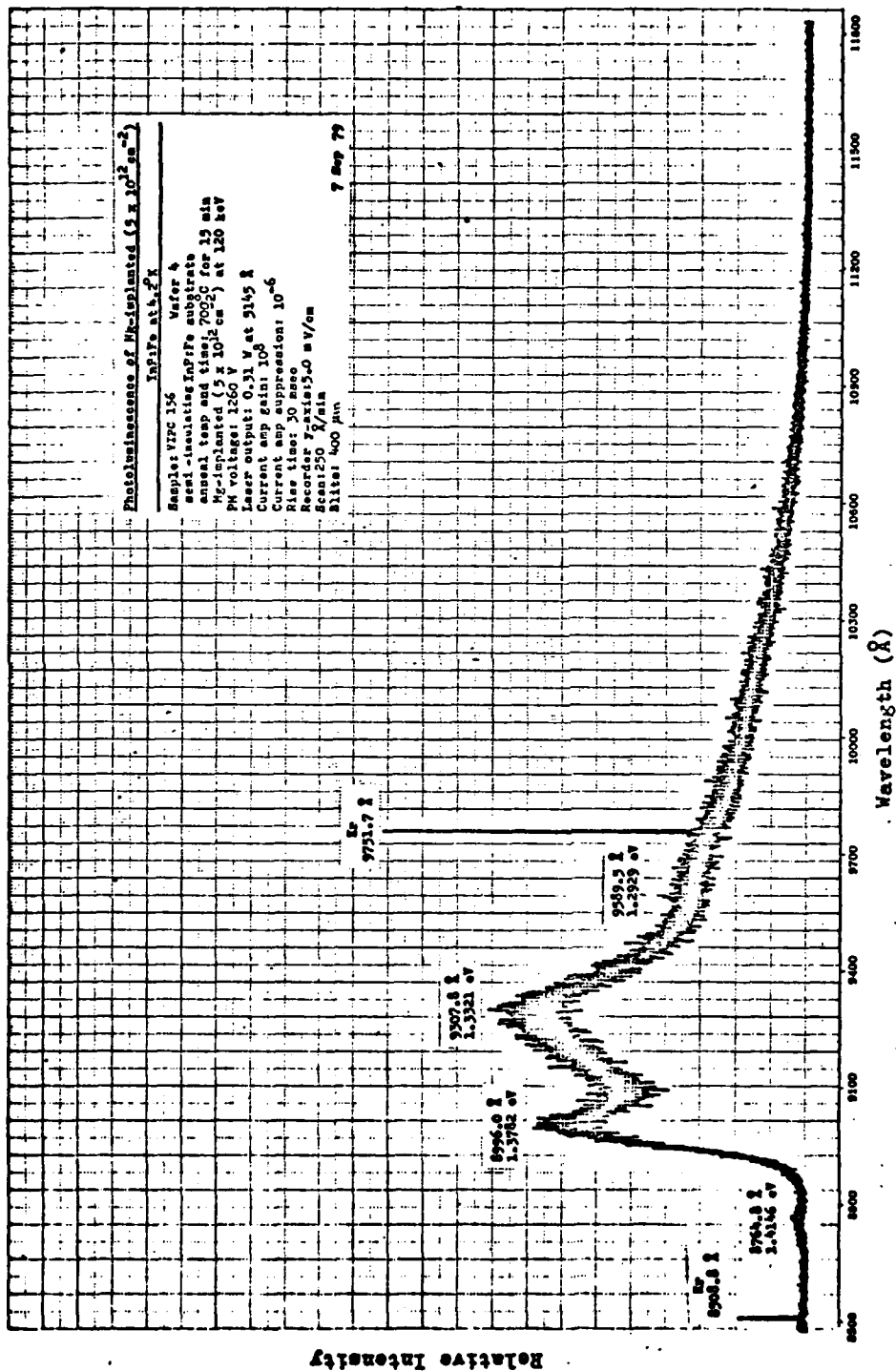


Figure I-8 Photoluminescence of Mg-implanted ($5 \times 10^{12} \text{ cm}^{-2}$), 700°C Annealed InP:Fe at 4.2°K

Appendix J

Photoluminescence of Mg-implanted, 700°C Annealed InP:Fe at 50°K

Identification of anomalies in spectra:

- 1 Improper placement of krypton calibration lamp
- 2 Due to laser turning off and due to premature and improper placement of the calibration lamp, spectra became excessively disrupted. Hence, a separate scan was made from 9100 Å to 9360 Å and was placed over the original.
- 3 Line of connection of the continued spectrum to the original spectrum
- 4 Laser turned off due to low water pressure or overheating

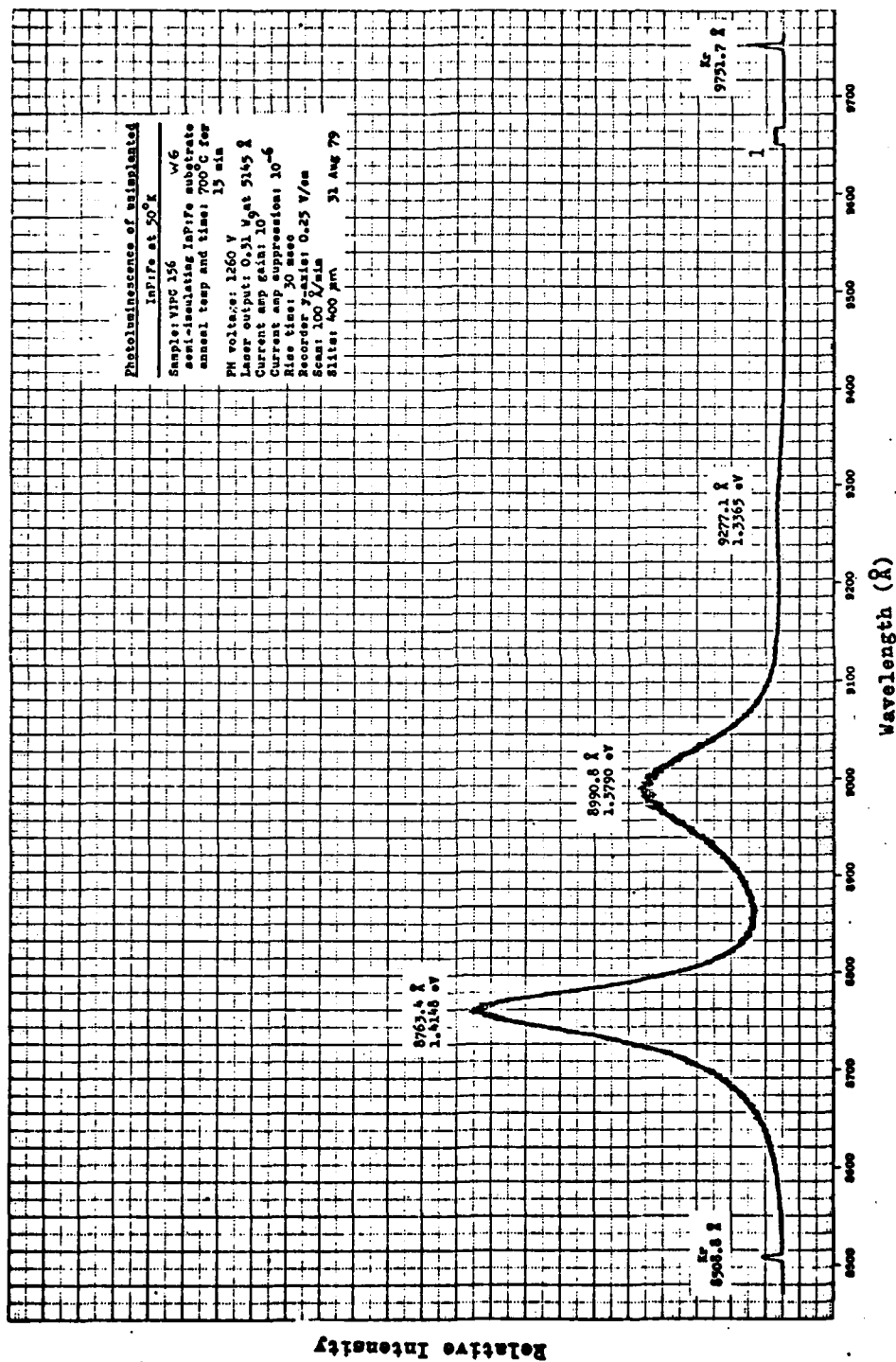


Figure J-1 Photoluminescence of Unimplanted, 700°C Annealed
InP:Fe at 50°K

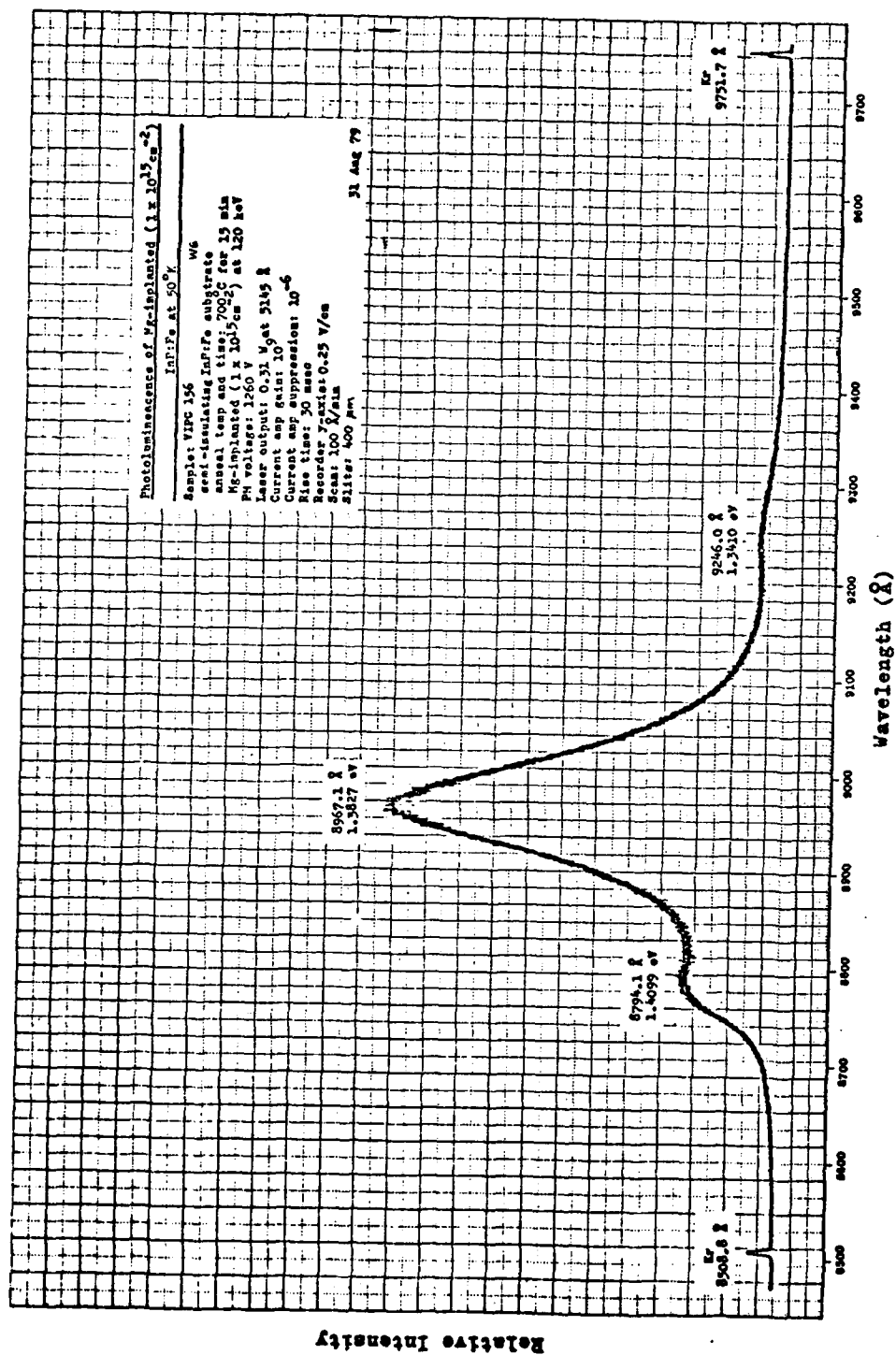


Figure J-2 Photoluminescence of Mg-implanted ($1 \times 10^{15} \text{ cm}^{-2}$),
 700°C Annealed InP:Fe at 50°K

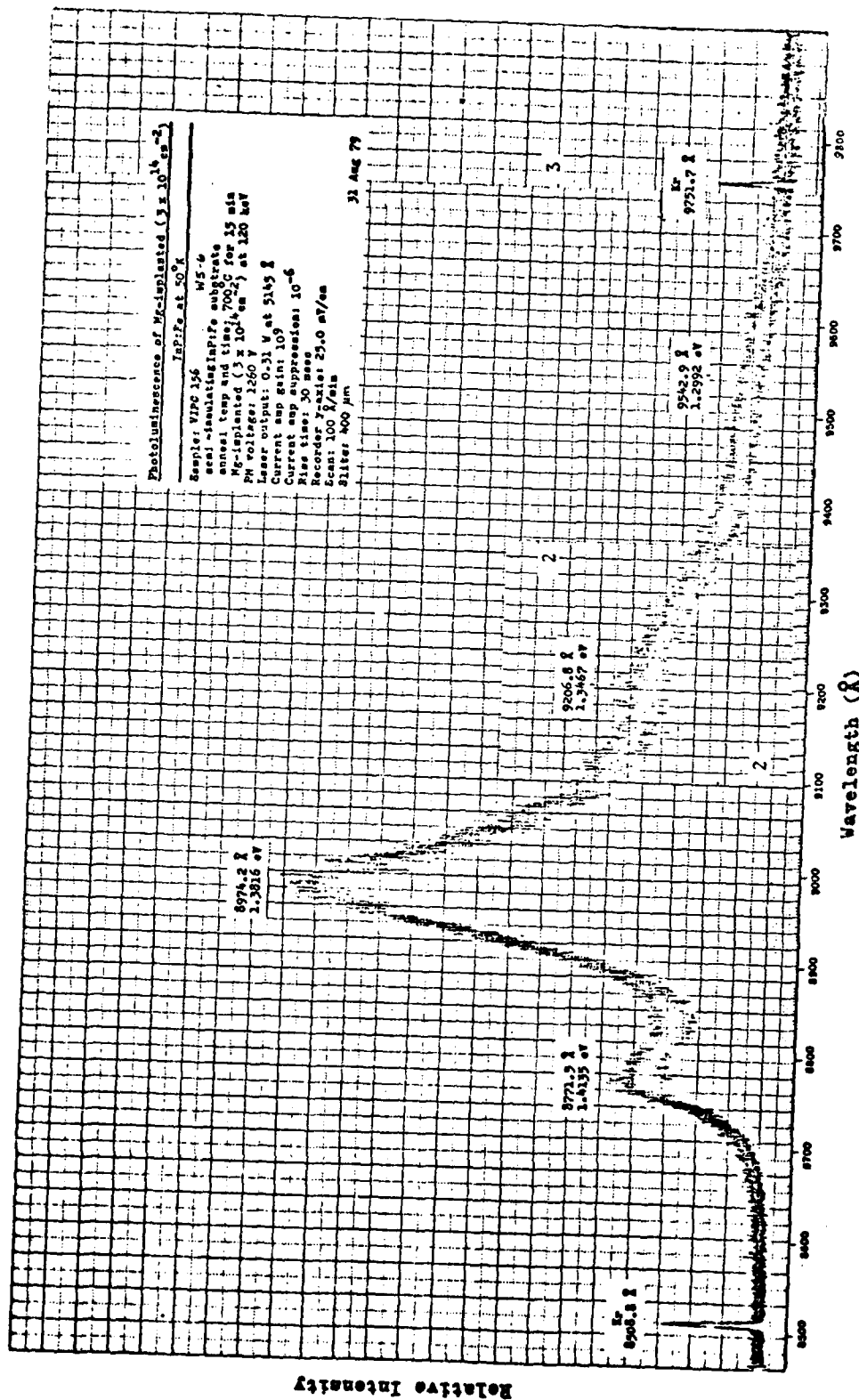


Figure J-3 Photoluminescence of Mg-implanted ($3 \times 10^{14} \text{ cm}^{-2}$),
 700°C Annealed InP:Fe at 50°K

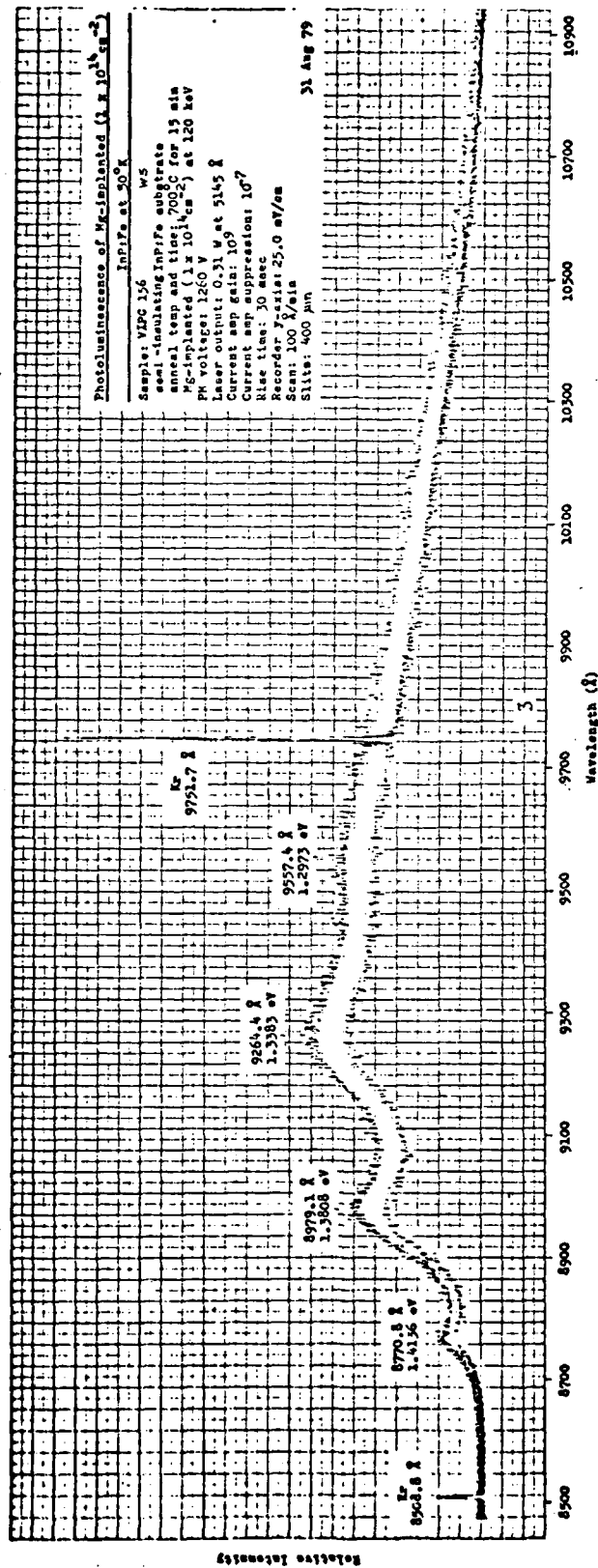


Figure J-4 Photoluminescence of Mg-implanted ($1 \times 10^{14} \text{ cm}^{-2}$),
 700°C Annealed InP:Fe at 50°K

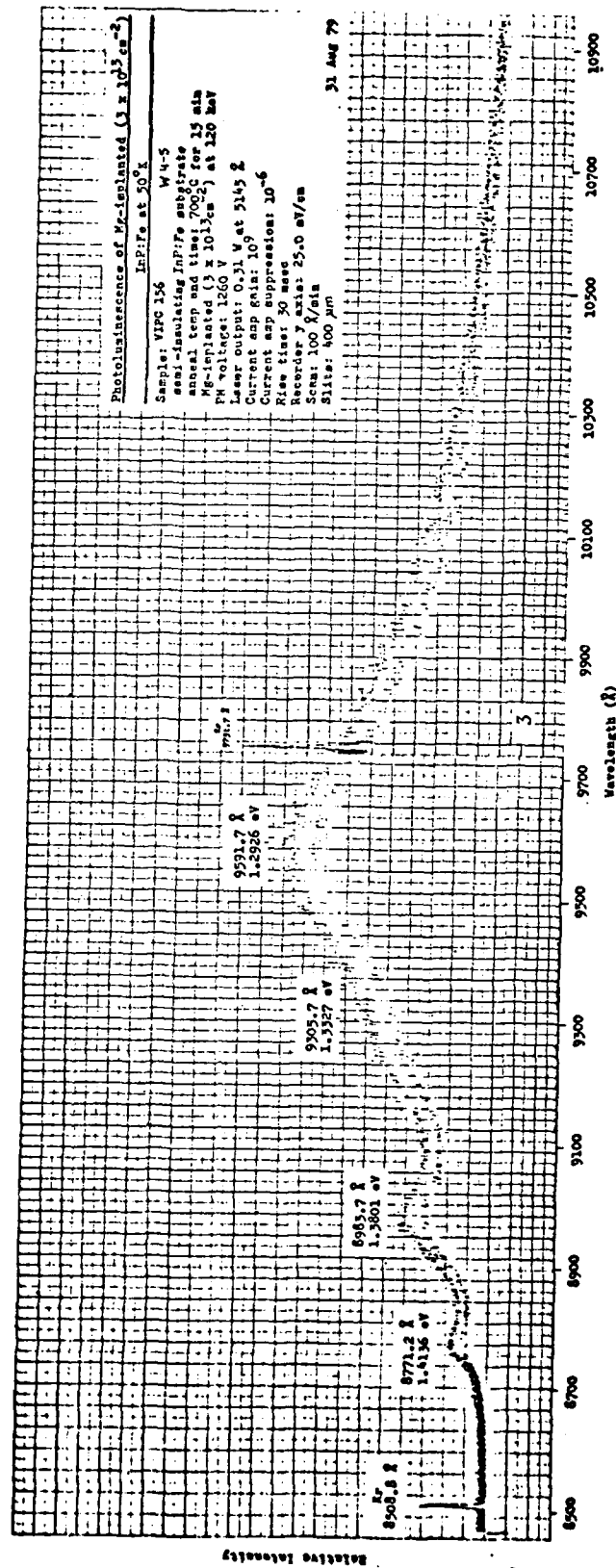


Figure J-5 Photoluminescence of Mg-implanted ($3 \times 10^{13} \text{ cm}^{-2}$),
 700°C Annealed InP:Fe at 50°K

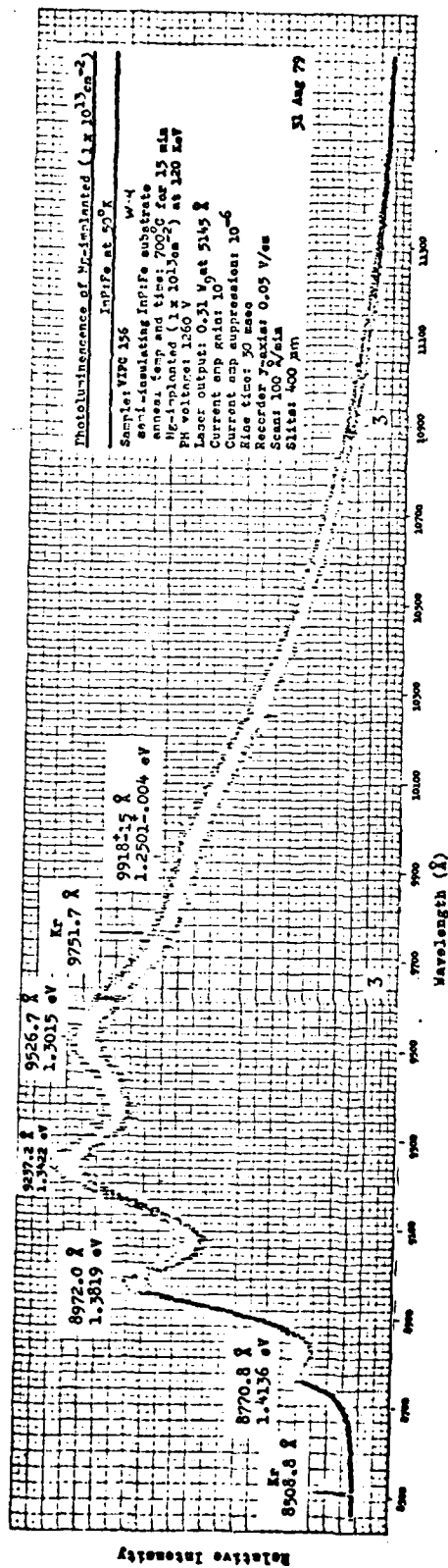


Figure J-6 Photoluminescence of Mg-implanted ($1 \times 10^{13} \text{ cm}^{-2}$), 700°C Annealed InP:Fe at 50°K

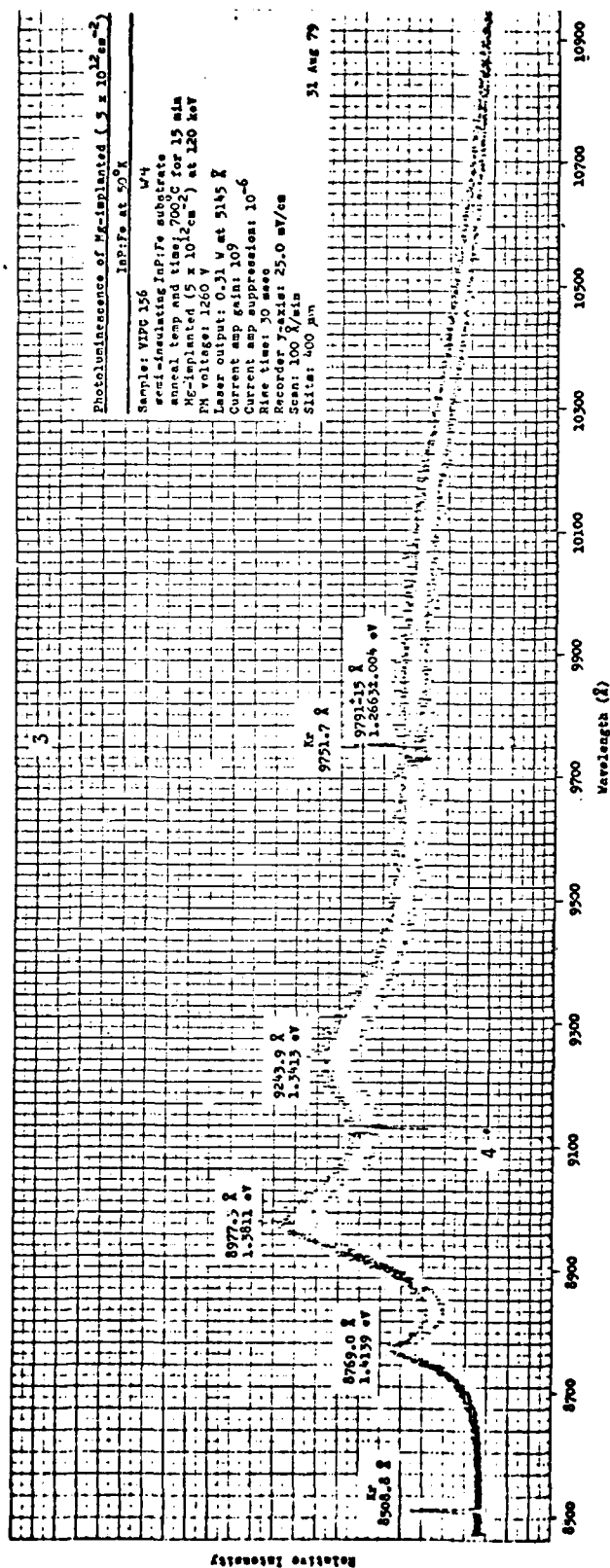


Figure J-7 Photoluminescence of Mg-implanted ($5 \times 10^{12} \text{ cm}^{-2}$), 700°C Annealed InP:Fe at 50°K

Appendix K

Photoluminescence of Unimplanted (wafer 6), 700°C Annealed InP:Fe
from 4.2°K to 100°K

Identification of anomalies in spectra:

- 1 Laser turned off due to low water pressure or overheating
- 2 Temperature change in sample environment

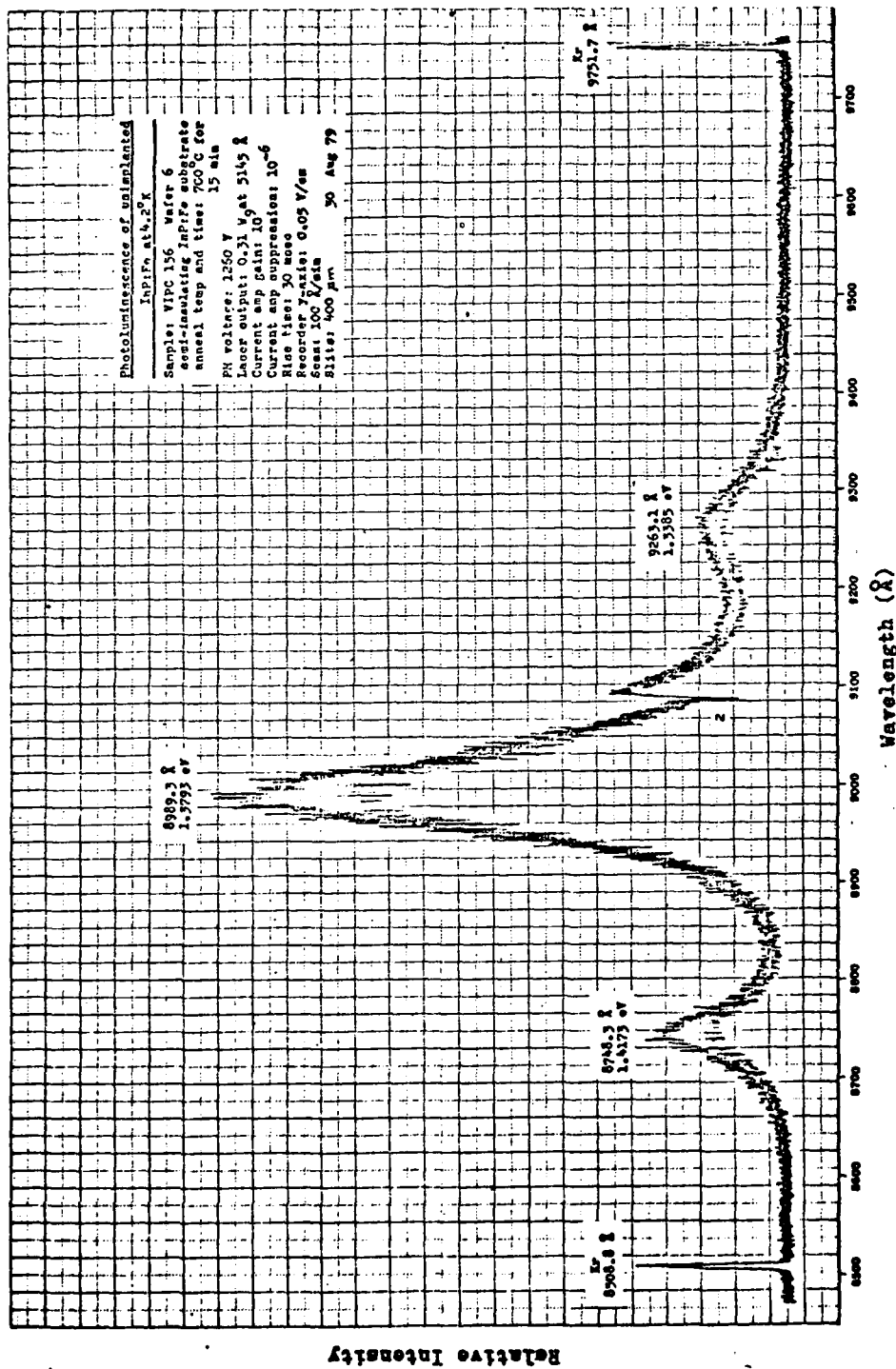


Figure K-1 Photoluminescence of Unimplanted (Wafer 6), 700°C
Annealed InP:Fe at 4.2°K

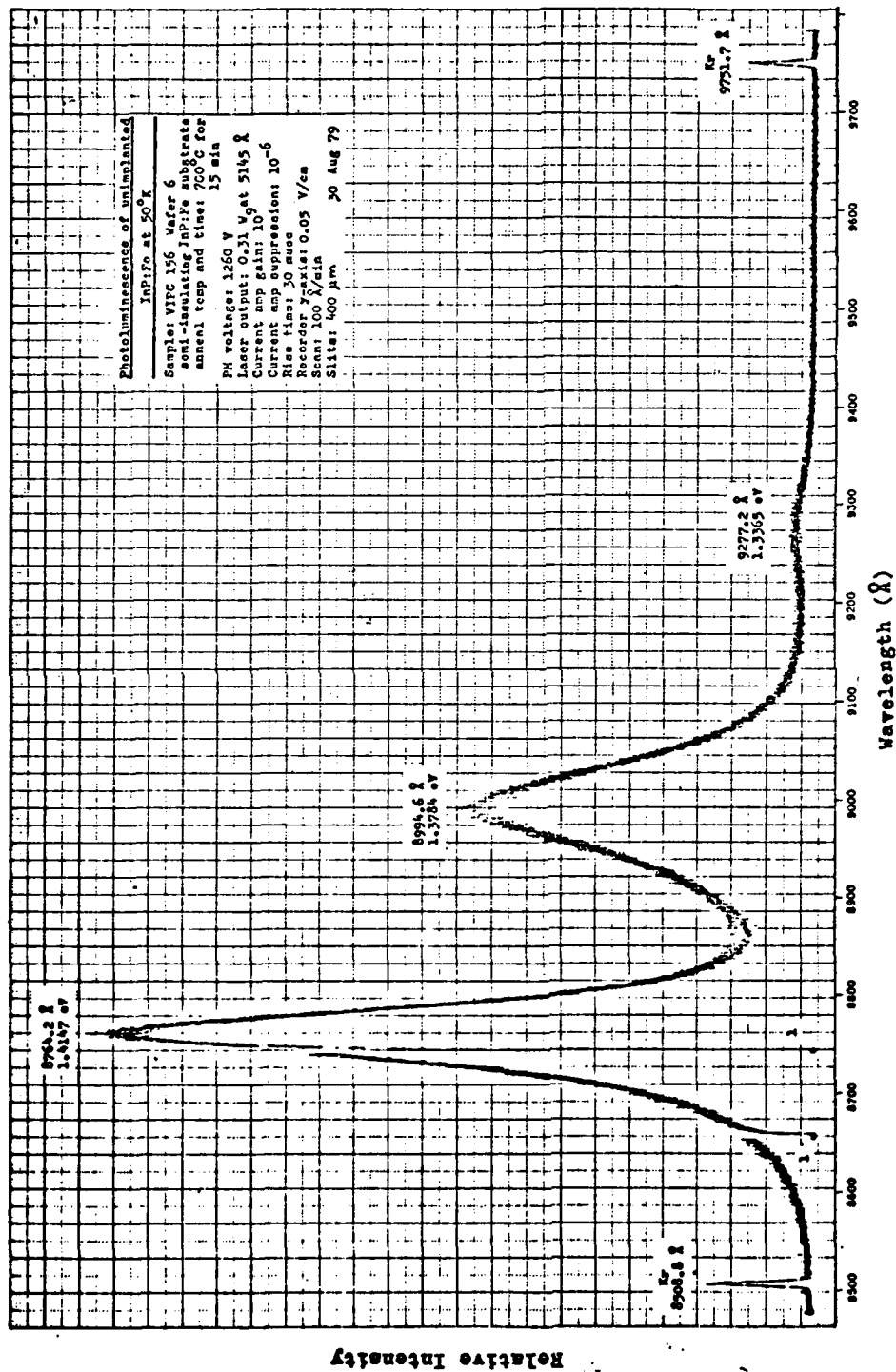


Figure K-2 Photoluminescence of Unimplanted (Wafer 6), 700°C
Annealed InP:Fe at 50°K

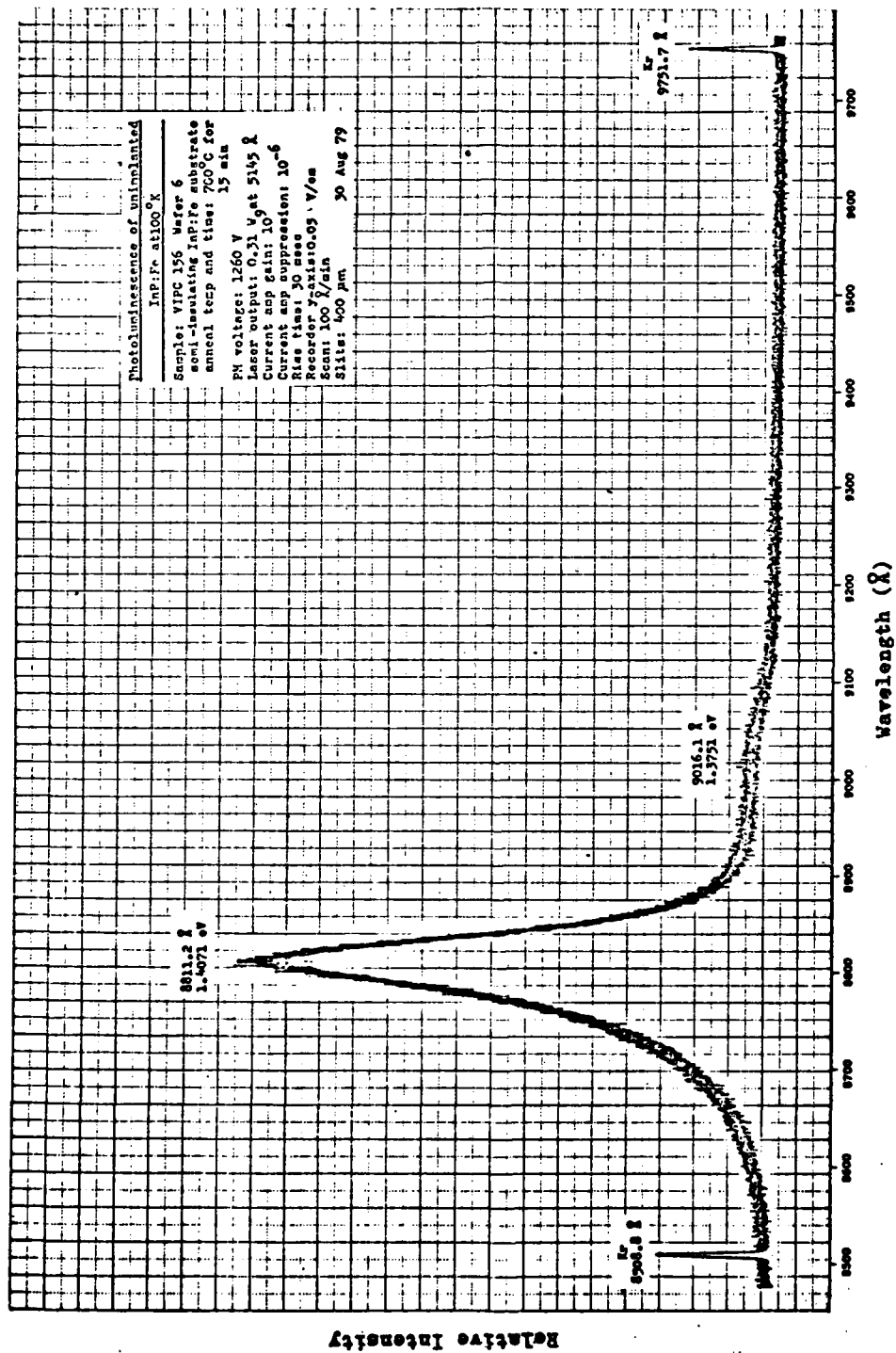


Figure K-3 Photoluminescence of Unimplanted (Wafer 6), 700°C
Annealed InP:Fe at 100°K

Appendix L

Photoluminescence of Mg-implanted ($1 \times 10^{15} \text{ cm}^{-2}$), 700°C Annealed

InP:Fe from 4.2°K to 100°K

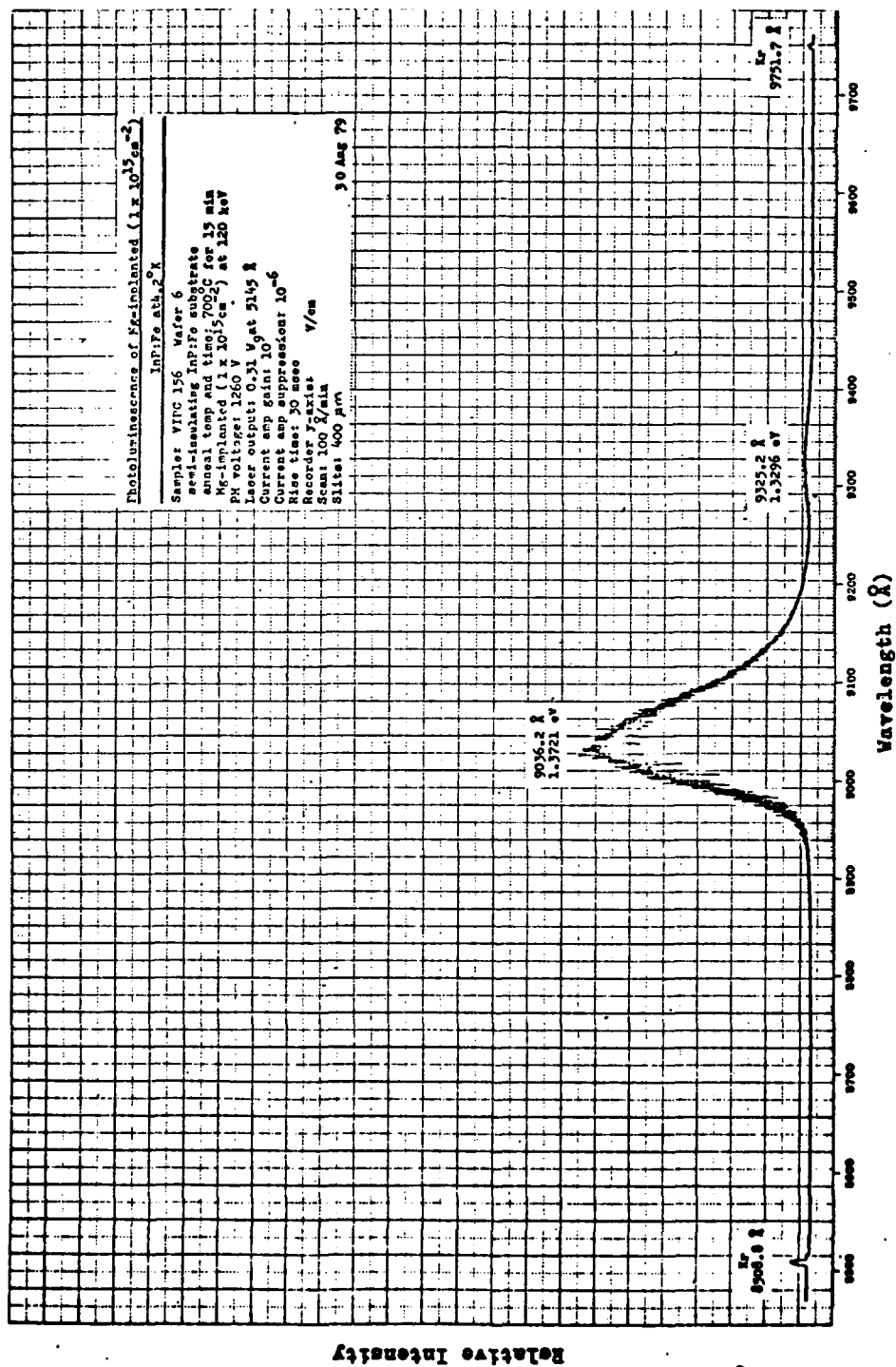


Figure L-1 Photoluminescence of Mg-implanted ($1 \times 10^{15} \text{ cm}^{-2}$), 700°C
Annealed InP:Fe at 4.2°K

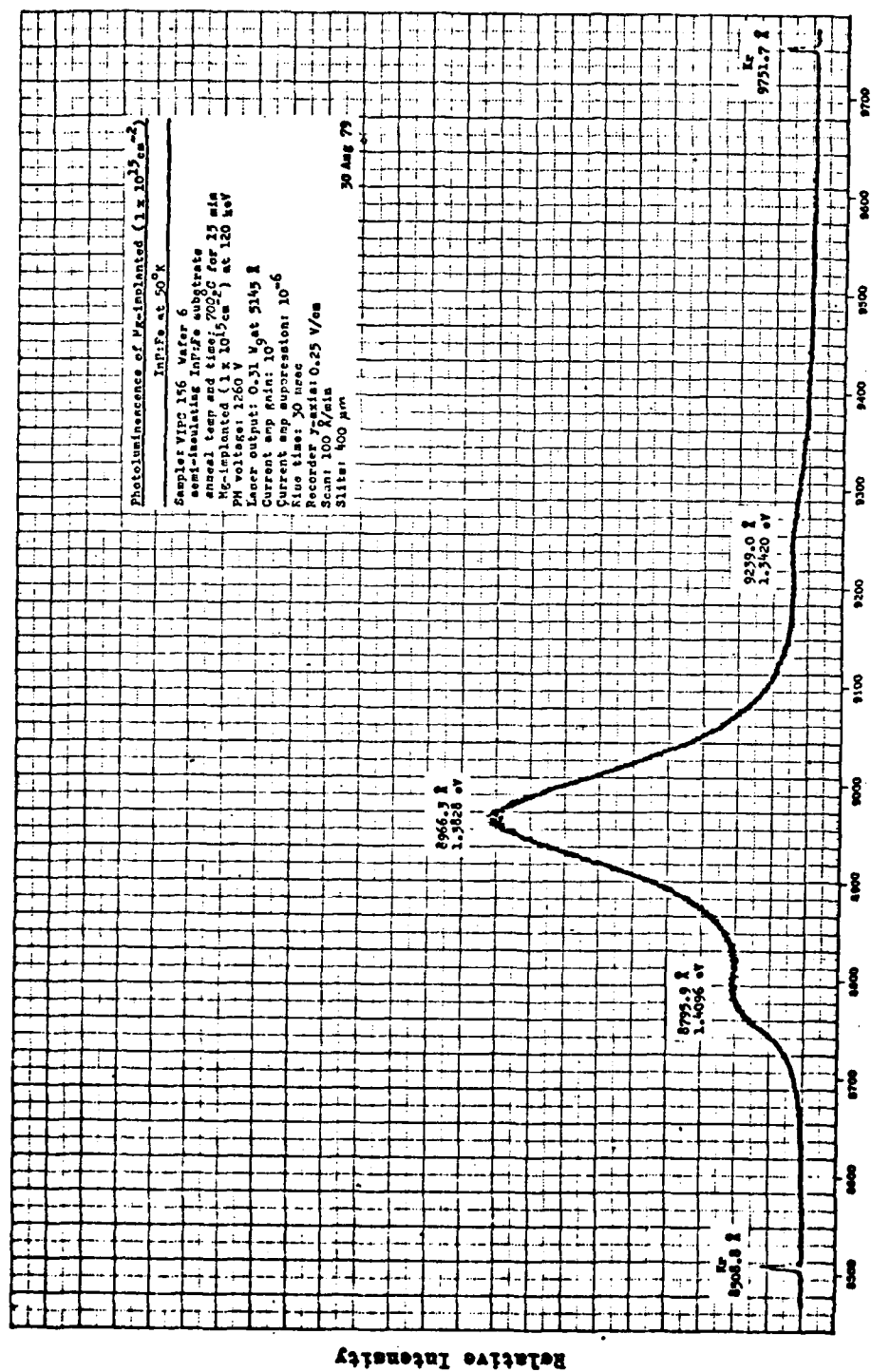


Figure L-2 Photoluminescence of Mg-implanted ($1 \times 10^{15} \text{cm}^{-2}$), 700°C
 Annealed InP:Fe at 50°K

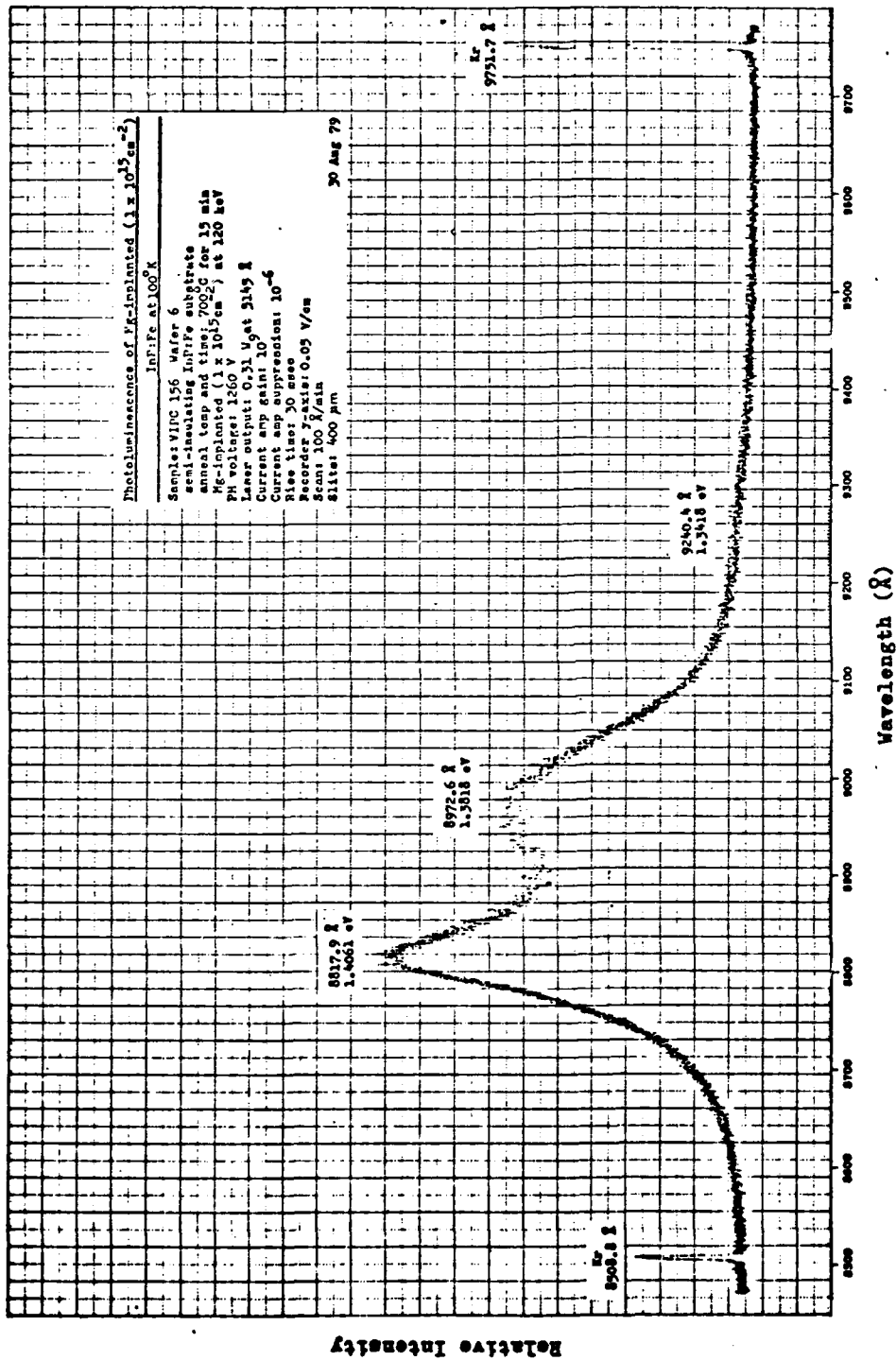


Figure L-3 Photoluminescence of Mg-implanted ($1 \times 10^{15} \text{ cm}^{-2}$), 700°C
 Annealed InP:Fe at 100°K

Appendix M

Photoluminescence of VPE InP

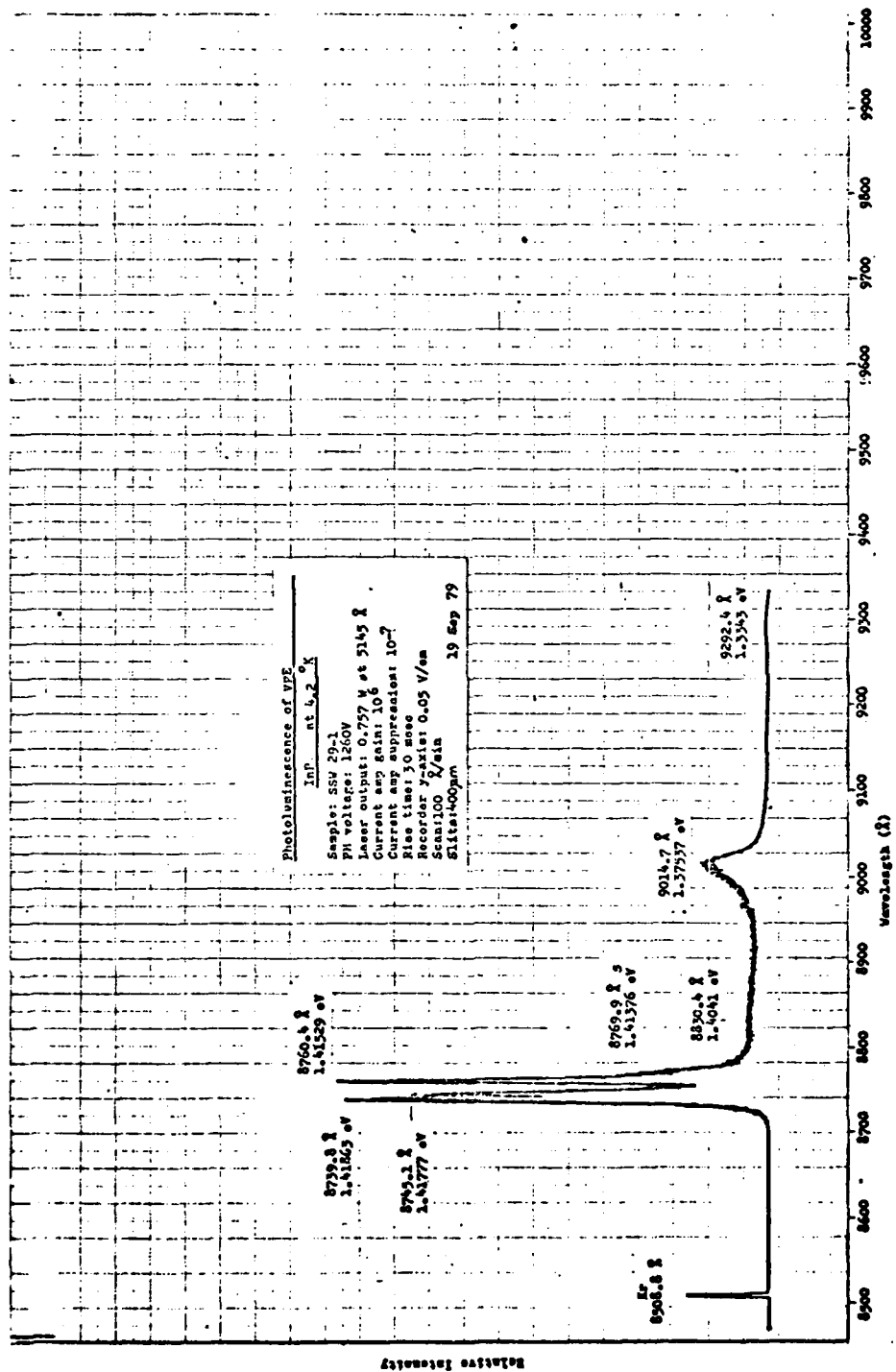


Figure M-1 Photoluminescence of Undoped VPE InP at 4.2°K

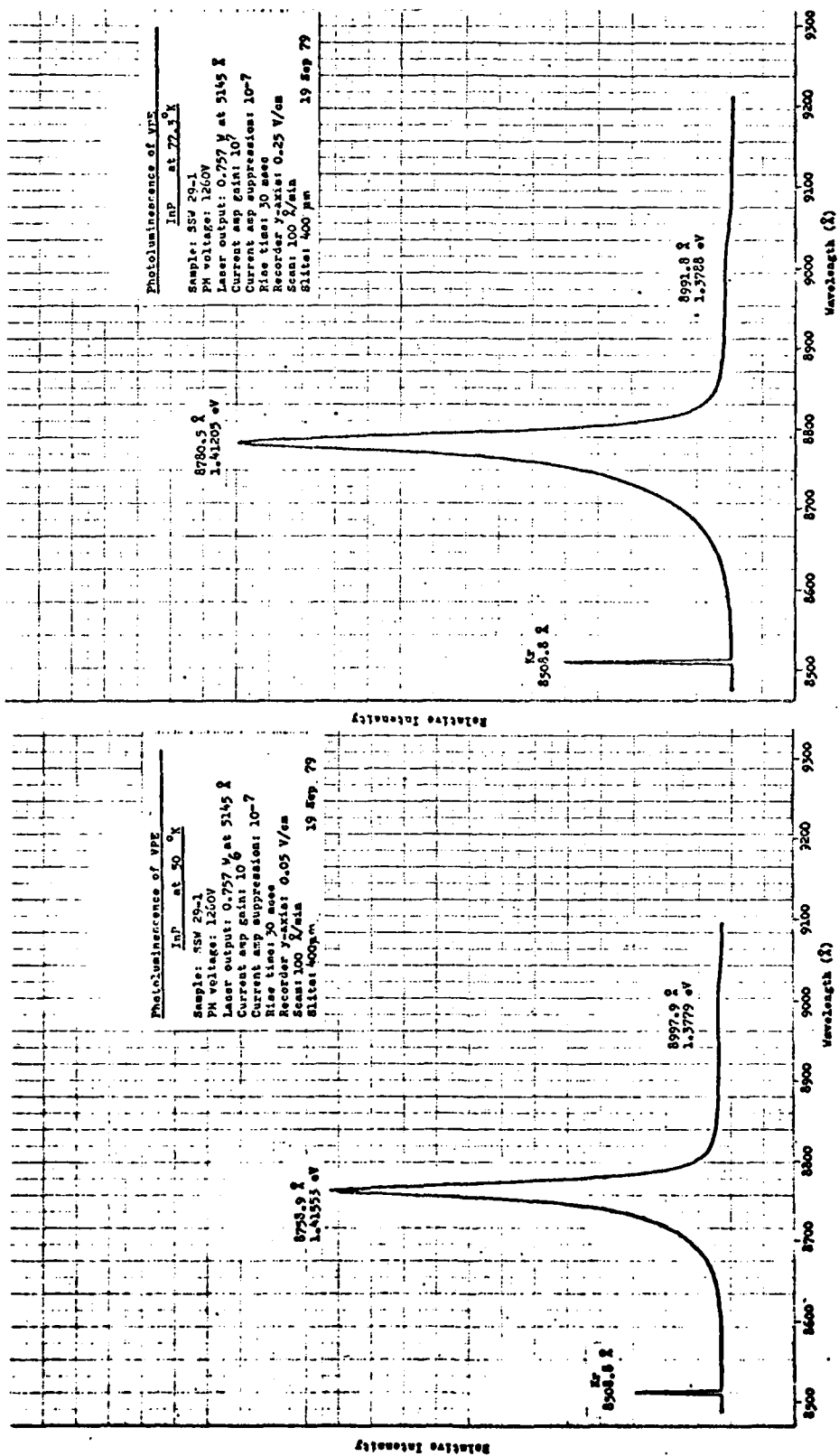


Figure M-2

Photoluminescence of Undoped
 VPE InP at 50°K

Figure M-3

Photoluminescence of Undoped
 VPE InP at 77.3°K

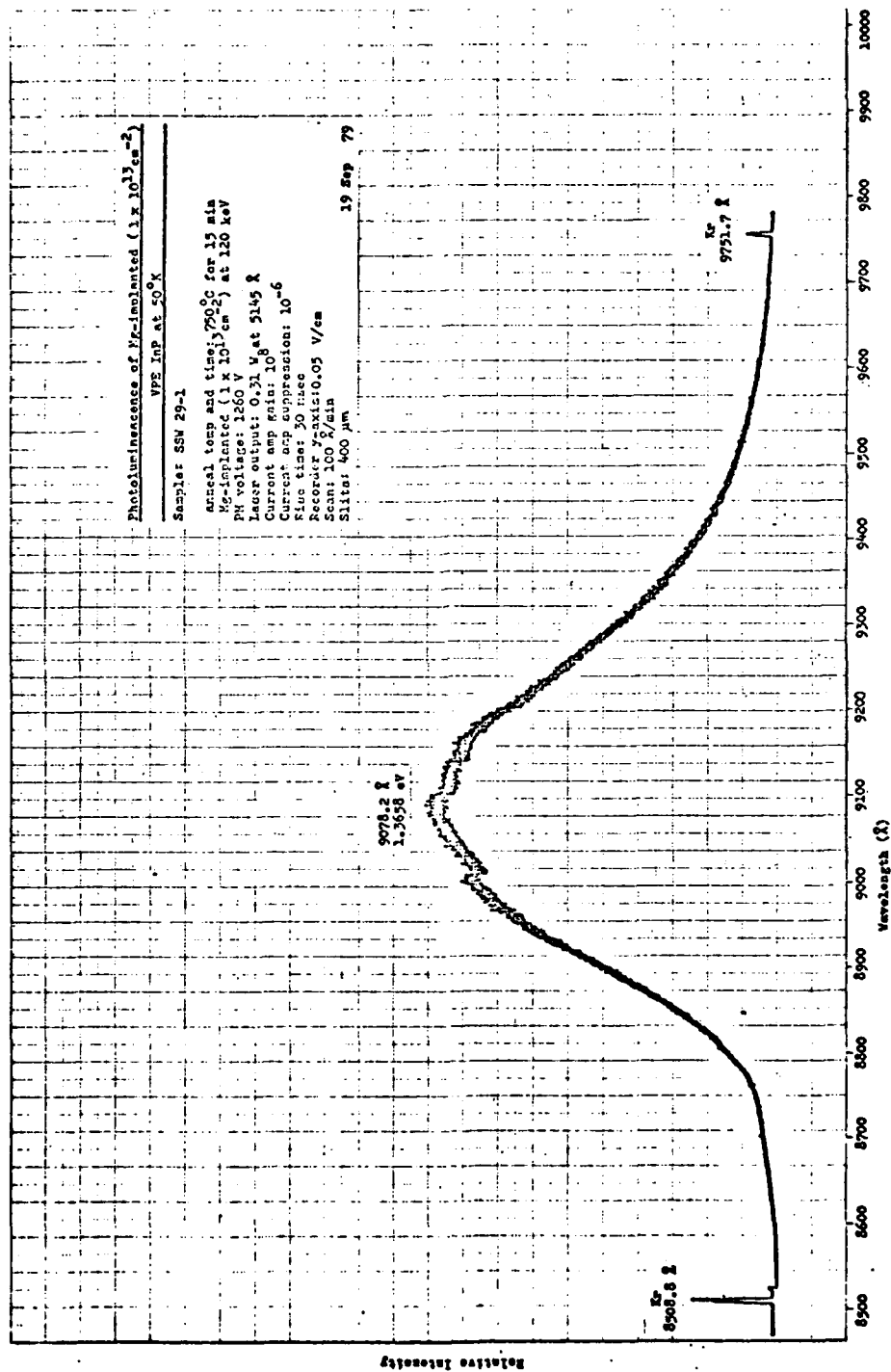


Figure M-4 Photoluminescence of Mg-implanted ($1 \times 10^{13} \text{ cm}^{-2}$) VPE InP at 50°K

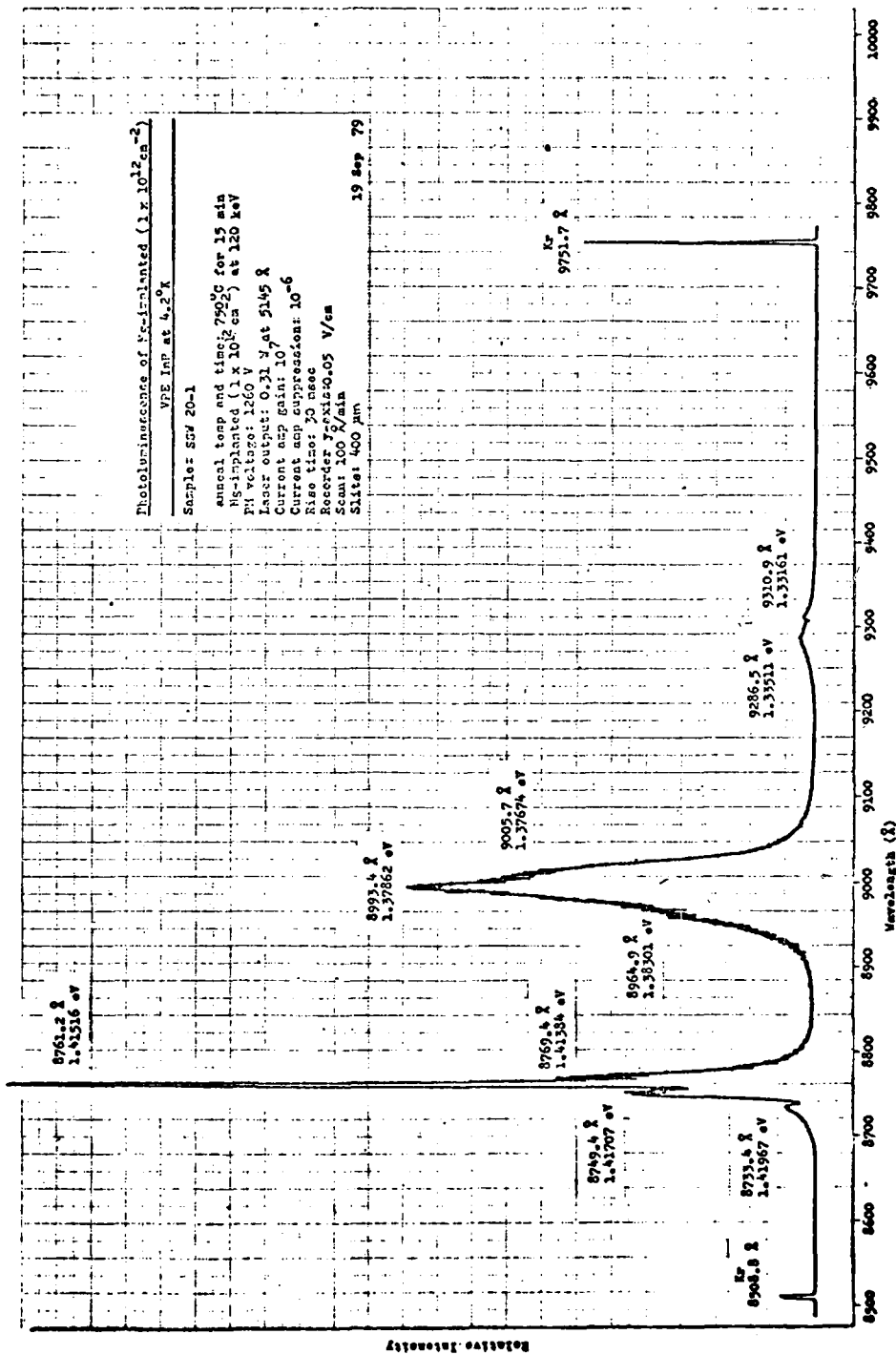


Figure M-5 Photoluminescence of Mg-implanted ($1 \times 10^{12} \text{ cm}^{-2}$) VPE InP at 4.2°K

AD-A080 366

AIR FORCE INST OF TECH WRIGHT-PATTERSON AFB OH SCHOO--ETC F/G 20/12
PHOTOLUMINESCENCE OF UNDOPED, SEMI-INSULATING, AND Mg-IMPLANTED--ETC(U)
DEC 79 G S POWRENKE
AFIT/CEP/PH/T90-6

UNCLASSIFIED

NL

3 of 3

AD-A080 366



END

DATE

FILMED

3 - 80

DOT

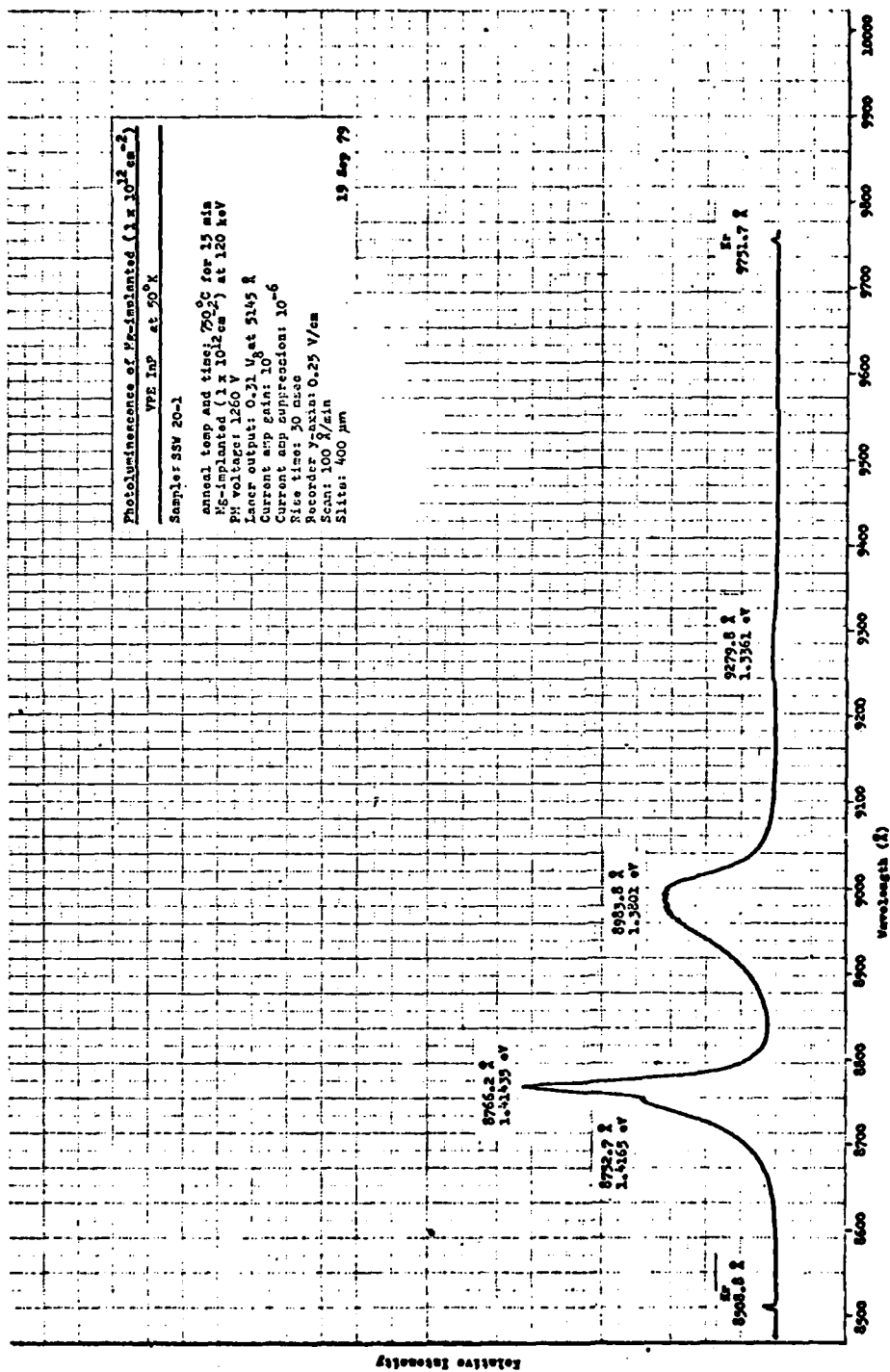


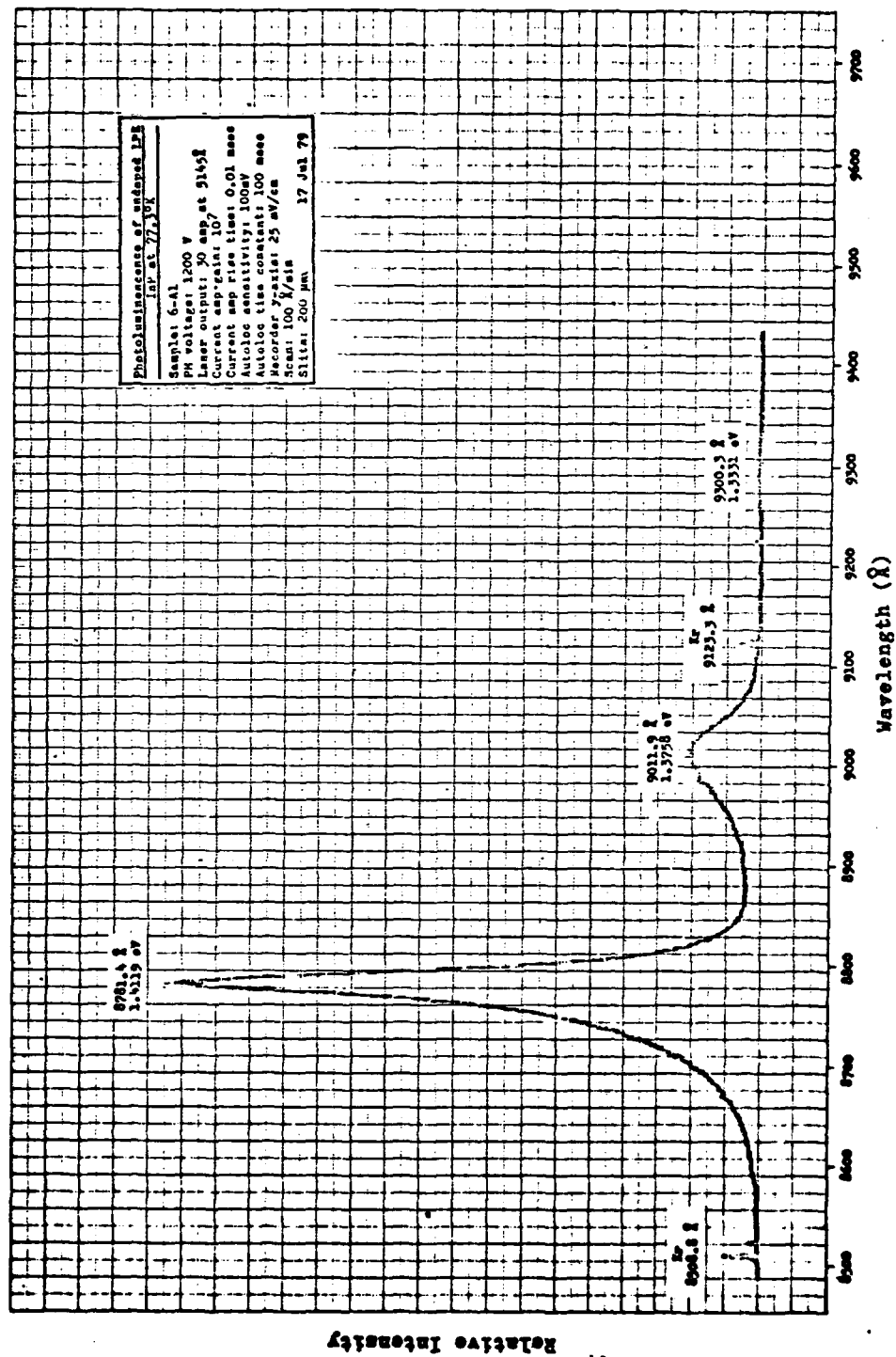
Figure M-6 Photoluminescence of Mg-implanted ($1 \times 10^{12} \text{ cm}^{-2}$) VPE InP at 50°K

Appendix N

Photoluminescence of Undoped LPE InP at 77.3°K and 100°K

Identification of anomalies in spectra:

- 1 Laser turned off due to low water pressure or overheating
- 2 Unidentified peaks, due to unfiltered background



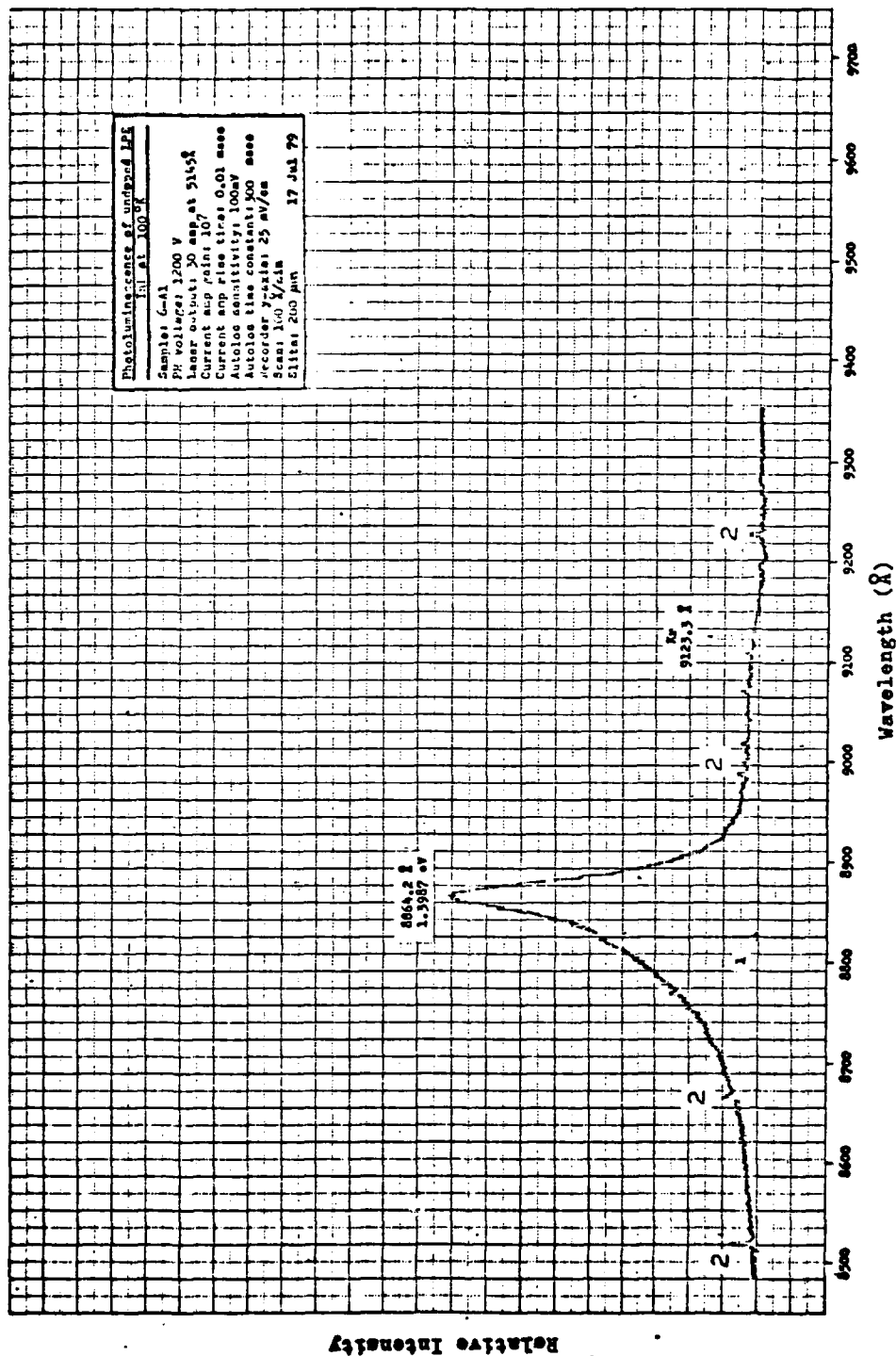


Figure N-2 Photoluminescence of Undoped LPE InP at 100° K

Vita

Gernot Siegfried Pomrenke was born on 9 June 1952 in Pirmasens, Germany. In 1963 he moved with his parents, Gudrun and Karl Pomrenke, to the United States and became a U. S. citizen in 1967. Upon graduation from Southside High School, Fort Smith, Arkansas, in 1971, he entered the USAF Academy under a congressional nomination. In June 1975, he graduated with a Bachelor of Science degree in physics and geography, and was commissioned in the United States Air Force. Subsequent assignments included positions with the 475th Test Squadron and the Test and Evaluation at Tyndall Air Force Base, Florida. In May 1978, he was assigned to the Air Force Institute of Technology.

Permanent Address: 2508 South 22nd Street
Fort Smith, Arkansas 72901

or

Fjólugata 25 Box 439
Reykjavík, Iceland

UNCLASSIFIED

SECURITY CLASSIFICATION OF THIS PAGE (When Data Entered)

REPORT DOCUMENTATION PAGE		READ INSTRUCTIONS BEFORE COMPLETING FORM
1. REPORT NUMBER AFIT/GEP/PH/79D-8	2. GOVT ACCESSION NO.	3. RECIPIENT'S CATALOG NUMBER
4. TITLE (and Subtitle) PHOTOLUMINESCENCE OF UNDOPED, SEMI-INSULATING, AND Mg-IMPLANTED INDIUM PHOSPHIDE		5. TYPE OF REPORT & PERIOD COVERED MS Thesis
		6. PERFORMING ORG. REPORT NUMBER
7. AUTHOR(s) GERNOT S. POMRENKE Capt USAF		8. CONTRACT OR GRANT NUMBER(s)
9. PERFORMING ORGANIZATION NAME AND ADDRESS Air Force Institute of Technology (AFIT-EN) Wright-Patterson AFB OH 45433		10. PROGRAM ELEMENT, PROJECT, TASK AREA & WORK UNIT NUMBERS Program Element 61102A Task/WU: 2306-R2-13
11. CONTROLLING OFFICE NAME AND ADDRESS Air Force Avionics Laboratory (AFAL/DHR) Wright-Patterson AFB OH		12. REPORT DATE December 1979
		13. NUMBER OF PAGES 195
14. MONITORING AGENCY NAME & ADDRESS (if different from Controlling Office)		15. SECURITY CLASS. (of this report) UNCLASSIFIED
		15a. DECLASSIFICATION DOWNGRADING SCHEDULE
16. DISTRIBUTION STATEMENT (of this Report) Approved for Public Release; Distribution Unlimited.		
17. DISTRIBUTION STATEMENT (of the abstract entered in Block 20, if different from Report)		
18. SUPPLEMENTARY NOTES Approved for Public Release; LAW AFR 190-17 JOSEPH R. HIPPS, Major, USAF Director of Public Affairs		
19. KEY WORDS (Continue on reverse side if necessary and identify by block number) III-V Compound Magnesium Indium Phosphide Photoluminescence Ion Implantation		
20. ABSTRACT (Continue on reverse side if necessary and identify by block number) A photoluminescent investigation was made of undoped, semi-insulating, unannealed and annealed Mg-ion implanted indium phosphide originating from Czochralski, vapor, and liquid grown crystals. Ion implantation was performed at fluences of 5×10^{12} ions/cm ² to 1×10^{15} ions/cm ² with an energy of 120 keV at room temperature, followed by annealing at 700° C and 750° C for 15 minutes using a Si ₃ N ₄ encapsulant. (Continued on Reverse)		

DD FORM 1 JAN 73 1473

EDITION OF 1 NOV 68 IS OBSOLETE

UNCLASSIFIED

SECURITY CLASSIFICATION OF THIS PAGE (When Data Entered)

UNCLASSIFIED

SECURITY CLASSIFICATION OF THIS PAGE(When Data Entered)

BLOCK 20 (Cont'd)

Luminescence of undoped InP was studied with respect to temperature, emission intensity, and excitation intensity; results included the possible identification of the following radiative recombinations: free exciton, bound exciton, donor-to-valence, and donor-to-acceptor. Broad, low intensity peaks were identified at 1.0541 eV, 0.9374 eV, and 1.15 eV. Spectral results of the less intense semi-insulating InP:Fe were identical to undoped InP aside from a 1.38 eV high energy shoulder and low intensity peak at 1.31 eV.

Photoluminescence of unannealed, implanted samples resulted in a 0.9643 eV peak with a long, low energy shoulder. Emission intensity and peak energy of annealed, implanted samples were studied as a function of dosage and anneal temperature. The post-implantation annealing at 750° C was sufficient to obtain efficient luminescence. Analysis of the 750° C annealed samples indicate that the peak due to recombinations involving implanted Mg acceptors is located between 1.384 eV and 1.388 eV at 50° K. Superior spectral results from VPE InP places the Mg peak position at 1.3801 eV.

UNCLASSIFIED

SECURITY CLASSIFICATION OF THIS PAGE(When Data Entered)